Offshore migration of coastal sand-bars at Wanganui, New Zealand

A thesis presented in partial fulfilment
of the requirements for the degree of

Doctor of Philosophy

in

Geography

at

Massey University, Palmerston North,
New Zealand

Roger Duncan Shand

March 2000

MASSEY UNIVERSITY LIBRARY

Thesis Copyright Conditions

Title of thesis: *Offshore migration of coastal sand-bars at Wanganui, New Zealand*

1. I give permission for my thesis to be made available to readers in the Library at Massey University under the conditions determined by the Librarian.

2. I agree that my thesis may be sent to another institute on temporary loan under conditions determined by the Librarian.

3. I agree that my thesis may be copied for Library use **only if** published copies are not available through the Geography Department.

Signed R D Shand

Date 22 November 2000

The Library
Massey University
Palmerston North
New Zealand

The copyright of thesis belongs to the author. All readers must sign their name in the space below to show that they recognise this. They are asked to add their permanent address.

Name and Address Date

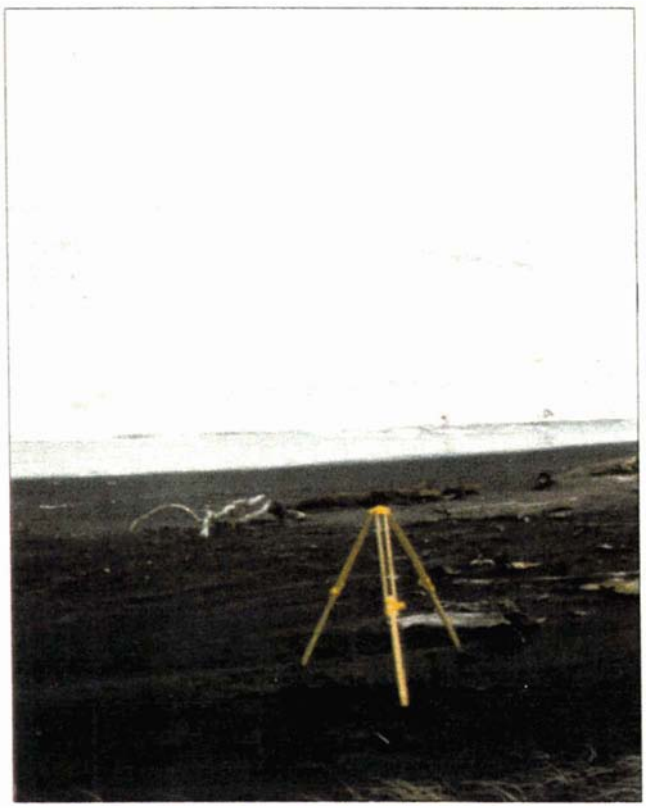

The mystery of the universe, the layer upon layer of new meaning and new discovery, will never be revealed to those who do not look for it.

Veitch (1990)

ABSTRACT

Net offshore bar migration (NOM) refers to the systematic seaward migration of coastal sand-bars across the surf zone. These bars form near the shore-line and disappear in the outer surf zone. NOM behaviour is repetitive and has been described as cyclic. Over the past decade NOM has been recognised on the North Carolina coast, the Dutch coast and by the author on the west coast of the New Zealand North Island. The aim of this project is to elaborate on the behaviour and causative processes of NOM.

The New Zealand data used in this study comprise a 6.3 year bar-crest record from an approximately six kilometre long field site at Wanganui. These data were collected using aerial and terrestrial photography and supplemented with ground surveys. Image processing techniques were developed for photographic data abstraction and analysis. Published data from the other 'global' NOM sites were analysed and compared after data compatibility procedures had been developed and applied. The NOM cycles were quantified using parameters for NOM width (cross-shore migration distance), duration and rate, together with return period.

The global NOM sites are characterised by multiple sand-bars, the predominance of sea waves and a narrow band of storm strength wind and wave conditions. The longer-term (average cyclic) parameter values for the global data-set were as follows: NOM width ranged between 195 and 930 m; duration ranged between 1.2 and 13 years; NOM rate ranged between 35 and 196 m/yr, and NOM return period varied between 1.2 and 14.4 years. NOM characteristics for the global sites were found to be correlated with cross-shore slope, coastal orientation and extreme wave height.

The Wanganui bar-crest data were also analysed for shorter-term (within-cycle) bar behaviour. Cross-shore bar migrations had a bimodal frequency distribution. The group of larger migrations, termed 'episodic seaward jumps', significantly influenced the characteristics of individual NOM cycles. Episodic seaward jumps appear to be preceded by the degeneration of the adjacent seaward bar. Longshore non-synchronous variation in NOM characteristics were found to be mainly related to 'bar switching' (longshore bar realignment).

Based on the above results, a conceptual morphodynamic model for NOM was formulated. The model incorporates three main components: a drive mechanism; a morphodynamic modification mechanism; and a timing mechanism.

Net offshore bar migration is a significant mode of morphological behaviour within the surf zone. Its influence upon other aspects of coastal geomorphology such as shoreline change, and its relationship with existing 'beach-state' based models, require further investigation.

ACKNOWLEDGEMENTS

First I wish to thank my main supervisor, Dr Mike Shepherd, who introduced me to the fascinations of coastal geomorphology. My world quickly became a different place as the continuous and multi-scaled changes which characterise the coastal environment were revealed. I hope that I am also able to open the eyes of others to see the wonders of this world. Thanks Mike for your patience and help in dealing with the numerous obstacles I faced.

Professor Bob Kirk, now Pro-Vice Chancellor of Research at the University of Canterbury, played a vital role in keeping the project on track with his astute overview and insistence on coherence, clarity and adherence to the principles of scientific research - thanks Bob.

The project relied upon the imaging system VIPS, devised by Dr Don Bailey as part of his own PhD. I well remember wandering into Don's office with the Lippmann and Holman (1989) seminal paper on obtaining morphological bar-crest data from photographs and video, handing him the paper and then asking if he could do this sort of thing. In hindsight I realised this was a silly question to ask an engineer! Don willingly adapted his operating system to processing my surf zone photos and providing the bar-crest data for my subsequent geomorphological analysis. Don became a secondary supervisor and his advice concerning mathematics, statistics, physics and imaging were greatly appreciated. The National Institute of Water and Atmospheric Research (NIWA) subsequently commissioned Don to modify some of the algorithms for use in a national video-based automated coastal monitoring system.

Assistance with data and error analysis from Drs S. Ganesalingam and T. Moore of the Massey University Statistics Department is acknowledged.

I wish to thank Professor Rob Holman (Oregon State University) for the initial time-lapse photographic equipment and suggestions on how to go about developing techniques for its use. Thanks also to Drs Gerben Ruessink (Utrecht University) and Phil Osborne (Auckland University) for guidance on preparing papers for publication and to Professor Andy Short (Sydney University) for his instruction on coastal morphodynamics.

Funding and field support for the project came from many sources. I acknowledge with thanks the Massey University input: the Post Graduate Research Fund; the Massey University Research Fund; the Special Vice Chancellor Grant, and financial and equipment support from the Geography Department (now incorporated within the School of Global Studies).

Organisations in Wanganui were also very supportive. The Wanganui Port Company, the Wanganui District Council and the local NIWA office provided survey equipment and labour. The Wanganui Surf Lifesaving Club provided inflatable craft and highly skilled operators. Thanks to all of you - especially for braving winter days when conditions were marginal.

Finally, I wish to give special thanks to my parents who helped me develop an enquiring mind and acquire practical skills for problem solving, and also to my wife Susan and to my family and friends who for so long put up with me as I struggled through a project that, at times, seemed to have no end. You all supported me in so many ways - thank you.

TABLE OF CONTENTS

Title page i
Frontispiece iii
Abstract v
Acknowledgements vii
Table of Contents ix
List of Figures xiii
List of Tables xvii
List of Appendices xiv

Chapter 1 Introduction

1.1 Rationale 1
1.2 Background 5
1.3 Approach 8
1.3.1 Conceptual framework 8
1.3.2 Data collection issues 13
1.4 Objectives and thesis outline 15

Chapter 2 The field site

2.1 Introduction 17
2.2 Geomorphological setting 18
2.2.1 General background 18
2.2.2 Jetties and morphological influence 25
2.3 Morphology 30
2.3.1 Cross-shore morphology 30
2.3.2 Plan-view morphology 39
2.3.3 Rivermouth morphology 40
2.4 Sediment 40
2.4.1 Textural characteristics 40
2.4.2 Mineralogy 43
2.4.3 River sediment 44
2.5 Process regime 44
2.5.1 Surface waves 44
2.5.2 Wind 59
2.5.3 Longshore currents 59
2.5.4 River hydrodynamics 63
2.6 Relevance for NOM 63

Chapter 3 Morphological methods

3.1 Introduction 65
3.2 Image-based data 66
3.2.1 Field data 66
3.2.2 Image processing 74
3.2.3 VIPS 76
3.2.4 Data processing algorithms 76
3.2.5 Data-sets 80
3.2.6 Data analysis algorithms 82
3.2.7 Interpretation of intensity output 85
3.3 Ground profile data 86
3.3.1 Field data 86
3.3.2 Data processing 91
3.3.3 Data-sets 91
3.3.4 Data analysis 92
3.4 Summary 92

Chapter 4 Evaluation of morphological methods

4.1 Introduction 95
4.2 Errors 96
4.2.1 Definitions and concepts 96
4.2.2 Multiple errors 98
4.3 Image-based errors 99
4.3.1 Environmentally associated errors 99
4.3.2 Photogrammetric errors 116
4.3.3 Longshore and cross-shore resolution 121
4.4 Ground profile errors 129
4.5 Intensity and ground profile comparison 131
4.6 Summary and conclusions 136

Chapter 5 Longer-term aspects of NOM

5.1 Introduction 141
5.2 Study sites 147
5.3 Methods 151
5.3.1 Data acquisition methods 151
5.3.2 Methods of analysis 153
5.4 Wanganui sites 157
5.4.1 Results 157
5.4.2 Discussion 162
5.5 Global sites 164
5.5.1 Results 164
5.5.2 Discussion 170
5.6 Conceptual modelling 178
5.7 Summary and conclusions 180

Chapter 6 Shorter-term aspects of NOM

6.1 Introduction 183
6.2 Cross-shore bar migration 189
6.2.1 Methods 189
6.2.2 Results 191
6.2.3 Discussion 195
6.3 Episodic offshore bar migration 201
6.3.1 Methods 201
6.3.2 Results 204
6.3.3 Discussion 211
6.4 Morphological behaviour 216
6.4.1 Methods 216
6.4.2 Results 216
6.4.3 Discussion 220
6.5 Bar switching 220
6.5.1 Methods 221
6.5.2 Results 222
6.5.3 Discussion 228
6.6 Conceptual modelling 230
6.7 Summary and conclusions 231

Chapter 7 Conclusions

7.1 NOM objectives 237
7.1.1 Image-based data acquisition 238
7.1.2 Longer-term NOM characteristics 239
7.1.3 Shorter-term NOM characteristics 240
7.1.4 A conceptual model of NOM 241
7.2 Further research 243

References 247

Appendices 263

LIST OF FIGURES

1.1	Location maps of (global) NOM sites at mid 1991	3
1.2	Published NOM data for (global) sites at mid 1991	4
1.3	Additional Wanganui bar-crest time-series 1990/1991	6
1.4	Schematic representation of a coastal morphodynamic system	8
1.5	Space and time scales for coastal morphologies and associated processes	10
1.6	Schematic representation of morphological changes at a range of temporal scales	11
1.7	Cross-shore profiles at transects T150 , T500, T1500, T3000, T4000 and T5000.	15
2.1	Regional setting of study area	19
2.2	Structural geology affecting the study area	20
2.3	Construction of the northwestern river jetty	20
2.4	Photographs of the study area	22
2.5	Offshore profiles at cross-shore transects T200, T1500 and T5000	24
2.6	Shoreline change at T150 during the period 1876 to 1992	24
2.7	Rates of shoreline change along the Wanganui coast, 1876 to 1983	27
2.8	Bathymetric chart (23.1.68) of river entrance	27
2.9	Mean annual minimum depths at river entrance, 1926 to 1992	29
2.10	Cross-shore profiles at T150, 1879 to 1992	29
2.11	Cross-shore profile bundles for transects T200, T1500 and T5000	32
2.12	Morphological features and terminology	33
2.13	Cross-shore zonal nomenclature	34
2.14	Cross-shore mean profiles and fitted power curves	35
2.15	Cross-shore standard deviations for profile bundles	36
2.16	Alongshore sediment parameter values	41
2.17	Cross-shore sediment parameter values	42
2.18	Classification of surface waves	45
2.19	Field method for 'line-of sight' wave height measurement	45
2.20	Probability of exceedence curves for wave height data sets	47
2.21	Wave height variation at Wanganui during the study period	51
2.22	Examples of wave spectra for offshore wave data	54
2.23	Frequency spectra from a three hour run-up record	54
2.24	Time-series of seiche activity at Wanganui	57
2.25	Wind rose for Wanganui Airport data	60
3.1	Field equipment used for aerial photography	67
3.2	Example of a vertical aerial photograph	69

3.3	Example of an oblique aerial photograph	69
3.4	Field equipment for oblique terrestrial photography	71
3.5	An example of profile bathymentry and intensities from Duck	72
3.6	Examples of instantaneous and time-exposure photographs of the study area	73
3.7	An example of a video frame from the central study area	73
3.8	Examples of rectified aerial and terrestrial output images	77
3.9	An example of a time-averaged intensity profile taken from video images	80
3.10	Examples of rectified and straightened time-exposure output images	81
3.11	An example of monitor display for the algorithm PFIT.VIP	83
3.12	Examples of time-stack images	83
3.13	Equipment used for nearshore hydrographic surveys	87
3.14	Equipment used for offshore hydrographic surveys	89
3.15	Equipment used for foreshore profile surveys	90
3.16	Illustration of the 'maximum residual method' of bar-crest detection	93
4.1	Illustration of different error concepts and characteristics relevant to the study site	97
4.2	Method used to determine seiche influence on intensity maxima location	102
4.3	An example of tidal influence on intensity maxima location	107
4.4	An example of wave height variation on intensity maxima location	110
4.5	Cross-shore correlation function plots for longshore intensity maxima associated with different wave heights	112
4.6	Intensity maxima offset errors associated with breaking wave height study area	118
4.7	Distribution of random rectification errors across the study area	122
4.8	Longshore resolution lengths for rectified terrestrial and aerial images	123
4.9	Cross-shore resolution lengths for rectified terrestrial and aerial images	126
4.10	Error surface between rectified terrestrial and aerial images	128
4.11	Comparison between time-averaged ground profiles and time-averaged intensity profiles	132
4.12	Plot and fitted curve for the differences between ground-profile bar-crests and corresponding intensity maxima	134
5.1	Location maps for global NOM sites	143
5.2	Bar-crest time-stacks for Wanganui sites	144

5.3	Bar-crest time-series for global NOM sites	145
5.4	Diagrammatic representation of the parameters used to define NOM	155
5.5	Bar-crest generation and degeneration locations and boundaries for the zone of systematic offshore migration	155
5.6	Illustration of methods used to determine the time that bars underwent systematic offshore bar migration	158
5.7	Linear trend lines fitted to each NOM for the Wanganui sites	160
5.8	NOM parameter values for the Wanganui sites	161
5.9	Longshore linear trend lines for mean NOM parameter values at the Wanganui sites	163
5.10	Mean NOM parameter values for the global sites	165
5.11	Pearson correlation analysis results for mean NOM parameter values from the NOM sites	166
5.12	Plots of NOM duration with sediment size and cross-shore slope at the global sites	169
5.13	Non-linear relationships between angle of wind approach with NOM duration and angle of energy approach with relative strength of longshore energy component	171
5.14	Conceptual morphodynamic modelling for longer-term aspects of NOM	179
6.1	Examples of bar bifurcation, bar switching and oblique bar undergoing longshore translation	186
6.2	Bar-crest location time-series for sites T1600 and T5000	192
6.3	Bar migration distance histograms for sites T1600 and T5000	194
6.4	Bar migration distance versus inter-survey maximum wave height at T1600 and T5000	196
6.5	Episodic seaward bar migrations plotted on bar-crest migration time-series for sites T1600 and T5000	197
6.6	Illustrations of episodic and regular modes of bar migration	198
6.7	Classification scheme for morphological behaviour of the seaward bars relative to episodic offshore bar migrations	203
6.8	Migration start location and migration distance for episodic seaward bar migrations	205
6.9	Maximum wave height, storm duration and longshore wind speed for episodic seaward bar migrations	208
6.10	Plots and analysis of migration distance and start location for episodic seaward bar migrations versus maximum wave height, storm duration and longshore wind speed	210
6.11	Diagrammatic illustration of outer bar control concept	214
6.12	Examples of the four classes of morphological behaviour associated with episodic offshore bar migrations at Wanganui	218

6.13	Plots of morphological behaviour versus maximum wave height, storm duration and longshore wind speed	219
6.14	Plot of longshore location versus time for episodes of bar switching	222
6.15	Image sequence depicting bar switch episode 7 and time-stacks depicting the associated cross-shore bar migration	223
6.16	Bar migration rates for examples of positive and negative bar switching	225
6.17	Time-series for bars at T2800 and T5000 which underwent positive and negative switching associated with episode 7	227

LIST OF TABLES

1.1	Average durations and rates of NOM at global sites, mid 1991	7
2.1	Cross-shore profile zone boundaries and depths	38
2.2	Cross-shore profile zone widths and slopes	38
2.3	Wave height statistics	47
2.4	Wave period statistics	53
2.5	Significant wave height and peak spectral wave period distributions	53
2.6	Seasonal wind frequency distribution	60
2.7	Cross-shore and alongshore wind speed components	61
2.8	Longshore current statistics	61
4.1	Descriptive statistics for environmental parameter values at times of photographic sampling	101
4.2	Observed and predicted seiche wave heights	104
4.3	Variation of cross-shore intensity maxima location for different longshore segment widths associated with the environmental conditions experienced during photographic sampling	106
4.4	Descriptive statistics for tide-influenced intensity maxima variation	108
4.5	Descriptive statistics for wave height-influenced intensity maxima variation	108
4.6	Photogrammetric errors for rectified terrestrial and aerial photographs	117
4.7	Rectification errors associated with input parameter measurement precision	120
4.8	Errors associated with ground profile data acquisition	130
4.9	Time-averaged bar-crest data from ground profiles and intensity profiles	134
5.1	Morphological and sediment characteristics for global NOM sites	149
5.2	Energy characteristics for global sites	149
5.3	Details of data collection systems used at NOM sites	152
5.4	Maximum likely cross-shore distances traversed during successive seaward bar migrations	158
5.5	Pearson correlation matrices for NOM duration with morphological, sediment and process variables	168
5.6	Average NOM durations and bar volumes for global NOM sites	177
6.1	Descriptive statistics for inter-survey bar-crest migrations	193
6.2	Descriptive statistics for episodic seaward bar migration start distances and migration distances	206

6.3	Descriptive statistics for energy parameter values associated with episodic seaward bar migrations	209
6.4	Classification results for seaward bar behaviour associated with episodic offshore bar migrations	212
6.5	Episodic seaward bar migrations associated with different types of morphological behaviour	217
6.6	NOM parameter values for selected bars at T2800 and T5000 which were associated with switch episode 7	228

LIST OF APPENDICES

A	Conceptual surf zone models	263
B	Littoral drift estimates for the Wanganui coast	265
C	Shoreline change background information	267
D	Ground profile data-sets	269
E	Mineralogy of beach sediment	271
F	Line-of-sight wave height data	273
G	Oblique terrestrial rectification algorithm ETM_MAIN.VIP	275
H	Rectified images used in this study	281
I	Environmental conditions during error assessment sampling	293
J	Ground profile bar-crest data for site T1500	295

CHAPTER 1 INTRODUCTION

When your work takes you to the frontier there are no reliable maps and those that exist may be as misleading as they are helpful.

Veitch (1995).

1.1 Rationale for this study

Sand-bars are morphological features found on many of the world's sandy shorelines. Hardisty (1990) estimates that at least one third of the world's coastlines are sand-dominated and characterised by gently curving cross-shore profiles and plan shapes. Often superimposed upon this overall morphology are undulations on the sea-bed which are referred to as sand-bars. Sand-bars are usually aligned parallel to the shoreline and occur either singly or in multiple form. The morphological configuration and behaviour of sand-bars are a product of mutual interaction between fluid motions, material properties and surface forms (Wright and Thom, 1977). As the world's sandy coasts have numerous combinations of energy regime, sediment characteristics and geometry, a wide range of beach types occur. This thesis focuses on a coast characterised by multiple sand-bars, moderate levels of wave and tidal energy, and longshore currents.

Geomorphological surf zone models encompass a range of morphological configurations which are related to different environmental conditions. The earliest and simplest model involves two morphological configurations, both of which are uniform in the longshore direction. Beach morphology oscillates between a gently sloping or 'dissipative' profile with a seaward bar, and a steep faced or 'reflective' profile characterised by a landward (berm) terrace. Under fairweather conditions the bar migrates shoreward to form the berm while under storm conditions it is destroyed and a new bar reforms further seaward. This model was developed for single-bar oceanic coasts which display strong seasonality and is referred to as the storm/swell, summer/winter, or bar/berm profile model (see e.g. Komar, 1976a; Hardisty, 1990).

Conceptual models incorporating additional morphological configurations were subsequently developed by coastal researchers such as Davis and Fox (1972), Sonu (1973), Davis and Fox (1975), Fox and Davis (1976), Owens (1977), Chappell and Eliot (1979), Short (1979), Wright et al. (1979), and Sasaki (1983). A bench-mark in this work was Wright and Short's (1984) 'morphodynamic model' which consists of a sequence of six morphological assemblages or 'beach-states' (see Appendix A [i]). The end members of the sequence are the dissipative and reflective morphologies of the bar/berm

model. The four intermediate configurations have morphologies which vary in the longshore direction. Distinctive 'process-signatures' are associated with each beach-state. The morphology changes sequentially through these states in response to varying environmental conditions with the most frequently occurring configuration being referred to as the 'modal beach-state'. Geomorphological investigations on different coasts have identified variants of Wright and Short's model (e.g. Nummedal et al., 1984; Shaw ,1985; Marra, 1991; and Short, 1992). Sonnenfeld and Nummedal (1987) speculated that there is a single global nearshore bar sequence and each surf zone displays incomplete portions of the sequence in accordance with its own combination of wave and tide conditions.

The beach-state approach has been applied to multi-bar coasts by researchers such as Hom-ma and Sonu (1962), Goldsmith et al. (1982), Aagaard (1990), Short (1992), and Short and Aagaard (1993). The most comprehensive of these models (Short and Aagaard, 1993) is summarised in Appendix A(ii). While such beach-state modelling identified certain configurations and sequences, the task has been thwarted by the greater morphological complexity and spatial extent of surf zones with multiple sand-bars. The data-sets usually consisted of aerial photographs or relatively small areas of bathymetric map. In either case there were temporal limitations because of low sampling rates or the short time-spans of research projects. However, in a few instances temporally extensive data have been collected and new morphological phenomena identified. Of particular interest is an offshore migration trend which underlies sand-bar behaviour and this will now be discussed.

The recognition of *net offshore bar migration* (henceforth referred to as *NOM*) was made independently by different researchers. In mid-1991, when the present study was being planned, NOM had been observed and documented for sites on the North Carolina coast (USA) by Birkemeier (1984), on the Coast of Holland in The Netherlands by De Vroeg et al. (1988) and at the Wanganui Rivermouth on the west coast of the New Zealand North Island by Shand (1990). These locations are shown in Figure 1.1 and plots of the associated bar-crest time-series are depicted in Figure 1.2. Papers have subsequently been published which provide greater detail of NOM in these areas. These results will be considered in later chapters together with those from Terschelling Island (Figure 1.1B) where NOM has also recently been documented by Ruessink and Kroon (1994) and Ruessink (1998). The locations in The Netherlands, North Carolina and New Zealand where NOM has been identified will henceforth be referred to as the *global NOM sites.*

The bar-crest histories depicted in Figure 1.2 show that the bars are generated near the shoreline, systematically migrate seaward and finally

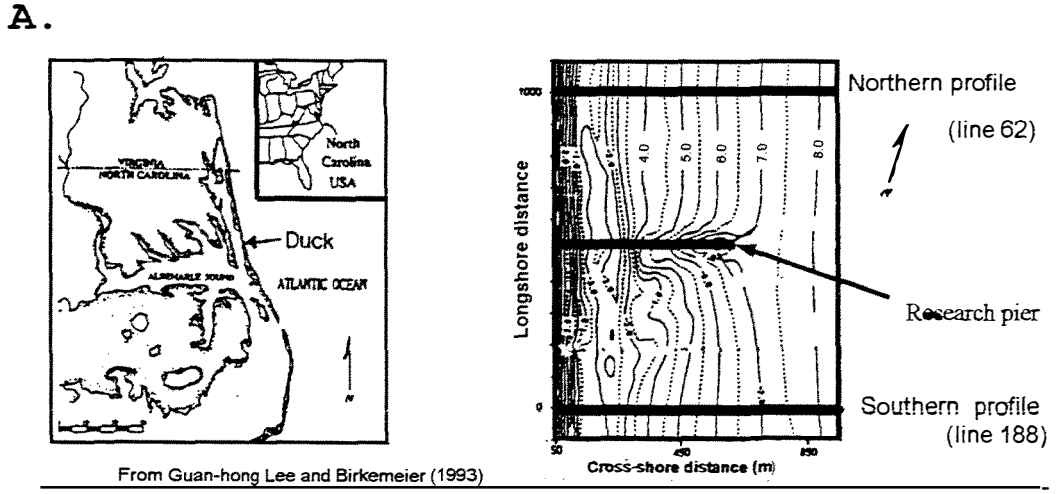

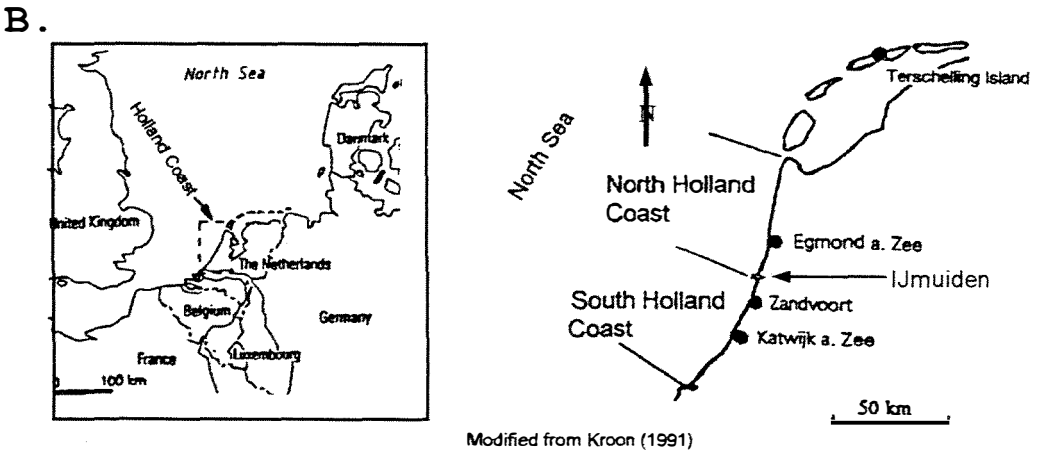

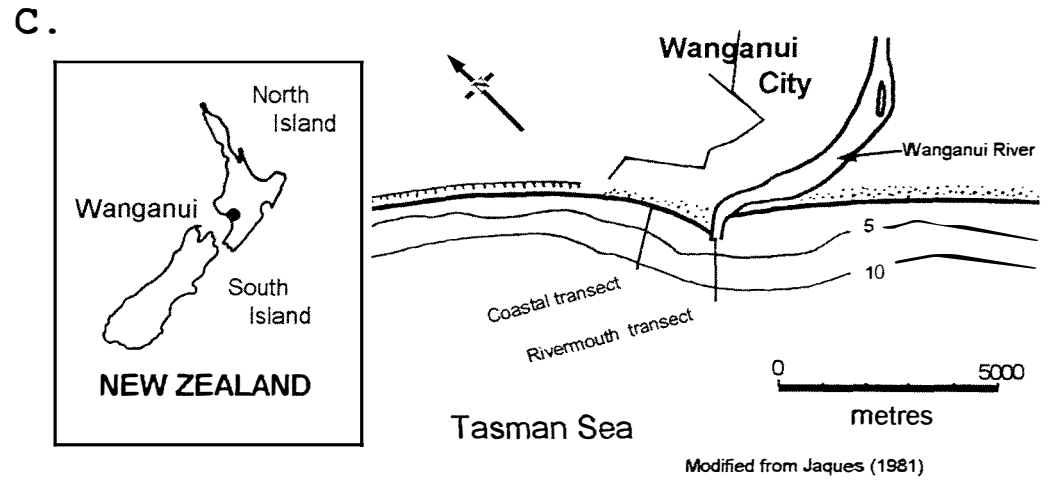

Figure 1.1 Location maps for sites where net offshore bar migration had been observed by mid 1991 - the time when this research project was being planned. These locations were at Duck, North Carolina (Figure A), the Northern and Southern Coast of Holland in The Netherands (Figure B) and at Wanganui, New Zealand (Figure C). Contour depths are in metres below MSL in Figures A and B but relate to chart datum (which is approximately 1.8 m below MSL) in Figure C.

A. North Holland coast South Holland coast

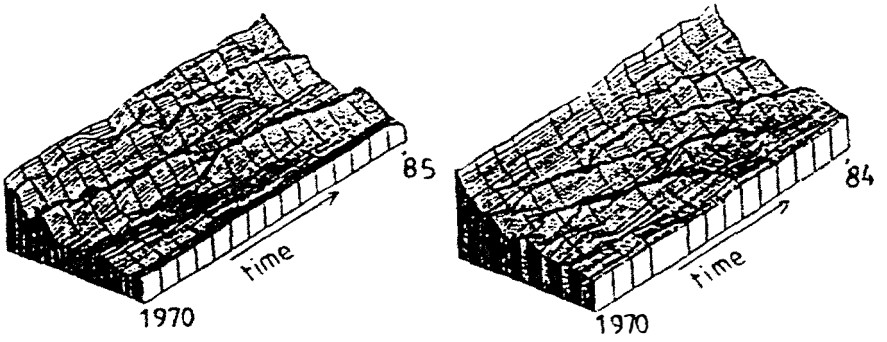

Modified from De Vroeg et al. (1988)

B. Duck

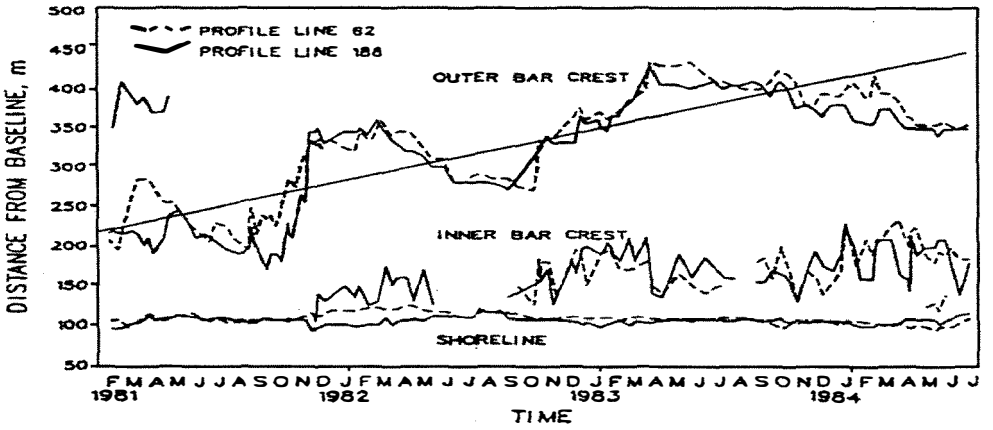

Modified from Birkemeier (1984)

C. Wanganui

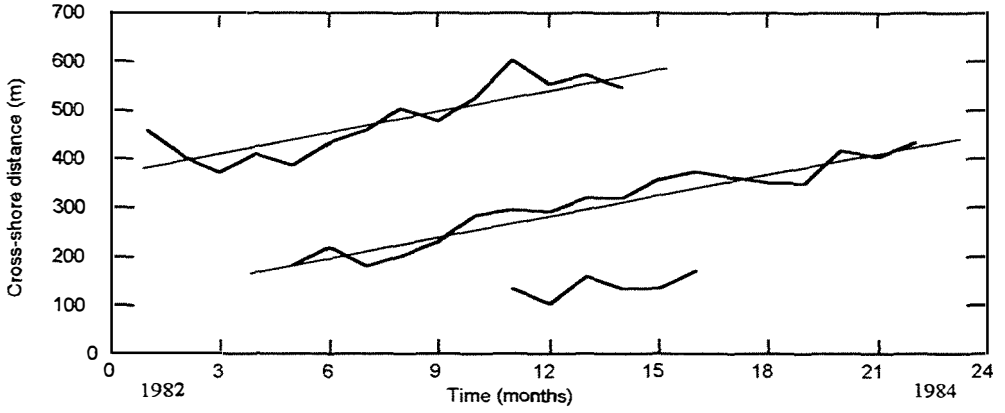

Modified from Shand (1990)

Figure 1.2 Published data depicting net offshore bar migration (NOM); these data were available when this research project was being designed in mid-1991. Data from the Northern and Southern Coast of Holland are shown in Figure A, data from Duck, North Carolina is shown in Figure B and data from the Wanganui Rivermouth (August 1982 to May 1984) is shown in Figure C. These locations are depicted in Figure 1.1. The diagonal trend lines in Figures B and C define NOMs.

disappear many hundreds of metres offshore. The diagonal trend lines overlain on the two-dimensional plots (Figures 1.2B and C) more clearly define the NOMs. Each sand-bar can therefore be viewed as having a 'life-cycle'. Furthermore, the successive occurrences of these seaward migrating sand-bars demonstrate a repetitive or 'cyclic' type of morphological behaviour. Such net offshore bar migration is the subject of this research project.

NOM has significant implications for coastal geomorphology. For example, NOM cannot be accommodated within the existing conceptual surf zone models depicted in Appendix A as these require, or infer, sand-bars to form at the approximate location where they are observed, while under a NOM regime they form near the shoreline. Furthermore, over the longer-term the present models indicate sand-bars attaining some average (modal) cross-shore location, while under NOM the bars systematically migrate in a seaward direction. Before this problem can be resolved, i.e. reconciliation of NOM with current geomorphological surf zone models, a more detailed understanding of the characteristics and controlling mechanisms for this intriguing and sparsely reported type of bar behaviour will be required.

NOM behaviour may also be relevant to other coastal workers. For instance:

- Coastal engineers may need to incorporate the influence of NOM into the design of surf zone structures and sediment renourishment projects.
- Planners need to consider whether NOM influences shoreline behaviour as this may be of relevance when establishing 'set-back' lines.
- NOM may be associated with cycles of rip-channel development which could be of relevance to surf-lifesavers when assessing/predicting bather risk.

The AIM of the present study is **to elaborate on the behaviour and causative processes of NOM by acquiring and analysing a temporally and spatially comprehensive set of field data from Wanganui, and also by comparing these results with those from the other sites where NOM is evident.**

1.2 Background to this project

The design of the present research project utilised the available published NOM results from Duck, the Coast of Holland and Wanganui (Figure 1.2), together with the following additional data for Wanganui. Between October 1990 and July 1991, morphological data had been collected by the author for a Port Development Study (see Patterson, 1991 and 1992). The most comprehensive bar-crest record obtained during this monitoring exercise

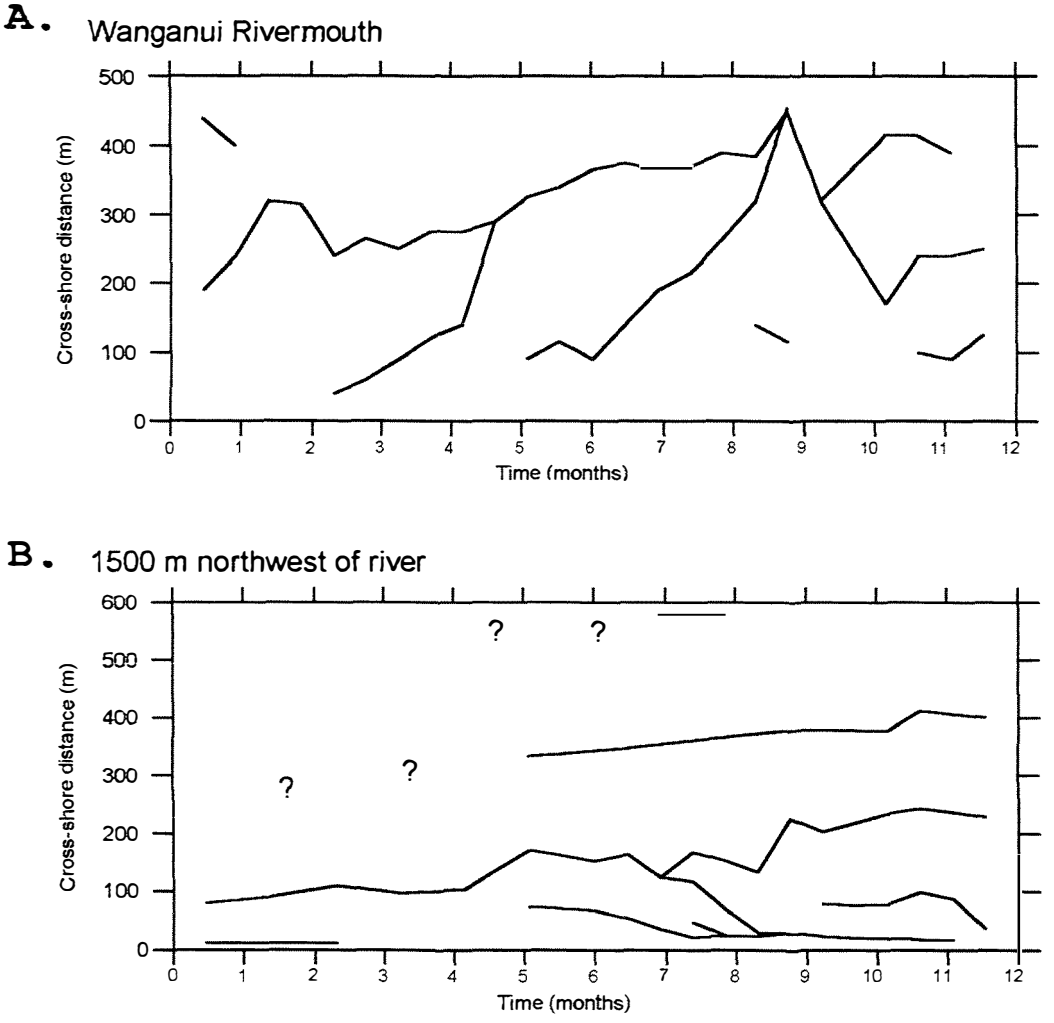

Figure 1.3 Wanganui bar-crest time-series depicting net offshore migration at the river-mouth for the period 27.7.90 to 11.7.91 (Figure A) and also at a site 1500 m northwest of the rivermouth for the period 24.7.90 to 11.7.91 (Figure B). The location of these sites is shown in Figure 1C.

was for a cross-shore transect located 1.5 km northwest of the rivermouth. These data, together with the contemporaneously sampled rivermouth bar-crest data, are shown in Figure 1.3. The rivermouth data were obtained from the bathymetric maps regularly produced by the Wanganui Port Company for navigation purposes. Although both the rivermouth and coastal records shown in Figure 1.3 were relatively short, an underlying NOM signal was evident. This result confirmed that NOM occurred at the rivermouth and indicated that it also occurred on the adjacent coast. It therefore appeared that a detailed study of NOM could be undertaken using morphological data from Wanganui.

It was found that there was considerable variation between the average cyclic NOM characteristics in the data from The Holland coast, North

Table 1.1 Average durations and rates of net offshore bar migration (NOM) at sites in The Netherlands, North Carolina and New Zealand (see Figure 1.1) using the data available in mid 1991 (see Figures 1.2 and 1.3).

Location	Average NOM duration (yr)	Average NOM rate (m/yr)
North Holland	20	15 - 20
South Holland	6 - 8	50
Duck, North Carolina	4	69
Wanganui Rivermouth	2	200
Wanganui coast	4	125

Carolina and Wanganui. Table 1.1 lists the average duration and the average rate of offshore bar migration for each of these global sites. The Wanganui Rivermouth result was obtained by averaging the earlier data reported by Shand (1990) with data from the 1990/91 Port Investigation Study. The averaged NOM duration ranged from 20 years for the North Holland coast to two years at the Wanganui Rivermouth. The average rates of offshore migration varied from ~15 m/yr (where ~ means approximately) on the North Holland coast to ~200 m/yr at the Wanganui Rivermouth. A negative correlation was apparent between duration and rate. Furthermore, there was a significant variation between the corresponding parameter values at the two Wanganui sites. These inter-site variations in longer-term (or average cyclic) characteristics of NOM, together with their associations with corresponding physical boundary conditions and energy regimes, provided a means of investigating NOM.

Differences in bar migration characteristics were observed within the bar-crest data from adjacent profiles at both Duck and Wanganui. The profile transects at Duck were separated by 1000 m (Figure 1.1A). While bar behaviour on the Duck profiles was often spatially synchronised, there were occasions when significant differences in the magnitudes of contemporaneous bar migrations occurred (see Figure 1.2B). There were also occasions when contemporaneous cross-shore bar migrations were in opposite directions. At Wanganui, bar formation and disappearance did not appear to coincide between the two monitoring sites (Figure 1.3) which were separated by 1500 m (Figure 1.1C). Bar 'merging' occurred at the rivermouth site and bar 'splitting' was evident at both sites, although the latter events were non-synchronous. This range of differing 'within-cycle' bar behaviour at adjacent monitoring sites indicate that antecedent morphology could control aspects of NOM. The apparent influence of local morphology upon NOM was also suggested by process-response relationships observed at Duck by Birkemeier (1984) who noted that while significant seaward migration events always occurred during

storm conditions, there were occasions when higher energy conditions did not induce such a morphological response. The study of variation in shorter-term (within-cycle or subcyclic) morphological behaviour between adjacent sites appears to offer an additional line of enquiry into NOM.

1.3 Approach

1.3.1 Conceptual framework

Systems

A systems-orientated approach is the usual framework used in geomorphological investigations (Phillips, 1992). A system is a structured set of objects and/or attributes which exhibit relationships with one another and operate as a complex whole (Chorley and Kennedy, 1971). Detailed consideration of systems characteristics and properties can be found, for example, in Chorley Schumm and Sugden (1984), Huggett (1985), and Phillips (1992). Aspects of systems theory used in the research design for this study will now be discussed.

A simple coastal system is represented diagrammatically in Figure 1.4. The inputs refer to independent variables, mainly energy, but to a lesser

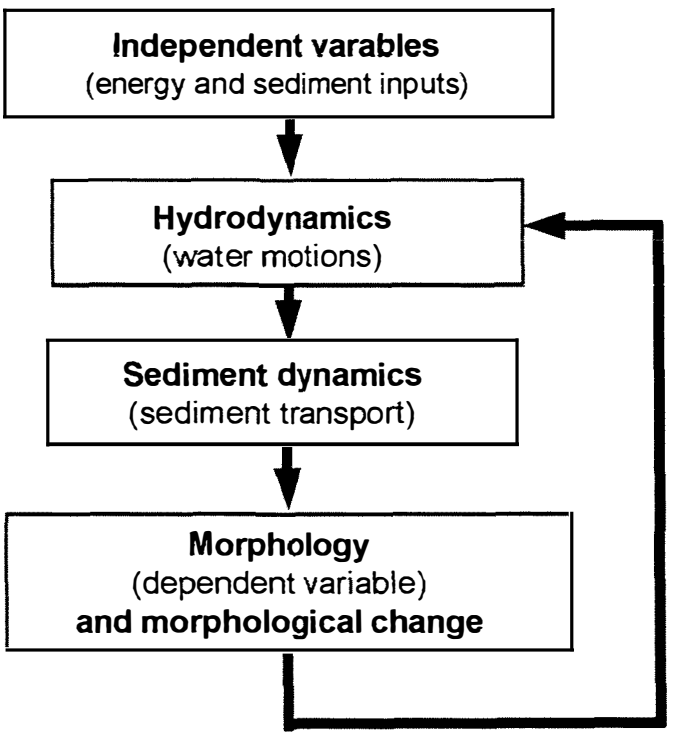

Figure 1.4 A schematic representation of a coastal morphodynamic system.

Modified from Hardisty (1990) and Wijnberg (1995)

degree water and sediment. Such a coastal system therefore functions as an open system. The system inputs, such as waves and currents, influence local water motion which then induces sediment transport. Over time, any net sediment transport will result in a change in the morphology. This adjusted morphology subsequently influences the hydrodynamics which further modify the sediment transport processes which further change the morphology and so on. Coupling and feedback mechanisms are therefore fundamental aspects of coastal systems. These mutual adaptations of the hydrodynamics, the sediment transport processes, the morphology and the background environmental conditions are termed 'morphodynamics' and the associated coastal system referred to as a *morphodynamic system* (Wright and Thom, 1977). The present study attempts to identify morphodynamic aspects of the NOM system.

Scale

A coastal geomorphological system can be viewed as a hierarchy of morphodynamic subsystems or compartments, each with its own temporal and spatial dimensions (De Boer, 1992). Lower order subsystems are influenced by inputs of lower magnitude and shorter duration than for the higher order systems. In addition, the morphological responses of lower order subsystems occur over a shorter time interval than for corresponding higher order systems. Similarly, the spatial dimensions for lower order subsystems are smaller than for higher order systems. These system properties indicate that a relationship exists between temporal and spatial dimensions (or scales) and this is considered further in the following paragraph.

In geomorphological systems a direct coupling is assumed to exist between temporal and spatial scales in which the time scale increases with the spatial scale (De Vriend, 1991; Phillips, 1992). Such apparent time/space coupling results in the notion of 'the' scale of coastal landform behaviour (De Vriend 1991). An example of the time/space relationship in terms of generally accepted size categories for coastal systems, is depicted in Figure 1.5. The spatial scale is often defined by the longshore length scale which is usually larger than the corresponding cross-shore length scale. The broadness of the space and time categories in Figure 1.5 reflects the gradual transition between scales and the site-specific nature of the scaling components (Terwindt and Kroon, 1993). Figure 1.5 depicts the coastal scale relationships for both morphological features (in bold) and the associated driving processes. Sand-bars within the NOM system fit the macro-scale category.

Coastal systems are characterised by changes simultaneously occurring at a range of scales; this is schematically illustrated in Figure 1.6. Terwindt and Wijnberg (1991) note that in a geomorphological system the smaller-scale processes are the most predominant, producing quick alterations to the

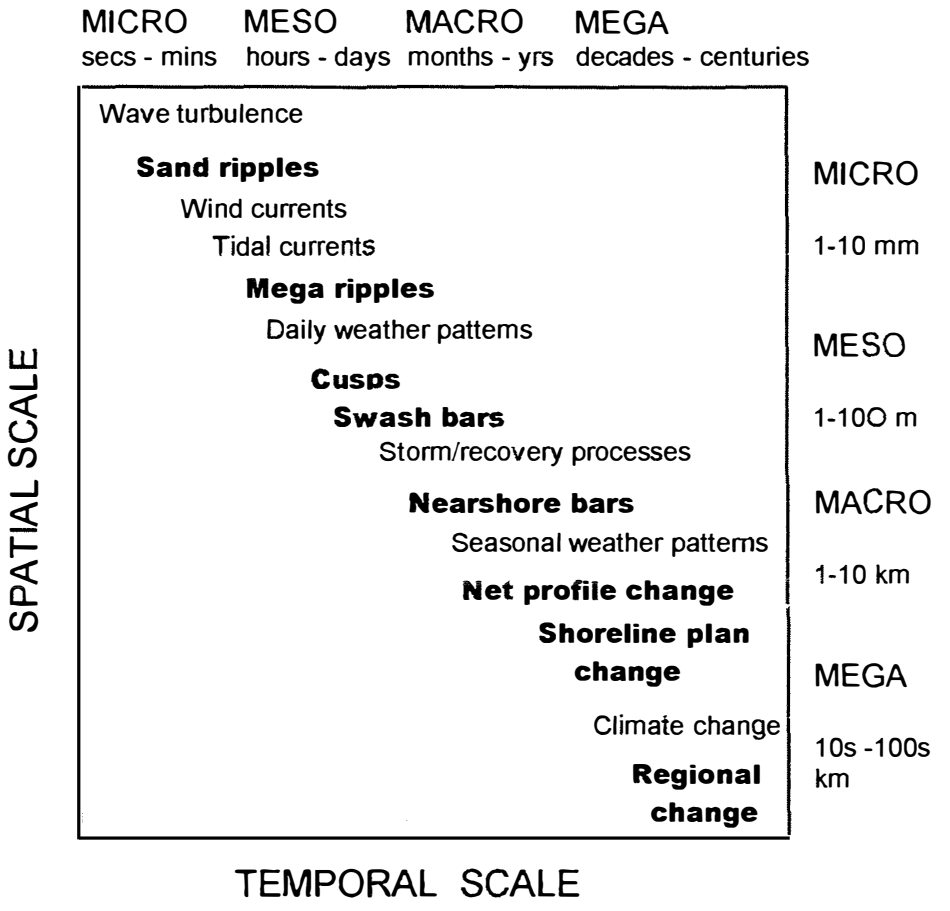

Figure 1.5 Space and time scales for coastal morphologies (bold) and associated processes. For the morphology, the temporal scale refers to the time the landform unit undergoes change (reaction plus relaxation time), while the spatial scale refers to the size of the unit. For the processes, the temporal scale refers to the duration of hydro-dynamic forcing, while the spatial scale refers to the net distance (area) over which sediment movement occurs.

Modified from Horikawa (1988), Larsen and Kraus (1993) and Kroon (1994).

morphology that reflect gross sediment fluxes, while at a larger-scale the more energetic processes are smoothed out and the net effect is apparent. This latter effect is depicted by the trend line in Figure 1.6. Both periodic and episodic changes in the energy and sediment inputs can produce responses in the morphology. Lakhan and Trenhaile (1989) note that it is important that coastal systems are studied for sufficiently long time periods to enable 'atypical' fluctuations to become evident and the intrinsic form and behaviour to be identified. In the present study, bar-crest time-series are used that contain enough data points to define both multiple life-cycles of NOM and also cross-shore fluctuations within the individual NOM cycles.

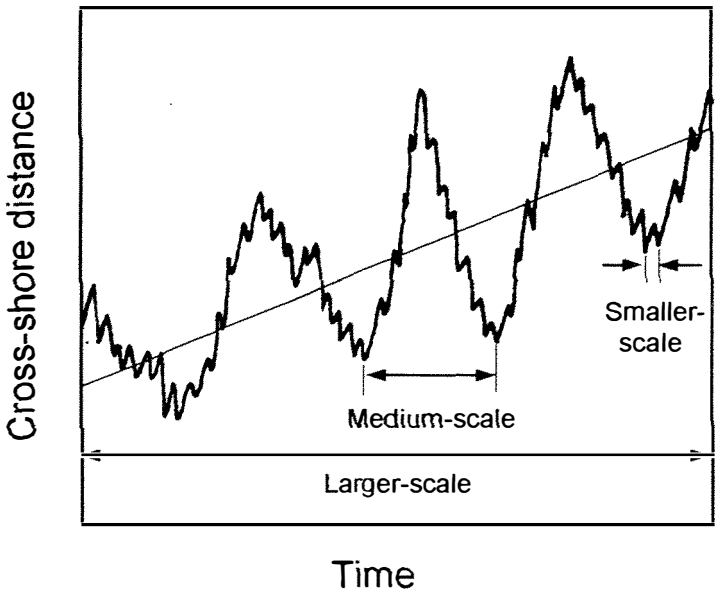

Figure 1.6 Schematic representation of morphological changes at a range of temporal scales. The straight (trend) line depicts the net long-term change and illustrates how smaller-scale changes are smoothed out over time.

Modified from Terwindt and Wijnberg (1991)

The study of larger coastal systems has been approached by either investigating the system at the 'scale-of-interest', or 'up-scaling' knowledge gained by studying subsystems (Wijnberg, 1995). Because larger systems inhibit conventional techniques of data-acquisition and analysis, subsystem decoupling followed by subsequent analysis and integration is commonly used (Jamshidi, 1983). However, the validity of this approach has been questioned. 'Holists' argue that the system must be studied as an indivisible whole due to synergistic and global qualities which cannot be possessed by its constituent parts (Blauberg et al., 1980; Capra, 1994). In contrast, 'reductionists' consider it is acceptable to trace complex phenomena or processes to their smallest parts, analyse them, and then by integration determine the dynamics of the whole system (Bunge, 1977; Lilienfeld, 1978). Because of the intrinsic non-linearity of coastal systems (see De Vriend, 1991; Carter et al., 1993; Holman and Sallenger, 1993), it would, if possible, seem prudent to avoid reductionist or upscaling approaches during the early stage of investigation into a new phenomenon. The present study therefore sets out to investigate NOM using the scale-of-interest approach.

Equilibrium

The concept of system equilibrium is fundamental to the study of geomorphological systems. Phillips (1992) considered that in geomorphology, equilibrium is generally taken to imply that a given set of processes and/or

environmental controls will produce (or result in a tendency toward) a particular landscape response. However, the increased recognition of hierarchies, thresholds and non-linearities in geomorphology has shifted the focus from a single stable equilibrium. Emphasis is now being placed on behaviour of geomorphological systems away from equilibrium; in particular, the presence and prevalence of non-equilibrium and disequilibrium in the landscape, and the occurrence of multiple equilibria - many of which are unstable (Phillips, 1992). The relevance of these systems concepts for the present study of NOM will be assessed in the latter chapters of this thesis.

Models

A common way to gain insights into the structure and functioning of complex systems is by developing models. These are abstract limitations or approximations which simplify reality (Lakhan and Trenhaile, 1989). A variety of model types have been used when investigating systems and the following summary is synthesised from Fox (1985), Lakhan and Trenhaile (1989), and Hardisty (1990).

- Deterministic (theoretical) mathematical models are based on classical physics; in particular, the principles of fluid mechanics. In such models the new state or output of the system is completely determined by the previous state and by the governing equations.

- Empirical mathematical models can be derived using physical modelling with wave-tanks where variables can be altered one by one. This is often combined with deterministic models to initially identify the equation parameters.

- Empirical statistical models result from the statistical analysis of field data. Applying a pseudo-random generator to a statistical model to move it forward through time leads to a probabilistic model.

- Computer simulation or numerical models are another form of physical modelling. Here both probabilistic and deterministic parts are used in computer subroutines.

- Conceptual models describe basic patterns or relationships evident in observed data with statistical techniques frequently being used to infer the associations. Conceptual models are often used to identify relationships that can subsequently be tested using more rigorous empirical and deterministic modelling approaches.

The present study will analyse bar-crest field data to develop a conceptual model for NOM.

1.3.2 Data collection issues

Sampling resolution

Both the temporal and spatial sampling resolution required for the NOM field data is guided by the scale relationships described earlier. Surf zone bars, the morphological feature with which this study is primarily concerned, are classified in Figure 1.5 as being macro-scaled features. These bars have a length (longshore) scale between 10^2 and 10^3 m. To identify features within these forms the longshore resolution of the morphological sampling should be at the lower limit, i.e. about 100 metres. Cross-shore sampling resolution to detect bar-crests would be ~10 m. Macro-scaled bar features in Figure 1.5 are subject to temporal changes over periods of weeks and months which suggests that morphological sampling for studying NOM should be carried out at two to four weekly intervals. As the hydrodynamic processes associated with change in nearshore bar morphology appear to relate to storm/fair-weather periods, a sampling regime capable of providing at least daily process values was used in the present study.

Temporal and spatial scales

The time-period over which data collection should occur is determined by the time-scale of the NOM phenomenon. The Wanganui data in Figures 1.2C and 1.3 depicted partial NOM cycles which, by extrapolation, suggested an overall duration of two to four years. The data-sets shown in Figure 1.2 indicate that behavioural regularity is a general property of NOM. To eliminate noise created by smaller-scale processes, or other atypical behaviour, a data-set twice as long as the maximum likely duration was considered desirable, i.e. eight years. The other global NOM data-sets were of a satisfactory length given the time scales indicated in Table 1.1.

The project was designed such that two to three years of Wanganui coastal data would be collected and this would be supplemented by the Port Company's archival rivermouth data to cover the required time-span. It was accepted that the spatially restricted nature of the rivermouth data, together with NOM interpretational complications and the lack of earlier process data, would compromise the overall effectiveness of the study. However, unforeseen circumstances[1] enabled coastal design data to be collected for a period of 6.3 years. This was found to provide a data-set of suitable length to identify NOM characteristics and meet the study objectives without having to incorporate rivermouth data.

---

1. The author experienced prolonged health problems during the study; this significantly delayed completion of the project.

The spatial extent of the area selected for study at Wanganui was influenced by the longshore physical characteristics of the northwestern coast. The jetty-controlled Wanganui Rivermouth is located upon an ebb tide delta which can be delineated by the 10 m contour in Figure 1.1C. The cross-shore width of the delta decreases from ~1500 m at the rivermouth to ~1000 m some 4000 m northwest of the rivermouth. Westward of this location the bathymetric contours remain approximately shore-parallel. This indicates that the jetties and ebb delta influence surf zone morphodynamics along the northwestern coast for a distance of ~4000 m. It was considered useful to include both delta and unmodified stretches of coast within the present study because of possible differences in NOM characteristics. The longshore length scale was therefore defined as extending approximately six kilometres to the northwest of the rivermouth.

The cross-shore width of the Wanganui study site was based on an echo-sounding survey carried out as part of the 1991 Port Development Study (section 1.2). The resulting profiles are shown in Figure 1.7. The seawardmost sand-bar was on the northwestern profile located ~5000 m from the rivermouth. The crest of this bar was ~650 m from the foredune toe. As this bar had a subdued form it was assumed its location was indicative of the likely seaward limit of bar migration. The cross-shore length scale of the study site was therefore defined as extending at least 700 m seaward of the dune toe.

New data acquisition techniques

To obtain Wanganui bar-crest location data at the specifications described above, new methods of data acquisition were developed. Morphological surveys are usually executed by sampling the sea-bed elevation at regularly spaced intervals along predetermined shore-normal transects. In the present study such methods, e.g. echo-sounding, will be referred to as 'ground profiling'. These techniques are relatively expensive, labour intensive, time-consuming, and require uncharacteristically calm atmospheric and sea conditions for the Wanganui coast. While ground profiling was clearly an inappropriate means of collecting data for the present study of NOM, this technique was used to provide data for other tasks relevant to the study such as determining physical boundary characteristics, e.g. time-averaged cross-shore slope. The method developed to obtain morphological data for NOM analysis was based on photographing the sea surface and using light intensity variation caused by broken waves to signal the relative elevation of the sea-bed. Digital image processing algorithms were written to capture and analyse these signals. This method was an extension of earlier work by Holman and Lippmann (1987) and Lippmann and Holman (1989). Obtaining bar-crest location data along cross-shore transects using image-based techniques will be referred to as 'intensity profiling'.

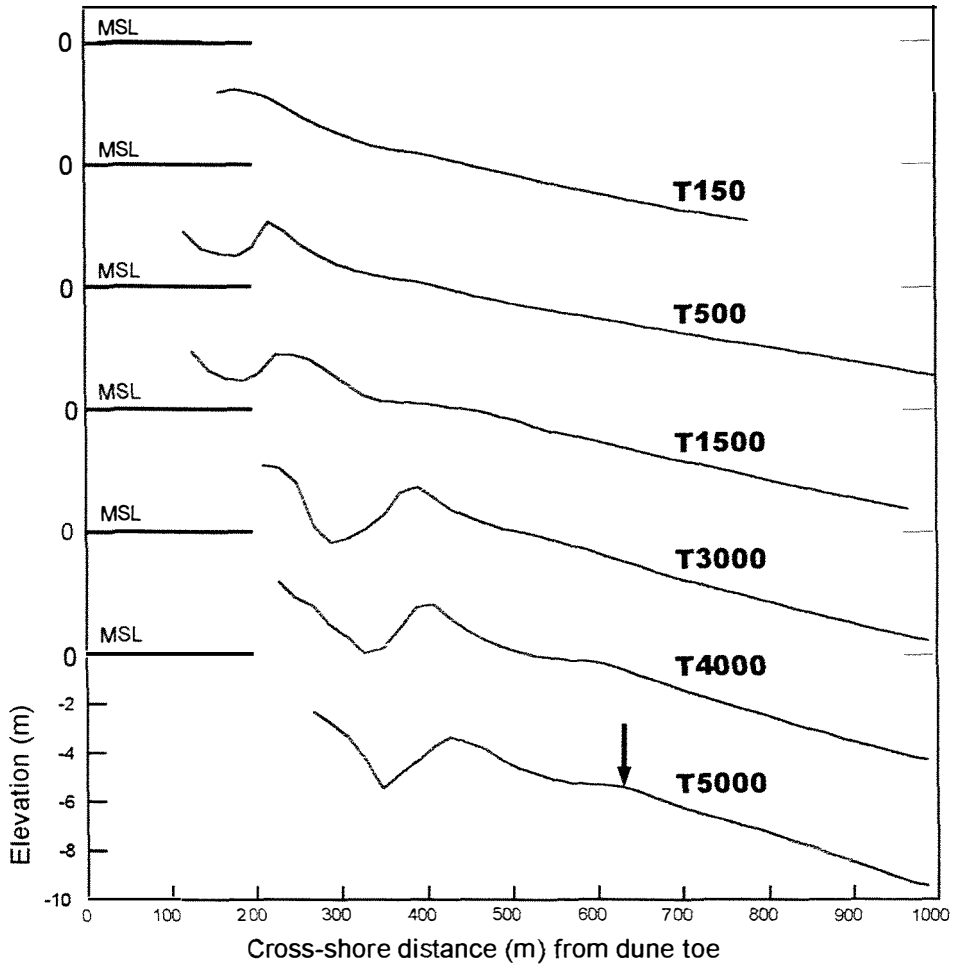

Figure 1.7

Cross-shore profiles at transects located 150 m (marked T150), 500 m, 1500 m, 3000 m, 4000 m and 5000 m to the northwest of the Wanganui Rivermouth. The arrow locates the seawardmost bar-crest. The survey was carried out using echo-sounding on 11.7.91.

1.4 Objectives and thesis outline

The considerations detailed above enabled the following general research objectives to be identified as a means of achieving the study aim:

- Development of photogrammetric methods of data acquisition and analysis;
- Determination of longer-term (average cyclic) characteristics of NOM behaviour based on the analysis of multiple cycles;
- Determination of shorter term (within-cycle or subcycle) characteristics of NOM behaviour, with emphasis on longshore non-synchronous variation;

- Comparison of the Wanganui results with those from other NOM sites;
- Identification of the environmental conditions associated with NOM characteristics;
- Development of a conceptual morphodynamic model to explain the observed NOM behaviour at Wanganui and the other global NOM sites.

These objectives will be addressed within the following chapters. Characteristics of the Wanganui study site are described in chapter 2. This includes the regional and local morphology and its evolution, the sediment characteristics and the energy regime. Chapter 3 describes the image-based and ground profiling methods developed to acquire morphological data capable of meeting the research design specifications. Chapter 4 consists of an evaluation of data acquired by these methods; this includes errors and the adjustments required to enable fusion of data obtained using the different methods. Longer-term characteristics of NOM at Wanganui and from the other global NOM sites are investigated in chapter 5. Shorter-term morphological behaviours which may influence individual cycles of NOM are identified in chapter 6. Relationships between NOM characteristics and environmental conditions, together with contributions to conceptual modelling of NOM, will be included in chapters 5 and 6. Chapter 7 summarises the findings for the specific research objectives and questions (for each chapter), and provides conclusions regarding the general research objectives (listed above). Of particular note is a general conceptual morphodynamic model of NOM applicable to all the global sites. Possible directions for future research into NOM are also included in the final chapter.

At the time this thesis was submitted, the following parts had been published: The method of automated swash-front tracking referenced in chapters 2 and 7 was described in Bailey and Shand (1994). The image-based data-acquisition techniques (chapter 3) were described in Bailey and Shand (1993, 1996, 1997). Comparison between the different methods of acquiring bar-crest data (chapter 4) were summarised in Bailey and Shand (1997). The NOM review materials included in chapters 1, 5 and 6 appeared in Shand and Bailey (1999). Comparison of NOM characteristics and environmental conditions at the global sites (chapter 5), together with the methods used to characterise NOM behaviour, appeared in Shand et al. (1999). The image sequences depicting bar bifurcation (Figure 6.1A) and bar switching (Figure 6.1B), along with the associated descriptions of these types of morphological behaviour, previously appeared in Shand and Bailey (1999).

CHAPTER 2 THE FIELD SITE

The Walrus and the Carpenter
were walking hand in hand.
They wept like anything to see
such quantities of sand.
"If only this were swept away",
they said, "wouldn't it be be grand".

"If seven maids and seven mops
swept it for half a year,
Do you suppose", the Walrus said,
"that they could keep it clear?"
"I doubt it", said the Carpenter,
and shed a bitter tear.

"I'm not so sure", the Walrus said,
"I've got a little scheme;
In place of seven maids and mops,
we'll concentrate the stream,
And then the sand will surely go
much further than you dream".

Wanganui Chronicle, 19 June 1923

2.1 Introduction

This chapter describes the study area and its environmental setting. The chapter begins (section 2.2) with a description of the regional and local geomorphology, including the coastal evolution. It is important to define longer-term morphological change as this may be causing NOM to occur or be influencing NOM characteristics. The morphological adjustment along the northwest coast during and subsequent to the construction of the rivermouth jetties, had a significant effect on the study area; the above quotation alludes to this situation. A somewhat detailed summary of this historical coastal change is therefore included so as to ascertain whether morphological adjustment may still be occurring. Section 2.3 considers the morphology within the study area and defines the associated terminology used in the thesis. Parameter values for morphological zones are derived for use in chapter 4 which evaluates the morphological methods, and also

for use in chapter 5 which compares different NOM sites. Sediment characteristics are considered in section 2.4. Sediment size is used when comparing global NOM sites in chapter 5. Sediment texture and mineralogical data are also included as these indicate sediment transport paths in and near the study area. Process conditions associated with wind and waves are described in section 2.5. These data and the associated parameter values are used in data processing (chapter 3), evaluating morphological data (chapters 4), during the analysis of NOM environments (chapter 5) and during the identification of NOM-associated morphodynamics (chapters 5 and 6). A description of the morphology in the vicinity of the rivermouth, together with the associated sediment and process characteristics, will be detailed within relevant sections.

2.2 Geomorphological setting

2.2.1 General background

The study area is situated along the northern margin of Cook Strait's western embayment (Figures 2.1A and B). The embayment is exposed to the Tasman Sea to the west and to the Pacific Ocean via Cook Strait to the south (Figure 2.2). The Wanganui-Taranaki shelf forms the floor of the embayment which generally has depths less than 125 m.

The Wanganui area lies within an extensive sedimentary basin - the Wanganui Basin (Figure 2.2). This geological structure is aligned northeast to southwest and is approximately 400 km long by 200 km wide. Four thousand metres of Plio-Pleistocene marine sediment have been deposited within this basin (Stern and Davey, 1989). These deposits consist of sequences of siltstone, shell beds and sandstone which represent late transgressive and highstand portions of Plio-Pleistocene sea-level cycles (Abbott and Carter, 1991).

The northern and eastern margins of the basin have been subject to uplift and along the northwest Wanganui coast the strata dip gently to the southeast at two to four degrees (Fleming, 1953; Naish and Kamp, 1995). The uplift rate along the contemporary coastline in the vicinity of the study area was estimated by Pillans (1983) to be ~0.25 to 0.3 mm per year with the rate increasing both inland and toward the west. Pillans (1983, p954) noted that 'a hingeline or zero isobath appeared to occur some distance offshore'. Continued sedimentation and subsidence occur further seaward. This is attributed by Stern and Davey (1989) to the subducting Pacific plate being locked with the Indo-Australian plate (see Figure 2.2). The possibility exists that such tectonics induce a landward sediment

A.

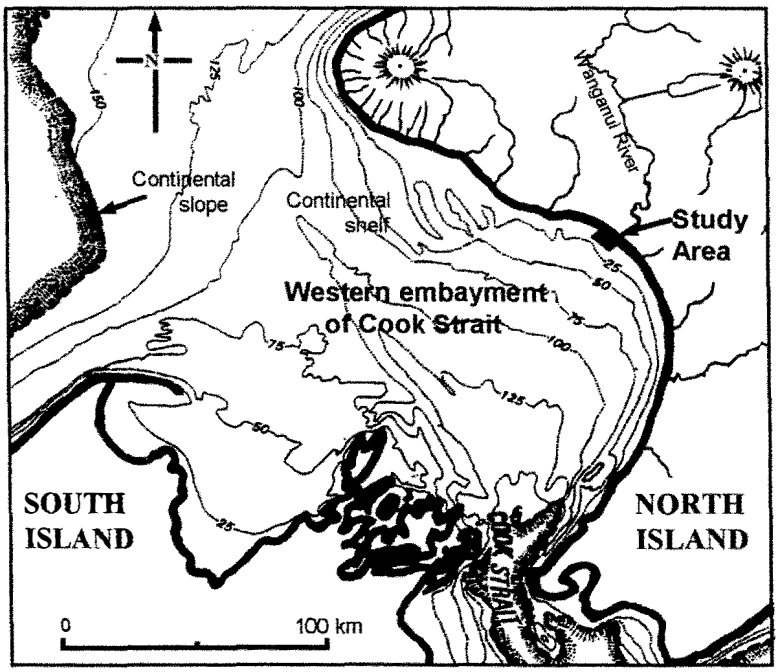

B.

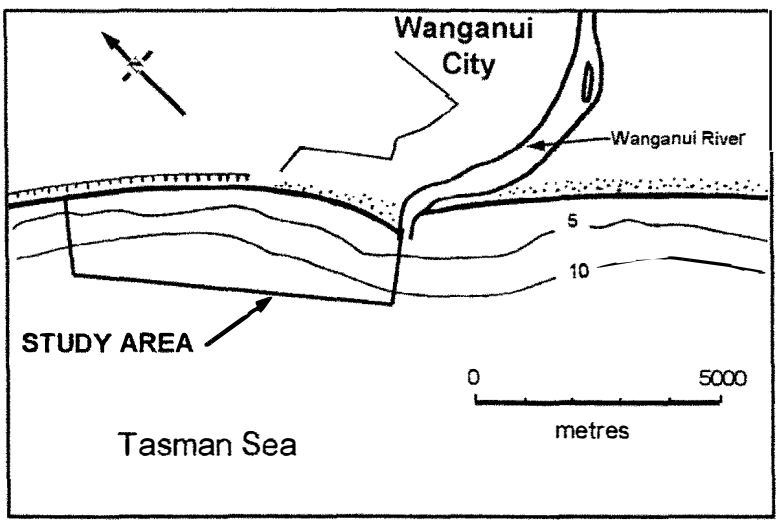

Figure 2.1 The regional setting of the study area is shown in Figure A and the local environmental setting is shown in Figure B. Depth contours are in metres below MSL in Figure A and metres below chart datum in Figure B (where chart datum is 1.8 m below MSL).

Sources: Figure A is modified from Lewis (1979)
Figure B is modified from Jaques (1981)

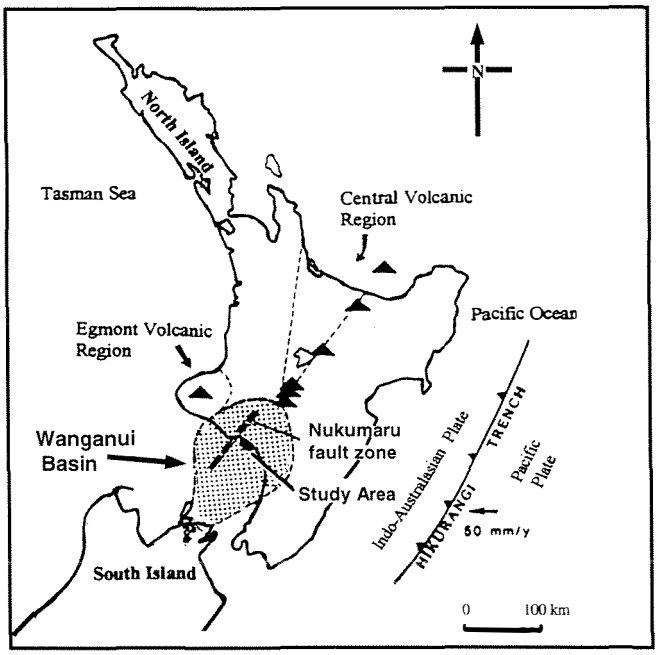

Figure 2.2 Structural geology affecting the study area.

Modified from Stern and Davey (1989)

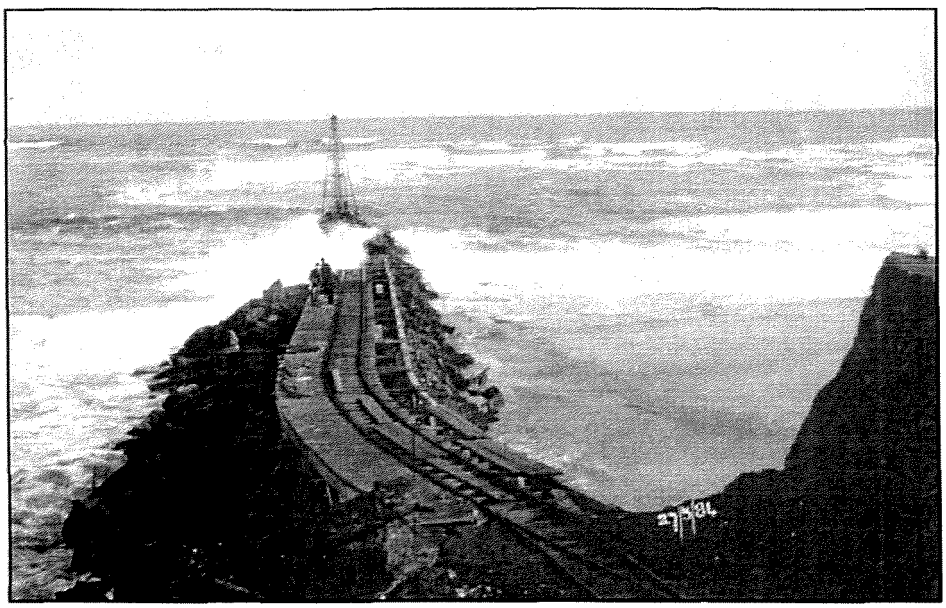

Figure 2.3 Construction of the northwestern jetty (the North Mole) at the Wanganui Rivermouth in 1884. The sea-cliff known as the North Head is evident on the right of the photograph.

Source: Wanganui Harbour Board archives

source-seaward sediment sink situation which may result in offshore sediment transport. West of the study area shoreline recession and an active sea-cliff are superimposed upon the uplifing coast. Such erosion is consistent with the landward sediment source concept. However, erosion along this coast is mainly attributed to longshore sediment transport and this situation is described later in the chapter.

A Holocene sea-cliff cut into Pleistocene sediment extends from the Wanganui River toward the northwest. Next to the river this cliff forms a siltstone bluff ~10 m high which was historically referred to as the 'North Head' (see Figure 2.3). The castle-like appearance of the North Head to approaching mariners resulted in the town that developed nearby being named Castlecliff (Burgess, 1971). For ~600 m to the northwest of the rivermouth the sea-cliff is obscured by dune sand which may have resulted from the coastal response to jetty construction (see Figure 2.3 and section 2.2.2). Further to the northwest the sea-cliff becomes increasingly better defined (Figures 2.4A and B) and reaches a height of ~45 m. Twelve ancient sea-cliffs have been identified on the uplifted marine surfaces further inland (Pillans 1983). To the west of the study area the toe of the sea-cliff is affected by wave action and historical data show that the cliff has recession rates of between 0.2 and 0.6 m per year (Johnston, 1985a).

As indicated above, the sea-cliff at Wanganui is relict for 6.2 km to the northwest of the rivermouth, i.e. for the approximate length of the study area. The cliff was cut off from the sea owing to shoreline progradation which occurred along this length of coast following jetty construction at the rivermouth. The accreted land seaward of the cliff is characterised by sand dunes (see Figures 2.4A and B).

Approximately 20 km northwest of the Wanganui Rivermouth uplift of more resistant beds of Pliocene limestone in the vicinity of the Nukumaru fault zone (Figure 2.2) has resulted in the development of a coastal salient which extends approximately two kilometres seaward. The foreland, together with its distinct bathymetric expression (Figure 2.1A), acts as a wave shadow for the coast toward the study area.

A platform cut into Pleistocene sediment by wave action extends seaward from the cliff-base. Fleming (1953) noted that a sand veneer at least one metre deep exists along the beach to the northwest of the study area, and the sand layer thickened to approximately 10 m near the rivermouth. The uplifted marine platforms further inland are also veneered by up to 12 m of marine sand with additional coverbeds comprising tephra, loess and dune

A.

B.

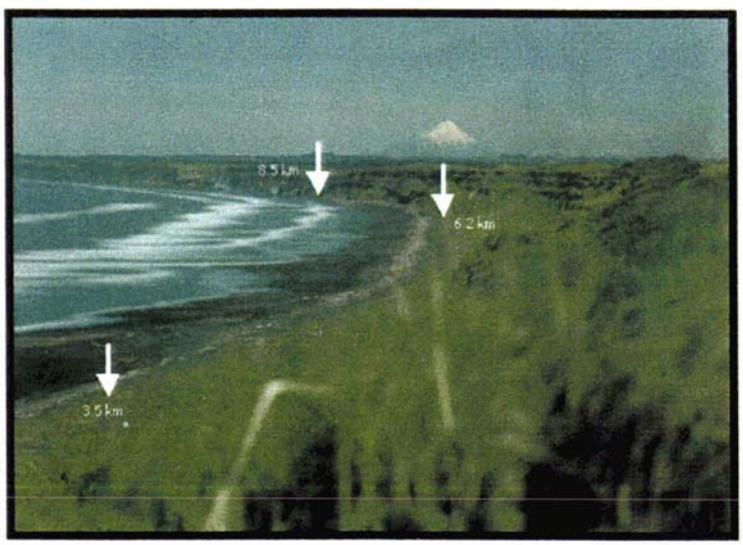

Figure 2.4

Aerial photograph (A) taken on (27.7.93) and terrestrial photograph (B) taken on 5.12.93 showing the study area and surrounding environment. Figure A illustrates the whole study area stretching from the Wanganui Rivermouth in the foreground to the location marked by the arrow in the distance (~6 km). The dashed line marks an ill defined sea-cliff. This cliff stretches westward for 25 km and is protected from the sea by a narrow coastal plain capped with sand dunes for the first 6.2 km. The asterisk in Figure A locates the camera site that was used for photographic data collection in the project. Figure B shows the relict sea-cliff and recently developed foredune in the northwestern section of the study area. Between 6.2 and 8 km colluvium, marine sand and driftwood are evident at the toe of the cliff; however, further to the west the cliff is directly exposed to wave action. The Nukumaru fault zone (see Figure 2.2) is located along the horizon and Mount Egmont - a major source of the sand for the study area, can be seen in the distance. Figure B was obtained using a time-lapse technique explained in chapter 3. The high intensity bands on this photo define multiple sand-bars.

sand (Pillans, 1983). Further offshore, the depth of sand mantling the wave cut Pleistocene formations is unknown.

The southeastern boundary of the study area is the Wanganui Rivermouth (Figure 2.1B) and a brief characterisation of the river is now given. The Wanganui River is 305 km long, has a catchment area of 7120 km^2, and its mountain headwaters in the central volcanic region attain a height of 2797 m (Tonkin and Taylor, 1978). For much of its length the river flows through well dissected Pliocene marine sediments (Fleming, 1953). At Wanganui, the mean flow of the river is 224 m^3/s and the annual sediment yield is 486 tonnes/km^2, ninety seven percent of which is estimated to be suspended load (Tonkin and Taylor, 1978). The tidal compartment (spring range) is 9.3 x 10^6 m^3 (Gibb et al., 1962). River hydrodynamics will be considered in greater detail in section 2.5.4, while the morphology and sediment characteristics in the vicinity of the rivermouth will be detailed in sections 2.3.3 and 2.4.3 respectively.

Ebb-tide delta

The contours in Figure 2.1B show that the ebb delta at the rivermouth has a southerly offset from the present entrance. The seaward extent of the delta reduces along the study area until the bathymetric contours become approximately shore-parallel beyond a location ~4000 m northwest of the rivermouth. To further define the cross-shore characteristics of the delta in the vicinity of the study area, transects located 200 m, 1500 m and 5000 m from the rivermouth were surveyed and the resulting profiles are shown in Figure 2.5. The methods used to acquire these data are described in chapter 3 (section 3.3). A distinct break in slope ~1900 m offshore in the profile closest to the rivermouth (T200 in Figure 2.5) appears to define the seaward extent of the delta. Longshore morphological gradients associated with the delta are expected to influence NOM; these morphological characteristics are described and quantified in section 2.3.1.

The plan shape of the delta (Figure 2.1B) suggests that wave energy is significant in controlling sediment transport in the vicinity of the rivermouth for the following reasons. The subdued form of the delta, i.e. its limited seaward extent, indicates the dominance of wave energy relative to river flow (see Wright and Colman, 1973), and also the dominance of wave energy relative to tidally induced flow near the entrance (see Davis and Hayes, 1984; Hayes, 1991). An offset in delta symmetry indicates wave-induced net longshore transport (littoral drift) of sediment in the direction of the offset (Wright, 1977; Wright et al., 1980).

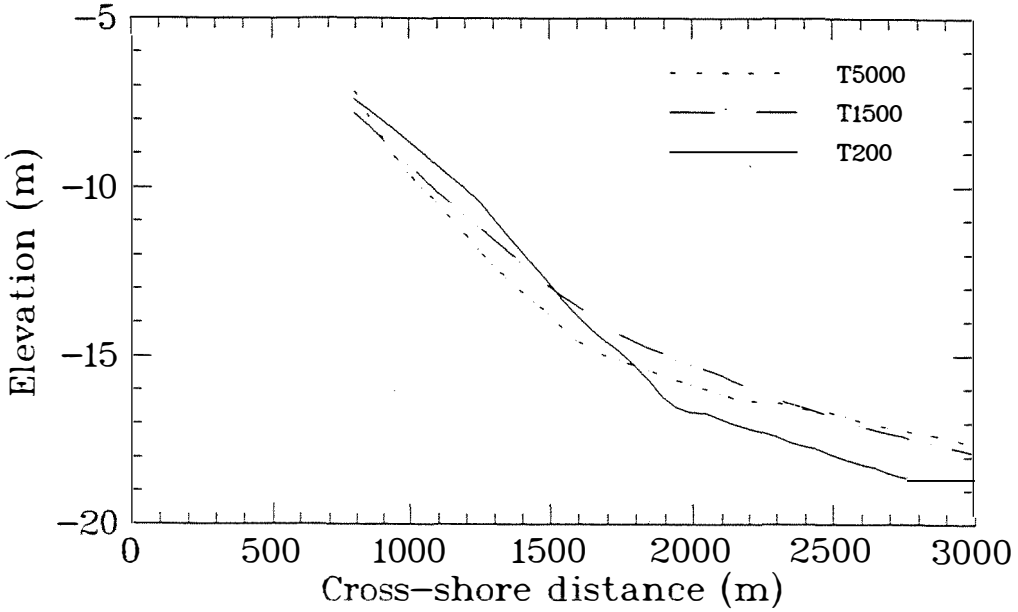

Figure 2.5 Offshore profiles for cross-shore transects located 200 m northwest of the rivermouth (T200), 1500 m northwest (T1500) and 5000 m to the northwest (T5000). Elevation refers to depth below MSL and cross-shore distances are measured from the dune toe. The survey was carried out on 1.9.92.

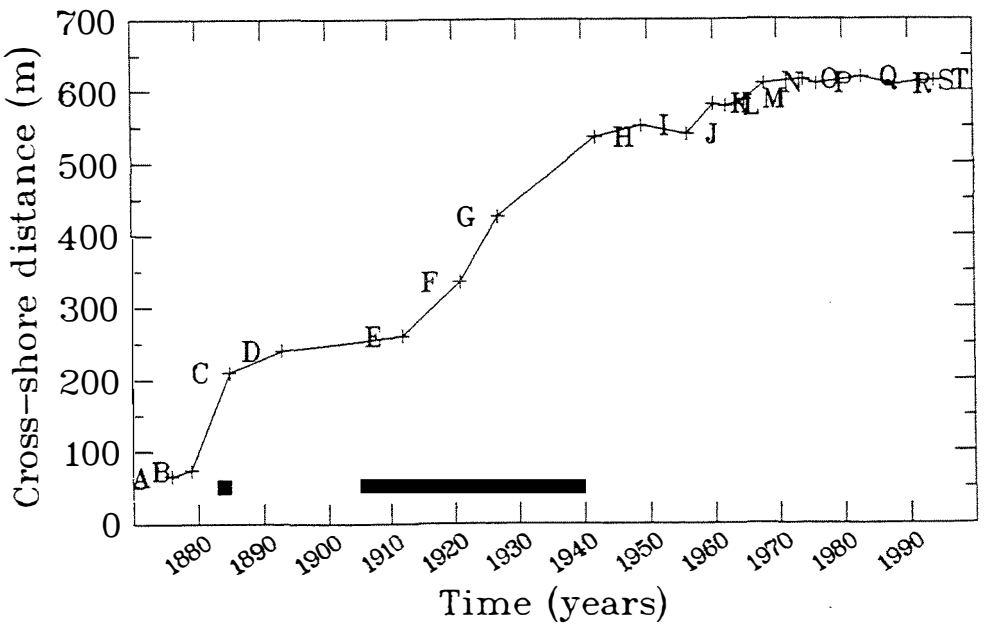

Figure 2.6 Shoreline change between 1876 and 1992 at a location 150 m northwest of the Wanganui rivermouth. The horizontal bars define periods of North Mole development (see text). The distance origin is the southwest side of Abbot Street (later named Egmont Street). This origin was used for consistency with previous surveys and to facilitate future surveys. Details on the data points are provided in Appendix C.

Studies into littoral drift along the Wanganui coast confirm the occurrence of net northwest to southeast sediment transport. Estimates of northwest to southeast rates vary between 142 000 and 597 000 m^3/yr, while estimates of the southeast to northwest rate vary between 60 000 and 277 000 m^3/yr (see Appendix B).

While the ebb tide delta has a notably subdued form, even this may be exaggerated as the seaward protrusion is at least partially a response to rivermouth jetty construction. The influence of the jetties on morphology, both within and beyond the study area, has been considerable. This change is now described in some detail as adjustment may still be occurring and this could influence NOM.

2.2.2 Rivermouth jetties and their morphological influence

The Wanganui River played an important transportation role for both indigenous and colonial economies (Chappell and Veitch 1939; King, 1964). Jetties were constructed at the rivermouth to prevent lateral migration of the channel and to increase depths (Gibb et al., 1962, King, 1964). A brief summary of jetty development is now given.

During 1884 and 1885 a 260 m long jetty was constructed in a seaward direction from the siltstone bluff on the northwestern side of the Wanganui Rivermouth (see Figure 2.3). In 1905 this jetty, referred to as the North Mole, was extended to 640 m. Smaller extensions subsequently increased its length to 730 m by 1912 and 884 m by 1930. Construction of the South Mole began in 1905 (670 m) and reached its final length of 975 m by 1912. During construction of the jetties the walls were only raised to low tide level. However, by 1940 the height had been increased to approximately three metres above mean sea level.

Following construction of the jetties, entrance depths increased from ~2.3 m below MSL in 1879 up to 5.8 m in 1932 (Gibb et al., 1962; Mclean and Burgess, 1974). This improvement has been attributed to seaward displacement of the rivermouth into deeper water, by ebb-stream scouring and by the moles acting as barriers which prevented littoral drift reaching the entrance (Gibb et al., 1962; Wallingford Hydraulic Research Station, 1967; Burgess, 1971; McLean and Burgess, 1974). The littoral barrier effect resulted in substantial morphological adjustment to both the northwest and southeast coasts and this change will now be described.

Shoreline change along a cross-shore transect located 150 m northwest of the rivermouth is shown in Figure 2.6. The data sources, shoreline indicators and error assessment are described in Appendix C. Two episodes of rapid seaward migration of the shoreline occurred: 170 m between 1879 and 1885 and 275 m between 1912 and 1942. These episodes broadly correspond with the two periods of jetty development. By 1970 the shoreline had extended to ~550 m and thereafter a state of dynamic equilibrium existed, i.e. the shoreline fluctuated about a constant cross-shore location.

Shoreline response to the jetty construction along nine kilometres of coast each side of the rivermouth is depicted in Figure 2.7. These annual rates of shoreline change for the time periods 1876 to 1942 and 1942 and 1982 (sources in Appendix C) were recently reported in Smith and Ovenden (1998). These data were derived by determining the average shoreline position over 500 m lengths of coastline. This approach removed noise caused by smaller scale changes associated with morphological configuration at the time of sampling (see section 2.3.2 and Appendix A[i]).

On the northwest coast, progradation occurred from the rivermouth to ~4000 m alongshore between 1876 and 1942. The greatest rate occurred near the rivermouth (5 m/yr) and resulted in the shoreline in this area prograding 330 m. From ~4000 m and ~7500 m alongshore the rate fluctuated between ± 0.2 m/yr. Further westward the coastline appears to have been unaffected with the regional erosion rate of 0.2 to 0.6 m/yr (identified by Johnson, 1985a) being maintained. By contrast, the results for the 1942 to 1982 period showed the rate of progradation reducing to ~2 m/yr (80 m) near the rivermouth but increasing to > 1 m/yr toward ~6000 m. The rate then diminished to near zero beyond ~7500 m. The occurrence of significant shoreline progradation northwest of 4000 m during the 1942 to 1983 period is also indicated by recent dune development to 6000 m and by the accumulation of colluvium and flotsam beyond 6000 m (see Figure 2.4B).

On the southeast coast, erosion occurred between 1876 and 1942 (Figure 2.7). The greatest rate (~3 m/y) occurred near the rivermouth and this resulted in shoreline retreat of ~200 m. The erosion rate then decreased to zero at ~9000 m southeast of the rivermouth. During the second survey period (1942 to 1982) the southeast coast experienced progradation at an annual rate of ~0.1 m/y (40 m) adjacent to the rivermouth. Further alongshore the rates diminished with erosion occurring beyond ~2000 m. The rate coincided with the 1876 to 1942 rate at ~7000 m and then dropped below the earlier rate beyond 8000 m.

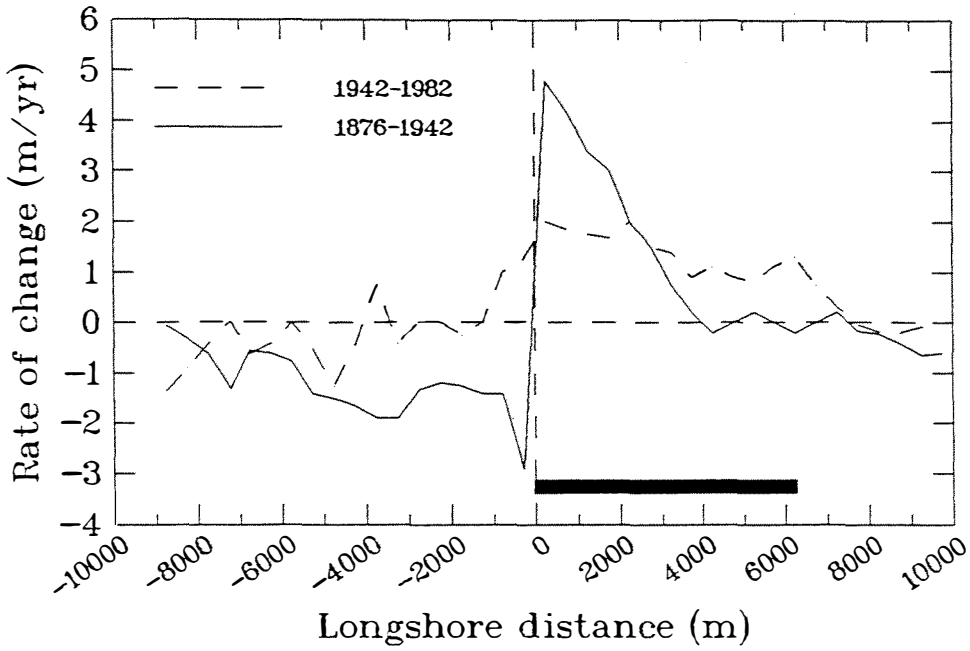

Figure 2.7 Rates of shoreline change along 19 km of Wanganui coast from 1876 to 1942 and from 1942 to 1983. The vertical dashed line locates the Wanganui Rivermouth. Negative distances refer to distance to the southeast of the rivermouth. The horizontal bar defines the study area. The data points were derived by Smith and Ovenden (1998). Details of the raw shoreline data are provided in Appendix C.

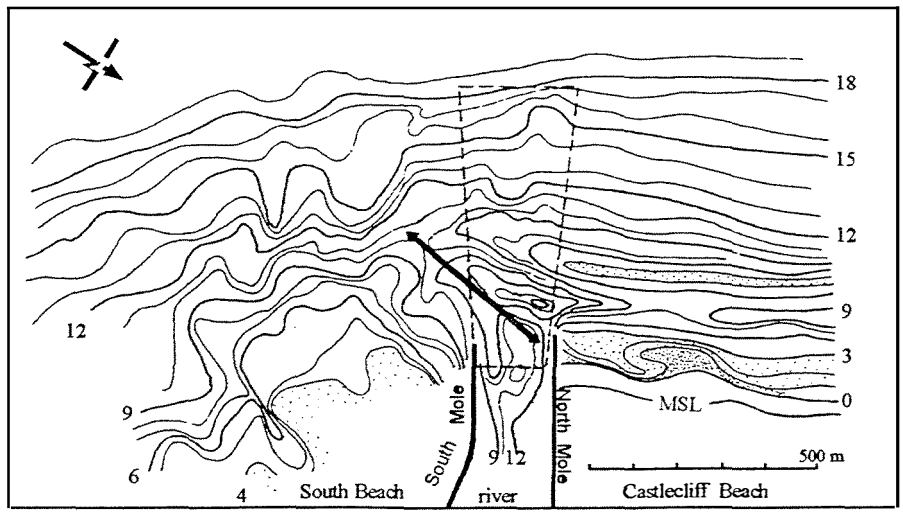

Figure 2.8 A bathymetic chart surveyed on 23.1.68 showing an example of rivermouth and adjacent coastal morphology. The double ended arrow defines the main inlet channel. The rectangular area enclosed by the dashed line depict the area regularly surveyed by the Port of Wanganui for navigation purposes. Contour depths are in feet below chart datum (MSL - 1.8m).
Source: Shand (1990)

These patterns of morphological change are consistent with the jetties acting as barriers for northwest to southeast directed littoral drift (Gibb, 1979; Komar, 1983b; CERC, 1984). The mechanism by which littoral sediment crosses a rivermouth such as at Wanganui involves sediment moving across an entrance bar under wave and current action (Burgess, 1971; Sutherland et al., 1990). This mechanism was referred to as bar bypassing by Bruun and Gerritson (1960) who described different bypass mechanisms together with defining criteria. Jetty construction at Wanganui caused increased depth at the entrance which prevented the bypass of littoral sediment. This resulted in significant progradation on the northwest coast nearer the rivermouth and severe erosion closer to the river on the southeast coast. These effects tapered off with increasing distance from the rivermouth. Over time, reducing entrance depths enabled sediment to once again bypass the rivermouth and renourishment occurred along the southeast coast. The data in Figure 2.7 also suggest that sediment renourishment is not yet complete along the southeast coast. Furthermore, on the northwest coast the shoreline progradation response to jetty construction has, over time, translated alongshore toward the northwest and this trend may still be continuing. Such an assertion is supported by the accumulation of colluvium and debris, together with incipient dune development beyond 6200 m (Figure 2.4B).

The only evidence of offshore morphological response to jetty development comes from bathymetic surveys carried out near the rivermouth. Two data sources are available. Firstly, bathymetric charts of the entrance have been produced at two to four weekly intervals by the Port of Wanganui since 1925. The 200 x 600 m survey area is shown on Figure 2.8. Sampling methodology and associated errors are described in chapters 3 and 4 respectively. The mean annual minimum depths along the northwestern boundary of the survey area - the transect closest to the study area, are plotted in Figure 2.9. These data have also been smoothed with a Lowess (locally weighted) filter[1]. By averaging the raw data points and then temporally filtering them the influence of short-term morphological change and sampling error on the long-term trend is minimised. The smoothed data indicate that depths decreased until about 1970 and, as with the shoreline change in this area, (Figure 2.6), a state of dynamic equilibrium occurred thereafter. Minimum depths along the northwestern transect were found to occur between 100 and 250 m seaward of the end of the North Mole by Shand (1990). The close coupling between shoreline change and depth change off the end of the North Mole, demonstrates the significance of littoral drift to entrance dynamics.

---

1. Unless otherwise referenced, all statistical analysis for this project was carried out using the SYSTAT software package. For further details contact: http://www.spss.com

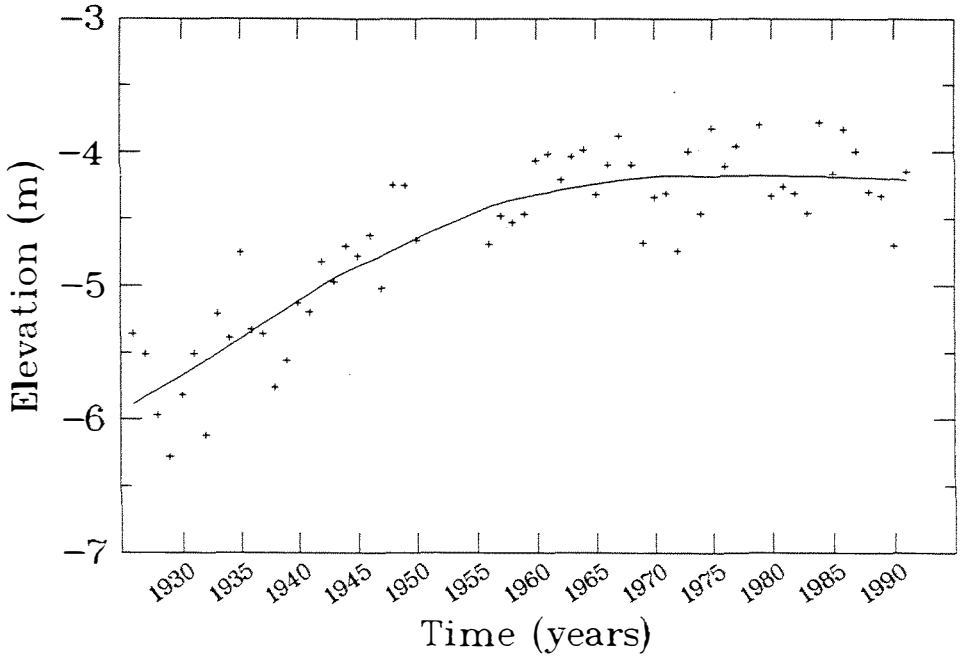

Figure 2.9 Mean annual minimum depths along the northwestern margin of the Wanganui Rivermouth survey area (see Figure 2.8) between 1926 and 1992. The curve represents a Lowess (locally weighted) filter. Elevation refers to depth below MSL.

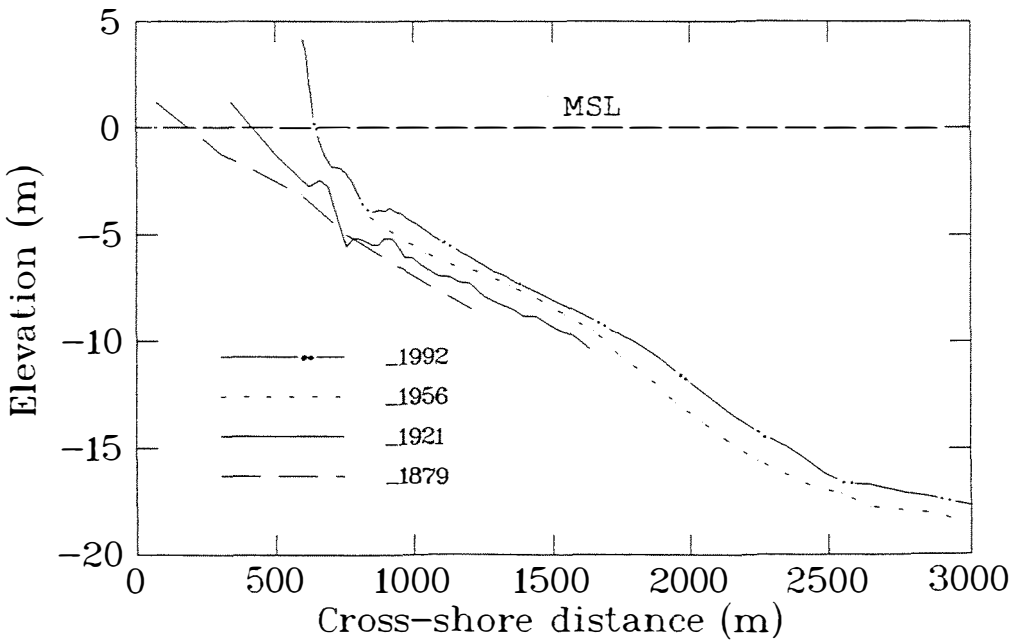

Figure 2.10 Cross-shore profiles at a site located ~150 m northwest of the Wanganui Rivermouth. The profiles were surveyed in 1879, 1921, 1956 and between 1991 and 1993. The latter data set, referred to as the 1992 survey, incorporates the mean nearshore profile obtained from analysing a bundle of profiles which were surveyed between 1991 and 1993 (see Figures 2.11 and 2.14).

The second set of data related to offshore morphological response to jetty development are cross-shore profiles for the transect located 150 m northwest of the rivermouth (see Figure 2.10). The profiles were surveyed in 1879, 1921, 1956 and 1991-93. Details of the 1879, 1921 and 1956 data are provided in Appendix C. The 1991-93 data utilised the offshore profile shown in Figure 2.5, together with the mean profile of the profile bundle (to be described in section 2.3) for the section closer to shore. The mean profile minimises the effects of sampling error and short-term variation which tend to be greater for a barred surf zone. As expected, the profiles in Figure 2.10 show that substantial seaward migration of the MSL shoreline had occurred by 1956. Further offshore, sediment accumulation resulted in the sea-bed rising between 0.3 and 1.3 m during the 1956 to 1992 period. The 1956 bathymetric survey was carried out by the Hydrographic Branch of the Navy Department so the data probably had an elevation accuracy within ± 0.25 m (Wallen[1], pers. comm.). The sea-bed elevation change between 1956 and 1992 therefore appears to be real and significant.

In summary, the shoreline and cross-shore data described in this section indicate that the morphological response to jetty construction was rapid closer to the rivermouth jetties with time-lags occurring in adjustment for areas located further offshore and alongshore. Furthermore, it appears likely that morphological adjustment is still occurring within, and in the vicinity of, the study area.

2.3 Study area morphology

In chapter 1 the study area was defined as extending approximately six kilometres alongshore to the northwest of the Wanganui Rivermouth and at least 700 m seaward from the dune toe. The study area is depicted in Figure 2.1B.

2.3.1 Cross-shore morphology

Profiles

The general cross-shore morphological characteristics of the study area were identified from ground profile surveys undertaken during the early stages of this research project. Sampling occurred at three monthly intervals along the same three transects used for the offshore profiles shown in Figure 2.5. These transects, located 200, 1500 and 5000 m to the northwest of the rivermouth, will henceforth be referred to as *T200, T1500* and *T5000* respectively. The intermediate transect (T1500) was offset toward the rivermouth to detect the expected transition between coast and inlet (see Wright, 1977; Gibeaut and Davis, 1991; Hayes, 1991; Fenster and Dolan, 1996). Sampling dates are listed in Appendix D(ii). Profile elevation data were reduced to MSL and cross-shore distances were measured relative to

1. Hydrographer, Royal New Zealand Navy.

the dune toe. Further details on the data acquisition methods are included in chapter 3 and an error assessment is made in chapter 4.

Profile bundle plots for the transect data are shown in Figure 2.11. Each transect is characterised by longshore bars and troughs with T5000 appearing to have a more stationary mid-profile configuration than the other transects. The average number (and range) of bars occurring on the individual profiles were 3.3 (2 to 5) at T200, 3.8 (2 to 5) at T1500 and 4.7 (4 to 6) at T5000.

Examples of the main morphological features evident on the profiles are shown in Figure 2.12. These features consist of seaward bars and troughs that are always submerged during the tidal cycle, a swash bar on the inter-tidal beach, a low tide step, a low tide terrace, and a berm (terrace) on the upper beach. These terms and morphologies are described in coastal geomorphological texts such as King (1972), Komar (1976a) and Davies (1980). The swash bar may also be referred to as a ridge and the adjacent shallow landward trough as a runnel. While submarine bars and troughs were always present on a profile, the smaller landward features were not always present.

Cross-shore zones and nomenclature

To facilitate profile description and analysis, cross-shore profiles are often divided into zones based on form and/or process characteristics (e.g. see Komar ,1976a; DCE, 1980; CERC, 1984; Horikawa, 1988). While a distinctive nomenclature has evolved for use in coastal science, zonal definitions are often adapted to suit the particular purpose of a study (e.g. Larsen and Kraus, 1989; Masselink, 1993). Figure 2.13 is a definition sketch of the zonal nomenclature used in this study. The swash, surf and shoal zonation is based upon different types of wave action. The *shoal zone* corresponds to the area seaward of the break-point where waves have begun to interact with the sea-bed and increase in height. The *surf zone* is the area from the wave break-point to the location of maximum backwash or backrush, while the *swash zone* extends from the limit of backrush to the landward extreme of the run-up or up-rush. However, these boundaries are not fixed in time or space, i.e they are 'dynamic or short-term'. This situation occurs because wave breaking happens when water depth is approximately the same as the wave height[1]. The zone boundaries therefore translate landward or seaward in response to a change in environmental conditions such as wave height, tide level, wind velocity or bar-crest location and depth.

1. Wave breaking occurs when the wave height to water depth ratio is ~0.8. This ratio is called the *breaker coefficient* (γ_b). However, the critical value at which wave breaking occurs is also influenced by cross-shore gradient, breaker type, wave steepness and wind velocity such that γ_b may range from < 0.75 to > 1.5 (Douglass and Weggel, 1988; Dalley, 1990; Hardisty, 1990).

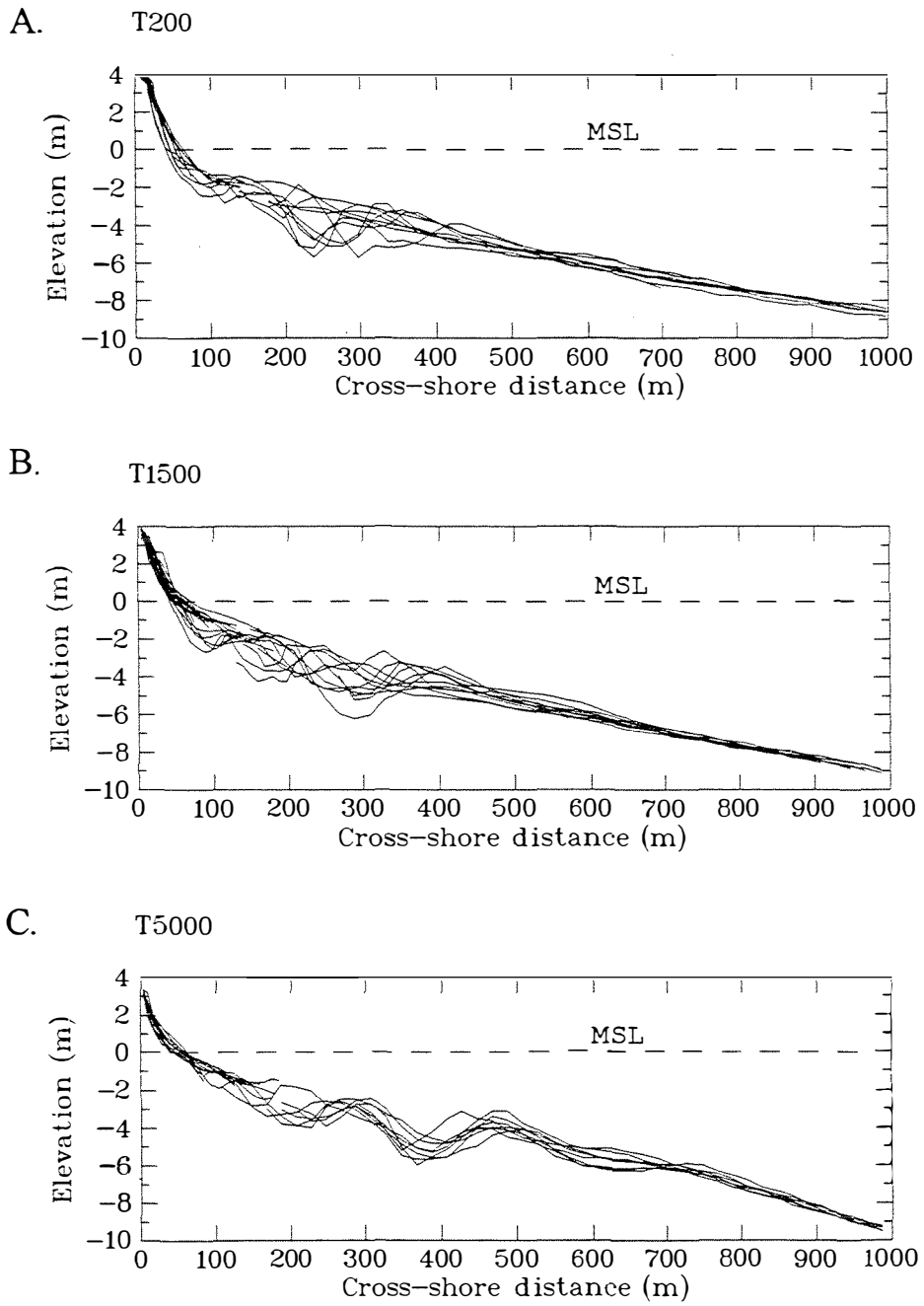

Figure 2.11 Profile bundles for cross-shore transects at sites T200 (A), T1500 (B) and T5000 (C). Individual profiles were surveyed at three monthly intervals between 1990 and 1994 (see Appendix D[ii]).

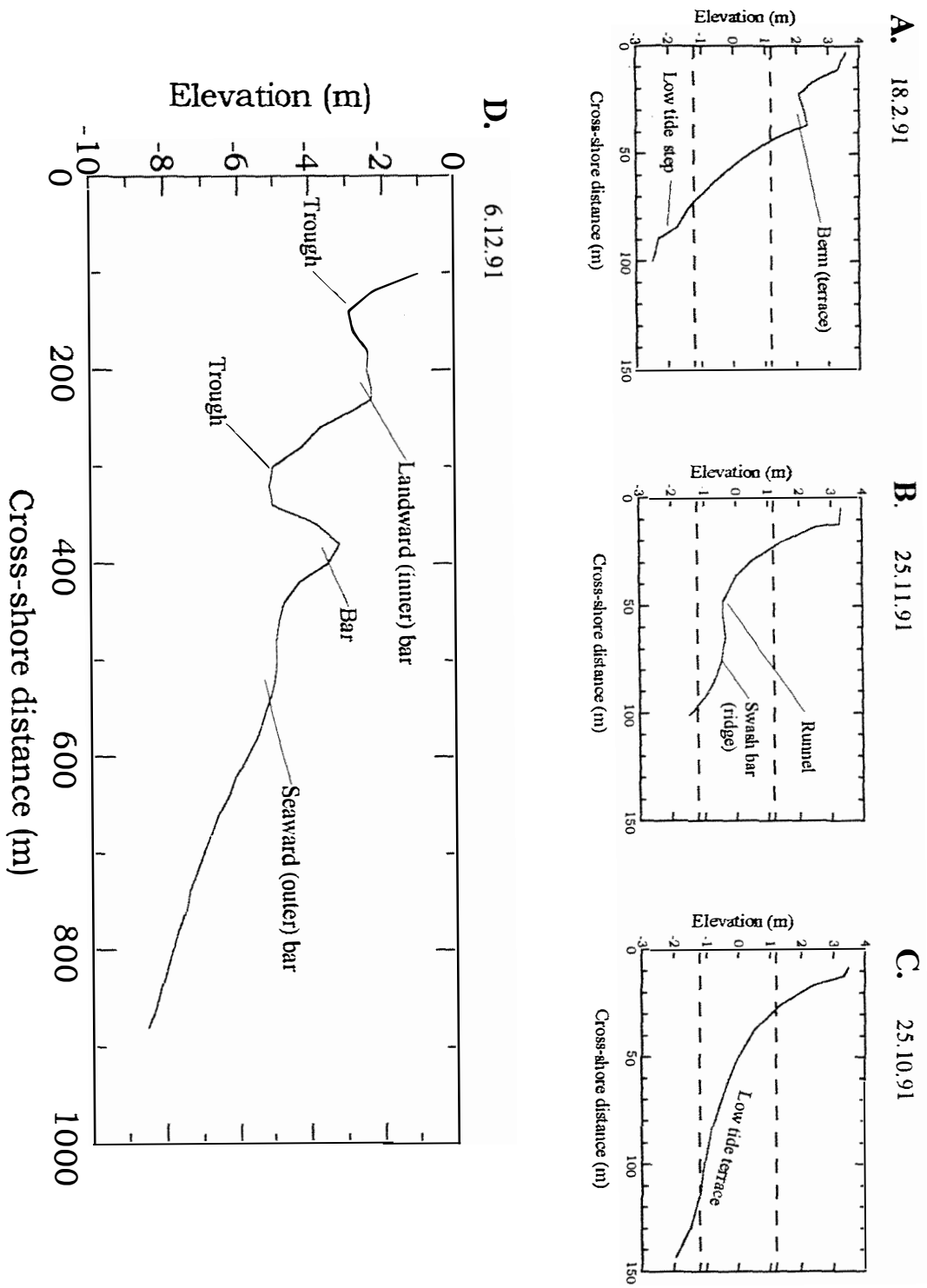

Figure 2.12 Profile representation of morphological features and terminology used in this study. Figures A to C illustrate features either within, or on the margins of, the inter-tidal beach, while Figure D illustrates submarine features located further offshore. All profiles were surveyed at site T1500.

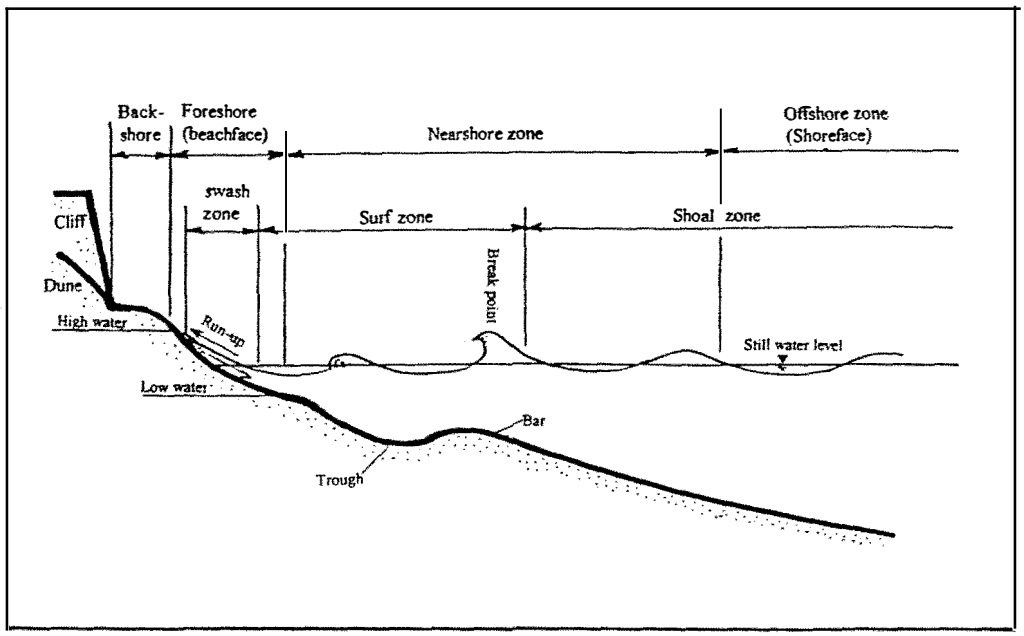

Figure 2.13 Sketch of a cross-shore profile illustrating the zonal nomenclature used in this study. Terms are defined in the text.

Modified from: Komar (1976a); DEC (1980); CERC (1984); Horikawa (1988)

A commonly used alternative set of terms that relate to cross-shore zonation is also shown in Figure 2.13. The foreshore or beach-face relates to that region of the cross-shore subjected to swash action. The low tide mark is often used as the seaward edge of this zone, while the up-rush maxima may be used to define the zone's landward edge. The nearshore refers to that area where the sea-bed is subjected to extensive surf-related effects (Birkemeier, 1985). The region seaward of the nearshore is termed the offshore zone or the shoreface and is subjected to wave induced currents. The backshore is any area that exists between the foreshore and dune or cliff. This is an accumulation area which may be subjected to marine (storm-wave overwash), terrestrial (mass movement) and aeolian (wind-blown sand) processes.

To compare profile characteristics between different sites a 'static' zonation based on long-term profile data can be used. The foreshore, nearshore and shoreface boundaries may then be defined using profile bundle variability with respect to elevation, together with the mean profile derived from the bundle. The mean profiles for the three sets of profile bundles in Figure 2.11, are shown in Figure 2.14, with the standard deviations about the mean values shown in Figure 2.15. The landward boundary of the 'static' or 'long-term' foreshore will be defined by the mean profile intersection with the most landward location of rapid

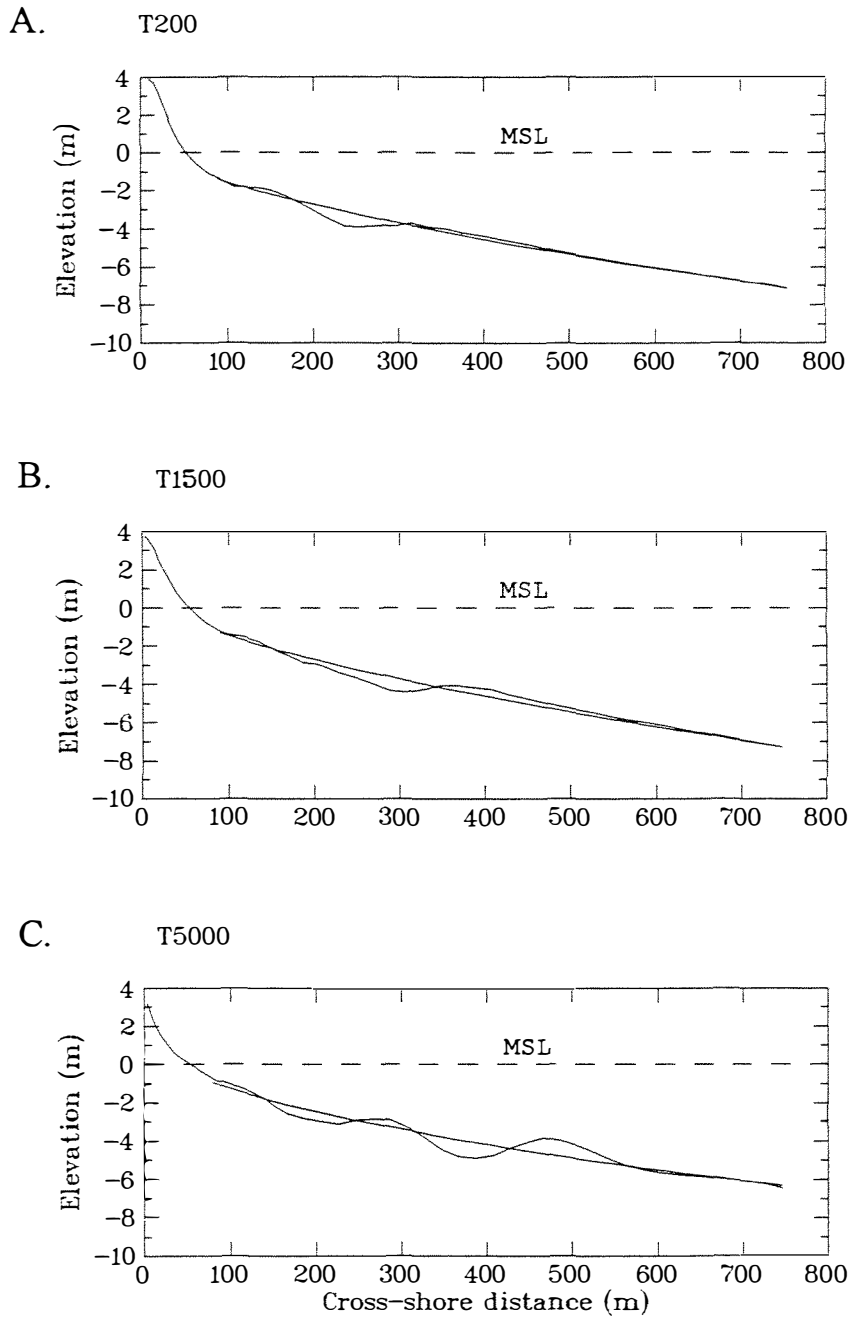

Figure 2.14 Foreshore/nearshore mean profiles, together with power curves fitted to the nearshore section, for transects T200, T1500 and T5000. Mathematical expressions for the curves are given in the text as equations 2.1, 2.2 and 2.3.

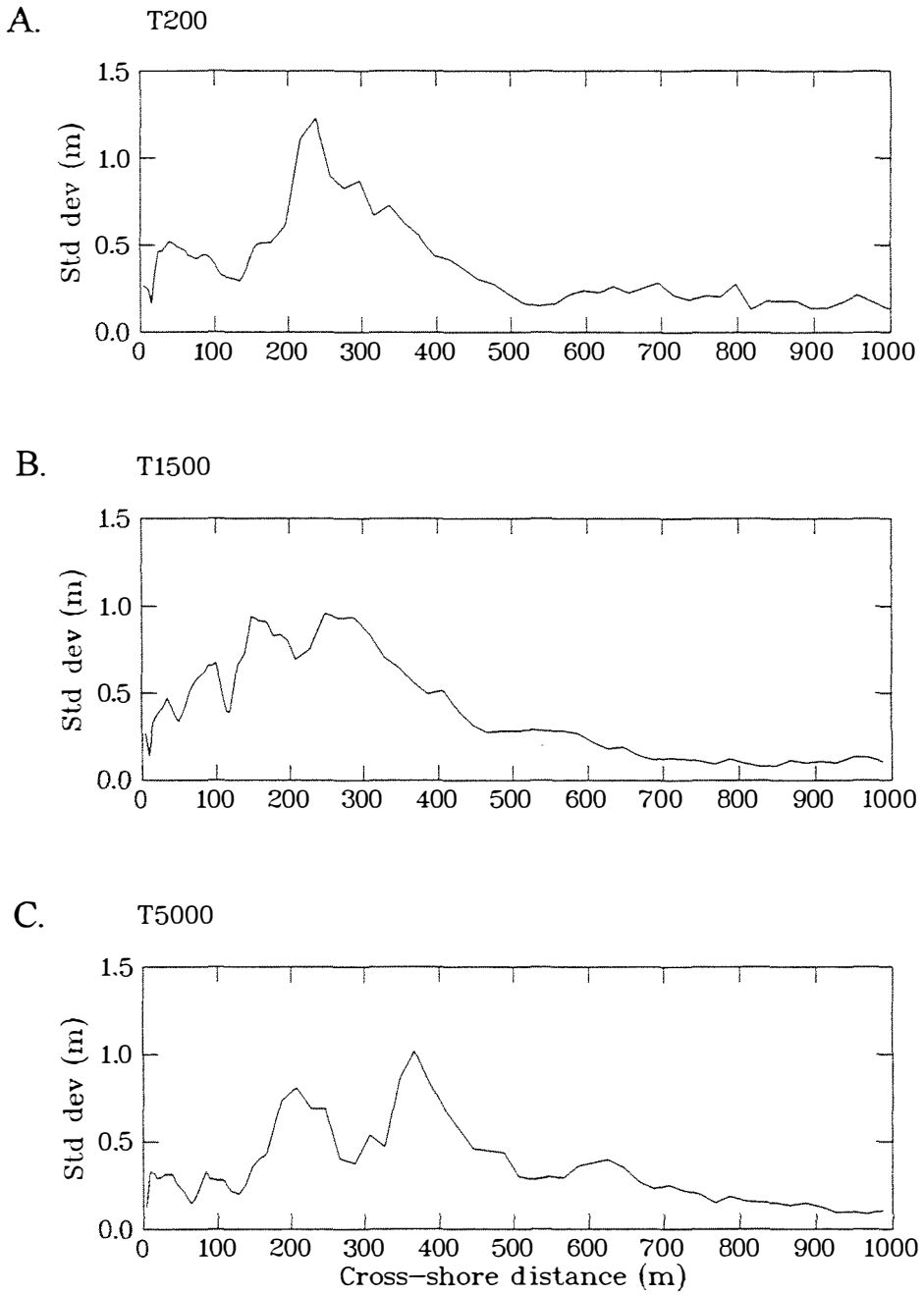

Figure 2.15 Standard deviations for profile bundle elevations at transects T200, T1500 and T5000.

reduction in elevation variance (see Figure 2.15). The long-term foreshore/nearshore boundary will be defined by the intersect of the mean profile and the spring low tide line. The long-term nearshore/shoreface boundary is defined as that location where vertical change in the profile bundle becomes constant in the seaward direction. The data in Figure 2.15 indicate that this occurs when the standard deviation reaches ~0.2 m. Kroon (1994) found that the same value occurred in data from the Holland coast. The seaward limit of the shoreface, which will be referred to as the shoreface/inner shelf boundary in this study, is often defined by a break in slope beyond the nearshore/shoreface boundary (Hesp and Hilton, 1996). Such offshore locations are evident on the Wanganui profiles (Figure 2.5) between ~1650 and 1950 m.

Study site zonal characteristics

The long-term zonal boundary locations and corresponding depths for the three Wanganui transects, together with the average slope across each zone, are summarised in Tables 2.1 and 2.2 respectively. Cross-shore slope is an important analysis parameter in the NOM inter-site study (chapter 5).

The results in Tables 2.1 and 2.2 show that longshore gradients exist for the cross-shore zones. The back-shore narrows (18 m to 9 m) and lowers (3.46 to 2.5 m) with increasing distance from the river and this results in an increase in slope (0.041 to 0.110). The foreshore widens (70.5 m to 116 m) and lowers with increased distance from the river and this results in a longshore slope reduction (0.069 to 0.034). Nearshore characteristics show a similar pattern to the foreshore with the width increasing from 426.5 to 625 m and the slope decreasing from 0.0094 to 0.0082. In contrast the shoreface width decreases significantly further from the river (1430 to 890 m) and the steepest shoreface slope (.0092) occurs at the site furthest from the river-mouth. In summary, the long-term foreshore and nearshore profile slopes are both steeper near the rivermouth compared with the northwest of the study area, while the long-term backshore and shoreface slopes both increase further from the river. Intuitively, the delta morphology should cause the nearshore slope to be flatter near the rivermouth than at the northwestern end of the study area, and the shoreface slope to be relatively steeper closer to the river. The contradictory result evident in the Wanganui data possibly reflects rock control associated with the wave-cut platform to the northwest and the zone boundary locations used in this study.

Curve fitting

Cross-shore profiles typically have a concave upward form (King 1972, Dean 1977) and nearshore researchers often fit non-linear curves to the profiles to facilitate mathematical analysis (e.g. see Birkemeier, 1984; Larsen and Kraus, 1992; Inman et al., 1993; Lippmann et al., 1993; Kroon, 1994; Ruessink and Kroon, 1994).

Table 2.1 Boundary locations and depths for the long-term cross-shore profile zones defined in the text.

Site*	Dune/Backshore (benchmark)		Backshore/ Foreshore		Foreshore/ Nearshore		Nearshore/ Shoreface		Shoreface/ Inner-shelf	
	x	y	x	y	x	y	x	y	x	y
T200	0	4.20	18	3.46	88.5	-1.4	515	-5.4	1945	-16.6
T1500	0	3.75	12	3.27	97.5	-1.4	630	-6.3	1745	-14.2
T5000	0	3.49	9	2.50	125	-1.4	750	-6.5	1640	-14.7

* These codes refer to the cross-shore transects (T) at a given distance (e.g. 200 m) from the northwestern jetty of the Wanganui Rivermouth.
x = the cross-shore distance (m) from the dune-toe benchmark.
y = the elevation (m) from MSL.

Table 2.2 Width, height and average slope for the long-term cross-shore profile zones defined in the text.

Site *	Backshore			Foreshore			Nearshore			Shoreface		
	w	h	s	w	h	s	w	h	s	w	h	d
T200	18	0.74	0.041	70.5	4.86	0.069	426.5	4.0	0.0094	1430	11.2	0.0078
T1500	12	0.48	0.040	85.5	4.67	0.055	532.5	4.9	0.0092	1115	7.9	0.0071
T5000	9	0.99	0.110	116.0	3.90	0.034	625.0	5.1	0.0082	890	8.2	0.0092

* These codes refer to the cross-shore transects (T) at a given distance (e.g. 200 m) from the northwestern jetty of the Wanganui Rivermouth.
w = zone width (m), h = zone height (m), s = average slope ($\tan\beta$)

In the present project (chapters 4 and 5), power curves are fitted to individual profiles as part of a technique used to determine bar-crest locations. They are also fitted to mean profiles to locate modal bar-crests. The technique is described in chapter 3 (section 3.3.4). In Figure 2.14 power curves have been fitted to the nearshore section of the mean profiles for T200, T1500 and T5000 using a least squares routine. The associated mathematical expressions are given below as equations 2.1, 2.2 and 2.3 respectively.

$$E = -0.097*D^{0.657} + 0.401 \quad (2.1)$$

$$E = -0.102*D^{0.658} + 0.612 \quad (2.2)$$

$$E = -0.721*D^{0.387} + 2.966 \quad (2.3)$$

where E is elevation in metres with respect to mean sea level, and D is cross-shore distance in metres from the dune toe.

2.3.2 Plan-view morphology

When morphology is viewed in plan, i.e. from above, the configuration can be qualitatively described in terms of its 'dimensionality'. *Two-dimensional (2D)* morphology can be represented by a single shore-normal profile. Such configurations are (approximately) uniform in the longshore direction and may be described as shore-parallel. *Three-dimensional (3D)* configurations, however, vary alongshore and multiple profiles are needed to define such morphology. Three-dimensional configurations are often described as 'rhythmical'; however, three-dimensional topographies may take on a variety of non-symmetrical/irregular appearances. Three-dimensional configurations are frequently further categorised as either *weak, moderate or strong* depending on the level of longshore non-linearity. Typical morphological configurations found on the foreshore and nearshore are described in, for example, Komar (1976a), Wright and Short (1984) and Sunamura (1988).

Three-dimensional topography frequently occurs on coasts dominated by longer period waves (swell), smaller tidal ranges, steeper cross-shore slopes and a single bar (Short 1992; Short and Aagaard, 1993). However, on multi-bar coasts the most landward bar may have a 3D configuration, especially under prolonged fairweather condition which favour the development of more complex morphologies (Lippmann and Holman, 1990; Short and Aagaard, 1993). The configuration of seaward bars tends to be two-dimensional but three-dimensionality may occur (e.g. Goldsmith et al., 1982; Short, 1992; Short and Aagaard 1993, Ruessink and Kroon, 1994). The study area at Wanganui conforms to this pattern with landward bars having a higher level of three-dimensionality than seaward bars. This is

demonstrated in Figure 2.4B which is a 'time-exposure' photograph of the northwestern study area. The high intensity areas locate topographic highs (sand-bars); the technique is described in detail in chapter 3.

Morphological plan configurations have been classified into six 'beach-states' and, as noted in chapter 1, conceptual surf zone models relate environmental conditions to beach-state sequences (see Appendix A). In terms of dimensionality, the end members of the sequences are mainly two-dimensional while the intermediate states are mainly three-dimensional. Many of these configurations have been observed within the study area. For example, the inner bar in Figure 2.4B appears to be have a 'transverse bar and rip' state in the foreground and the 'rhythmic bar and beach' state in the distance, while the seaward bar is in the 'longshore bar and trough' state.

2.3.3 Rivermouth morphology

Coastal sand-bars in the study area have been shown to extend across the rivermouth at the southeastern end of the study area (Shand, 1990). This morphological continuity is illustrated in Figure 2.8. Shand (1990) analysed six and a half years of entrance charts that were surveyed by the Port of Wanganui at two to four weekly intervals. The results of this analysis showed a bar always existing beyond the jetties and a landward bar usually occurring between the ends of the jetties. These bars were dissected by an inlet channel which was usually orientated toward the south. As noted in chapter 1, the rivermouth bars were observed to undergo net offshore migration.

2.4 Sediment characteristics

2.4.1 Textural characteristics

The textural characteristics of surface sediment in the study area were determined by analysing samples collected along the high tide line and across shore-normal transects located 500 m and 3000 m from the rivermouth. Logistical constraints prevented a third transect further to the northwest from being sampled. The samples were sieved at 1/2 phi increments and the Folk and Ward parameters determined. Longshore and cross-shore values for mean size, sorting and skewness are plotted in Figures 2.16 and 2.17 respectively. These results will now be summarised.

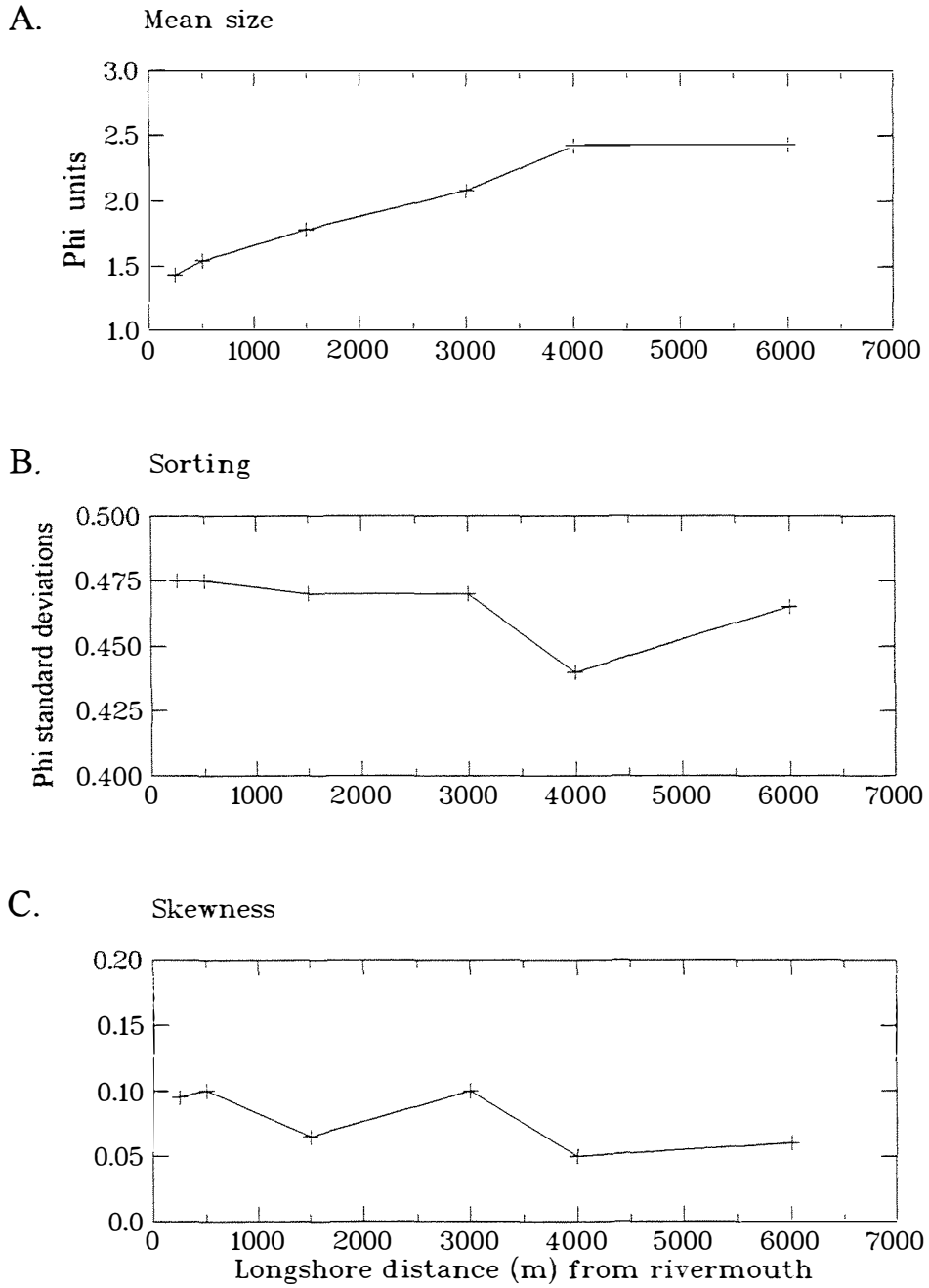

Figure 2.16 Folk and Ward parameter values for sediment samples collected along the high tide line of the study area on 22.2.92. Figure A shows the mean sediment size, B the sorting values and C the skewness values.

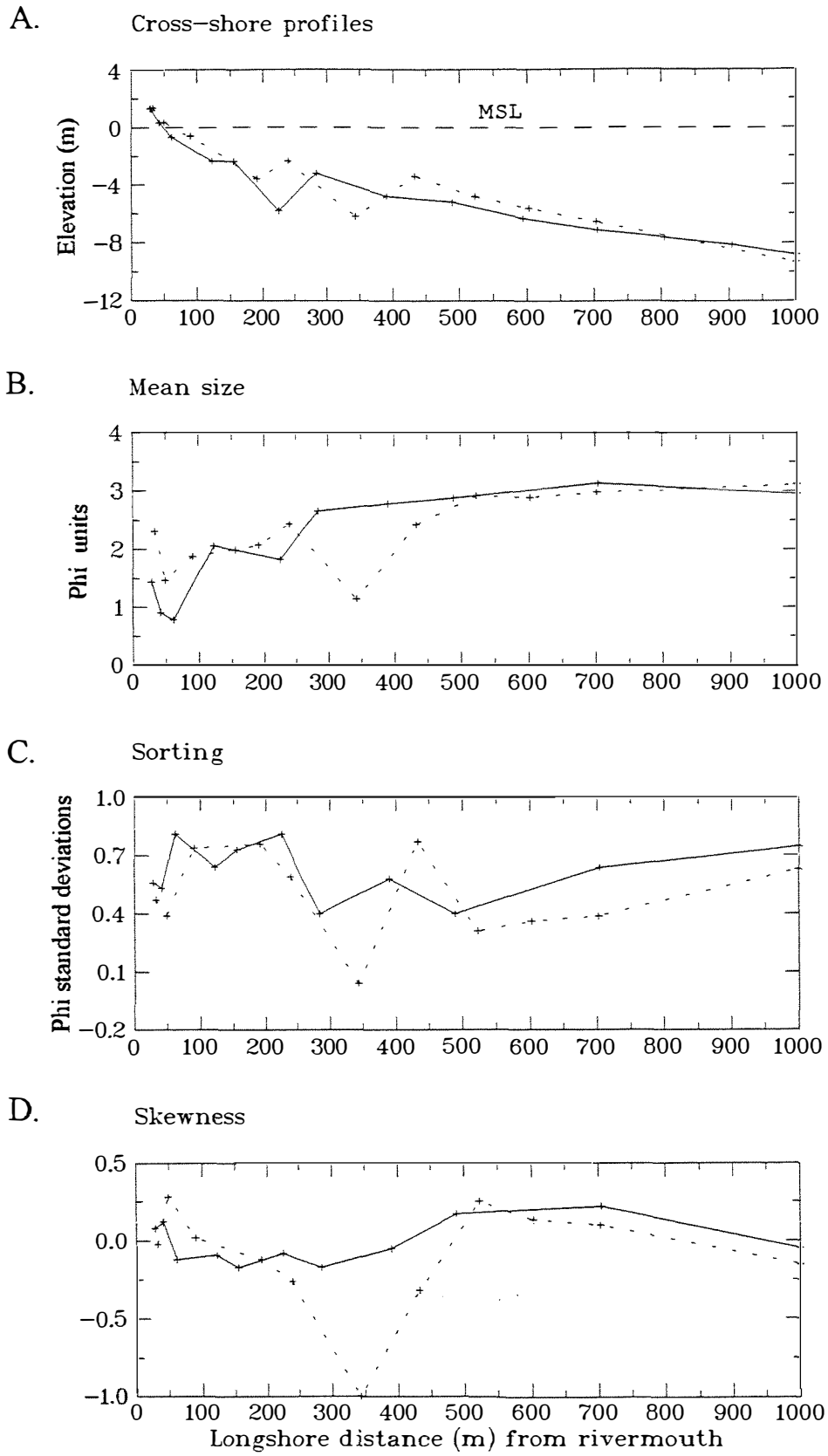

Figure 2.17 Folk and Ward parameter values for sediment samples collected across-shore to 1000 m at T500 (solid line) and T3000 (dashed line). Figure A shows the cross-shore profiles as determined by echo-sounding. Figure B depicts the mean sediment size, C the sorting and D the skewness values.

While beach sediments in the northwest of the study area comprise fine sand (2 to 2.5 phi) the sediment coarsens toward the river where values of ~1.5 phi were obtained. This coarsening appears to be a local phenomenon superimposed upon a trend of regional fining toward the southeast that was previously identified by Burgess (1971), Gibb (1979) and Lithgow (1986). Sediment coarsening adjacent to inlets has been observed elsewhere and attributed to tidal currents and inlet bypass mechanisms (Nordstrom, 1989). The beach sediments had consistent sorting values (0.45 to 0.475 phi standard deviations) and had a small positive skew (0.05 to 0.1).

Both sets of cross-shore samples have textural characteristics that change with increasing distance offshore. Sediment coarsened from high tide to low tide (2.3 to 0.9 phi). Further seaward the sediment fined across bars and coarsened within troughs before stabilising at ~3 phi (fine to very fine sand) in the outer nearshore. Across the foreshore and nearshore, sorting values fluctuated between 0.09 and 0.82 phi standard deviations. Sorting values were higher near the rivermouth indicating localised influence of fluvial processes. Skewness values fluctuated from being slightly positive on the foreshore to negative across the surf zone to slightly positive in the outer nearshore. Localised coarsening is evident in the seaward trough at the northwestern site. Sampling was also extended seaward along each transect; out to 3000 m on T500 and to 4000 m on T3000. However, textural parameter values were similar to those at 1000 m.

2.4.2 Mineralogy

The mineralogy of beach (foreshore) sediments in the Wanganui region has been reported by Fleming (1953), Gibb (1979) and Lithgow (1986). Gibb's (1979) results are reproduced as Appendix E. These studies all found that sediments to the west of the study area were dominated by heavy minerals (60 to 80%) such as augite and opaques (mainly titanomagnetite) which originate from the Egmont Volcanic Region (see Figure 2.2). The percentage of magnetic minerals declined along the study area to values between 30 and 40% at the Wanganui Rivermouth. Fleming (1953) attributed this reduction firstly to increased distance from the source, and secondly to dilution caused by the high concentration of non-magnetic minerals entering the beach system via the Wanganui River. Evidence that river-borne sand can travel northwest into the study area is provided by the distribution of hypersthene along the Wanganui coast. Hypersthene is a heavy mineral that originates in the Central Volcanic Region (Figure 2.2), and is delivered to the coast via the Wanganui River. While most hypersthene is carried to the southeast, some is deposited along the northwest coast.

2.4.3 River sediment

Burgess (1971) analysed 18 samples of rivermouth sediment. The range in sediment size was similar to that found in the surf zone samples. However, sorting values varied dramatically and ranged between 0.28 and 1.7 phi standard deviations. Such variation was expected in an area characterised by wave, tidal and fluvial interaction. Willett (1959) examined sediment samples collected along the Wanganui River and the size analysis suggests that river sand is marginally finer than coastal sand.

The southeasterly directed net littoral drift, the regional fining of sediment to the southeast and the reduction of heavy minerals southeast of the rivermouth indicate that most of the river's 114 kilotonne bedload yield of sand and gravel (Thompson, 1988) is deposited to the south of the study area. However, the mineralogical data and the sorting results for coastal samples, indicate that river sediment does reach the study area. The sand volume of the river bedload is unknown.

2.5 The process regime

2.5.1 Surface waves

Surface waves have been categorised by Kinsman (1965) into a range of types based on *wave period*, i.e. the time taken for a wave to travel one wave length. These wave types are depicted in Figure 2.18 which also shows the primary disturbing force, the primary restoring force and the distribution of ocean surface wave energy. These different types of wave frequently occur simultaneously; they have different influences on surf zone morphodynamics and require a range of monitoring techniques. This section identifies the characteristics of the different wave types at Wanganui. These waves consist of *gravity, infragravity,* and the longer period waves of *seiche* and *tide.* Surf zone studies since the development of Kinsman's classification have shown that gravity and infragravity waves with significance for surf zone morphodynamics have cut-offs at ~4 seconds and 20 seconds for gravity waves and 20 seconds to ~200 seconds for infragravity waves (CERC, 1984; Holman, 1983; Aagaard, 1990; Short and Aagaard, 1993).

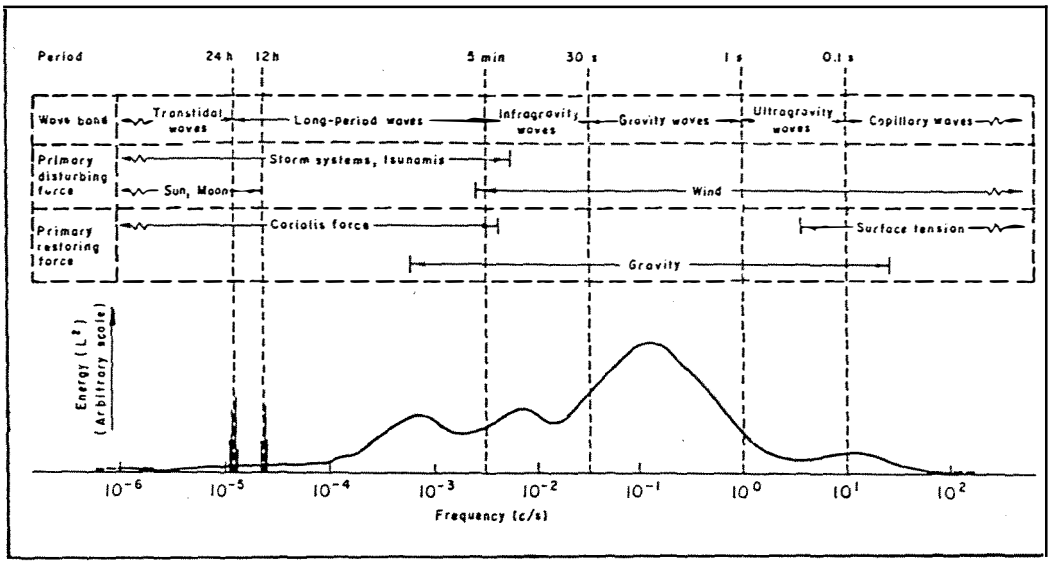

Figure 2.18 Classification of surface waves based on wave period bands. The primary disturbing force, primary restoring force and distribution of wave energy are also shown.

Source: Kinsman (1965)

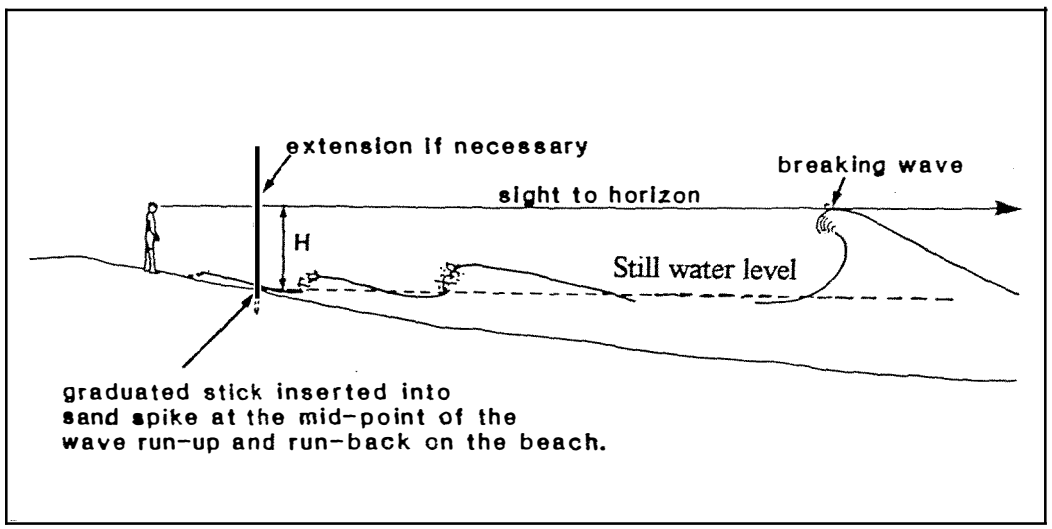

Figure 2.19 Illustration of the 'line-of-sight' field method used in this study to measure wave height at the breakpoint. Adjustments were subsequently made to derive the significant wave height (see text).

Source: Patterson (1985)

2.5.1.1 Gravity waves

Data sources

Gravity waves contain the greatest portion of surface wave energy (Figure 2.18) and larger gravity waves are the primary driving force for sediment transport and morphological change in the foreshore and nearshore zones (King, 1972; CERC, 1984). Gravity waves are also referred to as *incident waves*. Gravity waves can be further separated into two states: *sea* when waves are still under the influence of the wind in the generating area, and *swell* when they have moved out of the generating area. Sea waves have shorter periods, are steeper and refract less than swell waves (CERC 1984). Three sources of Wanganui incident wave data collected over time intervals greater than one year were available for analysis (see Table 2.3). These data-sets will now be described and analysed.

Between 27 September 1968 and 31 December 1969 the Wanganui Harbour Board collected daily wind and wave data from a site approximately 2.5 km northwest of the Wanganui Rivermouth. The purpose of this monitoring was to correlate process data with morphological change at the river entrance. The maximum wave height was determined using a technique involving a moored buoy and a theodolite. The buoy was located in the outer surf zone and the theodolite on top of the cliff. These data, henceforth referred to as the *Harbour Board data-set*, were initially analysed by McLean and Burgess (1969) and Burgess (1971). More recently Patterson (1992) reanalysed the raw data after computing the significant wave height at the break-point ($Hsig_b$); this wave height parameter is explained below.

Between 31 January 1986 and 25 February 1987 a Datawell (non-directional) Waverider Buoy was deployed off the Wanganui coast by the Ministry of Works and Development to provide data for coastal process investigations. The buoy was located 9 km offshore where the depth is ~30 m. The water surface was sampled at four Hertz (Hz) for nine minute durations every three hours. These data, henceforth referred to as the *Waverider data-set*, were initially analysed for deepwater significant wave height characteristics ($Hsig_0$) by Macky et al. (1988). This wave height parameter is explained below. Patterson (1992) subsequently undertook a record by record spectral analysis.

As part of the present study, daily wave conditions were recorded between 27 July 1989 and 10 January 1998 using the 'line-of-sight' method described by Patterson and Blair (1983) and Patterson (1985). The purpose of obtaining this data was to correlate wave parameter values with morphological change along the Wanganui coast. The line-of-sight method

Table 2.3 A summary of background details for Wanganui wave data-sets described in the text and the associated significant wave height parameter values.

Name of data-set	Harbour Board	Waverider	Line-of-sight
Collector	Wanganui Harbour Board	Ministry of Works and Development	Author
Method	Theodolite & buoy	Waverider buoy	Staff & horizon
Collection dates	27.9.68 to 31.12.69	31.1.86 to 25.2.87	27.7.89 to 10.1.98
Duration (days)	460	420*	3439
Mean wave height (m)	1.3	1.25	1.45
50% exceedence (m)	1.2	1.15	1.35
10% exceedence (m)	2.0	2.15	2.32
5% exceedence (m)	2.2	2.45	2.64
1% exceedence (m)	2.9	3.2	3.23

* 37% records lost or unrecoverable

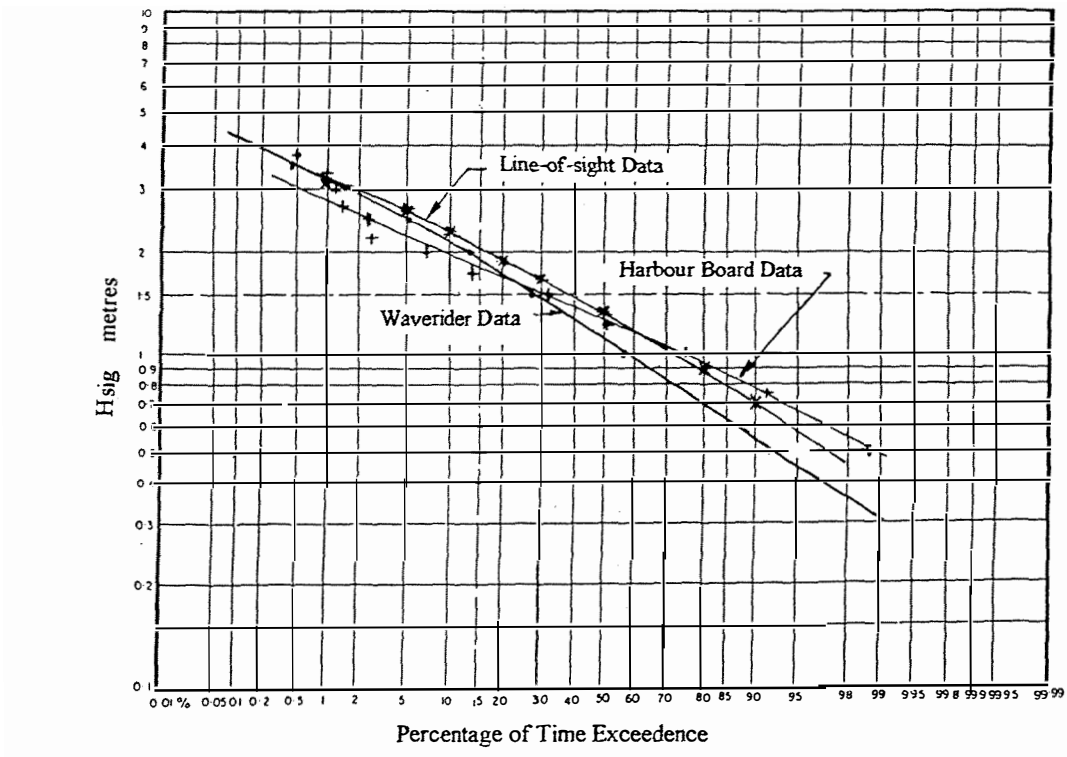

Figure 2.20 Probability of exceedence curves for three sets of non-contemporaneously sampled significant wave height data. Each data-set is described in the text. The Waverider and Harbour Board data points are from Patterson (1992), while the line-of-sight data points are derived from observations made during this study.

used a graduated staff positioned at the still water level (SWL). The observer then moves back up the beachface until the horizon is aligned with the breaking wave-crest (see Figure 2.19). The maximum breaking wave height over five minutes was recorded. These data were subsequently processed to provide estimates of deepwater significant wave height ($Hsig_0$) using conversions detailed in Patterson and Blair (1983) and Patterson (1985). This procedure incorporated adjustments for earth curvature, wave set-up above the SWL, trough depth below SWL, and wave deformation between deep water and the break-point. The resulting data, henceforth referred to as the *line-of-sight data-set,* is graphically presented in Appendix F. The line-of-sight method is used for daily wave height monitoring rather than the more commonly used visual estimation of breaking wave height, e.g. the LEO programme (Smith and Wagner, 1991), because of greater measurement consistency both over the range of possible wave heights and over time (Patterson, 1985).

Wave height

The three wave height data-sets were analysed with respect to the significant wave height either at the seaward break-point ($Hsig_b$) or in deepwater ($Hsig_o$). The *significant wave height* is defined as the mean value for the highest one third of wave heights. This wave height parameter is frequently used in scientific and engineering work because it is the most representative parameter of sea state (Goda, 1983). Further advantage of the significant wave height is its approximation to both visually estimated wave height and wave height determined from spectral energy density (Patterson 1985). Deepwater is defined as depth greater than half the wave length. Waves in such water depths have not been deformed through sea-bed interaction as occurs when they propagate across shallower water (Komar, 1983a; CERC, 1984; Hardisty, 1990).

Significant wave height exceedence curves for the three wave height data-sets are shown in Figure 2.20 and the wave height parameters most frequently used in this study are summarised in Table 2.3. These parameters consist of the mean wave height, the 50% exceedence value ($H_{0.5}$) which is also referred to as the 50th percentile value or median value, the 10% exceedence value ($H_{0.1}$) which is also referred to as the 90th percentile value or the *storm* wave height, the 5% exceedence value ($H_{0.05}$) which is also referred to as the 95th percentile value or the *severe* wave height, and the 1% exceedence value ($H_{0.01}$) which is also referred to as the 99th percentile value or the *extreme* wave height. The median values varied between 1.15 m for the Waverider data and 1.35 m for the line-of-sight data. For wave heights less than average the Harbour Board data has exceedence values

greater than the other data-sets with the Waverider data having the lowest values. However, this situation reverses for larger wave heights. By contrast, the line-of-sight exceedence values are greater than the Waverider values for all wave heights with the values converging at approximately the 1% exceedence value (~3.2 m).

Wave height variation between the three records was expected because of the non-synchronised sampling periods, the different record lengths, the different sampling methods and the different monitoring locations. The lower slope of the exceedence curve for the Harbour Board data may reflect the greater height loss larger waves undergo compared with smaller waves as the waves propagate over the shallow inner shelf between the deepwater location and the break-point. While wave deformation studies have not been undertaken for this coast, Burgess (1971) and Patterson (1991, 1992) considered that the wide and shallow inner shelf would result in the energy loss by friction and refraction outweighing height increase associated with wave shoaling.

Which incident wave height data and statistics to use?

This study requires knowledge of incident wave height firstly to enable comparison between global NOM sites, and secondly to correlate with NOM behaviour at Wanganui.

Statistics from deepwater wave data are better suited to the former purpose because data from all sites are free of wave height deformation. It is difficult to ensure equivalent deformation has occurred when instruments from different sites are located in shallower water closer to the coast. While some validation of line-of-sight data has been carried out by Patterson (1985), the processing procedures are subject to a range of systematic errors. Calibration with contemporaneously sampled data collected by a wave recorder located in deeper water would be required if the line-of-sight measurements are to be used in an absolute sense as would be required for inter-site comparison. The Waverider data therefore had to be used to provide Wanganui wave climate statistics despite its short record length. A comparison between wind records that corresponded to the period of Waverider deployment, with long-term wind climate statistics showed that wave conditions during the Waverider sampling period may overestimate the long-term frequency of higher waves and underestimate the occurrence of lower waves (Macky et al., 1988).

Wave data for morphodynamic studies must be sampled during the period of morphological monitoring. The line-of-sight data was collected for this purpose. While the line-of-sight data cannot be verified in terms of scale, the method provides a temporally consistent means of determining relative wave height.

Temporal variation in wave height

Possible patterns in wave height variation through time can be identified on the basis of relative wave heights so the eight year line-of-sight record was the most suitable data for this purpose. A 31-point running mean filter was first applied to the raw data to depict the continuous temporal variation at approximately monthly intervals (Figure 2.21A). The graph shows some evidence that high energy events occurred at approximately one to three monthly intervals throughout the study period. Because of the data smoothing, higher frequency events are unresolvable. There is also some indication that summer wave heights are lower than winter wave heights.

Seasonal characteristics were investigated further by plotting the average wave height for each month of the year (Figure 2.21B). Between December and April the average monthly wave heights were lower than the long-term mean, while the winter months were mainly above the mean. The data therefore indicate that 'weak' seasonality occurs in the wave height climate. However, high or low wave events can happen at any time of year.

Wave height pattern was also investigated by carrying out a spectral analysis and this output is shown in Figure 2.21C. Spectral analysis decomposes a time-series into sine and cosine waves of different frequency. The plot of each frequency's variance density (often called the wave energy density or the spectral energy density) is referred to as the periodogram (e.g. see Bendat and Piersol, 1971; Hardisty, 1993). Defining parameters used with spectral analysis are 'band width' which determines the frequency resolution and 'degrees of freedom' which shows the level of smoothing. While increased smoothing shows the spectral peaks more clearly, the confidence interval determining the significance of the peaks becomes smaller. In Figure 2.21C there is an indication of spectral peaks occurring at ~50 and ~7.5 days. The 50 day cycle is consistent with the peaks noted in Figure 2.21A. The 7.5 day peak is probably associated with the well recognised procession of eastward moving low pressure systems to the south of New Zealand (Tomlinson, 1976).

Spatial variation in wave height

No field data or theoretical assessment of wave height change along the study area has been undertaken as part of this study for the following reasons. Detecting wave height variation along six kilometres of coastline was beyond the resources of this project. Furthermore, any change over the relatively short length of the study area would probably be minimal and

A.

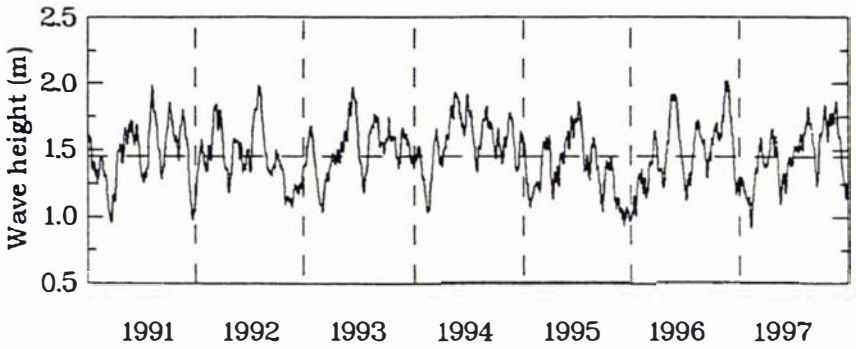

B.

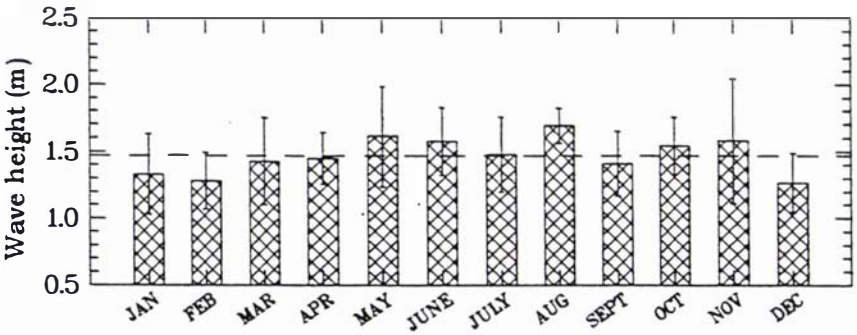

C.

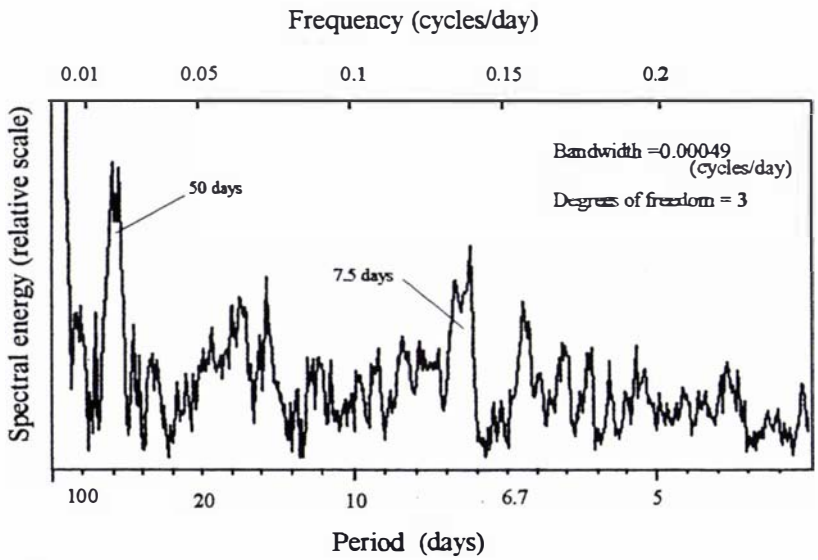

Figure 2.21 Wave height variation at Wanganui during the study period. Data were collected daily using the line-of-sight method described in the text and the raw data are depicted in Appendix F. Figure A shows the result of a 31 point running mean. Figure B shows the mean monthly wave height and corresponding range. The dashed horizontal lines in A and B mark the mean line-of-sight wave height. The periodogram in Figure C depicts the spectral energy for the daily wave height data.

therefore unlikely to cause differences in NOM characteristics. Nevertheless, the physical boundary conditions described earlier in this chapter show that bathymetric and topographic variation does exist and this could alter incident wave properties along the study area - in particular by differences in wave shadowing, refraction, friction and shoaling.

Wave period

Wave period statistics for the different data-sets are given in Table 2.4. Periods for the Harbour Board and line-of-sight data were obtained by timing the interval between wave-crests. Waverider periods were determined firstly from the spectral peak frequency (period = 1/frequency) and secondly by the time between successive upward directed crossings of the still water level (SWL) by the sea surface.

The descriptive statistics for the Harbour Board data, line-of-sight data and Waverider spectral peak periods are all very similar with minimum values ranging from 3.5 to 5 s, maximum values from 18 to 19.2 s and means from 9 to 10.3 s. Zero upcrossing statistics were consistently below these values, which is a characteristic of the method (Patterson, 1985).

The relationship between Waverider significant wave height and peak spectral period is depicted by the scatter diagram in Table 2.5. This result shows that higher waves (>2 m) correspond to shorter period waves (6 to 10 s).

Spectral analysis of the Waverider records (Patterson, 1992) found that distinct sea and swell populations were almost always present, with the sea waves usually predominating. The populations had a well defined cut-off at 10 to 11 s. Examples of periodograms illustrating this bimodal energy distribution are shown in Figure 2.22. In these examples the sea waves had periods of ~5 s and the swell had periods of ~14 s. Macky et al. (1988) found the time-averaged spectral peak for sea waves was 8 s and for swell it was 14 s. Patterson (1992) found that swell rarely exceeded 2 m and swell only predominated under light wind conditions.

Macky et al. (1988) used the width of the wave energy spectrum as an indicator of the distance waves had travelled from the generation area and concluded that most waves were generated within 320 km.

Table 2.4 Wave period statistics for the Wanganui data-sets described in text.

Name of data	Harbour Board	Waverider	Waverider	Line-of-sight
Method of period determination	Breakpoint counting	Spectral peak	Zero upcrossing	Breakpoint counting
Duration (days)	460	420*	420*	2053
Minimum (seconds)	5	3.5	4	3.5
Maximum (seconds)	18	19	11	19.2
Mean (seconds)	9	10.1	6	10.3

* 37% records lost or unrecoverable

Table 2.5 Two-way frequency distribution for significant wave height and peak spectral wave period for the Wanganui Waverider data-set (see text).

Significant wave height (m)	<4	4	6	8	10	12	14	16	18	>19
5										
4			1 1 2							
3		1 5 13 4						1		
2	9 25 26 6 1 2						2 2	2 1		
1	1 4 22 56 34 8 3 2						5 8	2 2 1	2	1
0	1 2 32 68 73 42 15 14 16						10 7	8 12 6	2	
	6 24 71 97 67 40 38 16 35						21 49	31 27 9	9 5	1
	23 40 88 37 22 42 35 31 42						45 78	55 48 40	19 4	3
	7 3 5 2 7 7 9 12 18						14 17	11 9 13	2	1

Peak spectral wave period (seconds)

Source: Macky (1991)

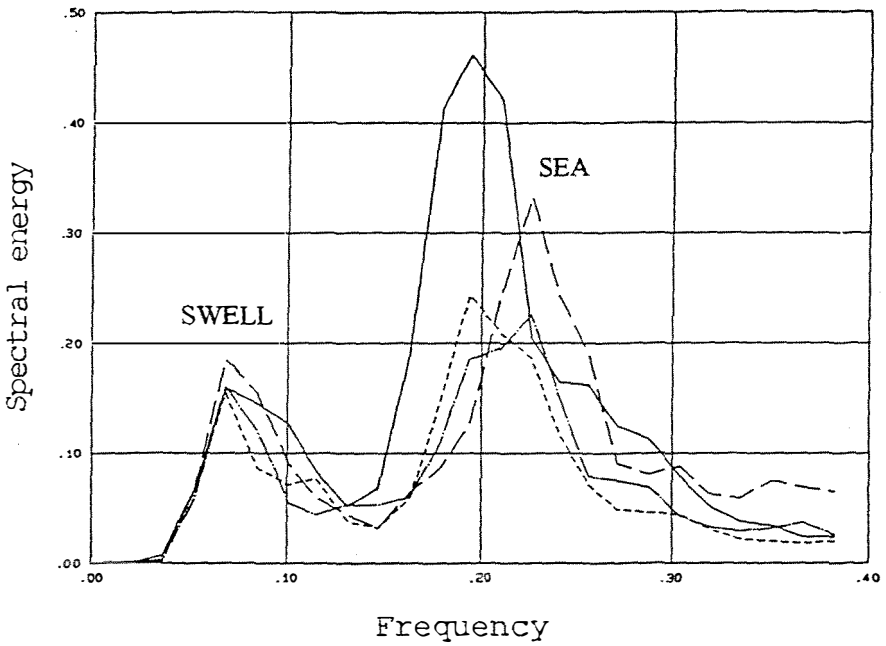

Figure 2.22 Examples of wave spectra from the Waverider data-set (see text). Energy peaks representing the sea and swell components are marked.
Source: Patterson (1992)

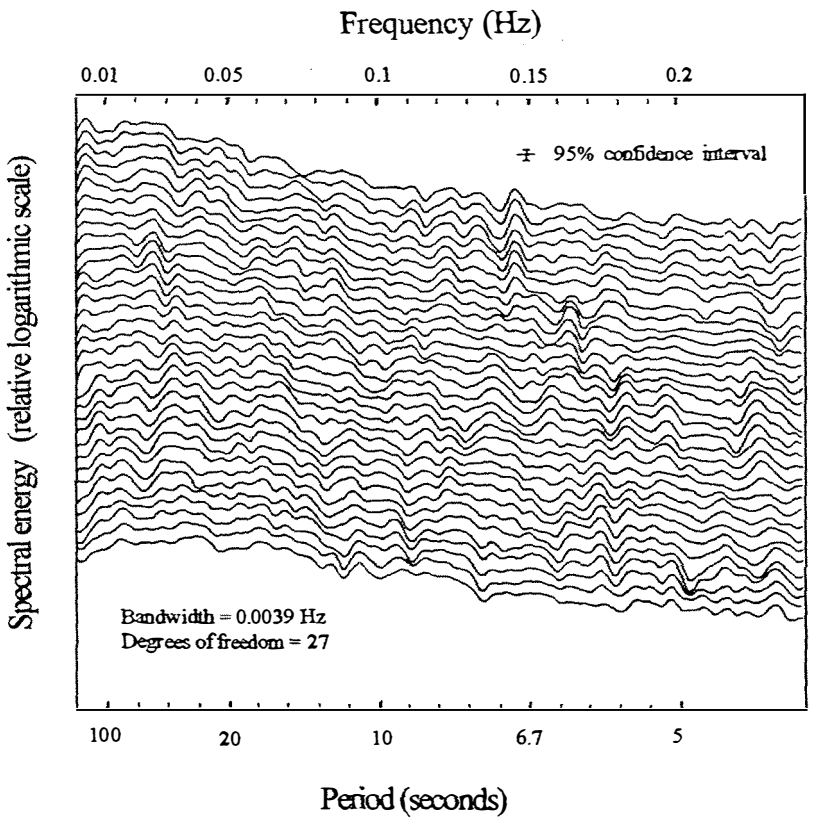

Figure 2.23 Wave frequency spectra from a three hour run-up record. Field sampling was carried out on 31.1.94 using a video camera located in the center of the study area (see Figure 2.4A). Run-up data was obtained using image processing techniques described in chapter 3. Each spectrum uses 34 minutes of record with subsequent spectra being stepped forward by 256 seconds (4.25 minutes).

Wave direction

Waves with 'unlimited' fetch can approach Wanganui from the Tasman Sea between angles of 250 to 300 degrees (from true north) or from the southern Pacific Ocean via Cook Strait between 290 to 300 degrees (see Figure 2.1A). Waves can also approach the study area from angles between 135 and 315 degrees; however, the curvature of the adjacent coastline together with the presence of the South Island restrict fetches to between 15 and 200 km.

Because most waves are generated by local winds, wind data (see section 2.5.2) indicates that the dominant direction of wave approach should be from west of shore-normal. Visual data collected during the Harbour Board monitoring programme in 1968/69 support this assertion, with 35% of waves approaching from shore-normal, 43% from the west and 22% from the east (McLean and Burgess, 1969).

2.5.1.2 Infragravity waves

The coastal geomorphological literature suggests that infragravity waves can play a significant role in foreshore/nearshore morphodynamics. The basis for this assertion lies firstly with the similarity in scale between infragravity water motions and sand-bars (e.g. see Short, 1975; Bowen, 1980; Holman and Bowen, 1982), and secondly because these waves dominate water motions and sediment transport in shallow water during storm conditions (e.g. see Holman 1981, Guza and Thornton 1982). Possible sediment transport mechanisms associated with infragravity waves which influence bar morphology involve drift velocity and orbital motion; these have recently been reviewed by Ruessink (1998). The best location to detect infragravity motions is in a beachface run-up record because an antinode occurs in surface elevation for all frequencies at this location (Sallenger and Holman, 1987).

To determine whether significant infragravity wave motion occurs at Wanganui, spectral analysis was carried out on a three hour run-up record. The field data was collected by video camera (see chapter 3, Figure 3.7) during moderate to high energy conditions on 31.1.94 (see Appendix I). The run-up data were subsequently derived using image processing firstly to identify the swash front (see chapter 3, Figure 3.12A) and secondly to track it through time (see Bailey and Shand, 1994). To observe if and how the spectral peaks changed during the 1.6 m tide shift, periodograms were determined for 34 minute subsets that were each stepped forward by 256 seconds.

This resulted in the stack of 34 periodograms displayed in Figure 2.23. Every eighth frequency spectrum is independent. Statistically significant frequencies in the infragravity range (20 to 200 s) are evident, with peaks undergoing both magnitude change and frequency shifting through time.

2.5.1.3 Seiches

Seiches are standing waves with periods greater than ~ 5 minutes which commonly occur in enclosed or semi-enclosed basins (CERC, 1984). Seiche activity, or seiching, has relevance to the present study in terms of potential influence on the cross-shore location of intensity maxima during morphological monitoring. This situation is considered in detail in chapter 4.

The occurrence and general characteristics of seiching at Wanganui was investigated using sea-level data obtained by pressure sensor and stationary echo-sounder, and also using video-based run-up records. In each situation the raw data was sampled at 4 Hz. Tidal change was subsequently removed using regression techniques and the residuals were assumed to define the seiching.

Figure 2.24A displays a 55 minute time-series of water levels collected using a pressure sensor that was deployed off the Wanganui coast between 30.1.91 and 11.3.91 (Bell, 1991). The pressure sensor was part of an S4 InterOcean instrument pack located approximately five kilometres southeast of the study area in a depth of ~12 m of water (below MSL). Sampling occurred every 10 minutes with logged data comprising two minute averages which removed the incident wave effect and most of the infragravity wave motions. This data will be referred to as the *S4 water-level data-set*. The cyclicity evident in Figure 2.24A identifies seiching with an ~45 minute period and an amplitude of ± 0.5 m. A harmonic at ~22.5 minutes may also be present.

Detail of higher frequency seiche components was obtained from data collected using a stationary echo-sounder. This equipment is described in chapter 3 (section 3.3.1). A two minute 'running mean' filter was applied; this made the data compatible with the pressure sensor output when it is used later in chapter 4. Two such sea-level records were obtained and the filtered results are plotted in Figures 2.24B and C. Periods of ~5 and ~30 minutes are indicated in Figure B, and ~5 and ~12 minutes in Figure C.

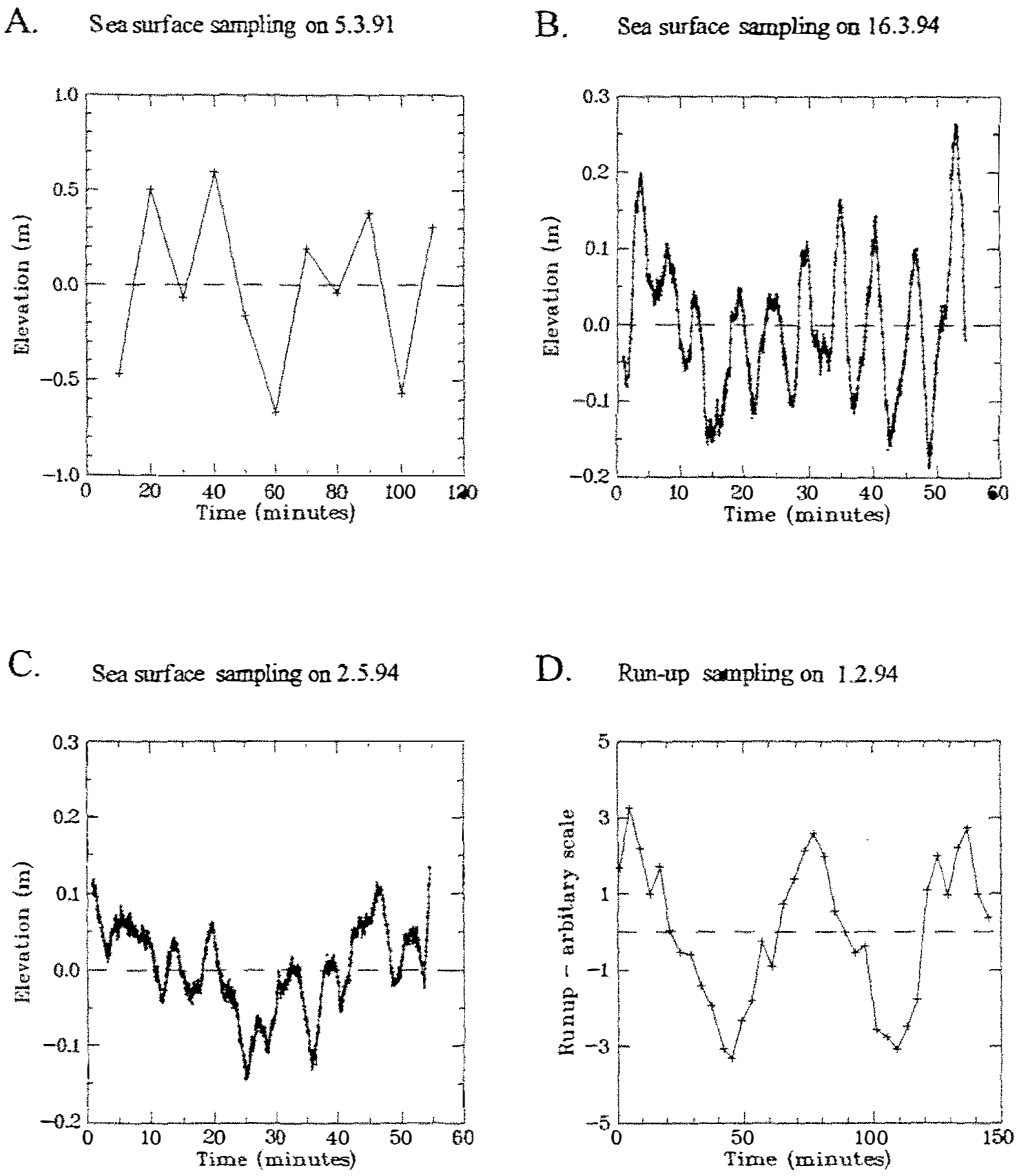

Figure 2.24 Time-series depicting seiche activity at Wanganui. In all cases the raw data was sampled at 4 hertz. Figure A shows offshore sea surface elevation at 10 minute intervals over 110 minutes. Data points were derived by averaging two minutes of data. Figures B and C show 54 minute long offshore surface elevation records after filtering with a two minute running mean. Figure D shows a 150 minute wave run-up record after filtering with a four minute running mean. All elevation measurements relate to the still water level (dashed line) and data-sets were detrended to remove tidal influence.

Detail of the periodicity of longer seiche waves was obtained by analysing a 180 minute run-up record. These data were acquired using the same video and image processing method referred to earlier in section 2.5.1.2. These run-up data were then filtered at 0.0042 Hz (four minutes) to enhance the low period signal. The result is plotted as Figure 2.24D. A well defined oscillation is evident with a period of ~60 minutes. Fluctuations with a shorter period are also apparent.

2.5.2.4 Tides

Tides can be considered as low frequency standing waves. While tidal range is an important control on coastal morphology (King, 1972; Short, 1991; Masselink and Short, 1993), the main significance of tide for the present study lies with its potential influence on the morphological monitoring systems; this is investigated in chapter 4.

The tide at Wanganui is diurnal with a mean spring range of 2.4 m and mean neap range of 0.8 m (calculated from data supplied by the Hydrographer, Royal New Zealand Navy). Chart datum, i.e. the lowest astronomical tide, is 1.8 m below MSL (Ministry of Transport, 1989). Chart datum is used as the elevation datum both for New Zealand Hydrographic Charts and for charts prepared by the Port of Wanganui. However, unless otherwise noted, in this study elevation datum will always be referenced to mean sea level (MSL).

The tidal stream is orientated parallel to the coast and sets to the northwest during the flooding tide and to the southeast during the ebbing tide (Ministry of Transport, 1989) at an approximate speed of 0.2 m/s (Williams, 1985).

Numerical modelling of oceanic circulation in the northern region of the western embayment of Cook Strait by Bowman et al. (1982), showed that surface wind stress and topography could cause substantial deviations in the time of high and low water, in the amplitude of the tide, and in the speed of the tidal stream.

2.5.2 Wind

Stronger winds play a significant role in nearshore and foreshore morphodynamics via their influence on wave size and current velocity (King, 1972; CERC, 1984).

A wind rose with eight directional sectors for Wanganui Airport data is shown in Figure 2.25. The Airport recorder is located five kilometres east of the study area, 500 m inland and elevated approximately five metres above ground level. Winds with speeds > 20 knots (10.4 m/s) approach mainly from west to northwest and to a lesser extent from the south.

Seasonal wind frequencies from airport wind data are shown in Table 2.6. While winds in excess of 20 knots (10.4 m/s) occur most frequently in the spring, strong winds can occur at any time of year.

Additional descriptive statistics for wind conditions at the study site were derived from Airport data obtained from the National Institute of Water and Atmospheric Research (NIWA) for the period 1.1.90 and 10.11.96. Observations were made every three hours and incorporated a ten minute average. The dominant wind direction was calculated at 290 degrees and the 90th percentile (10% exceedence) value was 10.8 m/s. Cross-shore and longshore wind speed components are shown in Table 2.7. These results show that longshore wind speed components are very similar in both directions; for example, the mean northwesterly component was 4.63 m/s and the southeasterly component was 4.46 m/s. However, over two thirds (70.4%) of the longshore components were from the northwest. While onshore wind components have similar magnitudes to the longshore components (for example, the mean value is 4.63) they occurred 47.5% less frequently.

2.5.3 Longshore currents

Longshore currents play a significant role in foreshore/nearshore morphodynamics by driving longshore sediment transport (littoral drift) and influencing morphological configurations (Fox and Davis, 1976; Hunter et al., 1979; Komar, 1976a, 1976b; Short, 1979; Goldsmith et al., 1982). Longshore currents may be generated by wind, waves, tidal stream and ocean currents (Williams, 1985) and these will now be considered with respect to the Wanganui coast.

Table 2.6 Seasonal frequencies per 1000 observations of winds for specified directions and speed categories at Wanganui Airport, 1977 to 1981. Source: Ministry of Transport (1982).

SPRING (Sep, Oct, Nov)

SPEED (KT) DIR	1-3	4-10	11-16	17-21	22-27	28+	TOTAL
N	17	102	40	7	1	0	166
NE	21	63	4	0	0		89
E	15	42	10	2	0		69
SE	3	26	22	6	1		61
S	5	38	32	15	12	1	102
SW	5	31	4	1	1	0	43
W	5	39	45	45	29	7	170
NW	4	47	101	70	36	5	262
CALM							39
TOTAL	75	389	260	147	79	13	
TOTAL OBSERVATIONS USED							10816

SUMMER (Dec, Jan, Feb)

SPEED (KT) DIR	1-3	4-10	11-16	17-21	22-27	28+	TOTAL
N	15	92	22	6	1		136
NE	17	45	2	0			64
E	10	32	12	1			55
SE	3	34	32	6	2		77
S	4	47	23	7	5	1	88
SW	9	55	6	1	0	0	72
W	5	67	61	49	23	4	209
NW	5	60	86	43	17	1	212
CALM							88
TOTAL	68	431	243	113	49	7	
TOTAL OBSERVATIONS USED							10693

AUTUMN (Mar, Apr, May)

SPEED (KT) DIR	1-3	4-10	11-16	17-21	22-27	28+	TOTAL
N	27	142	27	2			199
NE	46	85	4	0			135
E	28	62	20	2	0		111
SE	8	45	38	8	5	1	106
S	10	34	17	10	8	2	81
SW	10	24	3	1	1	1	41
W	4	28	34	17	12	3	98
NW	5	53	54	17	5	0	135
CALM							94
TOTAL	139	473	196	59	59	8	
TOTAL OBSERVATIONS USED							10612

WINTER (Jun, Jul, Aug)

SPEED (KT) DIR	1-3	4-10	11-16	17-21	22-27	28+	TOTAL
N	21	114	37	6	2	0	180
NE	46	127	12	0			185
E	32	68	15	2	0		117
SE	9	50	37	7	1	0	103
S	7	23	26	26	18	2	102
SW	7	12	5	3	1	0	27
W	5	17	17	11	6	2	58
NW	4	45	62	21	7	1	139
CALM							88
TOTAL	130	455	212	76	35	5	
TOTAL OBSERVATIONS USED							10803

Notes: A zero indicates occurrences <0.5, a blank indicates no occurences, 1 knot = 0.52 m/s

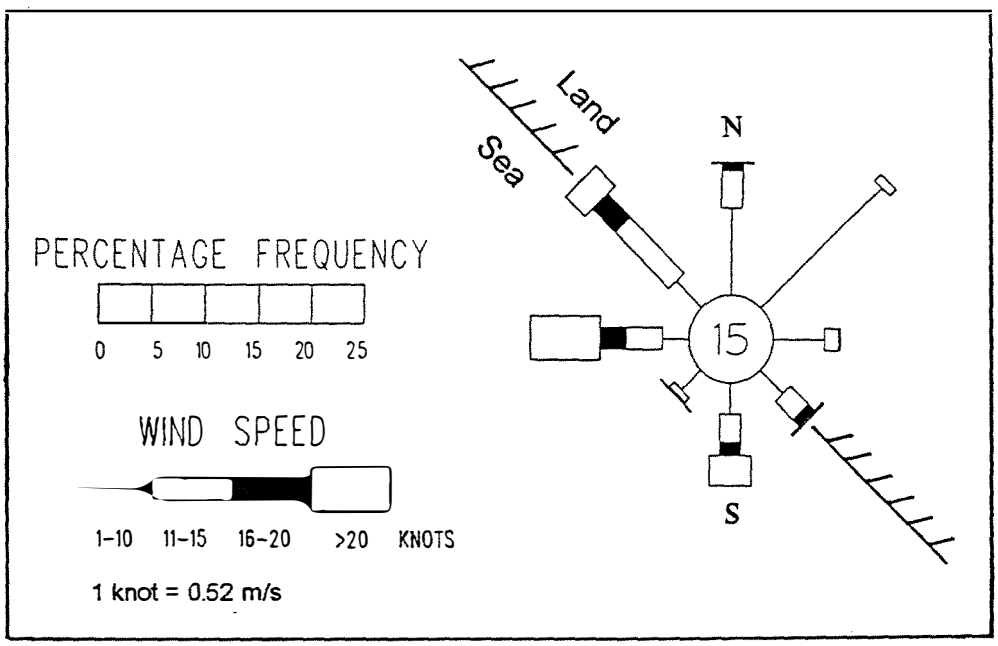

Figure 2.25 Wind rose for data from Wanganui airport during the period 1.1.90 to 1.7.95.

Source: National Institute of Water and Atmospheric Research

Table 2.7 Descriptive statistics for cross-shore and longshore wind speed components for Wanganui wind data. These data were collected at the Wanganmui Airport recording station at three hourly intervals between 1.1.90 and 10.11.96.

Statistic	Offshore (m/s)	Onshore (m/s)	Longshore northwesterly (m/s)	Longshore southeasterly (m/s)
Number	8708	7898	11731	4875
Minimum	0	0	0	0
Maximum	9.85	16.35	18.09	18.48
Mean	2.43	4.63	4.63	4.46
Standard deviation	1.38	2.99	3.33	3.37
50th percentile	2.46	4.14	4.43	3.86
90th percentile	4.43	8.98	9.37	9.49
95th percentile	4.89	9.95	10.90	11.20
99th percentile	5.62	12.42	13.16	14.03

Table 2.8 Longshore current statistics based on offshore and shoreline measurements (see section 2.5.3 for details).

Measurement method	Sampling periods	Current speed statistics (m/s) Minimum	Median	Maximum
Swashzone floats #	17.1.92 to 30.6.92	0	0.26	0.83
Offshore current meter @	22.3.90 to 1.5.90	0.02	0.18	0.77
Offshore current meter *	30.1.91 to 11.3.91	0.02	0.12	0.55

Data sources: # Patterson (1992), @ Bell (1990), * Bell (1991)

Wind and wave induced longshore currents

Wind and waves with oblique approach directions relative to the shoreline are considered to be the primary forcing agents of longshore currents (Komar, 1976b; Hubertz, 1986; Hardisty, 1990; Whitford and Thornton, 1993). Given the predominantly oblique wind and wave approach directions at Wanganui, this is also likely to be the case at this location. Previous longshore sediment transport studies at Wanganui were also based on this assumption (Burgess, 1971; Patterson, 1992).

Tide induced longshore currents

Bell (1991, 1992) found that tidal currents explained between 17 and 28% of the total variation in longshore flows at Wanganui and these currents were overridden by wind induced currents when the wind speed exceeded ~5 m/s. These results were obtained using data collected by electromagnetic current metre. The current metre was installed within the same InterOcean S4 instrument as the pressure transducer used to obtain the sea-level data described earlier (section 2.5.1.3).

Ocean-based longshore currents

The D'Urville Ocean Current has been detected flowing southeast along the Wanganui coast. Brodie (1960) attributed this current to local winds so it will not be considered as a separate morphodynamic influence.

Statistics for longshore currents measured at Wanganui are shown in Table 2.8. The values come from two sources: offshore current meters in the S4 instrument pack, and timing of floats launched from the shoreline. The shoreline data was acquired over six months as part of littoral drift investigations (Patterson, 1992). The maximum current speed near the shoreline was 0.83 m/s and the median value was 0.26 m/s. Such longshore current measurements incorporate the influence of waves, wind, tide level, tidal currents and morphology, e.g. rip feeders (Patterson, 1985). Analysis of offshore data by Bell (1990, 1991) found that up to 96% of the kinetic energy was associated with the longshore component and current speeds reached 0.77 m/s. The median was 0.17 m/s for the 1990 data and 0.12 m/s for the 1991 data. While the shoreline currents were faster, the general similarity indicates wind stress to be a significant forcing agent at Wanganui because wave induced longshore currents can only occur landward of the break-point (e.g. see Komar 1976b, Hubertz, 1986).

Nummedal and Finley (1978) used field data from the South Carolina coast to empirically model longshore currents in terms of other process variables. The longshore component of the wind velocity was the

independent variable explaining most of the observed variance (68.9%). Given the general environmental similarity between that field site and the Wanganui study area (see Tables 5.1 and 5.2) the longshore wind speed component will be used as a surrogate for longshore currents in the present study. However, strong correlation between waves and longshore wind speed at Wanganui ($r = 0.673$, $p << 0.01$) indicates that it may be difficult to separate out the influence of these two forcing agents on net offshore bar migration.

2.5.4 River hydrodynamics

Annual river flow statistics for the Wanganui River at Paetawa, a gauging site located 26 km upstream of the rivermouth, are summarised as follows. The annual seven day low flow is 45.5 m^3/s, the annual mean flow is 224 m^3/s, the annual flood flow is 2221 m^3/s and the 10 year return period flood flow is 3180 m^3/s. In 1975 the mountain-fed headwaters were diverted north into the Waikato River system for hydro generation purposes. This reduced these river flow parameter values by approximately 30%, 8%, 2% and 1% respectively.

Tide-associated influence on river hydrodynamics are now summarised. The tide can affect the Wanganui River for ~37 km upstream from the mouth (Gibb et al., 1962). Salt-wedge penetration ranges between 10.2 km upstream during conditions of spring tide and low river flow (Dahm, 1988) and one kilometre upstream during neap tide and higher river flow (Gibb et al., 1962). The tidal compartment is 9.3×10^6 m^3 for the spring tide range and 3.3×10^6 m^3 for a neap range (Gibb et al., 1962). And finally, Macky (1991) reported peak tidal flows at the mouth of ~1000 m^3/s for the spring tide range and ~300 m^3/s for the neap tide range.

2.6 Relevance for NOM

The material presented in this chapter suggests that the following environmental characteristics may influence NOM at Wanganui.

- Long-term tectonic tilt in the vicinity of the study area could cause offshore sediment transport.

- Coastal adjustment to the rivermouth jetties (constructed between 1884 and 1940) may still affect the study area despite littoral drift now freely bypassing the entrance. Contemporary morphological adjustment

appears to consist of net seaward sediment transport across the study area and deposition within the central and western study area.

- Longshore gradients in cross-shore slope, surf zone width and nearshore width may affect NOM-associated morphodynamics.

- The energy regime may influence NOM characteristics. Incident waves and winds are characterised by relatively high magnitudes (10% exceedence values of 2.15 m and 10.8 m/s respectively) and oblique approach directions. This results in frequent and relatively strong longshore currents. The dominance of these processes is indicated by the morphological configuration of the ebb tide delta, net littoral transport estimates, and sediment characteristics. Surface waves with non-incident periods may also affect NOM characteristics.

Physical and process parameter values identified in this chapter are used when processing data (chapter 3), evaluating the different methods of morphological data acquisition (chapter 4) and analysing NOM characteristics (chapters 5 and 6).

CHAPTER 3 MORPHOLOGICAL METHODS

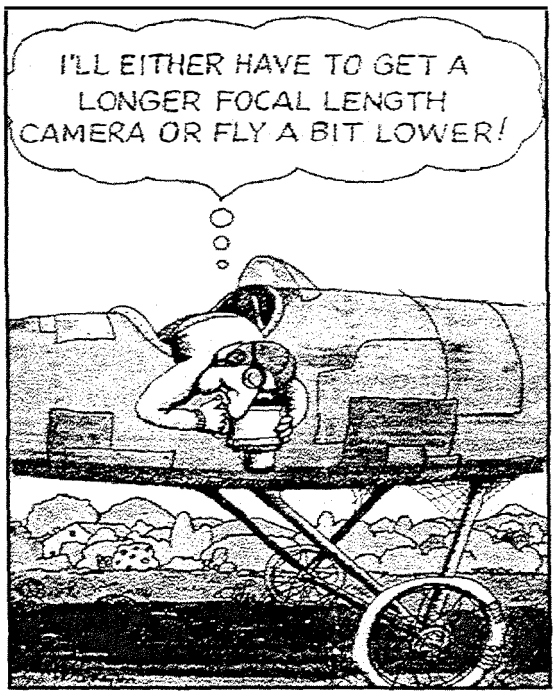

Wolf (1974)

3.1 Introduction

This chapter describes the methods used to obtain and analyse the spatially and temporally extensive data-set required to identify NOM characteristics at Wanganui. In chapter 1 it was determined that data had to be sampled alongshore for approximately six kilometres at ~100 m resolution, across-shore for at least 700 m at ~10 m resolution, and that sampling should occur at two to four weekly intervals. In chapter 1 it was also noted that ground profiling would be unable to provide these data so an alternative approach was developed which utilised photographic field data, together with digital image processing for data abstraction and analysis. A variety of photographic techniques were trialed early in the research programme. These methods, together with the data processing and analysis procedures developed for the project, will be detailed in section 2. As image processing is a somewhat unfamiliar technique in geomorphological research, a general description of this approach is also included in section 2.

The present chapter will also describe the ground profiling methods used to obtain the data required to identify general morphological characteristics of the study area. These characteristics include average cross-shore

profiles, profile variability, cross-shore slopes and associated longshore variability. The resulting parameter values were given in chapter 2 (Tables 2.1 and 2.2). In addition, the ground profile data will be used in subsequent chapters for morphological data error analysis and as a supplementary source of bar-crest data. The foreshore levelling and nearshore/shoreface echo-sounding techniques used in the study will be detailed in section 3.3, along with the procedures used for subsequent data reduction (to MSL) and data analysis.

3.2 Image-based data

3.2.1 Field data

Breaking wave patterns on vertical or oblique aerial photographs have often been used by coastal geomorphologists to define nearshore morphology (e.g. Goldsmith et al., 1982; Short, 1992). As wave breaking is depth-dependent (see footnote 1, page 31), the areas on a photograph with the greatest light intensity represent relatively shallow areas, i.e. areas with relatively high elevation. The relationship between bar-crest location and intensity maximum has been field tested by Lippmann and Holman (1989). To ensure waves were breaking on all the nearshore bars at Wanganui, sampling was carried out under lower tide and higher wave conditions.

Vertical aerial photography
At the onset of the study period field images were obtained using vertical aerial photography. Sampling was carried out between 11.8.91 and 5.8.92 at approximately monthly intervals.

Customised equipment was developed to obtain the vertical aerial photographs (see Figure 3.1). The only available aircraft did not allow for vertical photography through the floor, so a jig was constructed which fitted to an open window. This equipment comprised a frame and a mirror angled at 45 degrees to the principal axis. Use of a window bracket and spirit levels mounted on the frame enabled the lens-tilt to be kept within 3 degrees of vertical. A non-metric 35 mm Pentax SLR Camera was used; photographs therefore incorporate the effects of lens distortion, lack fiducial marks and the internal camera geometry is unknown (Slama, 1980; Torlegrad, 1976; Van Wijk and Ziemann, 1976). However, the optical limitations of the non-metric camera can be satisfactorily overcome by discarding the periphery of the photograph and using analytical photogrammetry when abstracting data (Kolbl, 1976; Chandler and Moore 1989; Chandler et al., 1989).

A.

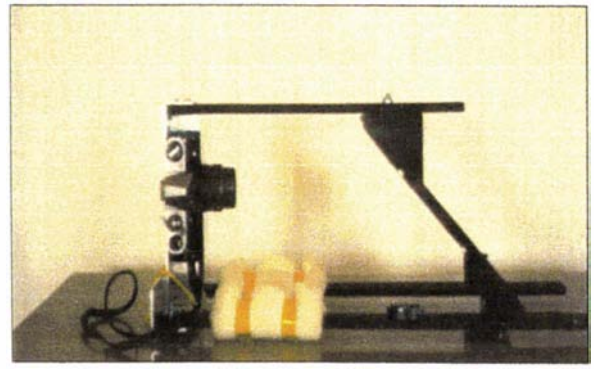

B.

C.

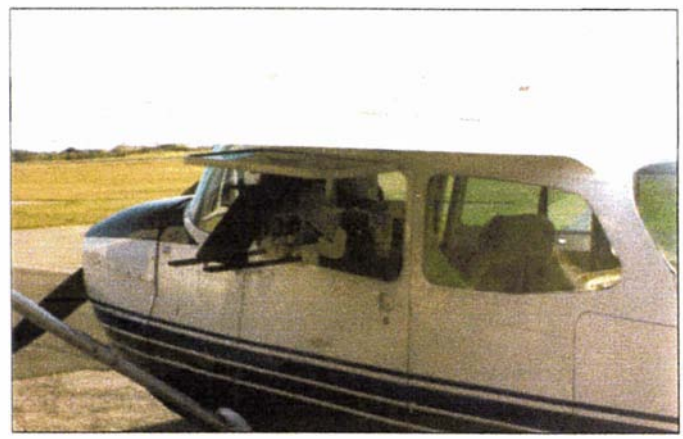

Figure 3.1 Field equipment used for vertical aerial photography. The camera frame, containing a mirror set at 45 degrees to the principle axis, is illustrated in Figures A and B. The window bracket used to position the frame in the aircraft is shown in the foreground of B. Figure C shows the camera frame and window bracket in operational position.

Operational requirements for this system are now described. To capture the entire surf zone a 55 mm focal length lens was used at an altitude of 6000 feet. A typical photograph is shown in Figure 3.2. Approximately 15 photographs were required to cover the 6 km long study zone. A photo run was made flying both up and down the coast to ensure complete coverage. Furthermore, averaging of intensity values on spatially corresponding photographs was carried out during subsequent image processing to (partially) compensate for cross-shore variability in the location of individual breaking waves. This technique is discussed in section 3.2.4.1.

Subsequent transformation of the digitised photographs to map coordinates required at least three ground control points to be visible in each photograph. This type of transformation is referred to as rectification and will be discussed in section 3.2.4. Sixty three control points were established at 100 m intervals along the foredune toe; these points are depicted later in Figure 3.8. Eight of these dune toe ground control points have been marked on the vertical aerial photo in Figure 3.2. Ground control points were also located on corners of buildings and other prominent features. A Topcon GTS-3B Total Station was used to assign geodetic coordinates, with an accuracy of ± 0.05 m, to all ground control points.

Vertical aerial photography had the following limitations. The method was expensive, the plane and pilot were not always available, and optimal sampling combinations of suitable light, cloudless sky, large waves and lower tides occurred infrequently. Variation in the sampling interval of up to 50 days occurred. It was therefore necessary to investigate other photographic techniques.

Oblique aerial photography

A data acquisition method using oblique aerial photography was also developed. The same camera and aircraft used for vertical photography was used and photographs were taken through an open window. The main advantage of oblique photography was that sampling could take place from beneath the cloud-base. This was important because clouds frequently accompanied high wave conditions. An example of an oblique photo is shown in Figure 3.3. A minimum of four ground control points bracketing the scene of interest had to be visible on each photograph for subsequent image processing. Whilst the technique did provide some useful rectified data, it was discontinued because of processing inaccuracies that occurred when ground control points did not bracket the scene of interest. Light reflection from the sea surface could also caused difficulties.

Figure 3.2 A vertical aerial photograph of a section of the study area taken on 20.1.99 from an altitude of 6000 feet. Ground control points used in the rectification procedure (section 3.2.4.1) are marked with small squares. These points are located at 100 m intervals along the foredune toe.

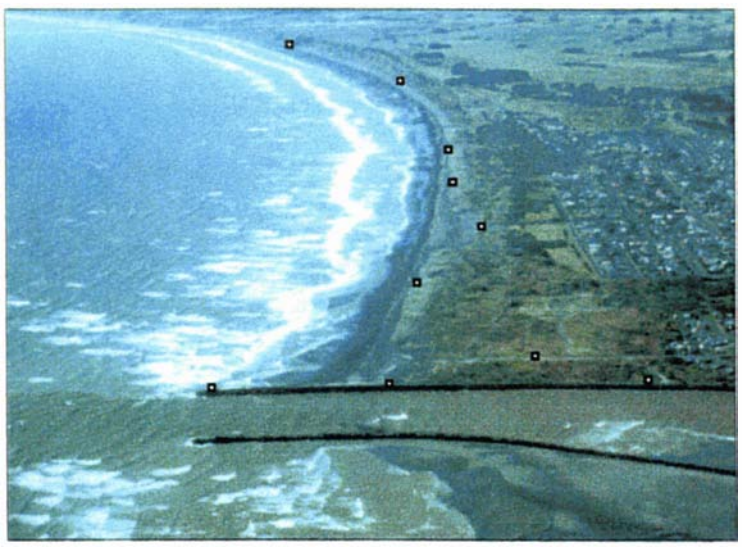

Figure 3.3 An oblique aerial photograph of the study area sampled on 9.1.93 from an altitude of 1500 feet. The small squares mark ground control points used in the rectification procedure (section 3.2.4.2). The Wanganui Rivermouth in the foreground marks the southeastern boundary of the study area and the most distant control point locates the northwestern boundary.

Oblique terrestrial photography

Elevated terrestrial photographic techniques were also trialled early in the study. Between 8.9.91 and 29.7.92 photographic panoramas were taken from a cliff-top location near the centre of the study area. These samples were taken at two to four week intervals using a variety of film types, lenses, filters, exposure times and ground control points. Some rectified data was obtained from these early photos and incorporated into the data-set used to investigate NOM. From 4.8.92 the field method used for the remainder of the study period had been developed. The field equipment used for the terrestrial photographic sampling is now described.

The same 35 mm SLR camera used for the aerial photography was fitted to a camera tripod which was mounted onto a survey tripod (see Figure 3.4A). This mounting arrangement enabled the camera orientation to be quickly changed and also provided support against wind vibration. A large lens hood was used to eliminate lens flare. A Polaroid filter was used to minimise light reflection from the sea surface. A neutral density filter (Kodak Wratten N.D. 4.00/96) was used to enable extended exposure times. A light-proof bag had to be placed over the camera to prevent light leaking in through the housing; this occurred because of the extended exposure times. The purpose of taking long exposure photographs is now discussed.

Photographic exposure times of several minutes were used to average out variations in the sea surface light intensity pattern that were caused by changes in the height and location of the breaking waves. Ocean wave heights tend to have a Raleigh distribution (Hardisty, 1990) so individual waves break at different cross-shore locations. This introduces a random error into the location of maximum intensity and hence an error will occur in locating the associated morphological feature, i.e. the bar-crest. However, this type of error can be filtered out by averaging the intensities from a series of images taken of the same scene. In this study, an alternative method was used to the averaging of multiple oblique terrestrial photographs. By using a neutral density filter and long exposure times, intensity variation associated with wave breaking was automatically averaged out. This method was initially developed by Holman and Lippmann (1987) and they referred to such an image as a *time-exposure*. Lippmann and Holman (1989) compared the location of time-exposure intensity maxima with contemporaneously sampled ground profile bar-crest locations (e.g. see Figure 3.5). While a distinct correlation occurred, changing environmental conditions were found to affect the location of intensity maxima. This situation is considered further in chapter 4 (section 4.3). Examples of an

A.

B.

Figure 3.4 Field equipment used for oblique terrestrial photography. Figure A shows the camera with filter mount, lens hood, release cord, light bag and support tripods. This equipment is in operational position at the camera site which is ~3200 m alongshore from the rivermouth jetties, ~42 m above mean sea level and ~130 m landward of the foredune toe. Figure B shows a typical ground control marker located at the rear of the foredune.

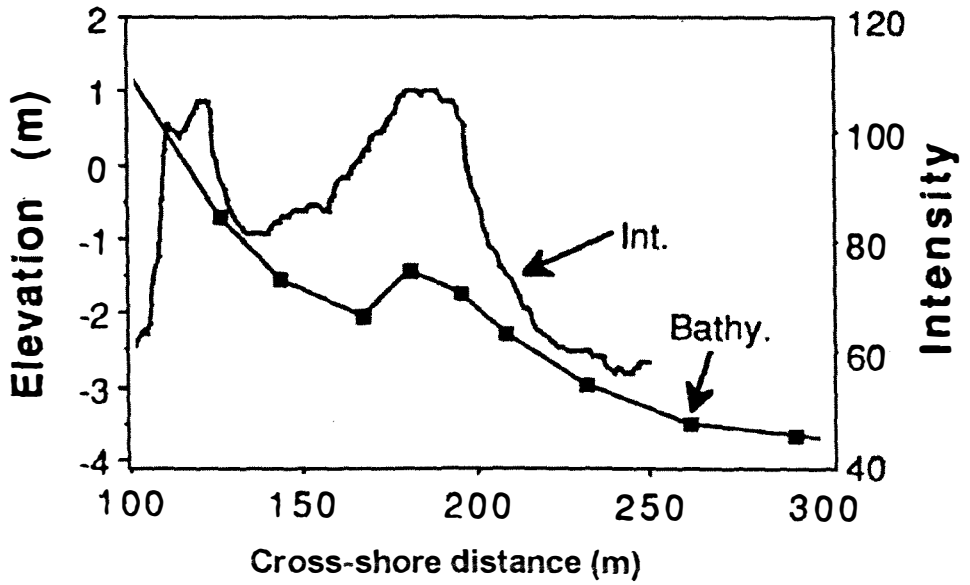

Figure 3.5 An example of conemporaneously sampled local cross-shore bathymetry and intensity profile from the Duck field site (Figure 1.1A). The correspondence between bar-crest location and intensity maximum is illustrated.

Source: Lippmann and Holman (1989)

instantaneous exposure (1/250th second) and the corresponding four minute time-exposure photograph are shown in Figures 3.6A and B respectively.

The camera was located above a benchmark situated on top of a cliff ~42 m above MSL, ~130 m behind the foredune toe and ~3200 m alongshore from the rivermouth. The site is depicted by the asterisk in Figure 2.4A. Nine ground control points were established behind the foredune. Geodetic survey co-ordinates were obtained for the control points and the camera benchmark. The horizon and two ground control points had to be visible in each photograph to enable subsequent rectification. An example of a ground control marker is shown in Figure 3.4B. During the rectification procedure, which will be described in section 3.2.4.3, control points in digitised time-exposure photographs were located manually using the mouse.

Operational requirements for this system are now described. To capture the entire study area a panorama of eight photographs was required. The end photos were taken with a 135 mm lens to increase feature resolution, while a 55 mm lens was used for the four central photographs. Sampling was carried out when wave heights were between two and three metres and sea-level was near low tide. These conditions produced optimum intensity variation on the photos and hence good morphological definition.

A.

B.

Figure 3.6 An instantaneous (1/125th second) exposure (A) and the corresponding four minute time-exposure photograph (B) taken of the southeastern portion of the study area on 22.11.93. The rivermouth jetties are evident in the distance. The small squares mark a ground control point used when running the rectification algorithm (section 3.2.4.3). The second control point required by the algorithm has been cropped off the lower edge of the photos when preparing these figures.

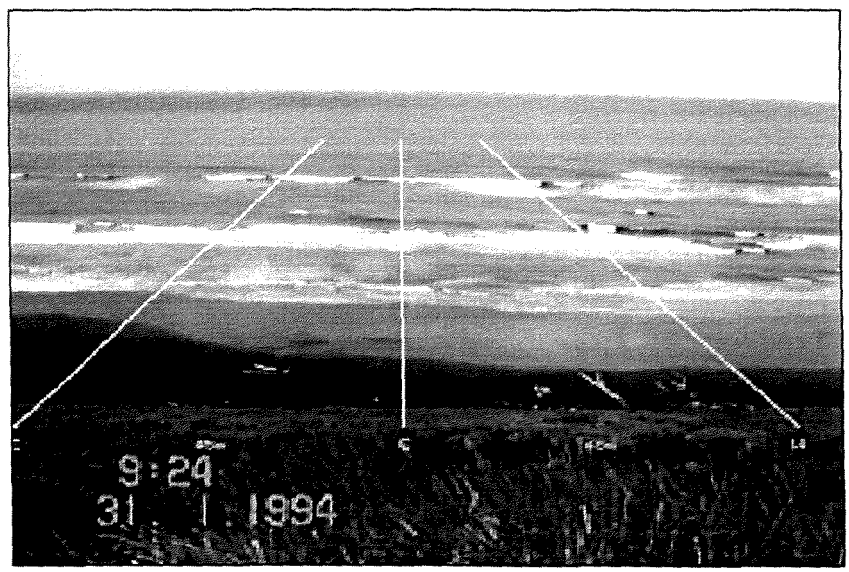

Figure 3.7 A video frame taken on 31.1.94. The camera was directed seaward and three shore-normal transects have been drawn at 100 m intervals.

Furthermore, sampling within these brackets minimised the extent of environmentally induced break-point variation; this is detailed in chapter 4 (section 4.3). To ensure minimal sea-level change during the sampling of a panorama, the photos were taken over the shortest possible time whilst still enabling satisfactory time-averaging to occur. Exposure times of approximately four minutes were used. This time interval was found to produce a relatively stable intensity image, although an exposure time of up to 60 minutes would have been necessary to average out all the low frequency seiche-associated wave modulations identified earlier in chapter 2 (section 2.5.1.3).

Oblique terrestrial video

Video images can be used to produce images similar to time-exposure photographs. This procedure involves the selection of a series of video frames of the same scene and averaging the spatially corresponding intensity values. This technique was first developed by Lippmann and Holman (1989). A video-based field system has the following advantages over a photographic system: electronic transmission of data; cheaper operation; audio input; and the provision of a continual/moving record (Everitt et al., 1988; Lillisand and Kiefer, 1987; Meisner and Lindstrom, 1985). However, an important disadvantage of video is the lower spatial resolution. The alongshore length of the Wanganui study area therefore precluded the use of video to acquire the required morphological bar-crest data for NOM analysis. However, the record continuity of video was utilised in this study to quantify the effect of seiche-associated sea-level change on intensity pattern stability (chapter 4, section 4.3.1).

A Panasonic MS1 Camera was used to obtain the video field data. The same camera location and platform used for the terrestrial photography was used for the video. When collecting video data, however, the camera was only directed seaward. An example of an image scene used for processing is shown in Figure 3.7.

3.2.2 Image processing

3.2.2.1 Background

The processing of images to obtain information began with analogue techniques in the 1950s (Marion, 1991); in particular, optical filters were used to enhance photographic images. Digital image processing became possible in the 1980s with advances in computer technology and these methods

have now found application in most disciplines. Image processing enables the huge amounts of spatial and temporal data contained in images to be rapidly utilised. Image processing also has sampling advantages as the spatial continuity of image data means that a flexible sampling strategy can be adopted. For example "retrodictive" data acquisition is possible, i.e. the required information can be sampled after the areas of major change have been identified (Lane et al., 1993).

3.2.2.2 Digital Image Processing

Digital image processing involves using a computer to apply a sequence of mathematical operations to a numerical representation of an object (Castleman, 1979). The light intensity pattern is sampled in a regularly spaced orthogonal grid to give a series of discrete picture elements referred to as pixels. The light intensity at each pixel is digitised, giving a two-dimensional array of numbers representing the original scene. The resolution of the digitised image is therefore a function of the number of pixels. By convention the assigned pixel values range between 0 (black) and 1 (white).

Applying image processing to a task consists of procedures involving object illumination, image digitisation, and algorithm development and implementation (Bailey, 1985). Image processing is often defined or described by the types of applications for which it is used (see Gonzalez and Wintz, 1987; Marion, 1991). The main applications are:

- Image coding where image processing is used to reduce the volume of data in an image.
- Computer assisted vision where image processing is used to improve pictorial information for human interpretation. Techniques include:
  - mathematical transformations to remove the effects of lens distortion or perspective distortion, or to achieve a particular map projection. These procedures are referred to as image *rectification*;
  - image enhancement which involves processes such as noise reduction, non-linearity compensation, contrast adjustment, and edge sharpening;
  - image restoration recovers information from a degraded image such as a blurred photograph;
  - image reconstruction which restructures information into a more convenient form for display or for further processing.

- Image analysis where image processing is used to extract information contained in the various objects in an image. Such algorithms often incorporate techniques already described for computer assisted vision as pre-processing steps.

3.2.3 The VIPS Image Processing System

The VIPS image processing system was used to carry out the image processing for this project. VIPS, standing for Vax[1] image processing system, is a command-based interactive system that was developed at the University of Canterbury during the early 1980's (Bailey and Hodgson, 1988).

3.2.4 Data processing algorithms

The algorithms used to transform photographs and video into rectified images suitable for analysis are now described.

3.2.4.1 Vertical aerial photographs

Vertical aerial photographs were rectified using rotation and stretch transformations and then scaled to geodetic co-ordinates. This algorithm, named AER_SING.VIP[2] requires a minimum of three ground control points to be entered (using the mouse). It also has a tilt correction option which requires four control points. When insufficient control points were visible in a single photo, adjacent photographs were mosaiced to increase the number of points. If more than three control points were available the additional points were incorporated using a least squares routine to minimise fitting errors.

Individual rectified photographs were synthesised into a single output image using a further routine (AER_AVE.VIP). Where duplicate photos were available from up-coast and down-coast sampling runs, the procedure averages the values from each individual view. An output example of such a synthesised image is shown in Figure 3.8A.

---

1. Subsequently renamed *vision* image processing system.

2. All algorithms written for this project will be referred to by their file name to facilitate subsequent reference and enquiries.

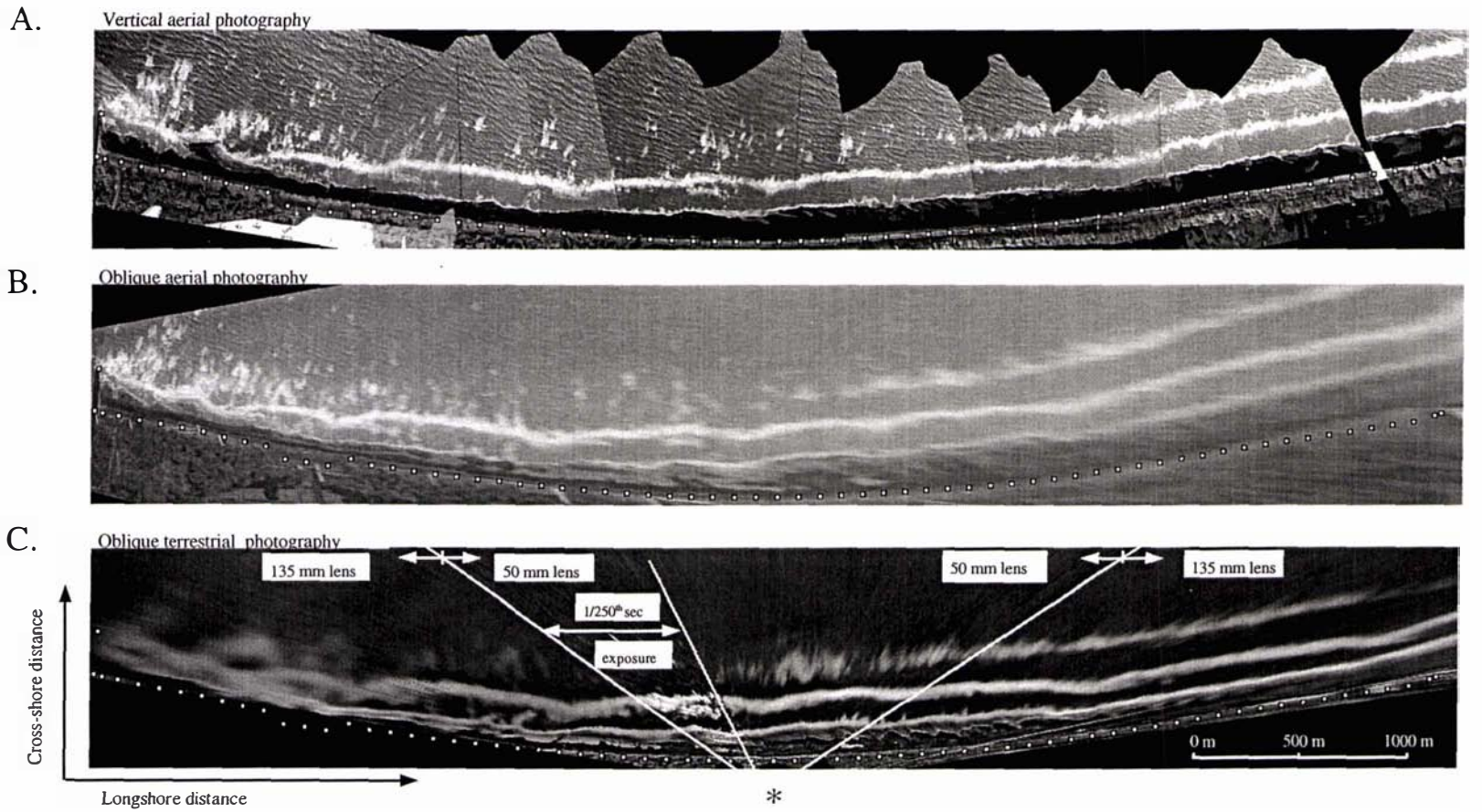

Figure 3.8

Output images of the study area based on the different types of photography and rectification procedures detailed in the text. Figure A shows the output obtained by rectifying and mosaicing a series of vertical aerial photographs sampled on 9.1.93. Figure B shows the rectified output from an oblique photograph also sampled on 9.1.93 (see Figure 3.3). Figure C shows the output from the rectification and mosaicing of a panorama of oblique terrestrial time-exposure photographs sampled on 12.1.93, i.e. three days after the aerial photography. For comparison, one of the input images incorporates an instantaneously exposed photo. The areas photographed with 50 mm and 135 mm focal length lenses are depicted. The asterisk locates the camera position. The row of dots along the base of each figure defines the foredune toe. These points are 100 m apart and were used when rectifying the vertical aerial photographs. The seaward point at the far left of the three images marks the end of the northern rivermouth jetty.

3.2.4.2 Oblique aerial photographs

Oblique aerial photographs were rectified using AER_SING.VIP with the four control point option, i.e. rotation, stretch, scaling and tilt transformations. An example of rectified oblique image output is shown in Figure 3.8B. Note that Figures 3.8A and B were sampled during the same aerial survey and that Figure 3.8B was rectified from the oblique aerial photograph reproduced earlier as Figure 3.3.

3.2.4.3 Oblique terrestrial photographs

Terrestrial photographs were rectified using the algorithm ETM_MAIN.VIP. This programme produced most of the data-set used in the project and has been described in detail by Bailey and Shand (1993, 1996). The relevant sections from these papers have been reproduced as Appendix G. Briefly, the algorithm consists of the following steps.

Pre-processing

Each photo was pre-processed to compensate for density variations associated with varying sun angle, cloud reflection, and glare from the sea surface. Various enhancements were also used to maximise intensity variation, i.e. inferred morphological detail, and to improve longshore coverage.

Perspective correction

Each photo was rectified by solving photogrammetric equations for the co-ordinates of each pixel. Rectification theory for single oblique terrestrial photographs is detailed in Wolf (1974), Slama (1980) and Lippmann and Holman (1989). The photogrammetry used in this project required the following input parameters: the camera position co-ordinates; four ground control point co-ordinates[1]; sea-level; the camera tilt and the lens focal length. The ground control points were indicated by the operator using a mouse. Subroutines were incorporated to automatically obtain the tilt and horizon location using the camera geometry and the dimensions of the digitised input image. Close range terrestrial photogrammetry uses a flat earth assumption. While this produces acceptable results for a study area that is less than 500 metres long, e.g. Bryant (1983), Lippmann and Holman (1990), Lippmann et al. (1993), its use over a range of >3000 m produced longshore errors of up to 300 m. Adjustments for earth curvature were therefore incorporated into the algorithm using the camera height and the radius of the earth.

---

1. The horizon could be used to provide two of these control points.

Post-processing

The eight output images were combined to create a single view or mosaic of the coast. By merging the overlap of adjacent images using a linear spline, artefacts from the photo edges were reduced and in most cases eliminated. A final intensity normalisation routine was applied across the mosaic to minimise inter-photo variation in the background grey shades. An output image example is shown in Figure 3.8C. Note that this terrestrial-based image was sampled three days after the aerial-based images in Figures 3.8A and B, so similar morphologies would be expected.

When evaluating the rectification routine ETM_MAIN.VIP, a systematic error was identified (chapter 4, section 4.3). An adjustment transformation (CORRECT.VIP) was therefore developed and built into the analysis algorithms described in section 3.2.6.

3.2.4.4 Oblique terrestrial video

Time-averaged intensity values along cross-shore transects were obtained by capturing and then averaging strips of intensity data from successive video frames. This produced the equivalent result to capturing a cross-shore slice from a time-exposure photograph. An example of such graphed intensity output associated with the central transect from the scene in Figure 3.7 is displayed in Figure 3.9. This graph resembles the expected profile morphology with intensity peaks corresponding to shallower areas where wave breaking is occurring.

3.2.4.5 Coastline straightening

All types of rectified coastal image were subjected to a straightening transformation (STRAIGHT.VIP). The natural curvature of the study zone's coastline is approximately one unit cross-shore to six units longshore. As morphological analysis would be assisted by using orthogonal axes the straightening transformation was developed. STRAIGHT.VIP fits a piece-wise parabolic curve to the 63 control points located at 100 m intervals along the foredune toe. The image was then incrementally rotated, i.e. unrolled, about the central shore-normal axis to achieve a straight base-line. The X-axis represents longshore distance and the Y-axis represents cross-shore distance. The transformed image was resampled at five metres per pixel alongshore and at two metres per pixel cross-shore. Finally the transformed data was truncated to exclude all points landward of 20 m and seaward of 512 m. This was done as the intensity values in the truncated areas usually did not provide morphological information and the file size

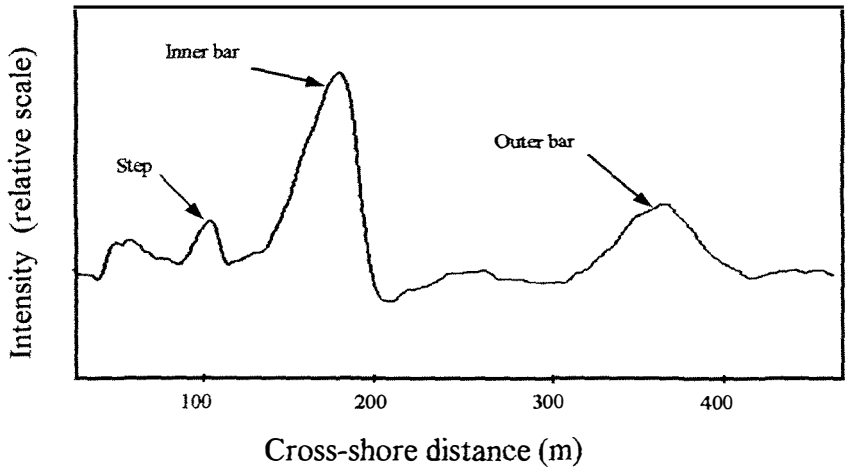

Figure 3.9 A time-averaged intensity profile created by capturing and averaging the cross-shore intensity values from four minutes of video tape. The data are from the same tape used for Figure 3.7 and were captured along the central transect. Morphological features associated with the intensity maxima have been marked.

could be reduced, thereby enabling faster analysis. Examples of a rectified image of the study site together with the corresponding straightened image, are shown in Figures 3.10A and B. The straightened image has a 4:1 cross-shore exaggeration and a 1000 m by 100 m grid overlay. Note that the time-exposure photograph in Figure 3.6B is part of the panorama of photos used to obtain Figure 3.10.

3.2.5 Image-based morphological data-sets

A total of 1894 individual photographs were sampled and rectified. These photographs were taken between 11.8.91 and 22.11.97. One hundred and thirty two mosaiced output images of the full study area and 162 images of part of the study area were produced. The latter images included the central photos sampled with the 55 mm lens. In addition, two series of vertical aerial photos sampled on the 18.12.90 and 5.2.91 by New Zealand Aerial Mapping Ltd. were rectified.

The rectified output images used in this study have been reproduced in Appendix H. The file name for each image is also shown. This code incorporates the date of field sampling, together with abbreviations which identify the field collection method and the spatial coverage. The images have been divided into two groups. The first group is a *monthly data-set* (mean = 29 days, standard deviation = 5.8 days); this is shown in Appendix H(i). Following exploratory analysis, monthly data were found to be

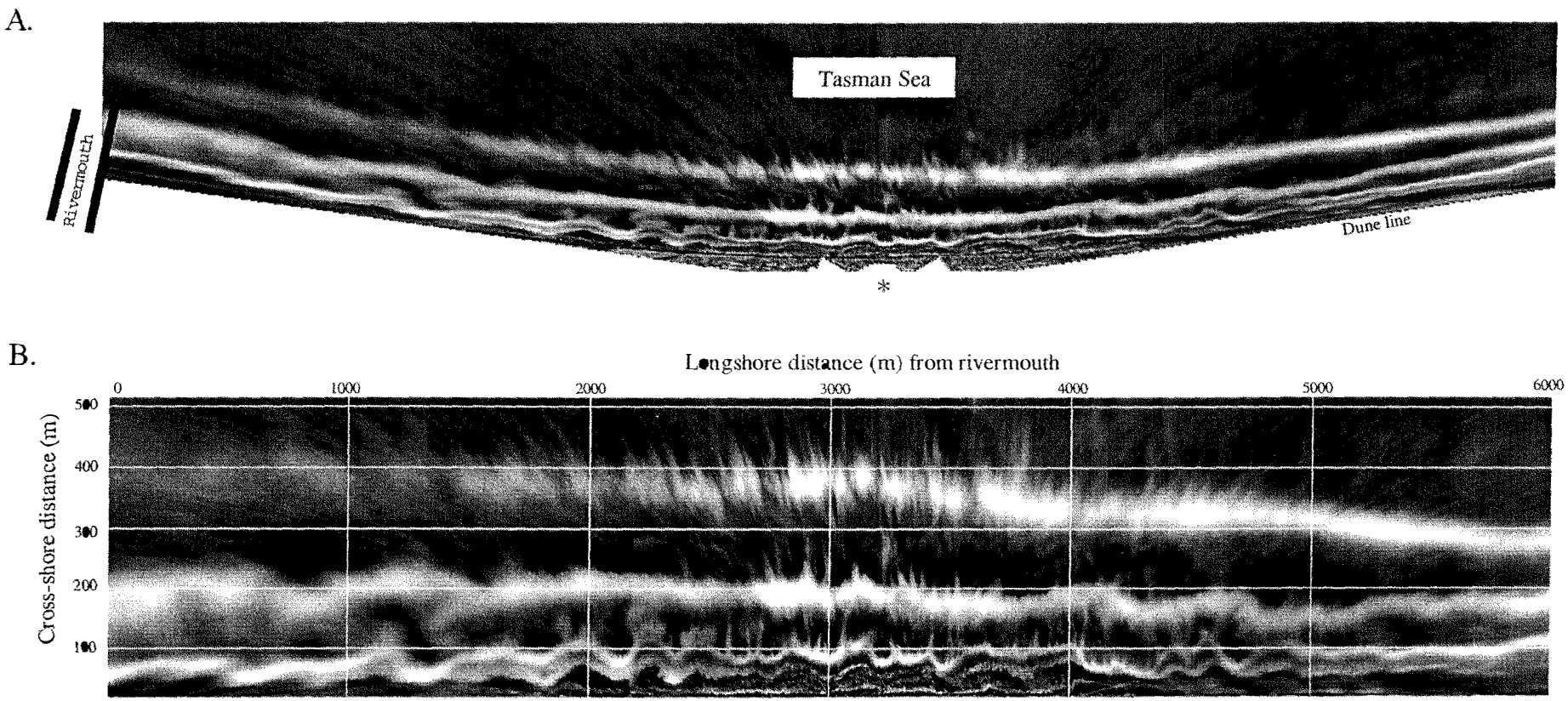

Figure 3.10

Examples of rectified time-exposure images of the study area. Figure A shows a panorama of eight rectified and mosaiced time-exposure photographs sampled on 22.11.93. The asterisk in A locates the camera site. Figure B shows the image after the coast has been straightened. Figure B has a 4X cross-shore exaggeration and has been overlaid by a 1000 m X 100 m grid.

suitable for most of the NOM-associated data analysis. Such exploratory analysis was carried out using fortnightly and weekly data-sets. The second group comprise data with shorter sampling intervals. These data were used either in form/process investigations, in the study of shorter-term morphological change, or for interpolating monthly image data when rapid or complex bar changes occurred. This second group of images is shown in Appendix H(ii).

3.2.6 Data Analysis algorithms

Bar-crest detection

An algorithm was written (PFIT.VIP) to identify the position that best represented the maximum intensity on the cross-shore intensity profile. A bar-crest's location was defined as corresponding to the location of maximum intensity on a rectified image. While a time-exposure image greatly reduces the noise associated with breaking waves on a cross-shore intensity profile, variability could still occur which influenced the selection of the point which was to represent the bar-crest. Figures 3.5 and 3.9 illustrate the localised intensity variation that could occur in the neighbourhood of locations of maximum intensity. A curve-fitting routine (PFIT.VIP) was written to estimate the location of cross-shore maxima in the presence of such noise. This routine will now be described.

The algorithm PFIT.VIP fits a parabola to the intensity points in the neighbourhood of a local intensity maximum and then determines the location of the parabola maximum to represent the bar-crest. Figure 3.11 shows an example of the monitor display while this algorithm is being run. PFIT.VIP has the following features:

- Cross-shore strips or segments of different longshore width could be analysed. The example of a highlighted cross-shore section shown in Figure 3.11 is 50 m wide. The segment is longshore intensity averaged and the resulting profile is plotted on the screen as depicted by the white curve in Figure 3.11. The advantage of processing a wider cross-shore segment is that this minimises the influence of rip-channels which have no intensity maximum, or small-scale rhythmic topography which can displace the intensity maximum either landward or seaward. The selection of the segment width is also determined by the need to maintain a constant longshore (image) resolution; this will be considered further in chapter 4 (section 4.3.3.1).

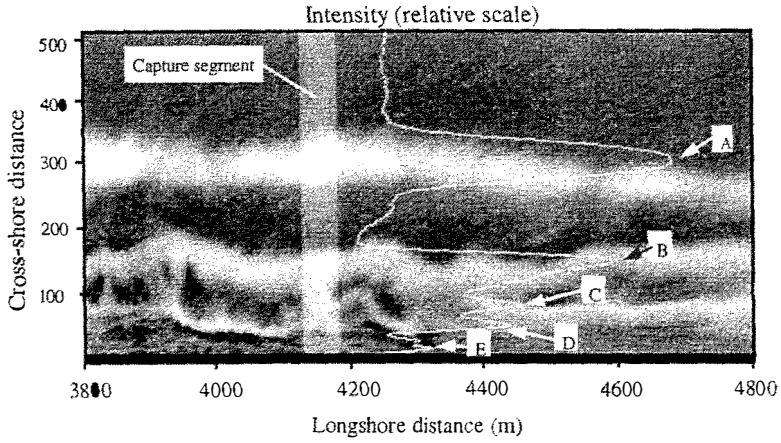

Figure 3.11 An example of the monitor display while running the intensity maxima detection algorithm PFIT.VIP (section 3.2.6). The highlighted vertical band shows the cross-shore segment being processed and the intensity curve depicts the longshore-averaged intensity values within this segment. The arrows (A to E) locate intensity maxima. When the operator detects such a location using a mouse then the algorithm fits a parabola in the neighbourhood of that point.

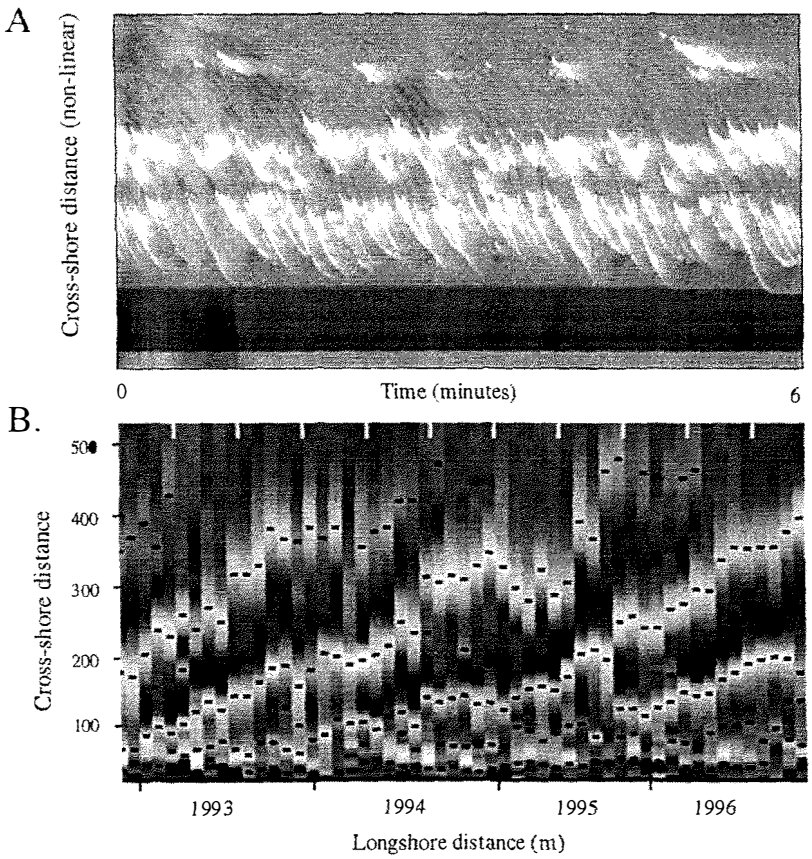

Figure 3.12 Examples of time-stack images. Figure A stacks cross-shore segments of a (non-rectified) video record sampled at four hertz over six minutes. This image contains hydrodynamic information because it enables individual waves to be tracked as they propagate shoreward and shoal, break, reform, break and run-up the beachface. Figure B stacks cross-shore segments of rectified time-exposure images sampled at monthly intervals over four years. This image depicts the behaviour of foreshore and nearshore morphological features. Intensity maxima representing these features are defined by the black rectangles which were fitted using the algorithm PFIT.VIP (see section 3.2.6 and Figure 3.11)

- The operator processes the intensity maximum of interest by pointing and clicking the mouse on the intensity curve, e.g. at locations such as depicted by the arrows in Figure 3.11. The algorithm then fits parabola to the neighbourhood of such a location, determines the point of zero slope and logs the associated cross-shore distance for subsequent analysis. By referring to the adjacent morphology displayed on the monitor, the operator can avoid clicking on intensity maxima other than longshore bars or the low tide step; the latter feature can be used to represent a landward bar when studying NOM. For example, arrows A and B in Figure 3.11 relate to longshore bars and arrow D signals the low tide step. By contrast, arrow C relates to a minor morphological feature (an inner bifurcate[1]) and arrow E relates to intensity artifacts associated with the saturation zone on the exposed foreshore. Interpretation of intensity maxima are considered further in section 3.2.7.

- Curve fitting could be repeated at successive longshore locations. This facilitated more comprehensive analysis. The transect locations are nominated during the programme initiation. After the first segment has been processed the algorithm automatically moves to the next one and the procedure is repeated.

Time-stack images

The time-stack image is constructed by arranging, along the horizontal or x-axis, a set of spatially corresponding cross-shore strips which are abstracted from a sequence of images. The time-stack image therefore depicts a time-history for characteristics within the input image and these characteristics depend on the type of input image being processed. If the raw images are from sequential video frames then the time-stack illustrates how individual waves are transformed as they propagate landward; this provides process or hydrodynamic information (e.g. see Figure 3.12A). By contrast, if the raw images comprise a sequence of time-exposure images, then the resulting time-stack depicts cross-shore bar migration (e.g. see Figure 3.12B). This latter approach was used extensively in the present study to investigate the morphological behaviour associated with NOM.

While the construction of time-stack images is well known to professional image processors, e.g. see Santaney et al.(1994), their use for oceanographic type applications is relatively new. Aagaard and Holm (1989) and Holland and Holman (1993) constructed time-stacks using video images to identify infragravity motions associated with wave run-up. Bailey and Shand (1996) constructed time-stacks using time-exposure images to identify bar-crest migration patterns.

1. Bar biurcation is a type of morphological behaviour described in chapter 6 (section 6.1).

The algorithm MORPHSTK.VIP was written to create the time-stacks used in the present study. When this programme is initiated the operator must nominate the longshore location of the cross-shore transect to be analysed, the segment width over which intensity averaging is to occur, and the set of input image file names. MORPHSTK.VIP also incorporates the transformation CORRECT.VIP which adjusts for the systematic error in the oblique terrestrial rectification routine that was noted earlier. PFIT.VIP was also incorporated into MORPHSTK.VIP so bar-crests could be detected and logged as each strip was processed. The location of each bar-crest is depicted on the output image by a black rectangle (e.g. see Figure 3.12B).

Image sequencing

The algorithm (SEQVIEW.VIP) was written to enable a set of input images to be displayed sequentially. Options include manual or automatic stepping through the sequence of images, a 1000 m X 100 m grid overlay and the highlighting of a particular cross-shore transect. An image sequencing capability was an invaluable aid in chapters 5 and 6 when tracking bar-crest migrations in time-stack images; in particular, where non-linear migration occurred, such as bar bifurcations (chapter 6, section 6.1), or where the sampling interval was long relative to the rate of morphological change. SEQVIEW.VIP was also useful when tracking plan-view morphological behaviour which was often complex, e.g. when identifying bar switching sequences (chapter 6, section 6.5). Image animation or flow visualisation (Kaufman, 1994) is a well recognised aid to research in that by visualising features and tracking their evolution, their nature, behaviour and causal associations may become apparent.

3.2.7 Interpreting cross-shore intensity output

Typical cross-shore intensity curves, e.g. Figure 3.9, show a strong intensity peak within the mid surf zone with weaker peaks to both landward and seaward. Ground truthing by Lippmann and Holman (1989) correlated the nearshore intensity maxima with bar-crests and the landward maximum was related to the 'shore break' and hence occurred 'in the vicinity of the shoreline'. In the present study, sampling was only carried out at times of lower tide level so the shore break would occur in the vicinity of the low tide step. Interpretation of nearshore and foreshore intensity features will now be considered further.

The relatively weak and broad seaward intensity peak in Figure 3.9, is associated with an outer bar located at greater depth and having a more subdued form. Such an outer bar is depicted in Figure 2.12D. Increased bar depth results in more intermittent wave breaking and greater spatial

variation of the break point in the cross-shore direction. This situation is illustrated by the seaward wave breaking in Figure 3.12A.

Strong intensity values associated with mid surf zone bars (e.g. Figure 3.9 and Figure 3.11 arrows A and B) result from the frequent and intense wave breaking that occurs in this region. During lower tide levels (when photographic sampling occurred) these bars are located in relatively shallow water so critical wave height to depth ratios for wave breaking (see footnote 1, page 31) are usually reached. This situation is illustrated by the wave breaking in the mid surf zone of Figure 3.12A.

The relatively weak intensity signal associated with the low tide step (e.g. Figure 3.9 and Figure 3.11 arrow D) occurs because at times of lower tide most wave energy has already been dissipated by wave breaking over the seaward bars.

Further intensity maxima are also evident within the foreshore region of Figure 3.9 and Figure 3.11 (arrow E). As this area was usually exposed during photographic sampling, these intensity peaks signal run-up characteristics and light reflection from the saturation zone, rather than morphological features relevant to this study.

In summary, photographic-based intensity maxima obtained from the Wanganui field data provide a satisfactory representation of surf zone bar-crests including the low-tide step. However, the signal becomes less well defined in the outer surf zone and less reliable as a morphological indicator when located on the foreshore.

3.3 Ground profile data

3.3.1 Field data

Echo-sounding

Nearshore surveys were carried out using a Rathyon XCD 600 (analogue) Echo-Sounder mounted on a five metre long inflatable boat. The field equipment used for the nearshore hydrographic surveys is illustrated in Figure 3.13. The craft was kept aligned with the transect by sighting along range markers set up on the crest and toe of the foredune. Benchmarks were established at these locations and assigned with geodetic position co-ordinates and elevation values relative to MSL.

Cross-shore distances were determined using a Topcon GTS-3B Total Station set in 'tracking mode' and located over the benchmark at the foredune toe. This benchmark was the transect zero point for all cross-shore distance measurements. Surveys began ~1000 m offshore and proceeded to a shoreward limit determined by vessel safety. Distances were relayed to the boat using two-way radios and the trace was 'event-marked' every 20 metres.

A.

B.

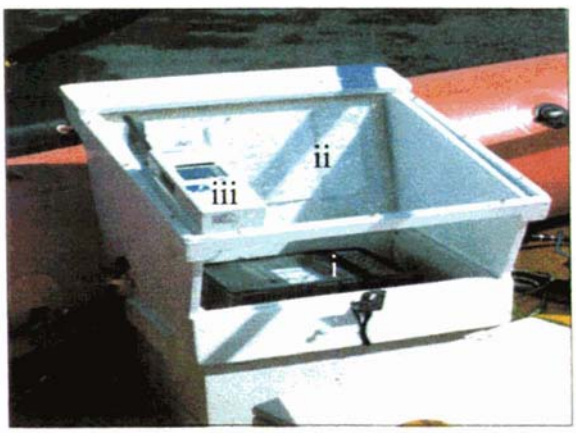

C.

Figure 3.13 Equipment used for nearshore hydrographic surveys. Figure A shows the inflatable (surf rescue) survey boat with electronic distance measuring reflectors in place (i) and the echo-sounder housing (ii) to the rear. Figure B shows the Rathyon Echo-Sounder (i), together with splash-guard (ii) and two-way radio (iii). A survey is underway in Figure C which shows the distance measuring instrument (total station) operator (i) and radio operator (ii). The survey craft (iii) is approaching the shoreline and the (white) seaward range marker (iv) is evident just beyond the distance measuring operators in the foreground.

Regular surveys were carried out along three cross-shore transects located 200 m from the rivermouth (T200), 1500 m from the rivermouth (T1500), and 5000 m from the rivermouth (T5000). The reason that these three transects were selected has been detailed earlier in section 2.3.1. Additional transects were also surveyed when environmental conditions and resources permitted. These transects were located at T50, T100, T150, T500, T1400, T1600, T3000, T4000, and T6000. Examples of the surveyed profiles from some of these transects were depicted earlier in Figure 1.7.

Sampling occurred at three-monthly intervals between 14.3.91 and 9.5.94. However, at times more frequent sampling was carried out. The most comprehensive record was obtained for T1500. Whenever possible, surveying was carried out at times of spring high tide to permit an overlap with the corresponding foreshore survey.

Shoreface/inner shelf profile surveys were carried out using an Elac LAZ 17 CT (analogue) Echo-Sounder mounted on a 30 m long hydrographic launch. A Del Norte SSK Trisponder was used in combination with range markers to determine cross-shore distance. Field equipment used in the offshore hydrographic surveys is illustrated in Figure 3.14. The cross-shore transects used for the shoreface surveys were the same as for the nearshore surveys, i.e. T200, T1500 and T5000. Recording began approximately 4000 m offshore and terminated approximately 500 m from the foredune benchmark. The trace was event-marked every 50 metres. While the shore-face/inner shelf was sampled several times during the study period only the results from the 1.9.92 survey were utilised (see Figure 2.5, Tables 2.1 and 2.2). The 1.9.92 survey was selected as it was carried out under particularly calm sea conditions thereby minimising processing errors. Errors associated with ground profile surveys are described in chapter 4 (section 4.4).

Levelling

Foreshore levelling was carried out using either a Wild NA-O Automatic Level or the same Topcon Total station used for measuring cross-shore distance in the nearshore surveys. Field equipment used for levelling is illustrated in Figure 3.15. A self-support device was designed for the target (staff or prism) to enable surveying to be carried out without a field assistant. A 'foot' was attached to the target to prevent subsidence in the foreshore saturation zone and scour from swash and breaking waves. The foot consisted of a 300 mm steel spike and a device for attaching it to the survey staff. The transect lines and zero points for levelling surveys were the same as described above for the echo-sounding surveys.

A.

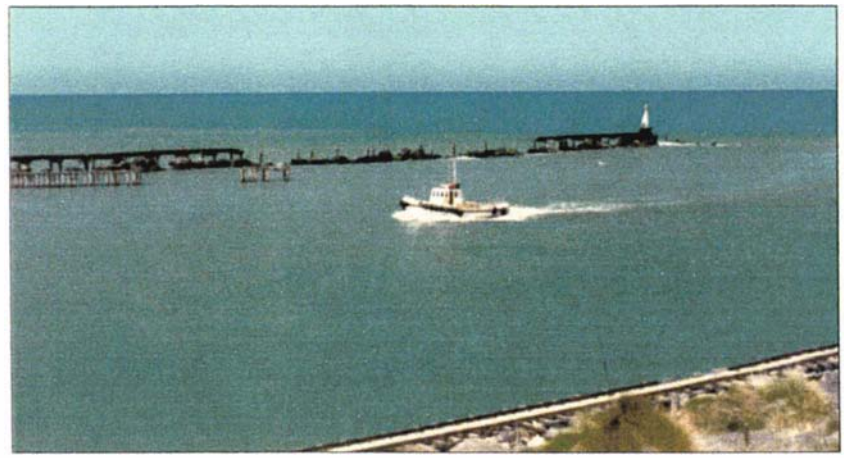

B.

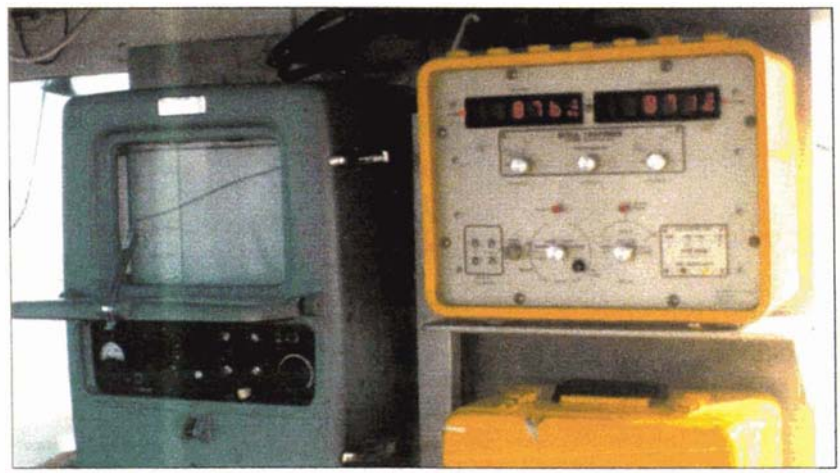

C.

Figure 3.14 Equipment used for outer nearshore, shoreface and inner shelf hydrographic surveys. Figure A shows the 30 m launch entering the Wanganui Rivermouth. Figure B shows the Elac Echo-Sounder (left) and Del Norte Trisponder, and Figure C shows the shore-based ranger markers and distance measuring equipment (on the ground near the vehicle).

A.

B.

C.

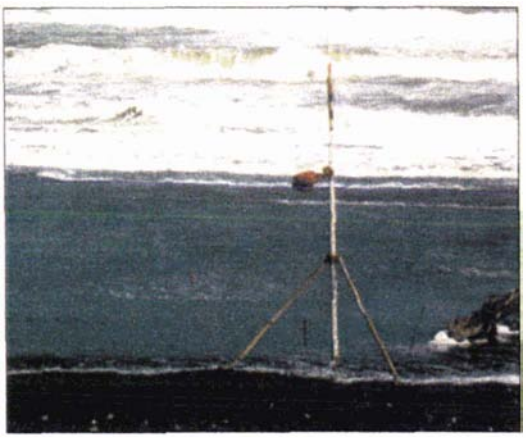

Figure 3.15 Equipment used for foreshore profile surveys. Figure A shows the Wild Automatic Level in use under fair-weather conditions. Figure B shows the Topcon Total Station in operational position. Figure C shows the staff with self-support apparatus being used under storm conditions. Note the pins holding the self-support legs in position and the 'foot' (at the base of the staff), which prevents subsidence. Under severe conditions the guy wire (to right of the staff) is also used for added stability against the wind.

Surveys were carried out at sites T200, T1500 and T5000. When resources permitted additional surveys were done at T500, T1400, T1600, T3000, T4000 and T6000. Surveys extended from the dune benchmark to the safe limit of wading at low tide. Sampling occurred every five metres from the benchmark out to 100 metres with 10 m spacing thereafter. Additional survey points were taken when required to define breaks in slope.

Surveys began on 31.12.89 at T200 and T1500 and on 20.5.91 at T5000. Surveying ceased at all sites on 14.5.94. Surveys were carried out at three-monthly intervals on spring low tides to ensure maximum beach exposure. Additional surveys were carried out when resources permitted. During much of this survey period two to four weekly monitoring was carried out at the T1500 site.

3.3.2 Ground survey data processing

Echo-sounding

All echo-sounded records (traces) were reduced to MSL using standard graphical techniques (see Ingham, 1975). This approach compensated for sea-level and transponder (sensor) depth; it also made some compensation for wave heave, boat pitch and boat roll. The adjusted profile of the sea-bed was then resampled at 20 metre intervals or at closer spacing when necessary to detect breaks in slope.

Levelling

Levelling records were reduced to MSL elevation and distance relative to the dune toe benchmark using algorithms written by the author. Data collected using the automatic level were reduced using PROFILE2.BAS, a programme which incorporated stadia-based distances. Total Station data were adjusted using the programme WDCPROF.BAS.

3.3.3 Ground profile data-sets

Fortyone foreshore records were reduced to MSL. This comprised 18 profile sets at T200, 23 at T1500 and 12 at T5000. These data were surveyed at three-monthly intervals and were used for the profile bundle analysis and morphological zone identification described in chapter 2. The survey dates for this data set are listed in Appendix D(ii).

Fortynine nearshore records were reduced to MSL. This comprised 16 profile sets at T200, 26 at T1500 and 7 at T5000. Monthly data were used either to help interpret images, or where long intervals occurred between

photographic sampling. Three-monthly data were used for the profile bundle analysis and morphological zone identification. Monthly and three-monthly survey dates are listed in Appendices D(i) and D(ii) respectively.

3.3.4 Data analysis

Profile bundle analysis

Each three-monthly set (or bundle) of nearshore and foreshore profiles from each transect were plotted (Figure 2.11) and statistically analysed. The descriptive statistics relating to each cross-shore sampling point were determined and these results were used to identify the morphological characteristics for each transect. These characteristics included the mean profiles (Figure 2.14), the profile standard deviations (Figure 2.15), the cross-shore morphological zone boundaries (Table 2.1) and the average cross-shore slopes for these zones (Table 2.2).

Bar-crest detection

At times during this study it was necessary to locate the bar-crest on an echo-sounded or levelled profile. To assure inter-site consistency, the method used at the other NOM sites was adopted. This method will be referred to as the *maximum residual method* as it locates a bar-crest by fitting a curve to the profile data points and determining the position where the associated residuals have a local maximum. The maximum residual approach can locate bar-crests when the bar has a subdued form, i.e. there is no discernible minimum depth such as for a low tide step (e.g. Figure 2.12 A), or a subdued outer bar (e.g. Figure 2.12D). This technique was advocated by earlier coastal researchers such as Holman and Bowen (1982). For the Wanganui data, power functions of the general form $y = Ax^B + B$, where y is elevation and x is cross-shore distance, were fitted by least squares to the average profiles. An example is shown in Figure 3.16. The method was also used in this study to determine the location of protuberance maxima on the time-averaged profiles, i.e. to locate 'modal' bar-crests. These results were used when comparing image and ground profile methods for acquiring bar-crest data (chapter 4, section 4.5).

3.4 Summary

This chapter described the image-based methods used to obtain and analyse the spatially and temporally extensive sets of bar-crest data required for determining NOM characteristics. Customised techniques of aerial photography and oblique terrestrial photography were used to collect

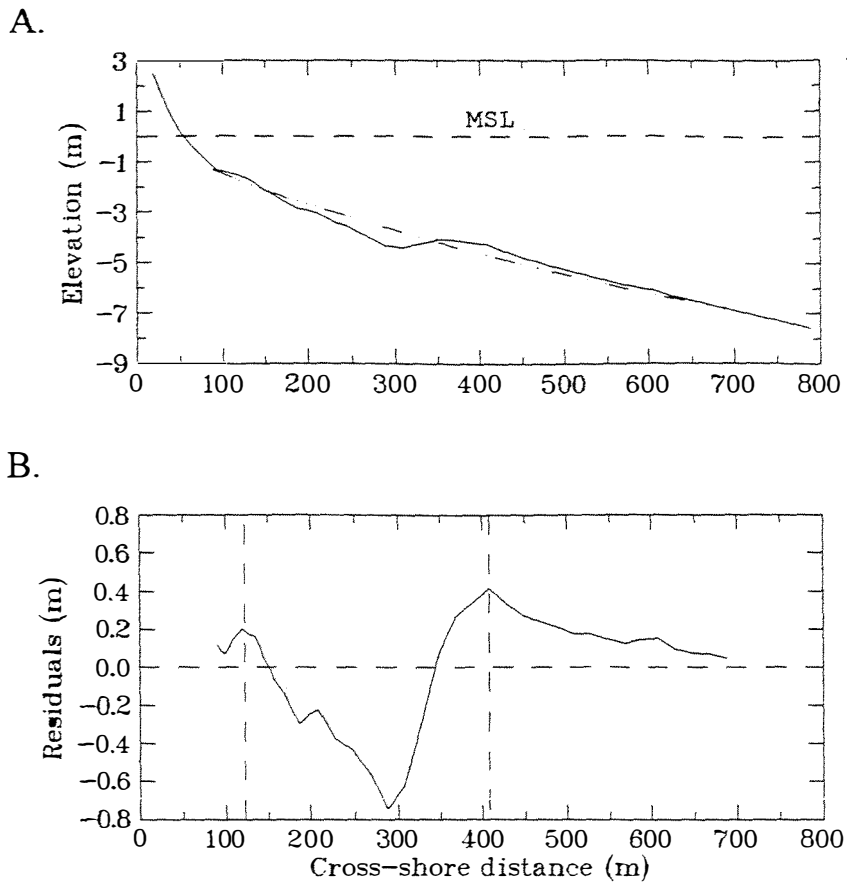

Figure 3.16 Illustration of the maximum residual method of detecting bar-crests from ground profile data. The continuous curve in A shows a cross-shore profile extending 800 m offshore. The dashed curve in A depicts a power function fitted to the profile data using using a least squares routine. Figure B graphs the residuals. The two vertical dashed lines correspond to the maximum positive residual values and these define the bar-crest locations.

images at monthly intervals over a 6.3 year time span. Periods of more frequent sampling were also carried out. Digital image processing algorithms were written to rectify photographs, determine bar-crest location and to facilitate error and data analysis. Intensity maxima obtained from the Wanganui field data were found to provide a satisfactory analogue for surf zone bar-crests and the low tide step. The signal became less well defined in the outer surf zone and was unreliable as a morphological indicator across the foreshore. However, such limitations did not prevent the realisation of the study objectives as the method used to define the zone of systematic offshore bar migration (chapter 5, section 5.3.2) excluded these problem areas.

This chapter also described ground profiling methods. These techniques were used to obtain data with high elevation resolution but lower spatial and temporal resolution. These data were collected to identify the general morphological characteristics at the study site, to help interpret and supplement the image-based data-set, and to assist with the evaluation of image-based errors. The methods consisted of levelling the foreshore, echo-sounding the nearshore and shoreface, and then reducing data to MSL using standard procedures. Three-monthly data were acquired for cross-shore transects located 200, 1500, and 5000 m to the northwest of the rivermouth. At times sampling occurred along other transects and periods of more frequent sampling also occurred. The methods used for the subsequent profile bundle analysis were also described, together with the method used to identify bar-crest location.

The bar-crest data obtained by the various methods described in this chapter are subject to a range of errors and compatibility issues; these matters are addressed in the following chapter.

CHAPTER 4 EVALUATION OF MORPHOLOGICAL METHODS

Measurement is fundamental to the growth and application of science. But making a measurement is not enough. When we come to use the result we must know if it is good enough for our purposes.

Barford (1985)

4.1 Introduction

This chapter assesses the errors associated with both sea surface intensity data obtained from photographs and also with ground profile data derived from echo-sounding and levelling. Such an assessment is required to determine whether apparent changes in bar-crest location are the result of bar migration or measurement noise (errors). The assessment also involves comparison of bar-crest data obtained from different sources, e.g. vertical aerial photographs and oblique terrestrial photographs. Any incompatibility that is identified must be reconciled if data obtained from such different sources are to be 'fused'. Data fusion involves combining differently acquired data sets either to produce a temporally more extensive dataset for a particular site, or to enable data from different sites to be compared (Bailey and Shand, 1997). Data fusion is an important aspect of the present study. The objectives addressed in this chapter are:

- To determine the cross-shore and longshore resolution of intensity-based and ground profile-based morphological data,
- To determine the compatibility between bar-crest data obtained from aerial images, terrestrial images and ground profiles.

A general discussion on errors is given in section 4.2. In section 4.3 the environmental and photogrammetric errors associated with intensity data acquired from aerial and terrestrial photographic images are identified. The cross-shore and longshore intensity resolution associated with data from these two sources will be determined, and the compatibility between aerial and terrestrially derived bar-crest data will then be investigated. Section 4.4 identifies the errors associated with ground profile data and section 4.5 compares intensity-based and ground profile-based bar-crest data.

4.2 Errors

Error concepts and characteristics relevant to this study are illustrated in Figure 4.1.

4.2.1 Definitions and concepts

Barford (1985) described errors as estimates of the uncertainty associated with an observation or measurement and categorised errors as follows:

- Systematic errors are those that remain constant between measurements; for example, where an instrument is miscalibrated. Such errors are defined when a measurement is compared with a known value.
- Random errors are those which differ if a measurement is repeated. Such an error is defined by the dispersion of the individual measurements; the 95% confidence interval about the mean is often used for this purpose. The 'true' value is therefore assumed to lie within the interval, while the sample mean is used as the estimate. If it can be independently established that this estimate differs from the true value then a systematic error is likely to account for the difference.

The following concepts are useful when describing either errors, or their effect on measurements:

- Accuracy refers to how close the measured value is to the 'true' value. Systematic errors and the mean value of a random error therefore influence accuracy.
- Precision refers to how tightly bunched repeated measurements are. The random error estimates the precision of an experiment.
- Resolution refers to the smallest spatial or temporal unit that can be distinguished, i.e. resolved. Factors such as film grain size, pixel size and environmental conditions influence resolution.
- Error notation is usually expressed by writing the ± symbol and then the error (E). Alternatively, the error may be expressed as a length (L) such that L/2 = E. While the ± notation relates more to random errors and the length notation to systematic and resolution errors, ambiguity and other complications arise. For example, a 'system' error incorporates both types of error (see footnote 1 in Table 4.6) or a systematic error may be suspected but it can only be defined in terms of a random error; this is the case for the systematic errors listed in

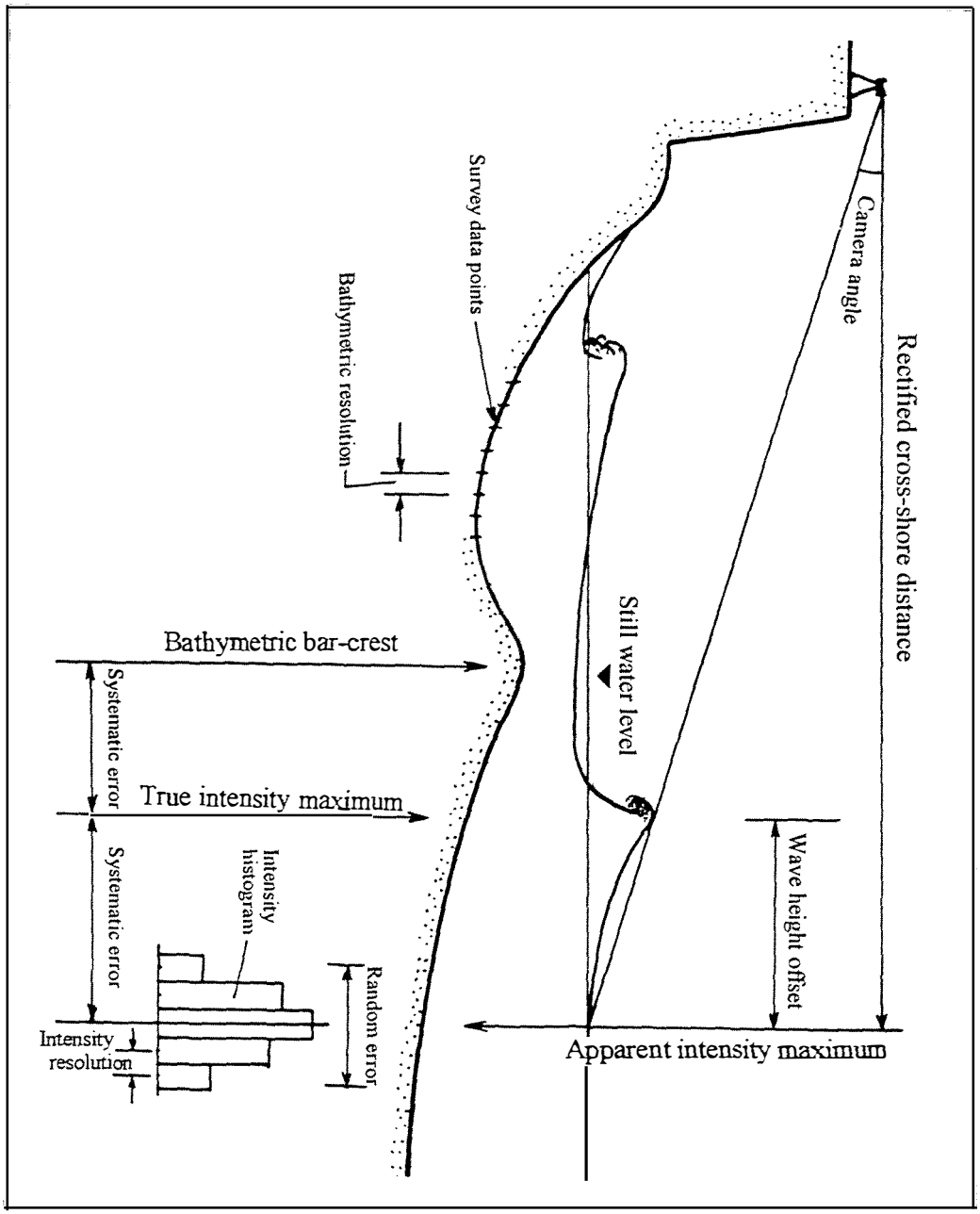

Figure 4.1 Illustrations of systematic errors, random error and resolution which are associated with the location of the sea surface intensity maximum corresponding to the bar-crest evident an the ground profile. Over time the cumulative intensities associated with breaking incident waves produce a stable frequency distribution. The rectified cross-shore location of the distribution centre is used to represent the bar-crest. However, if oblique terrestrial photographs are used as input then wave height causes a seaward offset in the location of the intensity maximum. The difference between this 'apparent' location of the intensity maximum and the 'true' location represents a systematic error. The location of the true intensity maximum may still not correspond with the bathymetrically defined bar-crest and any such difference represents a further systematic error. The dispersion of intensity values in the frequency distribution, e.g. the 95% confidence interval, represents a random error. The resolution associated with bathymetric and intensity measurements are also depicted.

Table 4.7B). In this study errors will be expressed using the most appropriate notation. However, if different types of error are included in the same table then a single type of notation will be used to facilitate comparison.

Where errors are based on a dispersion the 95% confidence interval will be used. When the number of data points is small this value usually approximates the value of maximum dispersion.

4.2.2 Multiple Errors

When data acquisition involves monitoring natural systems or requires extensive data reduction and processing, then measurements will invariably be subject to multiple errors. For example, different errors are associated with each stage of the data acquisition processes described in chapter 3. These errors consist of field-based errors, processing-based errors and transformation-based errors and they will be described later in this chapter.

The combined effect of multiple errors can be determined using the properties of variance addition. Errors are considered to be a form of statistical dispersion and therefore equivalent to the variance. Variance addition is described in texts on statistical analysis (e.g. Larson and Karl, 1986) and, in the context of combining errors, is explained as follows.

* As errors relate to measures of dispersion, it can be shown that:

$$Ec = [E_1^2 + E_2^2 + 2cov(E_1,E_2)]^{0.5} \qquad (4.1)$$

where Ec is the combined error, E_1 and E_2 are error terms and $cov(E_1,E_2)$ refers to the covariance between E_1 and E_2. This relationship holds for any number of error terms.

* For independent error terms the covariance term = 0, and equation 4.1 becomes:

$$Ec = [E_1^2 + E_2^2]^{0.5} \qquad (4.2)$$

* For dependent error terms the covariance term = $2(E_1*E_2)$, and equation 4.1 becomes:

$$Ec = [(E_1 + E_2)^2]^{0.5}$$

$$\text{or} \quad Ec = E_1 + E_2 \qquad (4.3)$$

Variance addition has previously been used in coastal studies for determining combined errors by Saville and Caldwell (1953) and Morang et al. (1997), who investigated depth sounding errors, and Crowell et al. (1991) who investigated shoreline change.

In this chapter, errors are combined using variance addition. Unless otherwise stated equation 4.2 will be used, as in most cases the error terms are independent.

4.3 Image-based errors

Image-based methods of morphological sampling infer the location of bar-crests from the position of light intensity maxima on the sea surface. This section investigates the errors for light intensity maxima location that are associated with environmental and photogrammetric factors. The longshore and cross-shore measurement resolutions are subsequently determined, and comparisons made between data obtained from aerial and terrestrial images.

4.3.1 Environmentally associated errors

The sea surface intensity pattern in the surf zone is primarily a product of light reflection off foam created by breaking waves. Wave height and water depth are the main controls of wave breaking (footnote 1, page 31). Water depth is affected by a range of local environmental conditions including infragravity wave height, seiche wave height, barometric pressure, wind stress and tides (Frisby and Goldberg, 1981; CERC, 1984). Secondary controls on wave breaking include cross-shore slope, wave steepness and wind velocity (footnote 1, page 31). Lippmann and Holman (1989) also found that strong onshore winds could blow foam landward, thereby translating the location of the intensity maxima in a landward direction. The influence of the main environmental influences on wave breaking will be considered further in the following (sub)sections.

The cross-shore variation of intensity maxima location (induced by breaking waves) that resulted from the environmental conditions experienced during photographic sampling, will be referred to as the *environmentally-associated intensity maxima location error.* The error resulting from each type of environmental condition will be referred to as, for example, the *seiche-associated intensity error.* This variation, which is quantified by the 95% confidence interval, is a random error that limits the resolution of the image-based bar-crest data-set. To define the component errors, the

variability of each process condition, e.g. wave height or tide level, that occurred during sampling throughout the study period must first be identified. This is carried out in the following section (4.3.1.1). The cross-shore intensity location error for each environmental condition will then be estimated (section 4.3.1.2) and the results will be discussed in section 4.3.1.3. Finally, it is noted that environmental conditions which affect the sea surface intensity pattern, equally influence aerial and terrestrial-based images.

4.3.1.1 Process data

The data used to identify the variability experienced by each of the environmental conditions during photographic sampling are now described:

- Incident wave heights were determined from daily wave observations (chapter 2, section 2.5.1.1 and Appendix F).
- Infragravity waves were not considered as the four minute time-exposure photographs would largely remove (average out) this influence.
- Seiche wave height was estimated from offshore sea-level records collected by the S4 InterOcean instrument described earlier in chapter 2 (section 2.5.1.3). Data points were logged every 10 minutes. The writer determined seiche elevation by analysing subsamples of nine successive data points. Such subsampling only occurred when the tide was near MSL; the tide shift was then removed by linear detrending. The residuals were assumed to define the sea-level motion, e.g. see Figure 2.24A. Furthermore, samples were only taken when the other environmental conditions were within their envelope of values experienced during photographic sampling - this was necessary as the S4 record only spanned a short portion of the 6.3 year study period. To ensure independent data, successive samplings were separated by at least 24 hours. Times of sampling, together with the associated environmental conditions, are detailed in Appendix I.
- Tide level data was obtained from the Wanganui Port Company's Foxborough (chart) Recorder located within the harbour approximately one kilometre inside the rivermouth.
- Wind and barometric pressure data were obtained from the official (NIWA) recorder located at Wanganui Airport which is approximately five kilometres east of the study area.

The descriptive statistics for the process conditions experienced during photographic sampling are summarised in Table 4.1. Wave heights (mean 1.9 m) were generally greater than the long-term values (mean 1.45 m, see

Table 4.1 Descriptive statistics for the environmental parameter values recorded at times of photographic sampling.

Statistic	Wave height (m)		Tide height (m)	Wind speed components (m/s)		
	Incident	Seiche	from MSL	Onshore	Offshore	Longshore
Sample size	58	14	92	50	16	90
Maximum (m)	2.8	1.26	-0.50	8.6	4.7	15.4
Minimum (m)	1.1	0.25	-1.55	1.2	0.7	0.7
Mean (m)	1.9	0.82	-0.88	4.5	2.9	6.5
Standard deviation (m)	0.38	0.33	0.23	1.6	1.1	3.4
95% confidence interval	1.2, 2.7	0.25, 1.25	-1.4,-0.55	1.2, 7.6	0.7, 4.5	0.7, 13.6

Table 2.3). While wave heights in excess of the long-term 5% exceedence value (2.64 m) were experienced during sampling, photography did not occur under the most extreme conditions. Seiche wave heights had a mean value of 0.82 m and range of 0.25 to 1.26 m. Tide levels during sampling ranged between 1.55 and 0.50 m below MSL which approximates the spring tide to neap tide range (Ministry of Transport, 1989). Offshore and onshore wind speeds (range 0.7 to 4.7 m/s and 1.2 to 8.6 m/s) were substantially lower than the long-term values given in Table 2.7 (0 to 9.85 m/s and 0 to 16.35 m/s). By contrast, longshore wind speed components (0.7 to 8.6 m/s) and were closer to the long-term range of 0 to 18.48 m/s. However, as with wave heights, photographic sampling did not occur under the most extreme conditions.

4.3.1.2 Intensity maxima location error

The change in cross-shore location of intensity maxima associated with each of the above environmental conditions is now determined using an empirical approach. The samples selected for analysis coincided with moderately three-dimensional morphology.

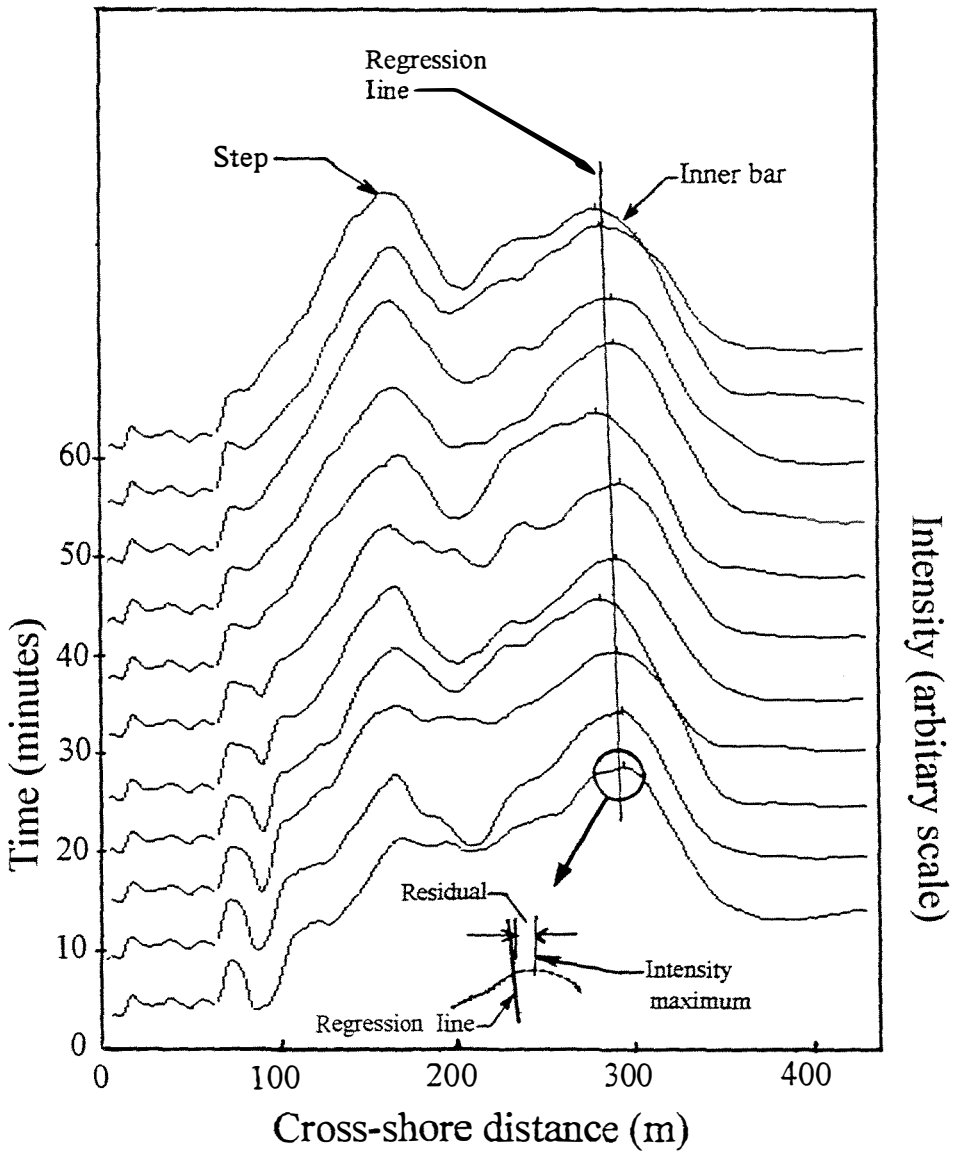

Figure 4.2 An example of a vertical time-stack of intensity profiles illustrating the method used to obtain data for determining the influence of seiching on the cross-shore location of intensity maxima. The intensity profiles were obtained by analysing video frames. Each profile was formed by intensity-averaging four minutes of video data along a shore-normal transect. The straight line represents a linear regression model fitted to the intensity maxima corresponding to the inner bar. The vertical offset of this line is interpreted as representing tidal change during the 60 minutes of sampling. The difference (residuals) between the tide (regression line) and the location of adjacent intensity maxima are assumed to represent seiche influence on the cross-shore location of intensity maxima.

Seiching

The influence of seiche-associated sea-level motion on the cross-shore location of intensity maxima involved the analysis of oblique terrestrial video data. These data were generalised to account for the range of seiching conditions experienced during photographic sampling by a multiple regression model

The video record was obtained on 31.1.94 during lower tide levels and the camera was directed seaward as illustrated in Figure 3.7. The environmental parameter values for 31.1.94 are listed in Appendix I. The video record was partitioned into five minute intervals. For each interval, four minute time-averaged intensity values were obtained along three cross-shore transects spaced 100 m apart (Figure 3.7). Each transect was one pixel (five metres) wide. Figure 4.2 shows one of the resulting stacks of output graphs; in this example the outer bar was cropped when compiling the figure. Cross-shore distances to maxima representing the low tide step, the inner bar and the outer bar-crest were measured and then linear trend (regression) lines were used to identify the tidal influence. This procedure is illustrated for the inner bar in Figure 4.2. The residuals were assumed to represent the seiche-associated cross-shore variation of intensity maxima locations and the 95% confidence interval was used to define the variation, i.e. the seiche-associated intensity error. The maximum error from the three transects for the step, inner bar and outer bar were used to represent these errors; the values were 8.0 m, 18.1 m and 18.0 m respectively.

Unfortunately no offshore seiche wave height data were available for the 31.1.94 so this was estimated using a multiple linear regression model which was developed in the following manner. A set of 20 seiche elevation values, were obtained from the S4 offshore sea-level record. These values included the 14 values that corresponded to photographic sampling conditions, which are represented by the statistics in Table 4.1, together with an extra six values whose associated environmental conditions were outside the photographic sampling range. These extra data points were included to reduce error terms in the regression model. The 20 seiche values along with the corresponding environmental parameter values, are listed in Appendix I. A stepwise routine was applied to these data to obtain the variables and coefficients which optimised the coefficient of determination (R^2) and the standard error of estimate. The resulting model is given as equation 4.4

$$S = 8.965 + .302*H - .014*T + .028*W - .009*P \qquad (4.4)$$

where: S is seiche wave height in metres;

H is the significant wave height in metres;

T is wave period in seconds;
W is wind speed in metres per second;
P is barometric pressure in hectopascals.

The seiche elevation model was evaluated using two sets of independently derived data (see Table 4.2). These independent data were obtained from sea-level records collected on 16.3.94 and 2.5.94 using stationary sonar. This exercise utilised the launch and survey equipment described earlier (chapter 3, section 3.3.1) for collecting offshore profile data. The launch was positioned ~3200 m alongshore from the rivermouth, ~1500 m offshore and at a water depth of ~15 m. The resulting sea surface records are depicted in Figures 2.24B and C. The environmental parameter values for the two samplings are listed in Appendix I and these values were used in equation 4.4 to determine the predicted seiche wave heights which appear in Table 4.2. While these results show qualitative consistency between the predicted and measured values, the predicted values overestimated the measured values (0.44 c.f. 0.34 m and 0.31 c.f. 0.21 m). The model was not not modified, however, as the observed values were within the model's standard error of estimate = 0.233 m.

The predicted seiche elevation for the environmental conditions on the 31.1.94 (using equation 4.4) is 0.4 m. A seiche elevation of 0.4 m therefore corresponds to the (maximum) cross-shore variation of intensity maxima of 8 m on the lower foreshore (low tide step) and 18 m across the surf zone further seaward (inner bar and outer bar) as determined earlier from the video data. It now remains to relate this particular result to the different seiche wave heights experienced during photographic sampling.

Table 4.2 Observed and predicted seiche wave heights (m). Predicted values are from equation 4.4.

Sampling dates	16.3.94	2.5.94
Observations	0.34	0.21
Predictions	0.44	0.31

To determine the seiche-associated intensity error a linear relationship was assumed between seiche height and horizontal intensity translation. The results for the 0.4 m seiche wave height of the 31.1.94 were therefore linearly adjusted to the limits of the 95% confidence interval for seiching, i.e. 0.25 and 1.25 m (Table 4.1). The results in Table 4.3A (row 1) show that the (maximum) seiche-associated intensity error was ~25 m on the lower foreshore and ~56 m across the surf zone further seaward. Note that the first row in Table 4.3A relates to five metre wide segments, this being the minimum segment width possible as one pixel equals five metres - see section 3.2.4.5. Results using wider segments are shown in the following rows of Table 4.3A and these will be considered later in this section.

Tides

The influence of tidal variation on the cross-shore location of the intensity maxima was determined by analysing rectified time-exposure photographs. The images used were sampled on 16.10.93 at tide levels of 0.51 and 1.53 m below MSL. These particular samples were selected because the tide levels approximately bracketed the tide levels experienced during photographic sampling (0.5 to 1.55 m below MSL, Table 4.1). Furthermore, the wave height and wind conditions remained approximately constant during sampling. The environmental parameter values accompanying these samplings are given in Appendix I.

A longshore range of 500 m centred on the camera site was used to detect if and how morphological variability would influence the tidal effect on location of intensity maxima. Cross-shore intensity was sampled every 10 m alongshore. The location of intensity maxima were obtained using PFIT.VIP (chapter 3, section 3.2.6) and these data have been plotted in Figure 4.3. The inter-survey differences were then computed for each longshore segment and the associated descriptive statistics are given in Table 4.4.

These tide-associated intensity variation results (Figure 4.3 and Table 4.4) indicate that an increase in tide level of 1.02 m is accompanied by landward movement of the intensity maxima. The (spatially) averaged intensity maximum translation distance was greatest on the lower foreshore (22.6 m) and least in the outer surf zone (1.2 m). However, substantial variation occurred for cross-shore change between the different longshore sites: from 18.0 m in a seaward direction to 59.2 m in the landward direction. Greatest variability occurred on the lower foreshore with a range of 51.5 m compared with 25.6 to 31.3 m further seaward. This contrasts with the seiche-associated result which had least variation on the lower foreshore and larger values further seaward.

Table 4.3 Variation of cross-shore intensity maxima location associated with environmental conditions (95% confidence intervals in Table 4.1) experienced during the times of photographic sampling period. Table A shows intensity variation associated with seiche wave height change, Table B shows intensity variation associated with tide change and C shows intensity variation associated with incident wave height change. The influence of cross-shore location (low tide step, inner bar and outer bar) and different segment widths (5 m, 50 m, 100 m and 200 m) on the location of intensity maxima are also shown in these tables. The cross-shore location of the bars and step relative to the camera (located 128 m behind the dune toe) are included at the base of each table.

A. Seiche wave height

Segment width (m)	Cross-shore variation of intensity maxima location Outer bar (m)	Inner bar (m)	Step (m)
5	55.80	56.10	24.80
50	40.70	40.90	18.10
100	28.40	28.60	14.00
200	14.00	14.00	6.20
Location (m)	472.0	300.0	235.0

B. Tide

Segment width (m)	Cross-shore variation of intensity maxima location Outer bar (m)	Inner bar (m)	Step (m)
5	22.4	15.4	38.4
50	12.4	12.4	30.8
100	9.7	9.7	22.4
200	3.8	7.4	12.5
Location (m)	489.0	303.0	230.0

C. Incident wave height

Segment width (m)	Cross-shore variation of intensity maxima location Outer bar (m)	Inner bar (m)	Step (m)
5	29.0	31.5	0.0
50	11.6	25.5	0.0
100	0.0	0.0	0.0
200	0.0	0.0	0.0
Location (m)	419.0	314.0	219.0

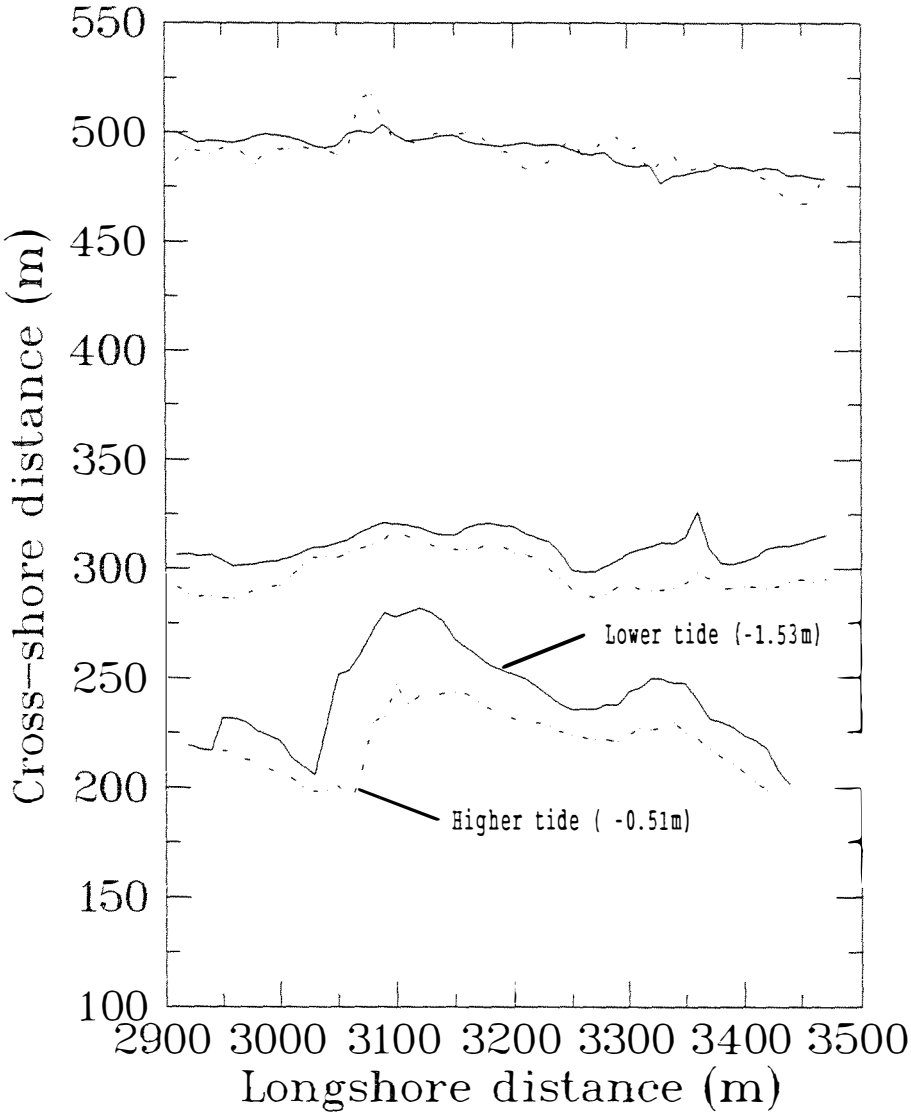

Figure 4.3 Cross-shore location of intensity maxima for a lower tide level of -1.53 m below MSL (solid lines) and a higher level of -0.51 m below MSL (dashed lines). The data points were obtained from rectified time-exposure images sampled on 16.10.99. The three bands of intensity maxima relate to the outer bar location, the inner bar location and the low tide step. Measurements were made along shore-normal transects located 10 m apart in the longshore direction. Cross-shore distance was referenced to the camera site which is located 128 m landward of the foredune toe.

Table 4.4 Descriptive statistics for longshore variation in the cross-shore location of intensity maxima during a tidal change from -1.53 m (below MSL) to -0.5 m (see Figure 4.3). Sampling was carried out on 16.10.93. Positive values relate to change in a seaward direction.

Statistic	Outer bar	Inner bar	Low tide step
Number of samples	57	57	48
Maximum (m)	18.0	-2.3	-7.7
Minimum (m)	-13.3	-28.0	-59.2
Range (m)	31.3	25.6	51.5
Mean (m)	-1.2	-12.4	-22.6
Standard deviation (m)	7.0	5.3	12.2

Table 4.5 Descriptive statistics for longshore variation in the cross-shore location of intensity maxima for a wave height change from 2.27 m to 1.25 m (see Figure 4.4). Sampling was carried out on the 25.10.99 and the 26.10.93. Positive values relate to seaward directed change.

Statistic	Outer bar	Inner bar	Low tide step
Number of samples	60	57	60
Maximum (m)	16.5	25.5	8.0
Minimum (m)	-20.8	-12.4	-6.0
Range (m)	36.3	37.8	14.0
Mean (m)	3.9	2.0	1.6
Standard deviation (m)	7.2	9.6	2.7

The tide-associated intensity errors corresponding to the 95% confidence interval in tide levels experienced during photographic sampling (-1.55 to -0.50 m, Table 4.1), are given in row 1 of Table 4.3B. The values in row 1 are for a segment width of five metres. These values were determined by removing seiche contamination from Figure 4.3 data using equation 4.2 followed by adjustment to the 95% confidence interval using linear interpolation. These results indicate that maximum tidal errors occur on the lower foreshore (38.4 m) with the value decreasing to 15.4 m in the inner surf zone and then increasing to 22.4 m in the outer surf zone.

Incident wave height

The influence of different incident wave height on cross-shore location of intensity maxima was determined by analysing rectified time-exposure photographs. These images were sampled on 25.11.93 when the significant (line-of-sight) wave height was 2.3 m and on the following day (26.11.93) when the wave height had reduced to 1.3 m. These two samples were selected because the wave heights approximate the 95% confidence interval values experienced during photographic sampling (1.2 to 2.7 m, Table 4.1); in addition, similar tide and wind conditions occurred during each sampling. The environmental parameter values for these dates are given in Appendix I. However, seiching and inter-survey bar migration possibly affected the intensity data so these effects will also be considered below.

Cross-shore intensity data were obtained along a 500 m longshore range centred on the camera site with sampling occurring at segments located every 10 m alongshore. PFIT.VIP was used to locate the intensity maxima. These data are plotted in Figure 4.4 and the associated descriptive statistics for the inter-survey differences are shown in Table 4.5. The (spatially) averaged results indicate that a wave height change from 1.3 to 2.3 m causes the intensity maxima to move seaward at all cross-shore locations with changes of 3.9 m in the outer surf zone, 2.0 m for the inner surf zone and 1.6 m on the lower foreshore. However, substantial variation occurred in cross-shore change between the different longshore sites; this variation ranged from 25.5 m in the seaward direction to 20.8 m in the landward direction. In contrast to the tide-associated change (Table 4.4), the wave height-associated change showed greatest variability on the lower foreshore (range 14 m) and least variability across the surf zone (~37 m). Wave height-associated change was qualitatively similar to the seiche-associated change, however, in that it was least on the lower foreshore and greatest further seaward.

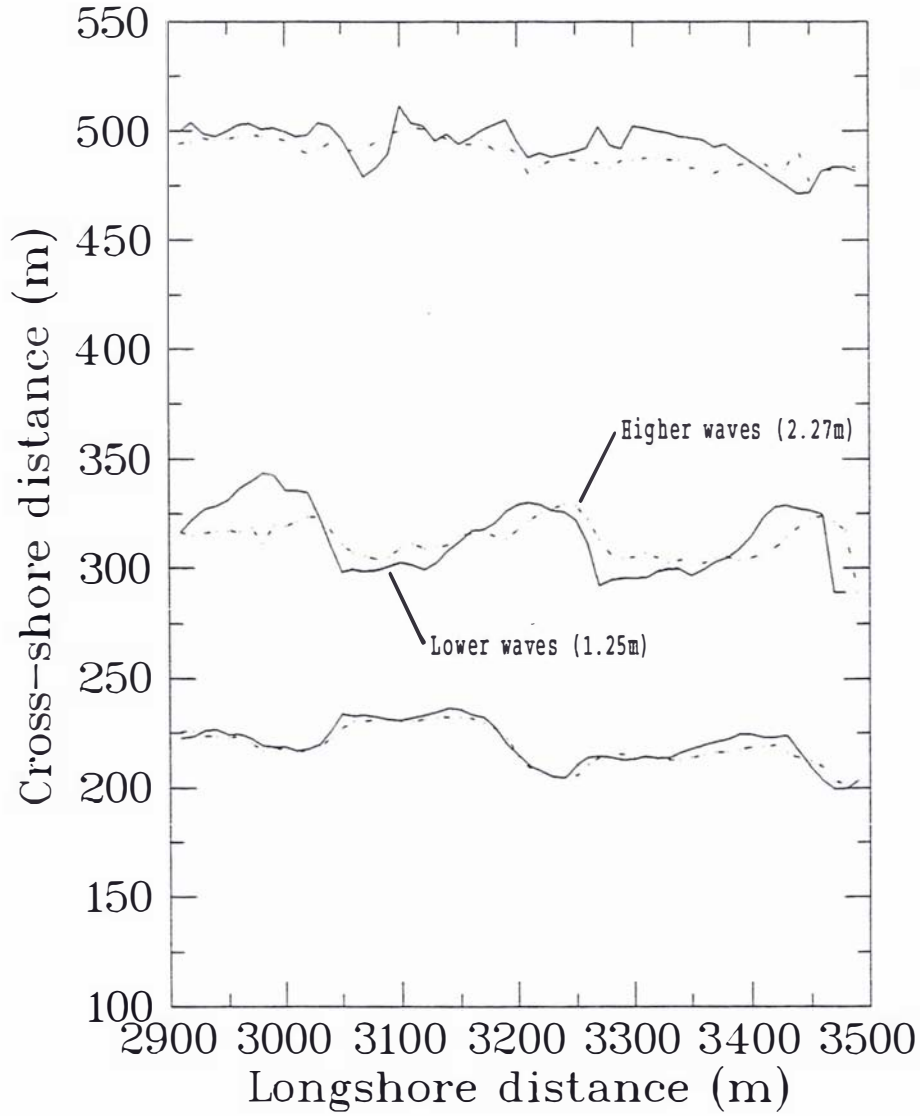

Figure 4.4 Cross-shore location of intensity maxima for wave heights of 1.25 m (solid lines) and 2.27 m (dashed lines). The two sets of data points were obtained from rectified time-exposure images sampled on 25.11.93 and 26.11.93 respectively. The three bands of intensity maxima shown in the figure relate to the outer bar location, the inner bar location and the low tide step. Measurements were made along shore-normal transects located 10 m apart in the longshore direction. Cross-shore distance is referenced to the camera site which is 128 m landward of the foredune toe.

Longshore translation of the morphology between sampling was estimated by cross-correlation analysis. Cross-correlation function plots for the low tide step, inner bar and outer bar data are depicted in Figure 4.5. Maximum correlation coefficients occur at lag zero for the step, minus two for the inner bar and zero for the outer bar. The inner bar morphology therefore migrated ~20 m (two lag units) toward the southeast (rivermouth) between the two photographic samplings. The inner bar data have been adjusted to account for this movement. By contrast the outer bar morphology and the step morphology did not undergo detectable longshore translation between the surveys.

Cross-shore bar-crest migration between sampling times was estimated as follows. Maximum (worst case) inner bar migration rates were determined using the bar migration models of Sunamura and Takeda (1984, 1993) with calibration using storm/recovery data from Duck, North Carolina (Sallenger et al;, 1985). Applying the result from Duck to Wanganui was justified as the two locations have broadly similar environmental conditions (see Tables 5.1 and 5.2). The bar migration rate was then related to beach-face and outer-bar locations by applying inter-bar cross-shore migration results from Duck (Larsen and Kraus, 1992; Lippmann et al., 1993). Finally, the influence of crescentic bar development on bar-crest migration was estimated using relationships identified in data from Duck (Sallenger et al;, 1985). The results showed landward migration of the morphology would have occurred between the two surveys with maximum expected movements of 5 m at the outer bar and low tide step, and 13 m at the inner bar. These morphological effects were subsequently removed from the wave height intensity change data.

The wave height-associated intensity errors corresponding to the 95% confidence interval for incident wave heights experienced during photographic sampling (1.2 m to 2.7 m, Table 4.1), are given in row 1 of Table 4.3C. The row 1 values are for a segment width of five metres. These values were determined by removing seiche and tidal contamination estimates from Figure 4.4 data using variance addition. Because the seiche influence involved a dependency on wave height, a non-zero co-variance term was incorporated into the subsequent error combination computations. The decontaminated data were then adjusted to the 95% confidence interval using linear interpolation. The results show that no detectable variation occurred on the lower foreshore and errors were approximately constant across the surf zone (29.0 to 31.5 m).

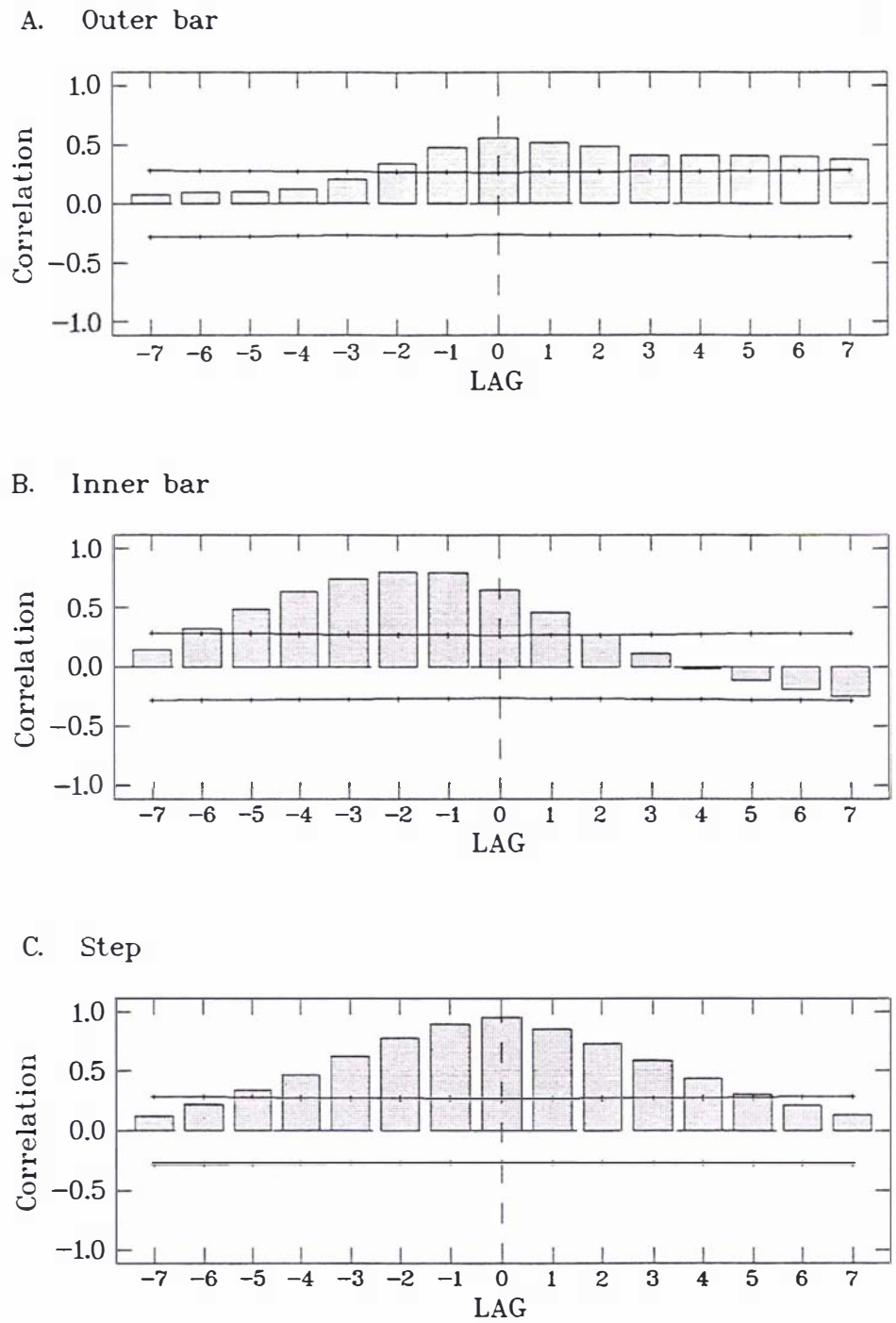

Figure 4.5 Cross-correlation function plots between intensity maxima associated with wave height variation (from Figure 4.4) for the outer bar (Figure A), the inner bar (Figure B) and the low tide step (Figure C). Intensity values were measured every 10 m alongshore, so the lag of one data-set relative to the other was 10 m. The solid lines mark the 95% confidence interval for the probability that the correlation coefficient values have arisen by chance alone. The dashed vertical line locates the correlation at lag zero. If the maximum correlation occurs at lag zero, then the morphologies did not undergo detectable longshore translation between sampling. By contrast, if the maximum correlation occurs at a negative lag, then the second sampling shows a translation toward the rivermouth.

Wind

The influence of wind on the location of intensity maxima was not investigated for the following reasons. Onshore wind speed components experienced during photographic sampling were usually low (range 1.2 to 8.6 m/s, Table 4.1). While much stronger longshore wind components occurred (range 0.7 to 15.4), these side winds were not expected to affect substantially the location of wave breaking and field observation indicated that they did not cause foam redistribution. Furthermore, as noted in the following discussion section (4.3.1.3), some allowance for localised wind stress variation on the location of intensity maxima may have been incorporated into the seiche-associated error.

Barometric pressure

The influence of barometric pressure on the location of intensity maxima was not considered as a separate influence because barometric pressure was incorporated into the seiche-associated error (see equation 4.4). Moreover, the effect of barometric pressure on sea-level change was compensated for by the sea-level parameter value during the oblique terrestrial rectification procedure ETM_MAIN.VIP (chapter 3, section 3.2.4.3).

Segment widths

Error values for environmental variables when intensities were averaged over different segment widths, are given in Table 4.3A to C. The first row in each table gives the result for five metre wide segments which have already been considered. The tide and wave height results for 50, 100 and 200 m wide segments were determined from the time-exposure images used for the five metre wide segments. The results in Table 4.3B and C show that errors reduced as intensity averaging occurred over increasingly wider segments. For tidal change, the widest segment (200 m) reduced the five metre wide segment intensity error values from between 52% and 83% depending on the cross-shore location. Errors associated with the differing wave heights also reduced with increased segment width, with errors being undetectable when the segment was wider than 50 m.

The inter-survey morphological adjustments required for calculating incident wave height-associated intensity errors for increased segment widths (previous paragraph), used a 'proportionality approach' which is considered further in the following paragraphs. For 200 m wide segments, a landward migration of 1.0 m was determined for the outer bar and low tide step, and 2.5 m for the inner bar.

Unfortunately, the only data available to determine seiche-associated errors were from the three (five metre wide) transects that were described earlier. These data were adjusted to give estimates for the wider segments

by using the same proportional changes derived for wave height and tide. The wave height proportions were based on data which did not include the seiche contamination adjustment (used when calculating the values in Table 4.3B). The proportional changes for wave height and tide for each segment width were averaged. The final proportions were as follows: for the 50 m wide segment, the intensity variation was 0.73 of the five metre variation; for the 100 m segment, the intensity variation was 0.51 of the five metre value and for the 200 m segment the intensity variation was 0.25 of the five metre value. The seiche-associated intensity errors for the five metre wide segments (row 1, Table 4.3) were then adjusted by these proportions. The resulting values, given in rows 2 to 4 of Table 4.3A, indicate that an increase in segment width from 5 to 200 m decreases the seiche-associated intensity error from 55.8 to 14 m at the outer bar, from 56.1 to 14 m at the inner bar and from 24.8 to 6.2 m at the low tide step.

Justification for using the 'proportionality approach' to determine intensity location errors for increased segment widths where comprehensive data were unavailable, was based on the following reasoning. At the same location, all processes which influence break point variation are themselves influenced by the same underlying morphology. Changing the segment width, should therefore result in proportionally similar intensity variation for the different environmental variables.

4.3.1.3 Discussion

The relative insensitivity of the location of intensity maxima to changes in the incident wave height (1.6 to 3.9, Table 4.5) is consistent with modelling by Lippmann and Holman (1989). These researchers investigated the light intensity pattern in time-exposure images by firstly assuming that the intensity was proportional to the dissipation of incident waves and then by modelling the energy dissipation over an arbitrary morphology using a random wave model. Their dissipation profile was consistent with the morphology. The weak sensitivity of dissipation maxima to wave parameters was attributed to 'saturation' of the local wave field, i.e. as incident wave height increases, the local wave height increases up to a maximum depth-dependent value and thereafter remains constant.

The greater tide-associated intensity error on the lower foreshore compared with the surf zone, may simply result from differences in cross-shore characteristics; in that the relatively wide, shallow and flat lower foreshore enables the breakpoint to have a greater translation range than can occur across nearshore bars.

Determining the seiche-associated intensity error proved to be particularly problematic. A lack of data acquired specifically for this investigation resulted in limitations and assumptions that in some cases were difficult to justify. The multiple regression model (equation 4.4), which expressed seiche wave height as a function of different environmental variables, had a relatively high standard error of estimate (0.233 m). Testing with independent data (Table 4.2) indicated that the output overestimated the seiche height. This overestimation may be due to residual infragravity water motion in offshore wave data from the S4 recorder (see chapter 2, section 2.5.1.3), or local variation in wind stress on the sea surface. This latter effect was observed by the author on the Wanganui Port Company's tide recorder; a drop in wind speed from ~15 to ~10 m/s over a 30 minute period, was accompanied by a drop in water level of ~0.2 m.

The linearity assumptions used when adjusting the experiment-based incident wave height, seiche wave height and tide-associated intensity errors to the 95% confidence interval experienced during photographic sampling, requires validation. Nonetheless, the apparent overestimation of seiche-associated intensity error resulting from the multiple regression model, together with the relative significance of the seiching component, should compensate for any underestimation of the combined environmental error resulting from the linearity assumptions.

The reduced environmental errors associated with intensity averaging over wider cross-shore segments is probably related to topographic variation. The moderate three-dimensional morphology, which occurred during the different sampling, results in different cross-shore slope characteristics along the study area which in turn leads to longshore variation in wave breaking location and intensity pattern. Intensity averaging over wider segments would reduce the variation between the different segments and hence lower the environmentally-associated intensity error. By contrast, for 2D morphological configurations the longshore variation in the location of intensity maxima was observed to be minimal. The environmental intensity errors for increasing segment widths (Table 4.3) would therefore overestimate the 2D situation.

The only compensatory adjustment made for environmentally-associated intensity errors in data used for investigating NOM was the selection of wider segments for analysis. While this reduced the magnitude of the errors, the error that remained was a resolution limitation that had to be incorporated into the analysis. Finally it is noted that while an increase in the segment width reduced the associated environmental error, this was achieved by trading-off longshore morphological resolution.

4.3.2 Photogrammetric errors

Photogrammetric errors are associated with the processes of recording, measuring and interpreting images (Slama, 1980). The errors considered in this section cover pixel effects, wave offset, rectification and output image sampling. These errors are described for both vertical aerial and oblique terrestrial data acquisition systems and the results are summarised in Table 4.6.

Pixel effects

Photographs were intensity-digitised over a 512 X 512 pixel array. With aerial mosaics this covered ~1000 m of coastline which gave a resolution of approximately two metres per pixel. When the rectification algorithm was applied to the oblique terrestrial images the square pixel shape was transformed into a narrow trapezoidal shape aligned with the optical axis of the camera lens. This produced a blurring of image features which became more severe with increased distance from the camera. The length of the trapezoid, i.e. the error, was ± 8.4 m at 500 m seaward of the camera, while at the far ends of the study site (3200 m from the camera[1]), the error was ± 38.3 m

Wave offset

With oblique terrestrial photographs, the height of a broken wave offsets the intensity maximum and this generates an error in the following manner. The rectification algorithm maps all points (in the pixel array) to the still water level (SWL). The height of wave foam above SWL therefore causes each point to be projected further away from the camera during the rectification transformation. The methods of estimating the wave offset error for both the cross-shore and longshore situations are graphically depicted in Figures 4.6A and B respectively, and mathematically expressed by equation 4.5 which is given in the caption of Figure 4.6. It was assumed that the maximum intensity corresponds to the breakpoint location. It was also assumed that a 2:1 ratio of wave height above SWL to height below SWL occurs. This latter assumption is consistent with non-linear wave theory (CERC, 1984) and such an approach has previously been used for a similar application by Patterson (1985). The wave-crest offset opposite the camera site (500 m from the camera) was ± 14.7 m in a cross-shore direction, while at the ends of the study area the offset was ± 76.8 m in the longshore direction.

Rectification parameters

The measurement precision of each input parameter used in the oblique terrestrial rectification algorithm (see chapter 3, section 3.2.4.3 and

---

1. A study-area length of 6400 m was used in (sub)sections involving photogrammetric error analysis.

Table 4.6 Photogrammetric errors for rectified aerial and terrestrial photographs. Each type of error is described in the text. Aerial errors were constant throughout the study area. Terrestrial errors varied both alongshore and across-shore and the table gives the maximum error at three longshore sites: opposite the camera site; at the river end of the study area; and at the northwestern end of the study area (6400 m from the rivermouth).

Error Sources	Aerial errors (m)	Terrestrial errors (m)		
		Opposite camera	River end	Northwest end
Pixel effects	+/-1.0	+/-8.4	+/-38.3	+/-38.3
Wave offset	0	+/-14.7	+/-76.8	+/-76.8
Rectification	+/-6.1	+/-6.3	+/-69.7	+/-126.5
Raw output sampling	+/-1.0	+/-1.0	+/-1.0	+/-1.0
Straightened: longshore	+/-2.5	+/-2.5	+/-2.5	+/-2.5
Straightened: cross-shore	+/-1.0	+/-1.0	+/-1.0	+/-1.0
Intensity maximum detection	+/-1.0	+/-1.0	+/-1.0	+/-1.0

Notes: 1. For aerial photos the rectification error refers to a 'system error' which includes camera and lens deformation, lens tilt, mosaic alignment, ground control point detection (see section 4.3.2).

2. For terrestrial photos the rectification error is the combined error associated with input parameter precisions (Table 4.7).

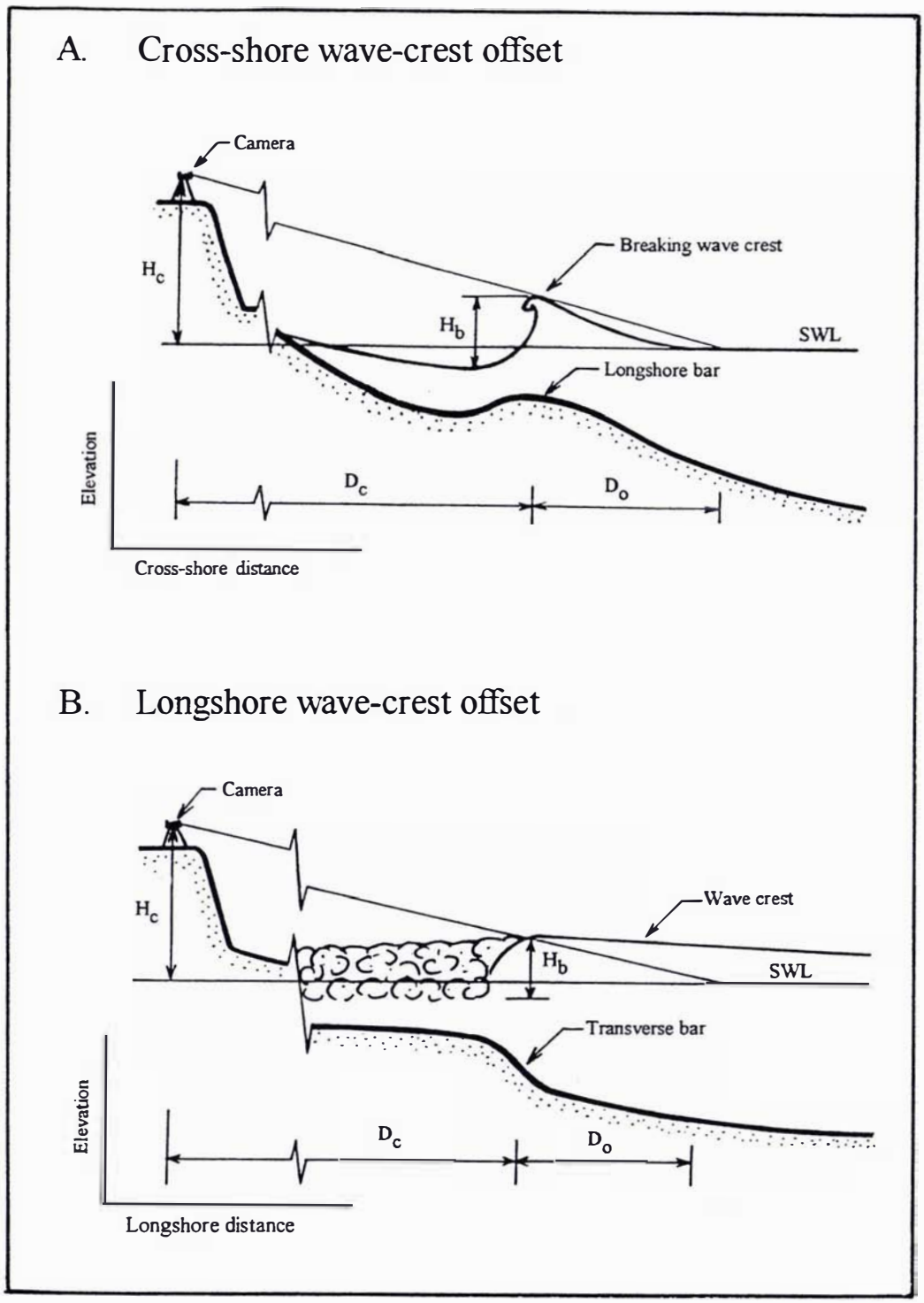

Figure 4.6 Wave-crest offset errors associated with the height of foam from a breaking-wave. Figure A shows the cross-shore offset in the location of the intensity maximum when the rectification transformation maps it to the still water level (SWL). Figure B depicts the longshore offset. The offset error is distance Do and this can be mathematically expressed by:

$$Do = (0.66Hb * Dc)/(Hc - 0.66Hb) \qquad (4.5)$$

where Hb = breaking wave height, Hc is the height of the camera above the SWL and Dc is the horizontal distance between the camera and the breaking wave.

Appendix G) defines an error in the transformed image. These parameters relate to the camera and the ground control point co-ordinates, ground control point detection, horizon detection, photograph edge detection, lens focal length and sea-level. To determine the relative significance of these errors a sensitivity analysis was carried out. This involved running the rectification transformation using the precision measurement of each parameter, while keeping the other parameter values constant.

The parameters, their measurement precision and the associated rectification errors are given in Table 4.7. These errors have been divided into random and systematic groups. Errors increased with increasing distance from the camera, with values of 0 to ± 4.7 m opposite the camera compared with ± 0.05 to ± 49.92 m at the rivermouth end of the study area and ± 0.05 to ± 105.30 m at the northwestern end. The difference in combined error values between each end of the study area resulted from greater atmospheric haze at the northwestern end which reduced the measurement precision from ± 1 pixel to ± 2 pixels. Horizon detection errors (± 20.83 to ± 105.3 m) and sea-level (± 21.74 m) were the largest random errors, while ground control point elevation co-ordinates (± 1.01 m to ± 6.04 m) and focal length (± 4.4 m) were the largest systematic errors. Table 4.6 gives the combined photogrammetric error values, i.e. all random errors and systematic errors. Errors vary across-shore, so values were selected which relate to the maximum error. Opposite the camera the combined error is ± 6.28 m, at the rivermouth end the combined error is ± 69.71 m and at the northwestern end the error is ± 126.45 m.

For aerial photos the rectification error was based on an overall error which will be referred to as a *system error.* This error includes systematic errors associated with the field equipment, e.g. lens deformation and survey co-ordinates for the ground control points, as well as random errors such as camera tilt, ground control point detection on the photos and misalignment of adjacent photographs and mosaics. The 95% confidence interval of the maximum least squares fit for individual rectified mosaics was used to estimate the error. For the 55 available mosaics this value was ± 6.1 m.

Post rectification

A variety of errors occur following rectification and these have also been included in Table 4.6. The (raw) rectified image has a two metre resolution as one pixel equals two metres (chapter 3, section 3.2.4.3). When the coastline was subsequently straightened, the longshore direction was resampled such that one pixel equals five metres and the cross-shore was resampled at one pixel equals two metres (chapter 3, section 3.2.4.5). Potential errors associated with the location of intensity maxima were reduced to two metres by using the detection algorithm PFIT.VIP described earlier in chapter 3 (section 3.2.6).

Table 4.7 Rectification errors associated with input parameter measurement precision for sites opposite the camera and at the ends of the study area. These rectification errors are directed along a ray from the camera. Random errors are listed in part A and systematic errors are listed in part B.

Parameter	Measurement precision	Errors opposite camera	Errors at river end	Errors at northwest end
A. Random errors				
Camera positioning:				
Northing	+/- 0.050 m	+/- 0.098 m	+/- 0.300 m	+/- 0.300 m
Easting	+/- 0.050 m	+/- 0.084 m	+/- 0.240 m	+/- 0.240 m
Elevation	+/- 0.050 m	+/- 0.090 m	+/- 1.570 m	+/- 1.570 m
Ground control point (GCP) detection:				
GCP1 vertical	+/- 0.5 pixel	+/- 0.090 m	+/- 13.500 m	+/- 13.500 m
GCP1 horizontal	+/- 0.5 pixel	+/- 0.045 m	+/- 0.020 m	+/- 0.020 m
GCP2 vertical	+/- 0.5 pixel	+/- 0.090 m	+/- 0.590 m	+/- 0.590 m
GCP2 horizontal	+/- 0.5 pixel	+/- 0.045 m	+/- 0.050 m	+/- 0.050 m
Photo edge detection:				
Top	+/- 1 pixel	+/- 0.090 m	+/- 1.340 m	+/- 1.340 m
Bottom	+/- 1 pixel	+/- 0 m	+/- 1.270 m	+/- 1.270 m
Horizon detection:				
Parallel	+/- 2 pixel	+/- 2.180 m	+/- 49.920 m	+/- 105.310 m
Tilt	+/- 2 pixel	+/- 1.050 m	+/- 20.831 m	+/- 45.110 m
Sea-level	+/- 0.150 m	+/- 4.700 m	+/- 21.740 m	+/- 21.740 m
B. Systematic errors				
Camera survey co-ordinates:				
Northing	+/- 0.100 m	+/- 0.392 m	+/- 0.600 m	+/- 0.600 m
Easting	+/- 0.100 m	+/- 0.330 m	+/- 0.480 m	+/- 0.480 m
Elevation	+/- 0.100 m	+/- 0.360 m	+/- 3.140 m	+/- 3.140 m
GCP1 survey co-ordinates:				
Northing	+/- 0.100 m	+/- 0.140 m	+/- 0.928 m	+/- 0.928 m
Easting	+/- 0.100 m	+/- 0.140 m	+/- 0.928 m	+/- 0.928 m
Elevation	+/- 0.100 m	+/- 0.428 m	+/- 6.038 m	+/- 6.038 m
GCP2 survey co-ordinates:				
Northing	+/- 0.100 m	+/- 0.150 m	+/- 0.216 m	+/- 0.216 m
Easting	+/- 0.100 m	+/- 0.150 m	+/- 0.216 m	+/- 0.216 m
Elevation	+/- 0.100 m	+/- 0.444 m	+/- 1.006 m	+/- 1.006 m
Lens focal length	+/- 0.001 m	+/- 0.240 m	+/- 4.400 m	+/- 4.400 m

4.3.3 Longshore and cross-shore resolution

4.3.3.1 Longshore resolution

Method and results

The longshore resolution for rectified oblique terrestrial data consists of the following types of error which were introduced in section 4.3.2:

- Pixel blur;
- Breaking wave offset - for which the resolution length is the difference in offsets for wave height variation experienced during sampling;
- Rectification parameter errors which consist of the combined random errors listed in Table 4.7. These random errors limit measurement resolution as they vary for each rectified image. This group of rectification errors are now discussed further.

The combined random rectification errors for the entire study area are depicted in Figure 4.7. Each line displayed in the figure represents an error (length) on the 100 m X 100 m grid. The combined error at each point was determined using vector addition (equation 4.2). The error values increase from 10.5 m opposite the camera site to 123 m at the rivermouth end of the study area and to 238 m at the northwestern end. The errors in Figure 4.7 also show that with increased distance from the camera the orientation of photogrammetric error becomes increasingly shore-parallel such that at each end of the study area the whole error comprises the longshore component while the cross-shore component is zero. By contrast, opposite the camera the longshore error component is zero and the whole rectification error comprises the cross-shore component which increases in length across the surf zone. The spatial depiction of the errors in Figure 4.7 also shows that at a specific distance the error associated with 55 mm lens photographs is greater than that for 135 mm lens photographs. The maximum error at each longshore location in Figure 4.7 was used when determining longshore resolution. The combined longshore resolution distribution described below therefore represents a 'worst case' situation.

The combined longshore resolution from pixel blur, breaking wave offset and rectification is depicted in Figure 4.8 (solid lines). Errors from these three sources were combined using variance addition (equation 4.2) and the longshore component was then derived. The 55 mm lens and 135 mm lens results have been plotted separately.

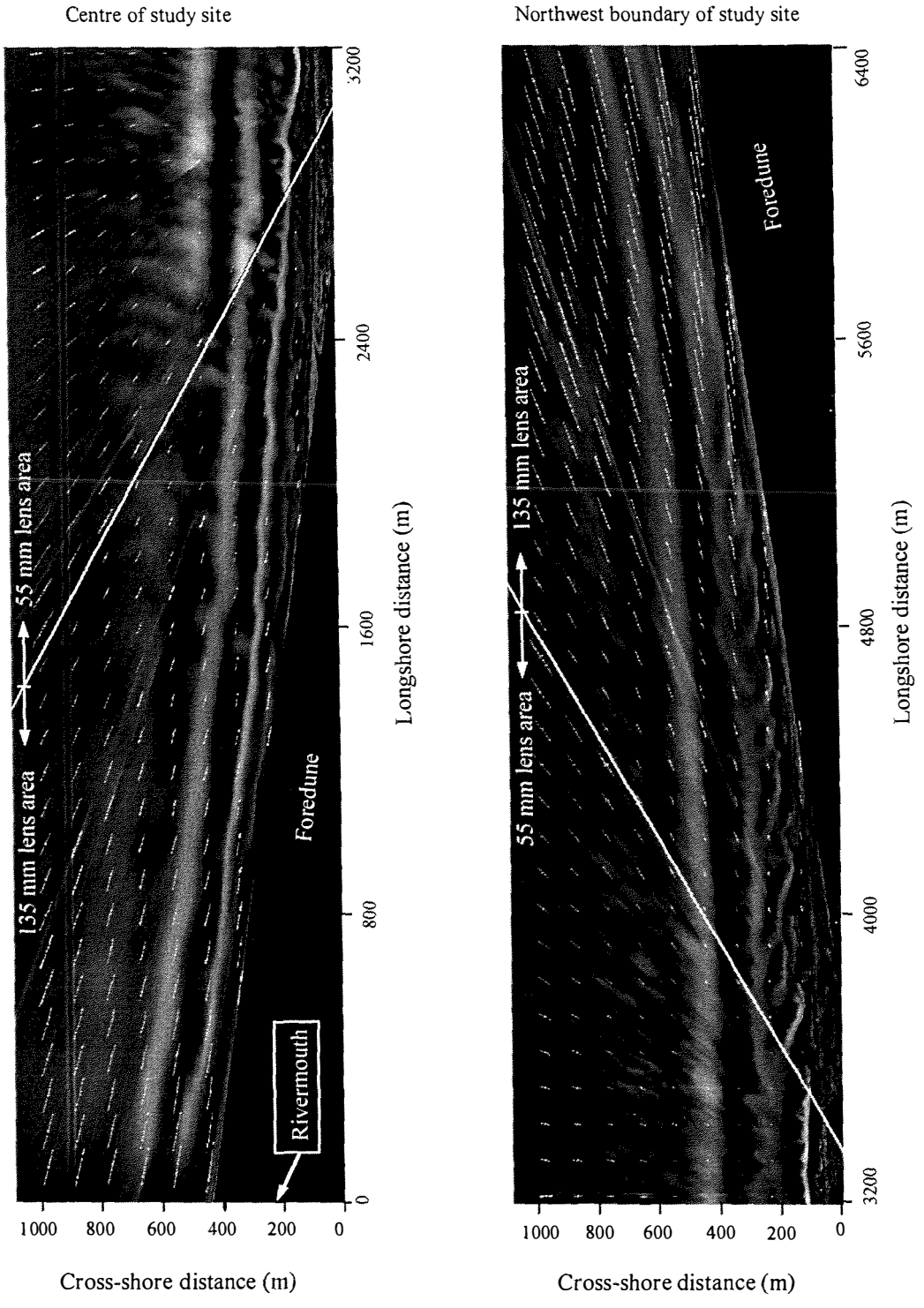

Figure 4.7

Distribution of random rectification errors across the study area over a 100 x 100 m grid. The length of each line represents the combined error (resolution) from the input parameter measurement precisions (see Table 4.6A). The error surface is underlain by a rectified panorama of photo-graphs to illustrate coastal curvature and bar-crest orientation relative to the error vectors. The areas covered by 55 mm and 135 mm lens photo-graphs have been marked on the image margins so the influence of focal length on rectification errors can be demonstrated.

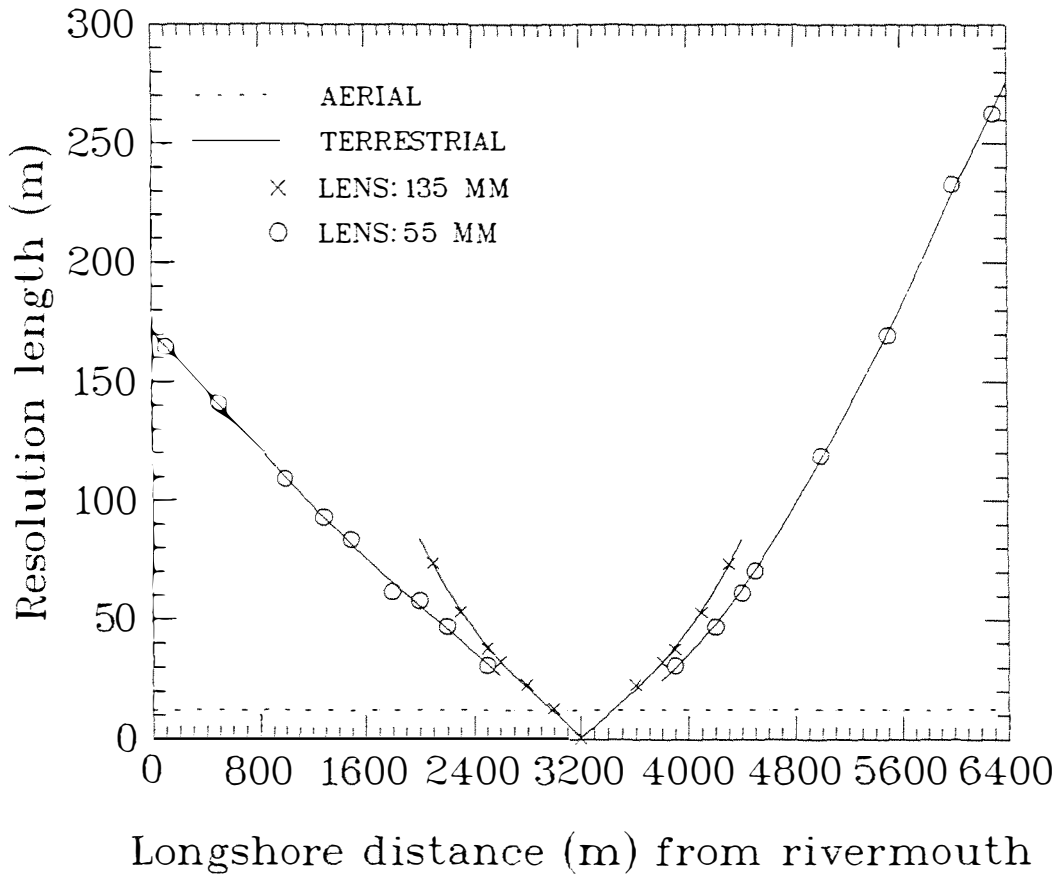

Figure 4.8 Longshore resolution lengths for rectified oblique terrestrial data (solid lines) and aerial data (dashed lines). For terrestrial data the component errors were associated with pixel blur, breaking wave offset and rectification parameter values (see sections 4.3.2 and 4.3.3). The resolution of 55 mm lens photos and 135 mm photos are also depicted. For aerial data the 'system' error was used (see sections 4.3.2 and 4.3.3).

The curves in Figure 4.8 show that the resolution decreases in a non-linear manner with increasing distance from the camera. Adjacent to the camera site the longshore resolution is two metres which is the pixel width. By contrast at the rivermouth end of the study area the error length is 170 m, while at the northwestern end the length is 275 m. The curves are asymmetrical about the camera location, which reflects the lower precision in detecting horizon points at the northwestern end of the study area; this was discussed in the previous section.

The longshore resolution for the aerial data is also depicted in Figure 4.8 (dashed line). The aerial photogrammetric resolution is equivalent to the system error discussed in the previous section, and the value of 12.2 m is constant throughout the study area.

Discussion

If a comparison in cross-shore bar migration is to be carried out between different longshore sites, then longshore resolution should be constant to ensure data compatibility. For example, analysis of data from a site closer to the camera may incorporate the effects of 3D bar behaviour, while this effect could be filtered from data further from the camera because of the lower photogrammetric resolution. If data from a 6.4 km long study area is to be analysed and compared then the minimum, or controlling, longshore resolution would need to be 275 m.

To compensate for such an imaging artefact, segment widths were selected so that the combined resolution of intensity averaging across the segment (chapter 3, section 3.2.6), plus the photogrammetric resolution (Figure 4.8), gave the predetermined (controlling) resolution. For example, suppose that a comparison of cross-shore bar migration is to occur between a transect located at the rivermouth end of the study area, say x = 100 (where x is the longshore distance from the rivermouth), and a transect located midway between the camera site and the rivermouth (say 1600 m from the rivermouth). From Figure 4.8, the photogrammetric resolution at T100 is 166 m, whilst the photogrammetric resolution at T1600 is only 77 m. The T100 resolution of 166 m is therefore the controlling resolution and the segment width at T1600 will need to be increased so intensity averaging will result in the same combined resolution for the two sites. The segment width was determined using equation 4.6.

$$A(x) = [Cr(x)^2 - Pr(x)^2]^{0.5} \qquad (4.6)$$

where A(x) is the number of points to be averaged, i.e. the segment width, and these points are centred about a longshore distance x which is measured from the rivermouth. Pr(x) is the photogrammetric resolution at longshore distance x which is obtained from Figure 4.8, and Cr(x) is the predetermined combined longshore resolution for location x. This equation was derived by rearranging equation 4.2 as the two types of error are independent. Substituting the values from the above example into equation 4.6 gives:

$$A(1600) = [166^2 - 77^2]^{0.5}$$

$$= 147 \text{ m}$$

So the cross-shore segment located 1600 m from the rivermouth needs to be 144 m wide to ensure the same longshore resolution for bar-crest data as at the site adjacent to the river.

4.3.3.2 Cross-shore resolution

Cross-shore resolution for the rectified oblique terrestrial data-set is plotted in Figure 4.9 (solid lines). Errors which contributed to these resolution values consisted of the cross-shore components of pixel blur, breaking wave offset, random rectification errors (section 4.3.3.1) plus the environmentally-associated intensity maxima errors (Table 4.3).

Only the results for the site opposite the camera are shown in Figure 4.9. A 'worst case' resolution distribution is therefore described, as cross-shore photogrammetric error components decrease with increasing longshore distance from the camera (see section 4.3.2). By contrast, the environmentally-associated cross-shore error was (assumed to be) constant alongshore.

The cross-shore resolution curves for terrestrial images in Figure 4.9 show that resolution decreased (i.e. the error length increased) with increasing distance from the camera and the resolution increased (i.e. the error length decreased) with wider longshore segments. In particular, the five metre wide segment resulted in cross-shore resolution lengths of 46.3 m at 200 m offshore from the camera location and 70.2 m at 600 m offshore. Increasing the segment width to 200 m resulted in the cross-shore resolution length decreasing to 16.8 m at 200 m offshore and 28.2 m at 600 m offshore.

The cross-shore resolution for the rectified vertical aerial data are depicted by the dashed lines in Figure 4.9. The aerial photogrammetric component was based on the system error which was explained earlier. The same environmental errors that influence cross-shore resolution for terrestrial images affected the aerial images. A five metre wide segment resulted in cross-shore resolution lengths of 47.3 m at 200 m offshore from the camera and 67.8 m at 600 m offshore. Increasing the segment width to 200 m resulted in the cross-shore resolution length decreasing to 19.1 m at 200 m offshore and 21.5 m at 600 m offshore.

4.3.4 Comparison of aerial and terrestrial bar-crest data

Contemporaneously sampled aerial and terrestrial rectified data were analysed to identify any variation in the intensity patterns (systematic error). This was necessary because Wanganui data used for studying NOM was obtained by fusing data obtained from both sources.

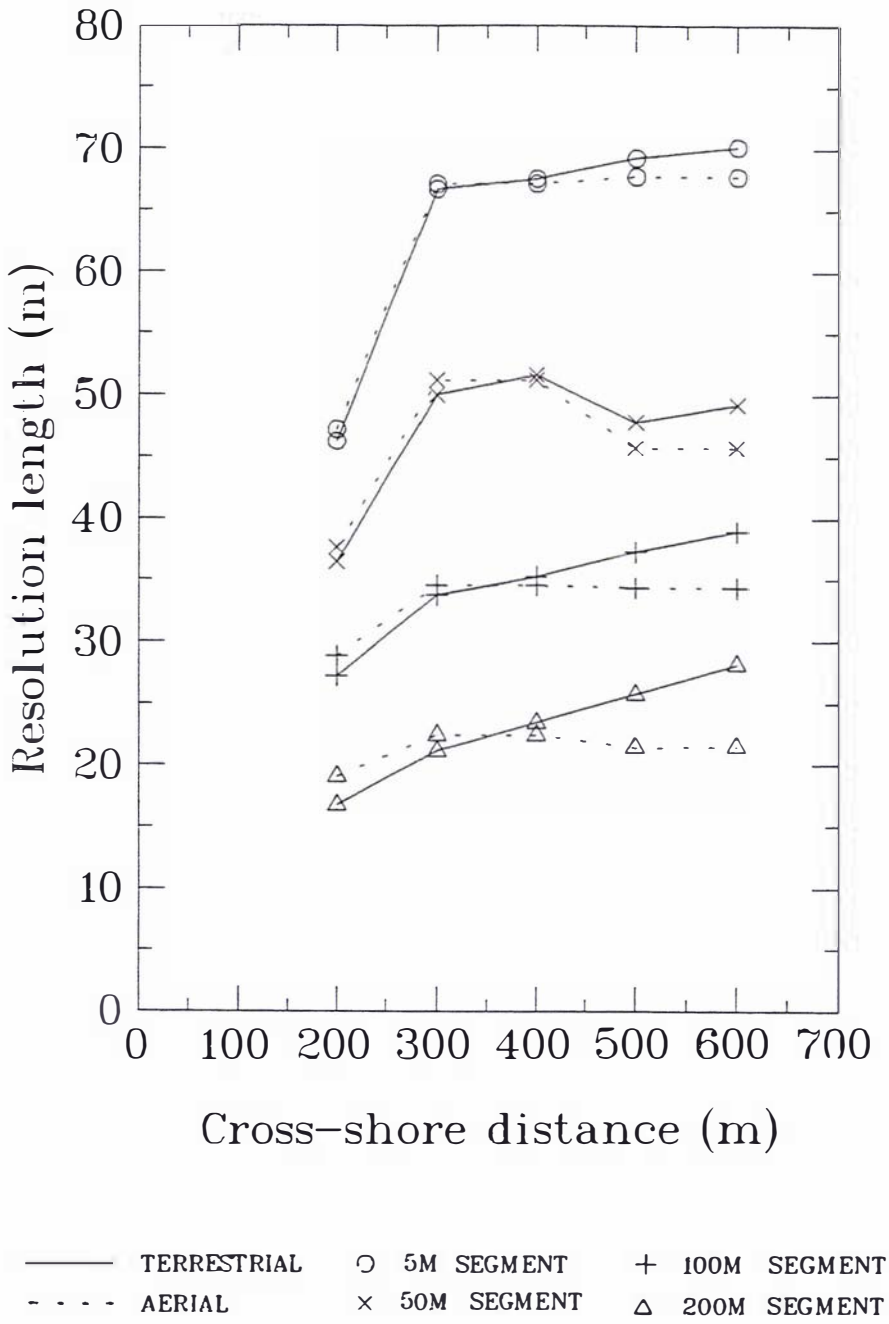

Figure 4.9 Cross-shore resolution lengths for rectified oblique terrestrial data (solid lines) and aerial data (dashed lines). Cross-shore distances have been set back to the camera site which is 128 m behind the foredune toe. These graphs show the result of intensity averaging alongshore over 5, 50, 100 and 200 m wide segments. For terrestrial data the component errors consist of the photogrammetric errors of pixel blur, breaking wave offset and rectification parameter precision, together with the environmentally-associated errors for incident wave height, seiche wave height, and tide level. For aerial data the photogrammetric system error was used together with the environmentally-associated errors listed above. The different errors are described in text (section 4.3.2).

Method

The location of intensity maxima on two sets of rectified aerial and terrestrial images were compared. The first set consisted of aerial photos sampled on 9.1.93 and the rectified image is depicted in Figure 3.8A. Two corresponding terrestrial images were used which temporally bracketed the aerial photo. These terrestrial images were sampled on 6.1.93 and 12.1.93. The rectified image from the former sampling is depicted in Appendix H(ii), while the rectified image from the latter sampling is depicted in Figure 3.8C. The second set of images were both sampled on 25.7.93. The terrestrial image is depicted in Appendix H(i) and the aerial image in Appendix H(ii). The environmental conditions at the times of photographic sampling are listed in Appendix I. Adjustments for differences in tide level and wave height between the corresponding samplings were made using relationships identified earlier in Tables 4.4 and 4.5.

On each rectified image, the location of cross-shore intensity maxima were determined at 200 m intervals alongshore using the detection algorithm PFIT.VIP. Segment widths were selected using equation 4.6 such that the combined resolution (photogrammetric and segment averaging) was 200 m. This resolution value was chosen to maximise both the longshore and cross-shore resolutions and will be discussed further in the final section (4.6) of this chapter. Differences in the location of corresponding aerial and terrestrial intensity maxima were then determined. Parabola were fitted to these differences for each 200 m wide longshore segment and this set of curves was used to define the error surface between aerial and terrestrially-based intensity data.

Results

The error surface covering the study area from the rivermouth to T5000 is depicted in Figure 4.10. For all positions, the bar-crest locations obtained from rectified aerial photographs are seaward of corresponding intensity maxima from rectified terrestrial photographs. This difference is less than 15 m at all locations between the rivermouth and T5000. The maximum difference for each cross-shore transect tends to occur in the mid-surf zone and the maximum difference in the longshore direction occurs at each end of the study area. In the northwestern portion of the study area, from T5000 to T6400, the maximum cross-shore errors (not shown) increased dramatically, from ~15 m at T5000 to ~45 m at T6400. A further point of interest in the shape of the error surface is the relatively elevated values between T2500 and T4500. This may be related to optical differences between the 55 mm and 135 mm lens as the upward bulge corresponds to that region covered only by the 55 mm lens.

The set of parabola which generated the error surface in Figure 4.10 formed the basis of the systematic error correction algorithm CORRECT.VIP discussed in chapter 3 (section 3.2.4.3).

Discussion

The increase in error values toward each end of the study area (Figure 4.10), together with the relatively higher values toward the northwest, is consistent with the photogrammetric error pattern in Table 4.6. It therefore appears likely that the error surface is dominated by a systematic error associated with the rectification procedure. In particular, increasing error values toward the rivermouth end of the study area would occur if the earth curvature correction was overestimated. The substantial increase in error value toward the northwest of the study area may also be horizon related for the following reason. No horizon occurred in this area so the line of the cliff-top (see Figure 2.4) was used as a surrogate. If this estimate of the horizon location was too high, and field inspection indicated that this may have been the case, then rectified terrestrial maxima from this part of the study area would be further from the camera, thereby causing increased aerial and terrestrial error values.

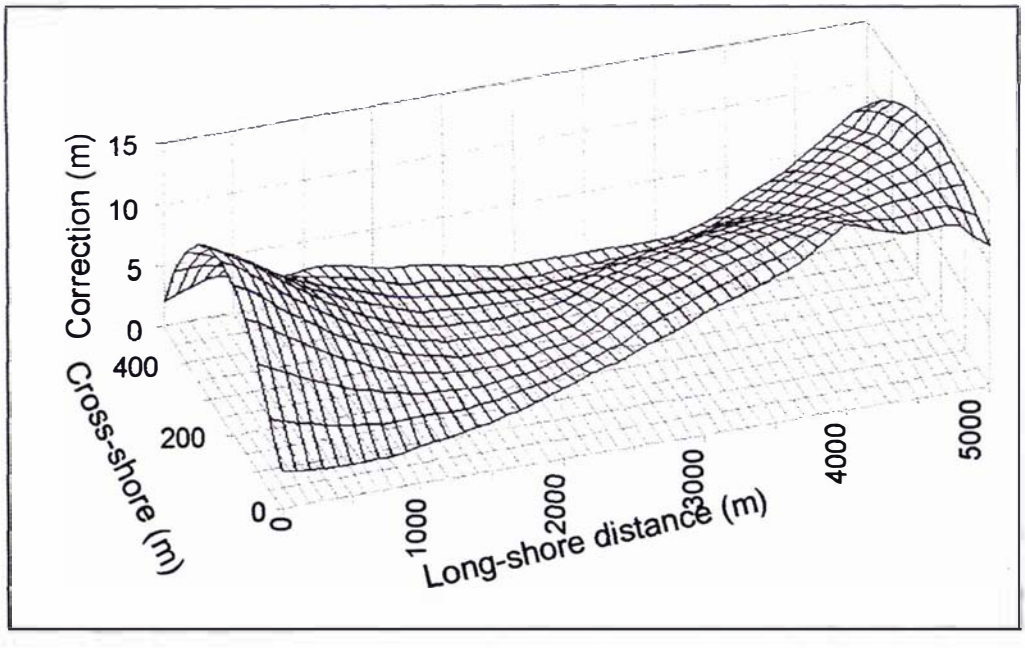

Figure 4.10

The error surface depicting the difference (labelled *Correction (m)*) between bar-crest location derived from rectified oblique terrestrial photographs and rectified vertical aerial photographs. Longshore distance is measured from the rivermouth and cross-shore distance from the dune toe. Bar-crest locations obtained from aerial photographs are located seaward of the corresponding bar-crest locations obtained from terrestrial photographs. To make the two types of data compatible, the cross-shore distance correction is added to terrestrial data or subtracted from aerial data.

4.4 Ground profile errors

A variety of equipment-based, operator-based and environment-based errors occurred when obtaining ground profile data. These errors will now be described, firstly for data obtained by levelling and then for data collected by echo-sounder.

Levelling

Levelling was used to survey cross-shore transects from the dune toe benchmark to the low tide step, a distance of between 150 and 200 m. The cross-shore error, longshore error, elevation error and sampling resolution for the levelling survey instruments, i.e. the Wild Automatic Level and Topcon Total Station which were described in chapter 3 (section 3.3.1), are summarised in Table 4.8A. The errors in this table were based on the manufacturers' specifications, together with observations made by the author.

The levelling errors in Table 4.8A are now described. Elevation errors ranged between ± 0.001 and ± 0.02 m, cross-shore location errors ranged between ± 0.005 and ± 1.0 m, longshore location error ranged between ± 0.5 and ± 2.0 m, and cross-shore resolution ranged between ± 1 and ± 5 m. Elevation and cross-shore errors were lower for the total station compared with the automatic level and the errors for the automatic level increased with distance from the benchmark. Most of the levelling error in Table 4.8A was associated with environmental influences such as wind (vibration), heat shimmer, or subsidence beneath the instrument or target.

Echo-sounding

Echo-sounding was used to survey cross-shore transects between ~100 m from the dune toe benchmark to ~4000 m from the benchmark. The cross-shore, longshore and elevation errors, together with sampling resolution for both survey instruments - the Raytheon and Elac Echo-Sounders which were described in chapter 3 (section 3.3.1), are summarised in Table 4.8B. The errors in these tables were based on the manufacturers' specifications and published materials (e.g. Hallermeier, 1978; Gable and Wanetick, 1984; Birkemeier 1985, Morang et al., 1997), together with observations made by the author.

The errors in Table 4.8B are now described. Elevations were estimated at ± 0.3 m for both systems. The instrument specifications indicated errors should be approximately an order of magnitude lower than those given in the table. However, the inexactness of manually removing the effects of vessel pitch, roll and wave heave, together with instrument miscalibration, and determining sea-level for data reduction (to MSL), caused errors to increase

Table 4.8 Errors associated with ground profile data acquisition. In Table A the elevation measurements are made using levelling instruments. In Table B the elevation measurements are made using echo-sounders. Methods used for determining position for the different systems are given in the footnotes.

A. Levelling

Survey instrument	Cross-shore width (m)	Elevation error (m)	Cross-shore error (m)	Longshore error (m)	Cross-shore resolution (m)
Wild Automatic Level	0-100	+/-0.005	+/- 0.5@	+/-0.5*	+/-1 to +/-2.5
	100-200	+/-0.02	+/- 1.0@	+/-2.0*	+/-2.5 to +/-5
Topcon Total Station	0-100	+/-0.001	+/- .005#	+/-0.5*	+/-1 to +/-2.5
	100-20	+/-0.001	+/- .005#	+/-2.0*	+/-2.5 to +/-5

Where: @ = stadia (automatic level); * = ranging poles; # = laser (total station).

B. Echo-sounding

Survey instrument	Cross-shore zone(m)	Elevation error (m)	Cross-shore error (m)	Longshore error (m)	Cross-shore resolution (m)
Raytheon XCD600	100-1000	+/-0.3	+/-5@	+/-5 to +/-10*	+/-2.5 to +/-5
Elac LAZ 17CT	500-4000	+/-0.3	+/-2.5 to +/-5#	+/-10 to +/-20*	+/- 10

Where: @ = laser (total station); * = ranging poles; # = micro wave (trisponder).

by approximately ± 0.2 m. This value was increased further to ± 0.3 m to allow for resolution and accuracy limitations of the Port Company's chart recorder that was used for measuring tide level, and error associated with the influence of river flow on tide level. While the distance measuring instruments had a specified accuracy to within one metre, this accuracy was reduced by operator error when using the 'event-marker'. This error source was caused by a combination of boat speed and operator reaction time. Cross-shore location errors were consequently estimated to range between ± 2.5 and ± 5 m. Longshore errors ranged between ± 5 and ± 20 m; this error increased with distance offshore because the range markers became more difficult to visually detect. Sampling resolution ranged between ± 2.5 and ± 10 m. However, resolution in the nearshore zone where bar-crests were detected and measured, ranged between ± 2.5 and ± 5 m.

4.5 Comparison of intensity-based and ground profile-based bar-crest detection

Because bar-crest data from different NOM sites were collected using both imaging and ground profiling, it was necessary to compare the output and compensate for any difference prior to inter-site analysis. This investigation is now described.

Method and results

It was beyond the available resources to carry out contemporaneous photographic and ground sampling so an alternative approach was adopted; a comparison was made between 'modal' bar-crest locations on time-averaged ground profiles and intensity maxima on time-averaged intensity profiles. The averaging process removed the need for exact synchronisation of pairs of samples, although sampling within the same overall time period was required. A further advantage of the time-average approach was removal of the need to accurately account for environmental influence as, over time, environ-mental variation is a random variable.

Ground profiles for transects T200, T1500 and T5000 were used for the comparison with intensity-based data. The ground profiles were sampled between 11.7.91 and 27.10.93 (see Appendix D[ii]). The maximum residual method (chapter 3, section 3.3.4) was used to determine the location of the modal bar-crests. Power curves fitted to the mean profiles are depicted in Figure 2.14. The residual plot for T1500 is shown in Figure 4.11A. The dashed vertical lines in this figure are aligned with the residual maxima and locate modal bar-crests at 122 m and 408 m offshore. These cross-shore locations, plus those for T200 and T5000, are listed in the first column of

A. Mean profile residuals

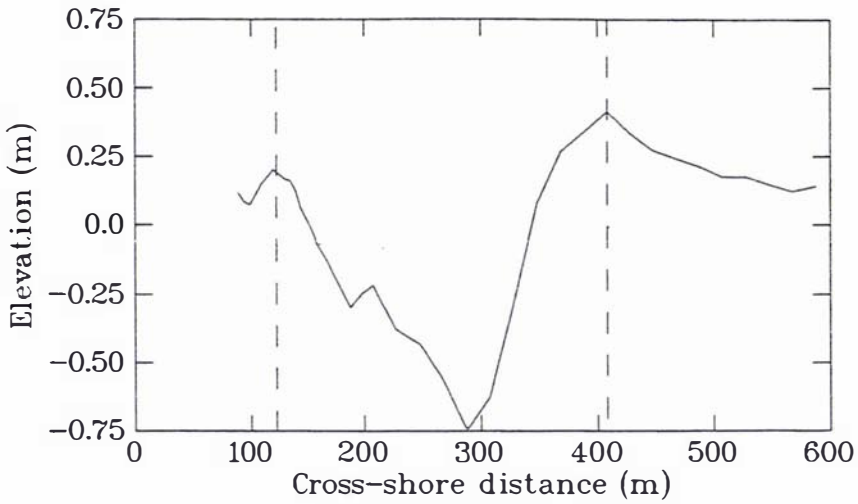

B. Average intensities

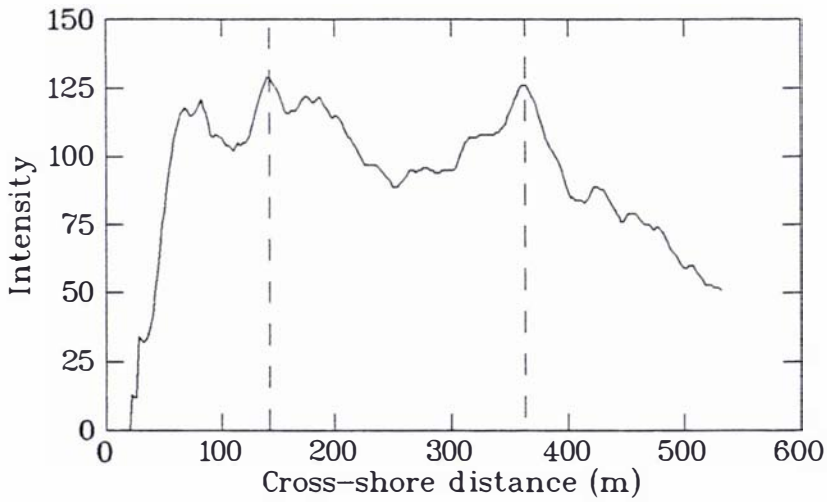

Figure 4.11 Figure A is a plot of the residuals between the mean ground profile and fitted power curve for ground profiles at transect T1500. The profiles were surveyed between 11.7.91 and 27.10.93. Figure B plots the time-averaged intensity values obtained from the T1500 time-stack for rectified images collected over approximately the same time-period (12.8.91 to 7.11.93). The intensity scale in Figure B is non-dimensional. The dashed vertical lines locate equivalent points of maximum residual (A) and maximum intensity (B). This result shows that the intensity-based maxima are located seaward (20 m) of ground profile-based maxima within the inner surf zone and landward (46 m) of the ground profile-based bar-crest location in the outer surf zone.

Table 4.9. Two crests occurred at T200 and T1500, while three crests were evident at T5000. The greatest distance between shoreward and seaward modal crests was at T5000 (113 m to 488 m), and the smallest distance was at T200 (148 to 320 m).

The closest corresponding time period over which rectified images were available was from 12.8.91 to 7.11.93 (see Appendix H(i)). Time-stacks were constructed for T200, T1500 and T5000. Time-averaged intensity curves were then derived from the time-stacks; the curve for T1500 is shown in Figure 4.11B. The points of maximum intensity were identified by fitting a parabola and determining the cross-shore location with zero slope using PFIT.VIP. These locations are identified by the vertical dashed lines in Figure 4.11B. The resulting locations of maximum intensity for all three transects are listed in the second column of Table 4.9. The greatest distance between shoreward and seaward intensity maxima was at T5000 (148 m to 438 m), and the smallest distance was at T200 (144 to 282 m). It should be noted that the location of intensity maxima in Table 4.9 differ from those shown in Figure 5.2 (chapter 5) because of the different sites (T1500 compared with T1600) and the different time-spans used for sampling.

Differences between corresponding image profile and ground profile maxima are listed in the third column of Table 4.9. These results show that on all three transects landward intensity maxima are located offshore from corresponding ground profile residual maxima, while further seaward the intensity maxima are located landward of corresponding ground profile residual maxima. This pattern reflects the depth dependency of wave breaking. These difference patterns represent a systematic error that will be 'generalised' below, thereby enabling data collected by the two methods to be reconciled.

Adjustment method and discussion

The above results were used to formulate an adjustment method by which bar-crest location data acquired from one data acquisition technique (ground profiling or intensity profiling) can be converted to the equivalent location as determined by the other technique. The method involves using a non-linear regression model which relates image and profile location differences (column 3, Table 4.9) to bar-crest depths, as wave breaking and associated morphodynamics are depth dependent. Depths from MSL to the curve fitted to the mean ground profile were used and these values have been included in the fourth column of Table 4.9. Figure 4.12 is the resulting plot of intensity and ground profile differences versus depth.

Table 4.9 This table lists the cross-shore 'modal bar-crest' (local maxima) locations on time-averaged ground profiles for T200, T1500 and T5000, the cross-shore locations of intensity maxima on time-averaged intensity profiles, the location differences between the intensity maxima and corresponding modal bar-crests, and the depths from MSL to the curve fitted to the mean ground profile at modal bar-crest locations.

Transect	Ground profile distance (m)	Intensity profile distance (m)	Intensity minus ground distance (m)	Depth to fitted curve (m) from MSL
T200	148	144	-4	2.2
T200	320	282	-38	3.9
T1500	122	142	20	1.8
T1500	408	362	-46	4.9
T5000	113	148	35	0.9
T5000	286	272	-14	3.3
T5000	488	438	-50	4.8

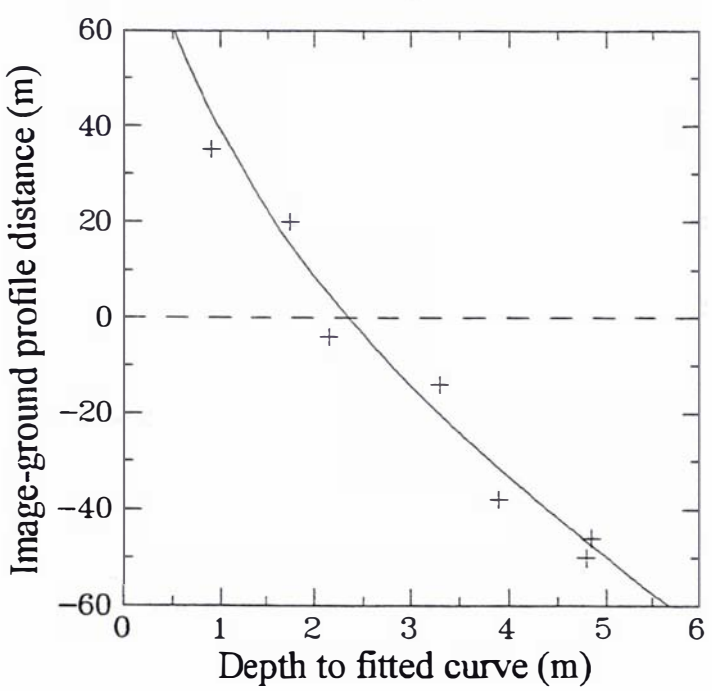

Figure 4.12 Cross-shore differences for intensity-based and ground-profile bar-crest locations plotted as a function of depth (below MSL) to the curve fitted to the mean ground profile. The data points are listed in Table 4.9 and their derivation was illustrated in Figure 4.11.

A non-linear regression model was found to provide the best fit to these data points using a least squares routine; the model is plotted in Figure 4.12 and is mathematically expressed by equation 4.7:

$$C = -79.765*D^{0.465} + 118.71 \qquad \text{for } D>1,\ D<5 \qquad (4.7)$$

where C = cross-shore intensity distance minus ground profile distance in metres, i.e. the systematic error adjustment, and D = depth (m) at the bar-crest between MSL and the curve fitted to the mean ground profile. The correlation co-efficient of 0.983 is highly significant ($p<<0.01$) for N = 7. The residuals (standard deviation = 5.757 m) may result from subtlety in the shape of modal bar-crests on the time-averaged ground profiles. The regression model was not improved by normalising the cross-shore distance data with respect to nearshore width.

This model only applies to bar-crests located at depths between approximately one and five metres below MSL. Ground profile bars at a depth of one metre are predicted to lie 39 m landward of the corresponding intensity-based crest, while ground profile bars at a depth of five metres are located 50 m seaward of the intensity-based crest. The model also shows that bars located 2.3 m below MSL have the same location regardless of which method is used for their detection.

The model is used in the following manner to convert bar-crest locations determined by one method to the equivalent location as determined by the other method. At the location of the ground profile bar-crest, the depth from MSL to the fitted curve is determined using Figure 2.14. The adjustment is then obtained via the conversion model expressed by equation 4.7. For example, if a ground profile bar-crest was located 300 m offshore at T1500, then the depth from MSL to the fitted curve (Figure 2.14B) is 3.7 m and an adjustment of -28.6 m (i.e. shoreward) is required. The equivalent intensity maximum is therefore located 271.4 m offshore. An iterative procedure is required for the converse transformation, i.e. determining the ground profile bar-crest location given an intensity maximum location. Estimates are made of the ground profile location and these are processed in the manner described above to obtain the equivalent intensity location. The required ground profile location is that value which results in the given intensity profile location.

Research has recently been carried out by Plant and Holman (1999) in which they compared bar-crest locations on ground profiles with intensity maxima identified on contemporaneously sampled images. Unfortunately the resulting data were not compatible with the Wanganui data as bar-crests on

the ground profiles were detected by fitting a Gaussian curve. Furthermore, the landwardmost and seawardmost bars were not analysed. Nonetheless, their results were qualitatively similar to those from Wanganui, in that differences between ground profile bar-crest location and the intensity maximum appeared to increase with increasing seaward distance.

4.6 Summary and Conclusions

The objectives of this chapter were to determine the cross-shore and longshore resolution of intensity-based and ground profile-based morphological data, and also to determine the compatibility between bar-crest data obtained by the different methods of data acquisition. To achieve these objectives the environmental and photogrammetric errors associated with each method were first defined. Contemporaneously sampled data were used to compare bar-crest locations from rectified vertical aerial and rectified oblique terrestrial photographs, while time-averaged data were used to compare image profile-based and ground profile-based bar-crest locations.

A range of systematic errors, random errors, and measurement resolutions characterised the image and ground survey data from Wanganui, e.g. see Figure 4.1. Multiple errors were evaluated using the principles of variance addition (equations 4.2 and 4.3).

Image-based errors were based on either environmental or photogrammetric factors. Environmentally-associated errors are caused primarily by variation of incident wave height, seiche wave height and tide level, all of which affect wave breaking and hence the location of intensity maxima. Environmentally-associated error values ranged between 0 and 31.5 m for incident wave variation experienced during photographic sampling, between 24.8 and 56.1 m for seiche height variation and between 15.4 and 38.4 m for tidal variation (see Table 4.3). However, when intensities were longshore averaged over a 200 m wide segment prior to analysis the errors were reduced by 48% to 100% (Table 4.3). Environmentally-associated errors had a similar effect on both aerial and terrestrial image data.

Photogrammetric errors cover pixel effects, wave offset, rectification and output image sampling. These errors influence aerial and terrestrial images differently. The results summarised in Table 4.6 show the most substantial errors occur for terrestrial-based images with magnitudes increasing as distance from the camera increases. Pixel effects ranged from ± 8.4 m opposite the camera, to ± 38.3 m at the ends of the study

area. Wave offset ranged between ± 14.7 m opposite the camera and ± 76.8 m at the ends of the study area, and rectification parameter errors ranged between ± 6.3 m opposite the camera and ± 126.5 m at the northwestern end of the study area. The aerial error was associated with photo rectification (± 6.1 m) which was constant across the whole study area.

The longshore resolution for the rectified images is controlled by photogrammetric errors. The resolution values depicted in Figure 4.8 show that the resolution for terrestrial images decreased with increasing distance from the camera; with error lengths of 2 m opposite the camera, 170 m at the eastern end of the study area, and 275 m at the western end. By comparison the longshore resolution for aerial images was constant at 12.2 m throughout the study area.

The cross-shore resolution for the rectified images is controlled by both environmental and photogrammetric errors. The resolution values depicted in Figure 4.9 were similar for both terrestrial and aerial images. Resolution decreased with increasing seaward distance. For terrestrial images the error lengths increased from 46.3 m at 200 m offshore from the camera to 70.2 m at 600 m offshore, and for aerial images the values increased from 47.3 m at 200 m to 67.8 m at 600 m. Increasing the segment width and then intensity averaging (alongshore) prior to analysis increased the resolution. For example, with terrestrial images the error lengths in the mid-surf zone decreased from 67.6 m for a 5 m wide segment to 23.5 m for a 200 m wide segment. For aerial images the error values decreased from 67.2 m for a 5 m segment to 22.5 m for a 200 m segment.

To meet the cross-shore resolution requirements (~10 m) stipulated in chapter 1 (section 1.3.2) it is necessary to intensity average wider segments. For cross-shore resolution, the segment width would need to be in excess of 200 m as such segments had a resolution of ~20m. However, while increasing the segment width significantly improves cross-shore resolution it decreases longshore resolution. In chapter 1 the longshore resolution requirement was set at ~100 m. As a compromise 200 metres was selected as the longshore resolution. This value could be achieved at all locations between the rivermouth and T5750 by combining segment width and photogrammetric resolution using equation 4.6. Data from cross-section transects to the northwest of T5700 were not used in the NOM analysis. While the 20 X 200 m resolution combination imposed a limitation on the detection of bar migration, the data were still able to be used to identify morphological change at a level of detail satisfactory for meeting the NOM objectives outlined in chapter 1 (section 1.4).

A comparison between aerial and terrestrial bar-crest data identified an error surface (Figure 4.10) in which terrestrial intensity maxima were located landward of corresponding aerial maxima. While this difference was less than 15 m at all locations between the rivermouth and ~T5000, it increased substantially beyond 5000 m to reach a value of ~45 m at T6400. The error surface was interpreted to represent systematic errors that were primarily associated with the rectification of terrestrial photographs.

Ground profile data were affected by errors associated with equipment, operators and environmental conditions. The summary of these errors in Table 4.8 shows they increase with increasing seaward distance. Foreshore data was obtained by levelling. Elevation errors ranged between ± 0.001 and ± 0.02 m, cross-shore location errors ranged between ± 0.005 and ± 1.0 m, longshore location errors ranged between ± 0.5 and ± 2.0 m, and cross-shore resolution ranged between ± 1 and ± 5 m (Table 4.8A). The nearshore and offshore data were collected by echo-sounding. The elevation error was ± 0.3 m, cross-shore location errors ranged between ± 2.5 and ± 5 m, longshore location errors ranged between ± 5 and ± 20 m, and sampling resolution ranged between ± 2.5 and ± 10 m (Table 4.8B). Levelling data were less affected by errors than the echo-sounded data which were particularly susceptible to environmental conditions and operator skill.

A comparison between bar-crest location determined from time-averaged ground and intensity data identified a depth-dependent association in which intensity-based maxima were located up to 35 m seaward of corresponding ground profile bar-crests on the lower foreshore (approximately one metre below MSL) and up to 50 m landward of the ground profile crests in the outer surf zone (approximately five metres below MSL). This systematic error was quantified by a regression model (Figure 4.12, equation 4.7) which enabled bar-crest location determined by one method to be converted to the 'equivalent' location determined by the other method.

Error evaluation methods and results in this chapter were undoubtedly affected by the lack of data available to carry out some aspects of the investigation. Examples include the assumptions of linearity when quantifying environmentally-associated errors, the limited number of data points used in both the aerial vs terrestrial comparison (two pairs of data sets) and the ground profile vs intensity maxima comparison (seven data points). However, some supporting evidence for the evaluation results was available. While differing methodologies prevented quantitative comparison, qualitative confirmation as to the influence of tide and wave height on the location of intensity maxima is contained in the work of

Lippmann and Holman (1989). Similarly, the ground profile vs image intensity results of Plant and Holman (1999) qualitatively support the conversion developed for the Wanganui data.

While further work is required to increase the quantitative accuracy of the error assessment, the use of 95% confidence intervals and the 'worst case' approach will, in general, have overestimated errors. Measurement resolution throughout the study area (20 m cross-shore and 200 m longshore), and data fusion conversions (aerial image with terrestrial image and ground profile with intensity profile) enable reliable data to be acquired that is suitable for the NOM analysis.

CHAPTER 5 LONGER-TERM ASPECTS OF NOM

Nature creates ever new forms; what exists has never existed before, what has existed returns not again - everything is new and yet always old. There is an eternal life, a coming into being and a movement in her; and yet she goes not forward".

Goethe: Essay on Nature.

5.1 Introduction

This chapter deals with the average cyclic characteristics of NOM from Wanganui and the other sites where NOM has been reported. In chapter 1 (section 1.1) NOM was described as a cyclic type of morphological behaviour because it consisted of "successive occurrences" of seaward migrating sandbars. Cycles of NOM will now be identified within the bar-crest data for each site and then analysed for NOM characteristics. As the average timespan of NOM cycles at the different sites ranged between 1.4 and 13 years, this chapter is concerned with *longer-term* aspects of NOM. *Shorter-term* or *within-cycle* aspects will be covered later (chapter 6). The present chapter will focus on the following general research objectives from chapter 1 (section 1.4):

- Determination and comparison of the longer-term characteristics of NOM behaviour at Wanganui and at the other sites where NOM has been observed.
- Determination of the relationship between NOM characteristics at these sites and the corresponding longer-term environmental conditions.
- Contribution towards a conceptual morphodynamic model for NOM.

Since 1991, when the present study began, further description and analysis of NOM phenomena have been published. As noted in chapter 1 (section 1.1), early reports of the systematic offshore migration of coastal sandbars were made by De Vroeg et al. (1988) on sections of the coast of Holland, Birkemeier (1984) at Duck on the North Carolina coast, and Shand (1990) at the Wanganui Rivermouth in New Zealand. More recent NOM documentation has been provided by Kroon (1991), Kroon and Hoekstra (1993), Kroon (1994), Wijnberg (1995) on the Holland coast; Ruessink (1992), Hoekstra et al. (1994), Ruessink and Kroon (1994) and Ruessink (1998) on

the Terschelling coast; Larsen and Kraus (1992), Lippmann et al. (1993) and Plant et al., (1999) at Duck; Patterson (1991), and Bailey and Shand (1996) on the Wanganui coast. A review of NOM by Shand and Bailey (1999) has also recently been published. The locations of these NOM sites are shown in Figure 5.1. Bar-crest time-series for sites along the Wanganui coast are shown in Figure 5.2. Data from the Dutch sites, the Duck sites, the Wanganui Rivermouth site and two 'representative' sites from the Wanganui coast are depicted in Figure 5.3; in the present study these locations are referred to as the *global NOM sites* and the associated data as the *global data-set*.

Ruessink (1992) appears to have been the first researcher to report on a NOM system as consisting of three distinct stages. After studying a 26 year data-set of cross-shore profiles from Terschelling Island, Ruessink described NOM at this location in terms of a simple conceptual model in which a bar was formed (generated) near the shore-line then moved (systematically migrated) offshore across the inner nearshore until it finally flattened out and disappeared (degenerated) in the outer nearshore. These three stages therefore describe the 'life-cycle' of a coastal sand-bar. Support for the application of this three stage model to other NOM coasts has recently been provided in an inter-site study by Shand et al. (1999). This work investigated bar migrational behaviour within three cross-shore zones that were used to represent the three NOM stages. At each site a similar inter-zonal pattern of bar migration occurred. This chapter will determine the migrational characteristics for bars in stage 2 of the NOM life-cycle, i.e. bars undergoing systematic offshore migration.

It was necessary to develop a set of NOM-defining parameters before any inter-site comparison of NOM characteristics could be performed. To achieve this the following specific objectives were addressed:

- To develop a set of parameters that quantitatively characterise NOM behaviour along a cross-shore transect.
- To develop a method that identifies comparable start and finish locations to the zone of systematic offshore migration for any data-set.

The following research questions were then addressed:

- What NOM parameter values characterise the Wanganui field site, and which of these values are representative of the Wanganui data?

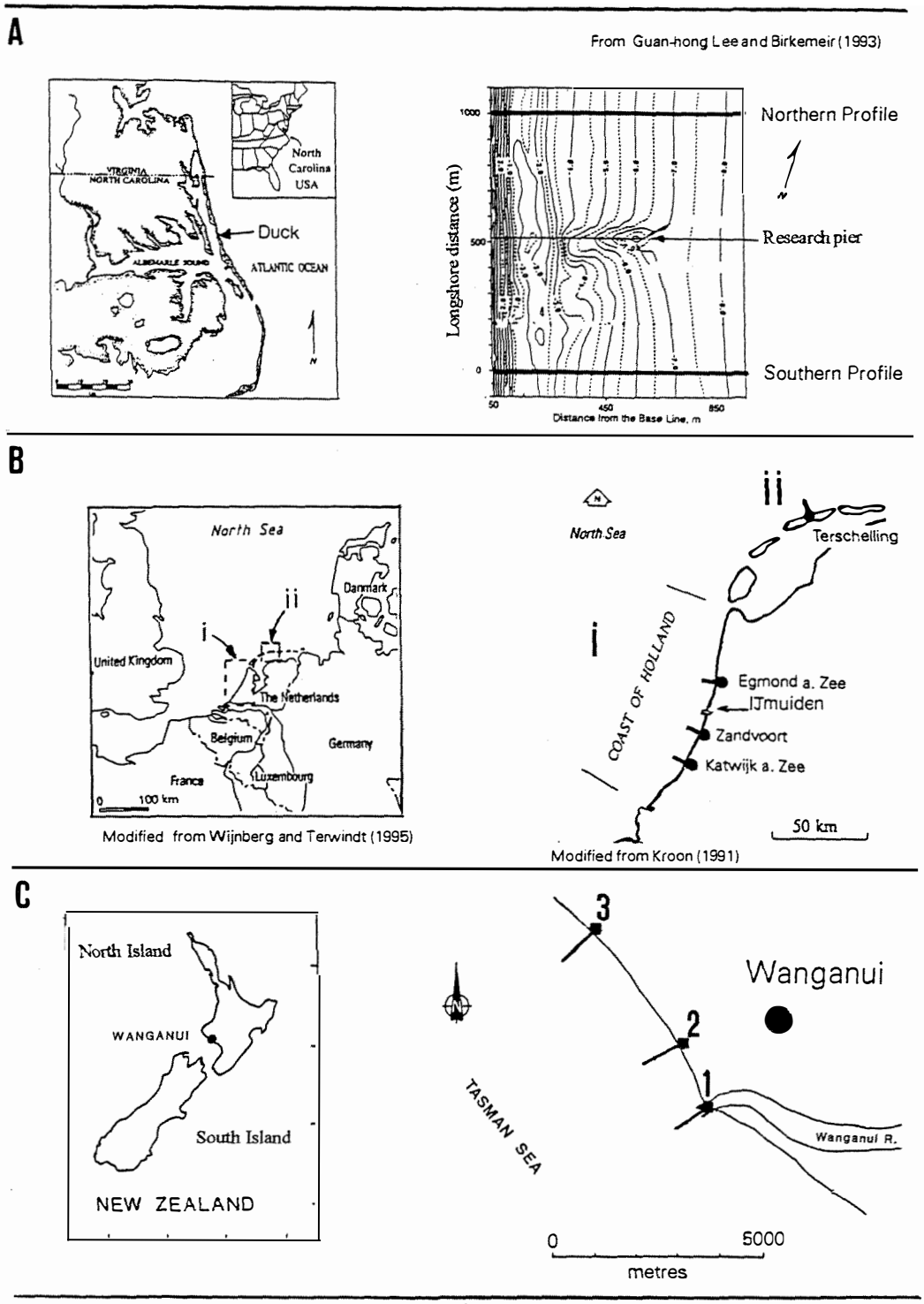

Figure 5.1 Location maps for the global net offshore bar migration sites in North Carolina (Figure A), The Netherlands (Figure B) - where (i) refers to sites along the Coast of Holland and (ii) refers to the Terschelling Island site, and New Zealand (Figure C). The bold shore-normal lines mark survey transects used when collecting the data depicted in Figure 5.3.

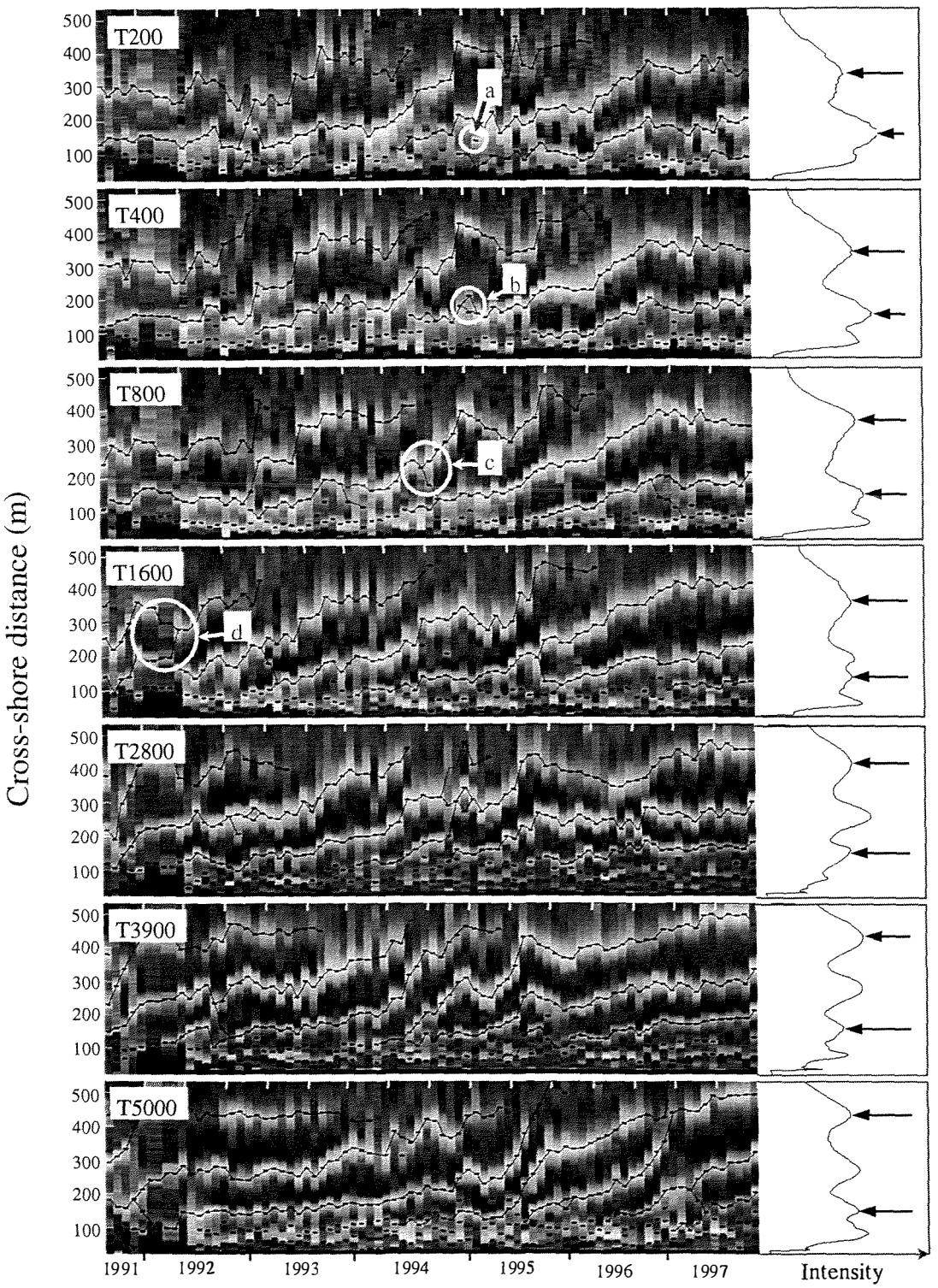

Figure 5.2

Time-stack images showing bar-crest migration tracks for cross-shore transects T200 (200 m northwest of the Wanganui Rivermouth), T400, T800, T1600, T2800, T3900 and T5000. Sampling occurred at approximately monthly intervals between 11.8.91 and 22.11.97 (see Appendix H[i]). The black rectangles locate intensity maxima which represent bar-crests. The circles marked **a** to **d** depict examples of intensity artefacts or atypical morphological behaviour which complicate the identification of NOMs (see section 5.4.1). The curves along the right side of the figure show the time-averaged cross-shore intensity (relative scale) for each time-stack and the arrows point to the intensity maxima which define landward and seaward boundaries of the zone of systematic offshore migration (see section 5.3.2).

A. Egmond

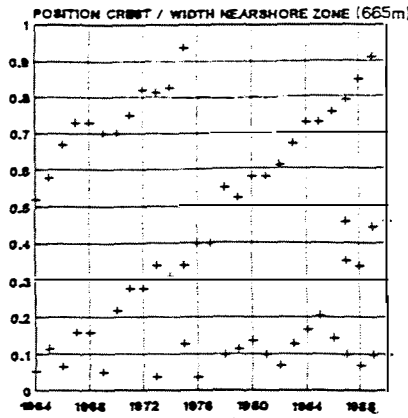

From Kroon (1994)

B. Zandvoort

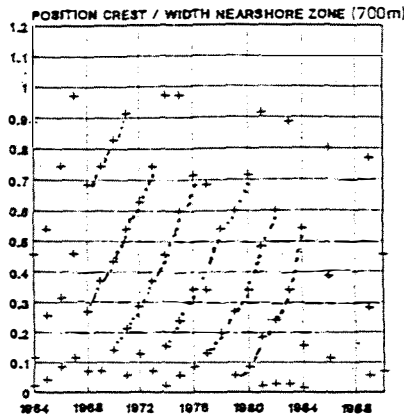

From Kroon (1994)

C. Katwijk

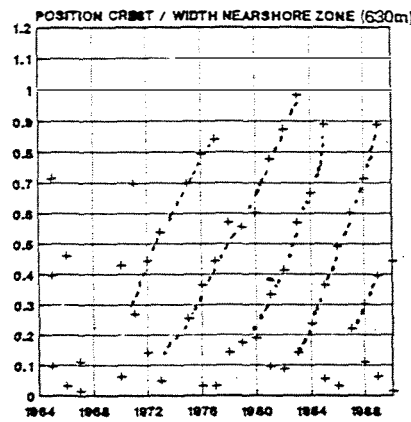

From Kroon (1994)

D. Terschelling

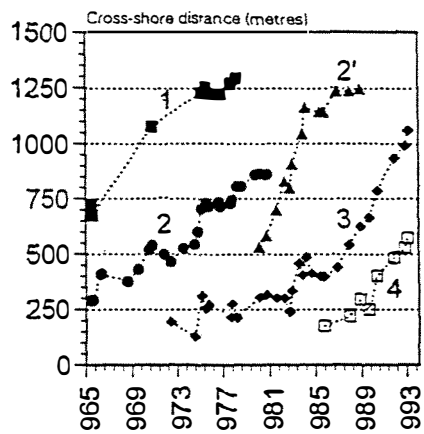

From Ruessink and Kroon (1994)

E. Duck South

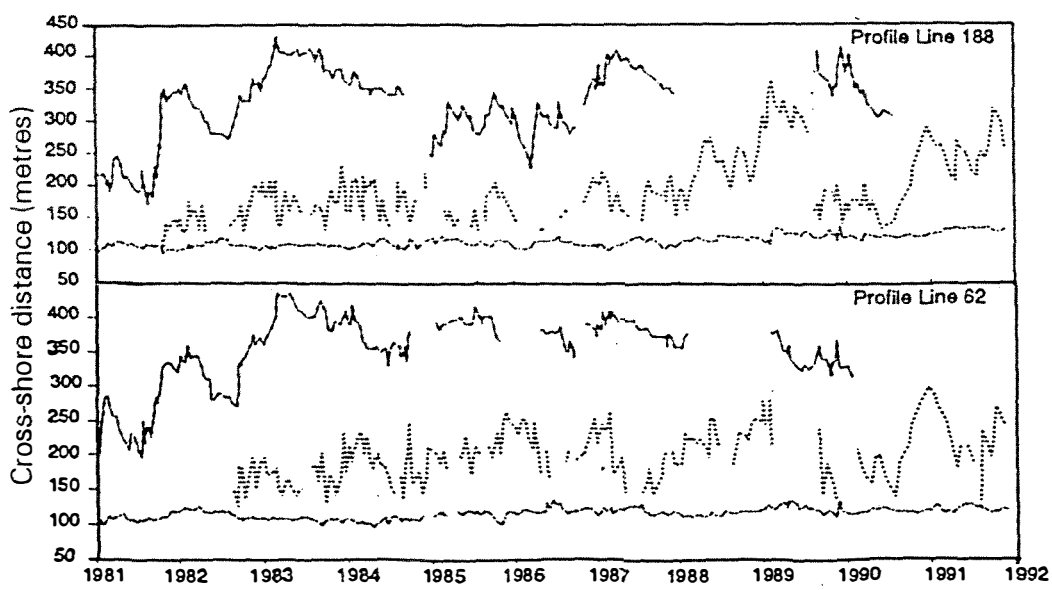

F. Duck North

— Shoreline ---- Inner Bar — Outer Bar

Modified from Lee and Birkemeier (1993)

continued

G. Wanganui Rivermouth (Wanganui 1)

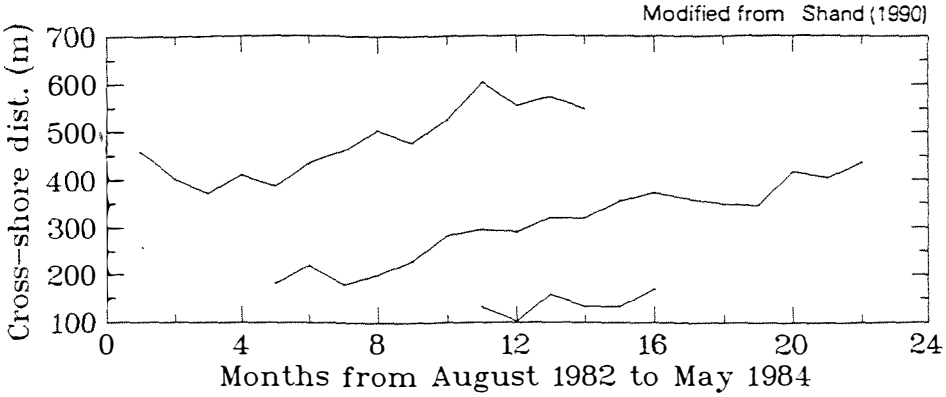

H. Wanganui coast at 1600 m from river (Wanganui 2)

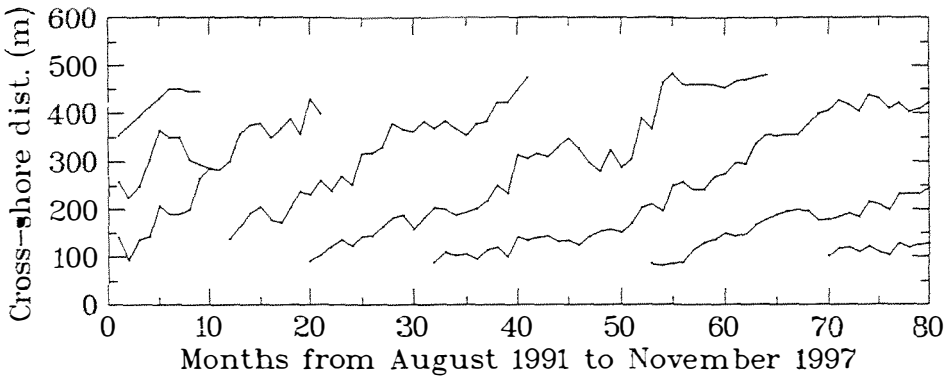

I. Wanganui coast 5000 m from river (Wanganui 3)

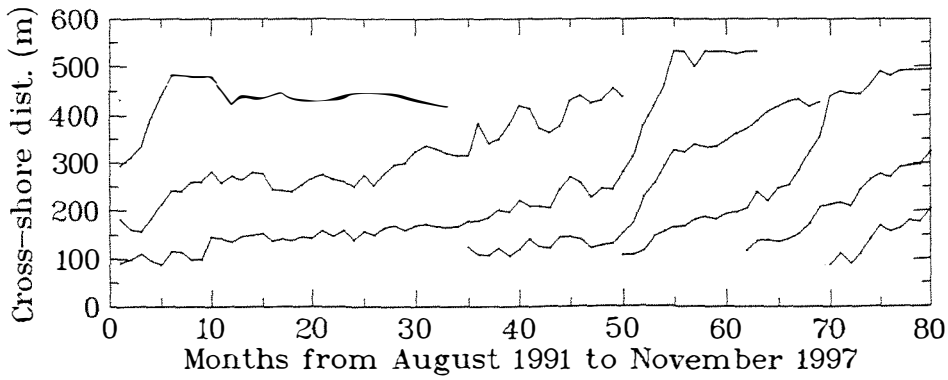

Figure 5.3 Bar-crest time-series showing net offshore bar migration at the global NOM sites in The Netherlands (Figures A to D), North Carolina (Figures E and F), and New Zealand (Figures G to I). For the Wanganui coast (Figures H and I) the data points are intensity maxima derived from time-stack images, while data for all other sites were obtained from ground surveys. For Figures A to C the cross-shore distance is referenced to the foreshore/nearshore boundary, for Figure D the cross-shore reference is the intersect between MSL and the mean profile, for Figures E and F the reference is ~75 m landward of the dune toe, and for Figures G to I the reference is the dune toe.

- What NOM parameter values characterise the global field sites, and what parameter is most representative of the NOM morphological system?
- What environmental conditions (physical boundary and process/sediment) occur on the NOM coasts?
- What are the associations between the NOM characteristics and the corresponding environmental conditions?
- How do the longer-term results contribute toward a conceptual morphodynamic model of NOM?

The environmental conditions at the different NOM field sites are described in the following section (5.2). Section 5.3 describes data acquisition methods and methods developed to determine NOM characteristics. Section 5.4 identifies the NOM characteristics for sites along the Wanganui coast, while NOM characteristics for the global sites are considered in section 5.5. The associations between environmental variables and NOM characteristics are also considered in section 5.5. How the results concerning longer-term aspects of NOM contribute to conceptual morphodynamic modelling of NOM is considered in section 5.6.

5.2 Study Sites

The study sites in the Netherlands, USA and New Zealand are described using a range of environmental parameters which will be outlined below. These parameters are used to measure physical boundary, sediment and process conditions and their selection was based on likely associations with NOM characteristics suggested in the previous reports reviewed in Shand and Bailey (1999). Because of the variation in data available from the different sites, some specific definitions and assumptions had to be made to provide comparable statistics and these will also be described.

Scales and definitions

The scale of the environmental parameters is based on the system considerations in chapter 1, together with likely scale relationships suggested in earlier work on NOM. The minimum survey period for morphological data measurement was taken to be two NOM cycles. Based on the average cycle durations in Table 1.1 the survey period would therefore range between about 8 years at Duck and Wanganui up to about 40 years on the North Holland coast. Such time-spans required the use of long-term 'climatic' process data, i.e. the macro/mega scale processes in Figure 1.5. The scale

of relevant physical boundary parameters suggested by the scale-based couplings in Figure 1.5 range from the general morphology of the bar system itself to cross-shore profile characteristics and coastal orientation.

The physical parameter measurements were based on the cross-shore morphological zones. Because of limitations in the available data, the boundaries differed from those described in chapter 2 (section 2.3.1) and were defined as follows:

- The foreshore/nearshore boundary is the location on the average (ground survey) profile about spring low tide elevation where there is a distinct change in slope. The landward boundary of the foreshore was located at the intersect between mean sea-level and the average profile.
- The nearshore/shoreface boundary is that cross-shore location beyond which (to seaward) the elevation variability within the profile bundles converge to an approximately constant value.
- The foreshore and nearshore limits for the Wanganui Rivermouth (Wanganui site 1) were based on values from the closest available profile bundle which was for a site located 200 metres northwest of the entrance.

Physical and process characteristics

The physical parameters for inter-site comparison consist of: the average slopes ($\tan\beta$) of the mean sea-bed profile for the foreshore and nearshore zones; the nearshore width; the nearshore depth from MSL to the mean profile at the nearshore/shoreface boundary; the time-averaged number of nearshore bar-crests across each profile; and the median grain size (D_{50}) from locations approximating the mean high water level and the mid-nearshore. Representative sediment size values were obtained by averaging sample values taken in the vicinity of these two locations. This sediment size averaging was carried out to account for any size variation related to the particular morphological configuration that occurred at the time of sampling.

Physical boundary parameter values are presented in Table 5.1 together with the information sources. While all nine sites are characterised by multiple bars, inter-site variability occurs for all parameters. Average nearshore bar numbers range between 1.4 at North Duck and 3.2 at Zandvoort. Nearshore widths range between 313 metres at South Duck and 1250 m at Terschelling, while depths at the seaward limit of the nearshore range from

Table 5.1 Morphological and sediment characteristics for the global NOM sites

Site	Width (m) nearshore	Depth (m) nearshore (below MSL)	Slope (tan β): nearshore	Slope (tan β): foreshore	Bar number: nearshore	Sediment D_{50} (mm): foreshore	Sediment D_{50} (mm): nearshore
Egmond	670	6.8	0.0079	0.020	2.2	0.32	0.21
Zandwoort	705	5.0	0.0054		3.2	0.21	0.16
Katwijk	510	4.8	0.0064		2.4	0.27	0.17
Terschelling	1250	8.0	0.0041	0.015	2.5	0.21	0.17
Duck South	313	4.7	0.0096	0.052	1.5	0.47	0.18
Duck North	460	6.0	0.0098	0.060	1.4	0.47	0.19
Wanganui 1	405	5.4	0.0089	0.031	2.2	0.40	0.16
Wanganui 2	536	6.3	0.0092	0.034	2.5	0.41	0.18
Wanganui 3	662	6.5	0.0083	0.029	2.7	0.23	0.20
Minimum	313	4.7	0.0041	0.015	1.4	0.21	0.16
Maximum	1250	8.0	0.0098	0.060	3.2	0.47	0.21

Sources: Burgess (1971), Larson and Kraus (1992), Short (1992), Stauble (1992), Lee and Birkemeier (1993), Kroon (1994), Ruessink and Kroon (1994), Westlake (1995), plus Wanganui data collected and analysed by the author.

Table 5.2 Energy characteristics for the global NOM sites

Site	Wave recorder depth (m)	Mean wave height (m)	Extreme wave height (m)	Wave period (seconds)	Spring tide range (m)	Storm wind speed (m/s)	Wind/coast angle (degrees)
Egmond	21	1.35	4.10	6.00	1.78	13.4	82
Zandwoort	21	1.35	4.10	6.00	1.84	13.4	67
Katwijk	21	1.35	4.10	6.00	1.86	13.4	58
Terschelling	15 & 26	1.35	4.30	6.00	2.50	13.4	17
Duck South	18	1.10	3.05	6.40	1.20	12.3	40
Duck North	18	1.10	3.05	6.40	1.20	12.3	40
Wanganui 1	30	1.20	3.20	7.80	2.36	14.8	43
Wanganui 2	30	1.20	3.00	7.80	2.36	14.8	37
Wanganui 3	30	1.20	3.20	7.80	2.36	14.8	20
Minimum	18	1.10	3.05	6.00	1.20	12.3	17
Maximum	30	1.35	4.10	7.80	2.50	14.8	82

Sources: Wieringa and Rijkoort (1985), Macky et al., (1988), Ministry of Transport (1989), Patterson (1991), Larson and Kraus (1992), Patterson (1992), Short (1992), Lee and Birkemeier (1993), Hoestra et al., (1994), Kroon (1994), Ruessink and Kroon (1994), Westlake (1995), Wijnberg (1995), also: Birkemier (pers. comm.) for tidal information from Duck ; National Institude of Water and Atmospheric Research (NZ) for Wanganui wind data.

4.7 m (South Duck) to 8.0 m (Terschelling). Nearshore slopes vary between 0.0041 (Terschelling) and 0.0098 (North Duck) and the foreshore slopes range from 0.015 (Terschelling) to 0.06 (North Duck). Nearshore sediment size (median) ranges between 0.16 mm (Wanganui 1 and Zandvoort) and 0.21 mm (Egmond), while the foreshore sediments range from 0.21 mm (Zandvoort) to 0.47 mm (Duck).

Process characteristics are described using the parameters given in Table 5.2. All wave data are from instruments located where water depths are at least 18 m below MSL. It was assumed that at such depths the effects of shoaling and other sea-bed interactions would be insignificant. The average wave height was determined by reference to the mean daily significant wave height, and the extreme wave height is defined by the 1% exceedence value. The mean daily significant wave period was used. Empirical-based conversions from Patterson (1985) were used to convert spectral peak period, or zero upward crossing period, to significant wave period. Storm-strength winds (taken as the upper 10% of wind speeds) were used in this study. The wind direction parameter (for the predominant storm winds) was measured relative to the coastline.

Parameter values for the process variables are presented in Table 5.2 together with the information sources. Spring tides ranged between 1.2 m (Duck) and 2.5 m (Terschelling). Wave heights (1% exceedence) varied between 3.05 metres at Duck and 4.3 metres at Terschelling, while wave periods ranged from 6 seconds for The Netherlands sites to 7.8 seconds at Wanganui. For sites in the Netherlands, wind data from the centrally located Texel light-ship was used. The use of the Texel data is considered acceptable as Westlake (1995, p35) reported that "It has been established that there exists a strong correlation between wind velocities measured at IJmuiden (on the mid-Holland coast) and Terschelling... " Wind speeds (10% exceedence) ranged between 12.3 m/s (Duck) and 14.8 m/s (Wanganui). In contrast to the relatively narrow range for extreme wave heights and storm wind speeds, storm wind directions were highly variable and ranged from 17 degrees (to the coastline) at Terschelling to 82 degrees at Egmond. The energy values indicate that all sites are located in the storm-dominated environments as defined by Davies (1980).

Other environmental characteristics

A variety of anthropogenic, geomorphological and geological conditions occur at the global NOM study sites which may influence NOM characteristics. While these factors have not been included within the NOM/environmental parameter analysis, they are outlined for completeness. Both the Dutch and North Carolina regions may still be affected by submergence associated with glacio-isostasy, hydro-isostasy and possibly geoidal

deformation (Peltier, 1987). Tectonic deformation at Wanganui has resulted in seaward tilt across the coast (Pillans, 1990). Both Terschelling and the Wanganui sites are situated on, or near, active ebb tide deltas (Burgess, 1971; Ruessink, 1998). At Wanganui, Duck and on the mid Holland coast, jetties have been constructed (Burgess, 1971; Miller et al., 1983; Wijnberg, 1995), and beach nourishment has occurred along the Holland coast (Wijnberg, 1995). At the regional scale, coastal stability studies indicate shoreline and/or shoreface erosion exists at all sites. However, at the local scale, cross-shore and longshore variations in erosion and accretion often occur (Dolan and Hayden, 1983; Fenster and Dolan, 1994; Johnston, 1985; Wijnberg, 1995; Smith and Ovenden, 1998).

5.3 Methods

5.3.1 Data Acquisition Methods

Data sources

Details of the data collection systems used at the various NOM field sites are summarised in Table 5.3. Field surveys for the Dutch data began in 1964 and have continued at yearly intervals using vertical aerial photography and echo-sounding (Ruessink and Kroon, 1994; and Wijnberg, 1995). Data collection at Duck, North Carolina began in 1981 and has continued at approximately fortnightly intervals using ground contact instruments (Lee and Birkemeier, 1993). Wanganui Rivermouth data has been collected at fortnightly to monthly intervals since 1925 using lead-lining and echo-sounding; however, only a subset of 1980s data has been analysed for NOM activity in the present study. Data collection on the Wanganui coast began in 1991 at two to four weekly intervals, initially using levelling, echo-sounding and vertical aerial photography, then later using oblique terrestrial photography. The data acquisition techniques used at Wanganui have been described earlier in chapter 3 (section 3.2). The Wanganui monthly data-set sampled between 12.8.91 and 22.11.97 (Appendix H[i]) was used for the NOM investigation in this chapter. With the exception of the Wanganui coastal data, all bar-crest data referred to above were obtained from published reports.

Errors and corrections

Errors associated with the different raw data-sets are summarised in Table 5.3. Elevation accuracy varies between ± 0.02 m for levelling and ± 0.3 m for echo-sounding. However, for oblique terrestrial photogrammetry the bar-crest intensity signal only represents relative depth. Cross-shore

Table 5.3 Details of data collection systems used at the different NOM sites

Site	Record years	Field methods	Sampling rate (/yr)	Elevation accuracy (m)	Cross-shore accuracy (m)
Egmond &	1964-90	Nearshore: echo-sounder	1	+/- 0.25	+/- 10
Katwijk &	1964-90	Foreshore: aerial photo	1	+/- 0.10	+/- 2.0
Zandvoort	1964-90	theodolite	1	+/- 0.01	+/- 1.0
Terschelling	1965-93	Nearshore: echo-sounder	1	+/- 0.20	+/- 10
Duck: north	1981-92	Nearshore: theodolite	24	+/- 0.03	+/- 1.5
Duck: south	1981-92	Foreshore: theodolite	24	+/- 0.03	+/- 1.5
Wanganui 1	1981-84	Nearshore: echo-sounder	12	+/- 0.25	+/- 5
Wanganui sites	1991-96	Nearshore: aerial/terrestrial photography	12	relative	+/- 10
2 and 3	1991-93	Nearshore: echo-sounder	4	+/- 0.30	+/- 5
	1990-94	Foreshore: theodolite or level	4	+/- 0.001 to 0.02	+/- 0.005 to 1

Sources: Horikawa (1988), Shand (1990), Lee and Birkemeier (1993), Shand (1995), Wijnberg (1995) , Bailey and Shand (1996)

accuracy varies from ± 1.5 m for foreshore levelling to ± 10 m for nearshore echo-sounding and nearshore photogrammetry. It should also be recalled from chapter 4 that accuracy with respect to aerial and terrestrial nearshore photogrammetry relates to the position of sea-surface intensity maxima rather than to the location of morphological features on the sea-bed.

In all NOM studies the bar-crests were detected using curve fitting techniques and the crest location was based on cross-shore distance from the dune toe. Bar-crest detection for the ground profile data was based on the maximum positive residual from a fitted curve as described earlier in chapter 3 (section 3.4). Bar-crest detection for the intensity profile data was based on locating the point on a fitted parabola with zero slope using the algorithm PFIT.VIP (chapter 3, section 3.2.6).

Bar-crest locations obtained by sea-bed surveys (ground profiling) and sea-surface surveys (intensity profiling) are similar but they do not coincide and adjustments are required to reconcile these data (see chapter 4, section 4.5). Analysis of the Wanganui bar-crest records in section 5.4 used photogrammetrically derived data based on sea-surface intensity maxima. By contrast, all other global sites used ground profile-based data. Results of the Wanganui NOM analysis were therefore converted to ground profile equivalent locations when used in the global comparison.

Wanganui time-stack data

The image intensity data from the Wanganui coastal sites were arranged into time-stacks using the algorithm MORPHSTK.VIP (chapter 3, section 3.2.6) with segment widths selected to give a longshore resolution of 200 m (see chapter 4, section 4.3.3.2). The associated longshore intensity averaging reduced 3D detail and hence reducing evidence of smaller-scale morphological change associated with rip-channel migration; in effect this filtered out some higher frequency noise from the underlying pattern of NOM. At the Dutch sites, evidence of such 3D bar behaviour were reduced by the annual sampling interval used when collecting these data.

To determine the nature of longshore variability in NOM characteristics along the Wanganui coast, seven cross-shore transects were analysed. These transects were evenly spaced alongshore with closer intervals being used toward the rivermouth to detect any variation in morphological behaviour associated with the expected transition between coast and rivermouth (see chapter 2, section 2.3.1). The location of individual profiles were also selected so they were in close proximity to available ground profile transects (see chapter 3, section 3.3.1). The ground-based data were used to provide long-term physical boundary information corresponding to the imaging sites and to assist in the interpretation of image data. Time-stacks were constructed for the following transects; T200, i.e. 200 m from the rivermouth, T400, T800, T1600, T2800, T3900 and T5000.

5.3.2 Methods of Analysis

NOM parameters

A variety of parameters and terminology have been used by authors such as De Vroeg (1988), Kroon and Hoekstra (1993), Kroon (1994), Ruessink and Kroon (1994) and Wijnberg (1995) to define and describe NOM cycles. The time a bar exists has been referred to as the 'duration' or the 'life-span'. The frequency with which a bar recurs at any location in the surf zone has been referred to as the 'return period' or the 'passage

interval'. A third parameter required to characterise a NOM cycle is the 'cross-shore distance' over which a bar migrates. The 'average rate' of offshore migration has also been used as a NOM parameter. While rate is not an independent measure of NOM, the normalisation of migration distance with respect to time is useful when comparing different sites and it has been widely used by other writers when describing sand-bar dynamics. For completeness, all four parameters will be used in this study and the following terminology is adopted: *NOM width* for the cross-shore migration distance, *NOM duration, NOM rate, and NOM return period*. These parameters are diagrammatically illustrated in Figure 5.4.

The identification of NOM stages

In order to quantitatively define inter-site bar migrational characteristics within the zone of systematic offshore migration, i.e. the second stage in the NOM life-cycle, it was necessary to develop a method capable of partitioning any foreshore/nearshore area such that the NOM stages were isolated. A preferred method would have been to determine the actual stage boundaries by studying morphological characteristics of each bar sequence as depicted on ground profiles. However, this was impossible as complete ground profile data were not available for all sites. A method was therefore required that could utilise both the bar-crest time-series in Figure 5.3, together with the time-averaged ground profile data which were available for all sites.

The zone-defining methodology adopted here is based upon the indication in previous reports on NOM that preferential locations of bar residence may be associated with bar generation and bar degeneration. Reports on NOM have consistently described bars forming 'near' the shoreline (Lippmann et al., 1993, Ruessink and Kroon, 1994; Wijnberg, 1995; and Shand and Bailey, 1999). Ruessink and Kroon (1994) observed that new bars at Terschelling remained near this formation zone for 'some time' before trending seaward. This tendency for a new bar to remain approximately stationary should cause a peak (relative maximum) on the time-averaged profile. Bar degeneration in The Netherlands data has been found to occur relatively rapidly once a bar reaches a certain off-shore distance and/or depth (Kroon, 1994; Ruessink and Kroon, 1994; Wijnberg, 1995). Once again this temporary stationarity should produce a relative maximum on the time-averaged profile. These landward and seaward peaks would thus identify 'equivalent' locations at each site and these locations may separate out the cross-shore NOM stages. An example of a landward and seaward peak associated with time-averaged ground and intensity profiles based on Wanganui data were depicted earlier in Figure 4.11. To test the hypothesis that such

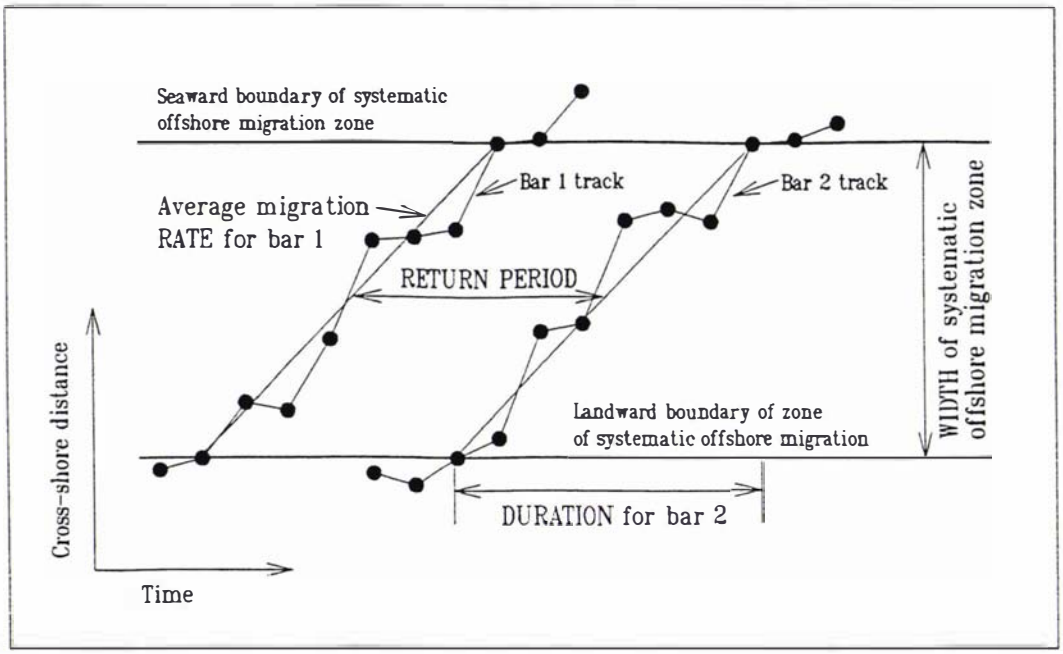

Figure 5.4 Diagrammatic representation of the parameters used to define net offshore bar migration across the zone of systematic offshore migration.

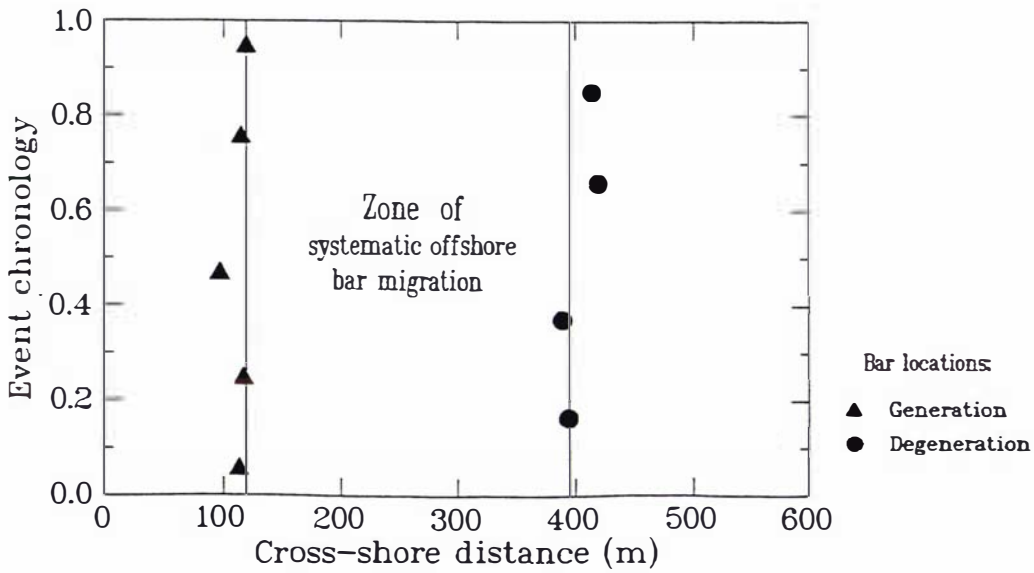

Figure 5.5 Bar-crest generation and degeneration onset locations for the Wanganui site T1500. Vertical lines define the zone of systematic offshore migration which was identified by peaks on the time-averaged profile derived from monthly data collected over the entire study period (see section 5.3.2). While both image-based and ground profile-based methods were used to acquire these data, all points were converted to equivalent ground profile distances using the technique described in chapter 4 (section 4.5)

time-averaged profile peaks will separate out bar generation and degeneration from the zone of systematic offshore migration, the bar-crest locations at a Wanganui site were analysed.

Locations of bar generation and the onset of bar degeneration from the Wanganui T1500 site, together with peaks from the time-averaged profile, are shown in Figure 5.5. Site T1500 was selected because it provided the most detailed ground survey record for identifying the times of bar generation and bar degeneration. The ground profile and image-based data used to compile Figure 5.5 were sampled at one to four weekly intervals over the period June 1990 to November 1997. All image-based data used in this exercise were converted to ground profile equivalent locations using the technique detailed in section 4.5. From Figure 5.5 it is evident that the time-averaged peaks identified by the two vertical lines, do, at least for these Wanganui data, separate the cross-shore into three zones which largely isolate generating and degenerating bars from those undergoing systematic offshore migration. It should be noted that the location of the peaks, i.e. the vertical lines in Figure 5.5, differ slightly from those shown earlier in Figure 4.11 because of the different time-spans over which data were collected in each case.

Intersection of bar migration track and zone boundary

Determination of the time when a bar crosses into, or out of, the zone of systematic offshore migration depends on the nature of the data-set. As noted earlier, the Dutch data-sets were effectively high frequency filtered because of their low sampling rate; this resulted in the intersection of the bar migration track and systematic offshore migration zone boundary usually being clear and unambiguous. By contrast, the higher sampling rates of the Duck and Wanganui data resulted in migration direction changes which make it more difficult to identify a particular time when a bar could be considered to have moved across a zone boundary. These cross-shore fluctuations in bar location were probably associated with morphodynamic forcing associated with alternating storm/fairweather conditions and longshore migration of rip channel systems. However, as discussed earlier, these effects would be somewhat reduced in the Wanganui data because of the 200 m longshore resolution. For the Duck and Wanganui data-sets a boundary was deemed to have been crossed by a bar when two sequential bar-crest positions were located across that boundary (see Figure 5.6A).

As relatively low levels of longshore variability in average NOM characteristics were found to occur along the Wanganui coast, it was desirable to define the time at which a bar crossed a zone of systematic offshore migration boundary as accurately as possible. Error band lines

representing a bar-crest's cross-shore location resolution were therefore constructed about the zone boundary lines as illustrated in Figure 5.6B. The bar migration intersection criterion (Figure 5.6A) were then applied at both the inner and outer error band line and the two intersection points were time-averaged to determine when the zone boundary crossing was deemed to have occurred.

Adjustment of the Wanganui bar-crest data for longshore variation in the rate of shoreline change was not considered necessary on the basis of the general uniformity suggested in Figure 2.7.

Incomplete NOMs

Each bar-crest time-series contained cases where NOMs were truncated at the start or end of the record. Owing to the erratic behaviour of cross-shore bar migration it was not acceptable to apply linear extrapolation techniques to all partially completed NOMs. However, in some situations partially completed NOMs could provide additional information. In particular, if a minimum completion time was used, and if the resulting duration parameter value was greater than the values from the other completed NOMs, then this result was included in the calculation of the average parameter values. The minimum completion time was derived using the 'maximum likely migration sequence' observed in the Wanganui data. This sequence was developed from the time-stacks in Figure 5.2 and is listed in Table 5.4.

5.4 Wanganui sites

5.4.1 Results

The time-stacks corresponding to cross-shore transects T200, T400, T800, T1600, T2800, T3900, and T5000 are shown in Figure 5.2. The black squares identify intensity maxima which represent bar-crest locations. The lines joining adjacent bar-crest locations depict the migrational histories of individual bars. The bar tracks in Figure 5.2 show that most bars migrate seaward across the zone of systematic offshore migration in an approximately linear manner. Isolated intensity maxima, e.g. **(a)** in Figure 5.2, may be associated with imaging artifacts or specific bar behaviour such as the longshore translation of larger-scale 3D morphology. Splitting or merging of an intensity sequence was found to be associated with the following behaviour: longshore translation of rip channels, e.g. **(b)** in Figure 5.2; bar bifurcation, e.g. **(c)** in Figure 5.2; or bar

Table 5.4 Maximum likely cross-shore distances traversed during successive seaward bar migrations based on inter-survey data from the Wanganui time-stacks depicted in Figure 5.2.

Month	Seaward migration distance (m)	Cumulative migration distance (m)
1	60	60
2	40	100
3	30	130
4	20	150

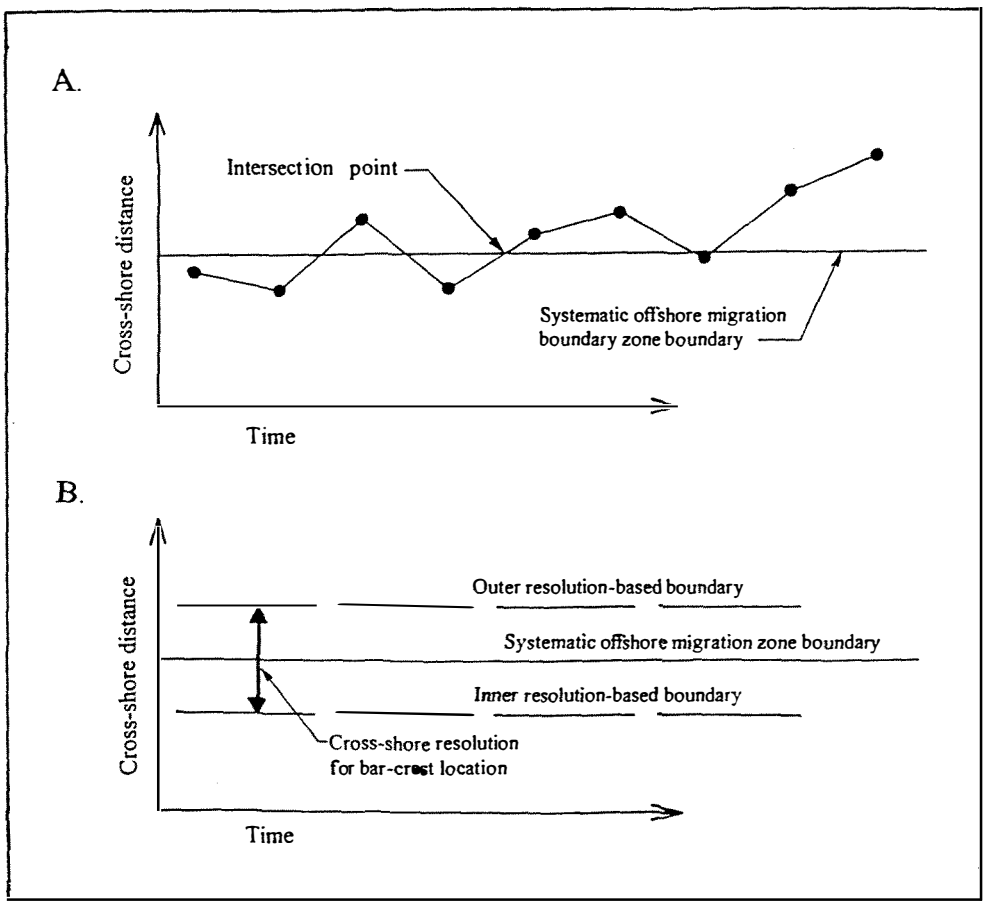

Figure 5.6 Methods of determining 'the time' when a migrating bar crosses the boundary of a zone of systematic offshore migration. Figure A illustrates the location of bar track and zone boundary intersection as described in the text. Figure B shows how cross-shore resolution for bar-crest measurement is accommodated by using inner and outer resolution-based boundary lines. The intersection procedure detailed in Figure A is applied to both boundary lines and the mean time is used as 'the time' when a bar crosses the zonal boundary.

switching, e.g. **(d)** in Figure 5.2. The latter two types of morphological behaviour, bar bifurcation and bar switching, are described in chapter 6 (sections 6.1 and 6.5).

Bar bifurcation and bar switching complicate the identification of NOMs and were dealt with in the following manner. With bar bifurcation, the landward bifurcate appeared to be smaller than the seaward bifurcate so the latter feature was incorporated into the NOM. By contrast, with bar switching all bars appeared to be of similar size so all bars were incorporated into NOMs. Accordingly, in the case of merging bar tracks, the associated NOMs had different times of entry into the landward side of the zone of systematic offshore migration, but the same exit time from the seaward side of the zone. This approach to identifying NOMs was also used for the global data (section 5.5) when apparent bifurcating or switch-associated bar migration patterns were evident.

On the right hand side of each time-stack image in Figure 5.2 is the corresponding time-averaged intensity plot. These graphs were computed by time-averaging the adjacent time-stack intensities. The two arrows on each curve locate the intensity maxima (via the fitting of parabola) which mark the boundaries of the zone of systematic offshore migration as described earlier in section 5.3.2. The increase in the separation between the arrows with increased distance from the rivermouth shows that average NOM width increases with increasing distance from the rivermouth.

Linear trend lines associated with each bar's NOM have been fitted between the boundaries of the zone of systematic offshore migration in Figure 5.7. The bold lines represent completed NOMs. The dashed lines represent uncompleted NOMs; these lines were extrapolated to the systematic offshore migration zone boundary as they contain additional information (see final paragraph of section 5.3.2). The diagonal orientation of these lines show that NOM dominates bar behaviour at Wanganui over longer time scales. However, the variation in slopes show that individual cycles can have quite different NOM characteristics.

NOM parameter values for each site are depicted in Figure 5.8. The parameter means have been joined by a line. Mean NOM widths vary between 177 m at T200 and 283 m at T5000. Mean durations vary between 1.4 yr at T200 and 2.4 yr at T5000. Mean rates vary between 130.9 m/yr at T3900 and 169.4 m/yr at T800, and mean return periods vary from 1.3 yr at T1600 to 1.5 yr at T2800. The (error) bars in Figure 5.8 represent the range of parameter values for duration, rate and return period. There is no range of values for NOM width because of the averaging method used to identify

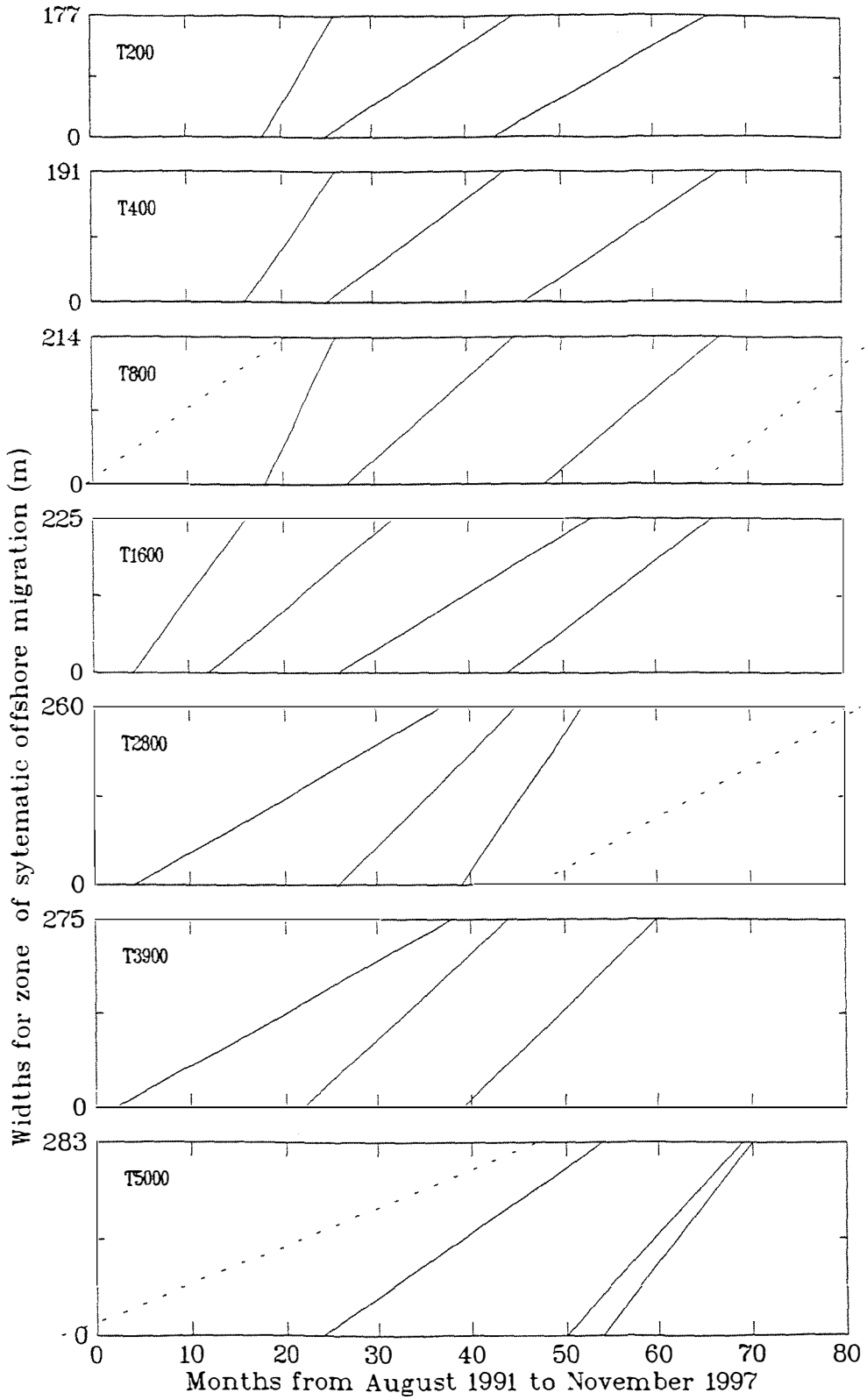

Figure 5.7 NOM trend lines fitted through each bar track's intersection points with the landward and seaward boundaries of the zone of systematic offshore migration for the seven Wanganui sites. These sites are located 200, 400, 800, 1600, 1800, 3900 and 5000 m to the northwest of the Wanganui River-mouth. Continuous lines represent completed bar migrations, while dashed lines represent those incomplete migrations which provide additional information on NOM parameter values (see section 5.3.2).

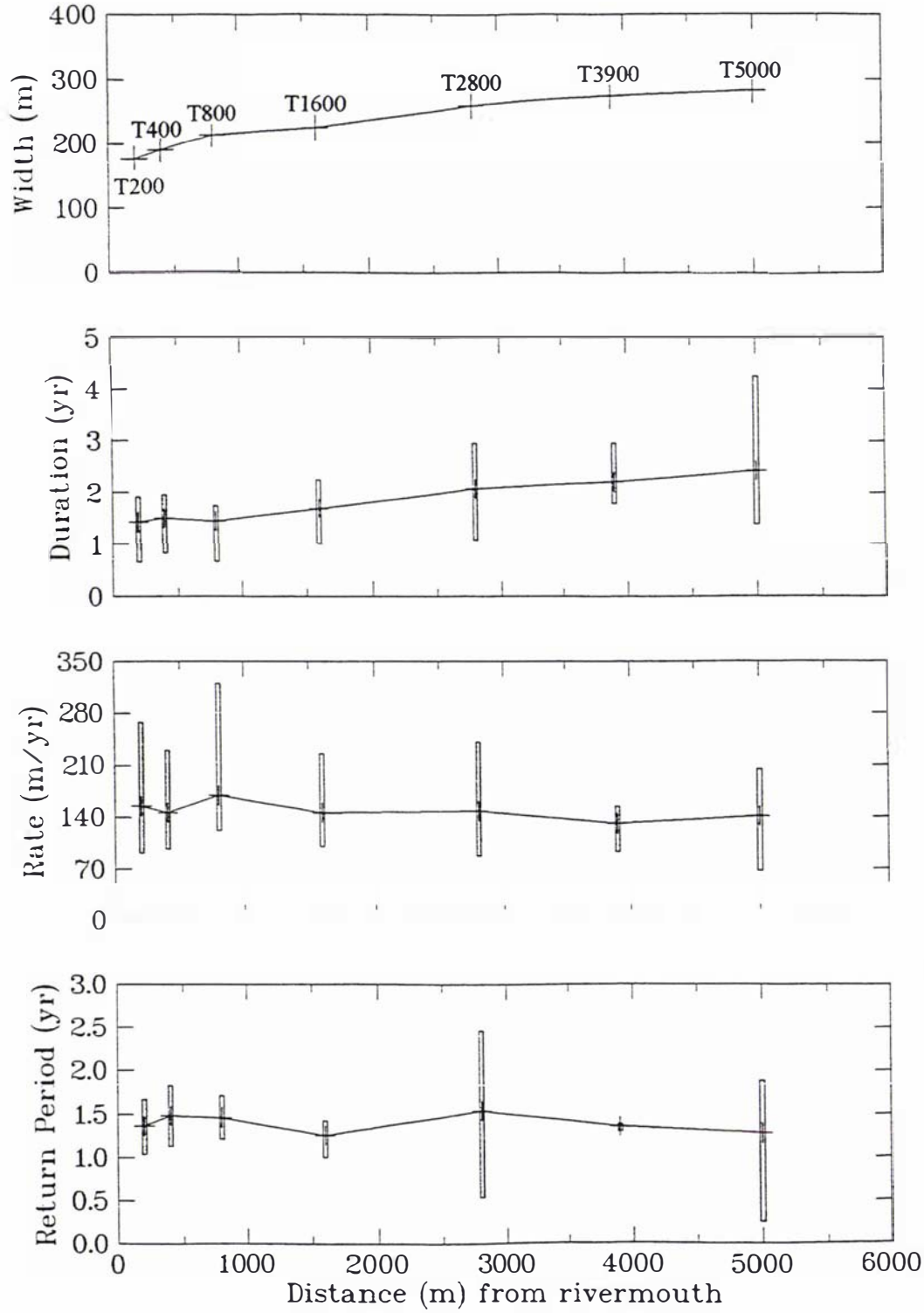

Figure 5.8 NOM parameter values for the seven cross-shore transects along the Wanganui coast. The means are depicted by points which have been joined by lines. The (error) bars for duration, rate, and return period illustrate the range of values experienced by individual cycles of NOM.

the zone of systematic offshore migration boundaries. The ranges for duration at T2800 and T5000 are greater than those experienced at the other sites. A similar pattern also occurs for return period. The variability in NOM rates is particularly high near the rivermouth with the lowest range occurring at T3900; this latter site also had the lowest range for duration and return period. The variability shown by these results will be considered further in the following chapter.

Longshore trends for the NOM parameter values are shown by the straight lines in Figure 5.9. These lines represent linear regression models fitted to the mean parameter values. The NOM width and duration values both increase with increasing distance from the rivermouth. Both these associations are highly significant with the F ratio probabilities being 0.0004 and 0.00003 respectively. In contrast, NOM rate shows a slight decrease with increasing distance from the rivermouth. However, this trend has only weak statistical significance ($p = 0.1$). Return period also shows a decrease with increasing distance from the rivermouth, but in this case the trend is not significantly different from zero ($p = 0.549$).

5.4.2 Discussion

The results from the Wanganui study area show that bar behaviour on this coast, when considered over a 6.3 year time span, is dominated by a repetitive pattern associated with cycles of NOM.

While the within-site variability in NOM parameter values for individual cycles suggests that energy inputs may influence NOM, the inter-site variability in contemporaneous bar behaviour evident in Figure 5.2 indicates that the existing morphology must also have a significant influence on NOM. These results and interpretation are consistent with the conclusion reached by Shand and Bailey (1999) in their review of NOM; i.e. that episodes of offshore bar migration are driven by smaller-scale events (storms), while the timing and nature of offshore bar migrations are influenced by small to moderate-scale antecedent morphology. The nature of these influences on NOM will be investigated in chapter 6.

The minimal longshore gradient in mean parameter values (Figure 5.9) suggests that in the longer-term NOM behaviour along the Wanganui coast may achieve longshore uniformity with respect to NOM characteristics. However, a longer data-set would be required to confirm this possibility. If such longshore uniformity did exist, then the observed statistically significant

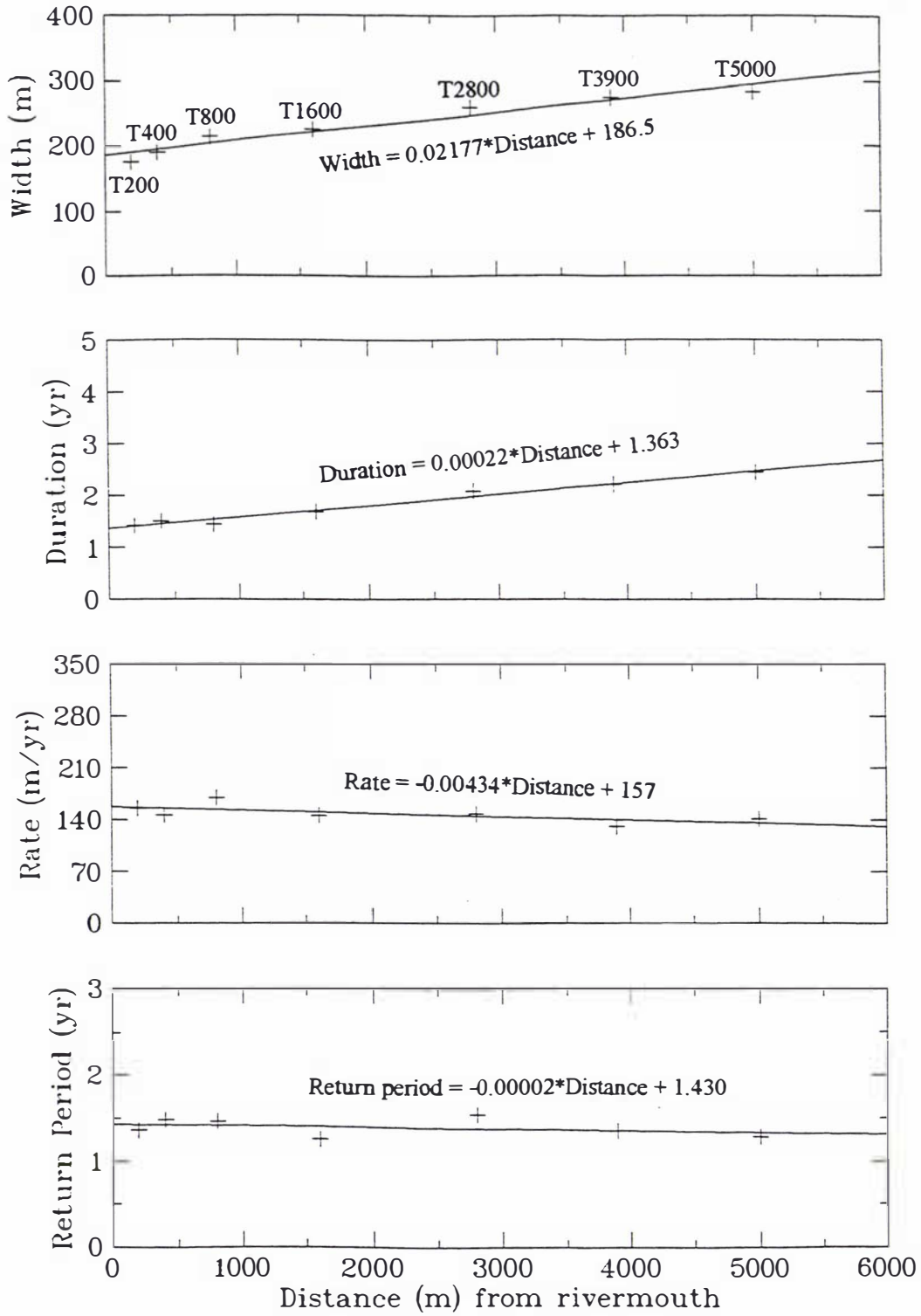

Figure 5.9 Longshore trend lines (linear regression models) fitted to mean NOM parameter values for the seven cross-shore transects along the Wanganui coast.

increase in duration values with increasing distance from the rivermouth is simply a reflection of the increasing distance over which the bars have to migrate to reach the more seaward located degeneration zone. The weak significance of the longshore trend in NOM rate and the insignificance of the return period trend also support the long-term longshore uniformity concept. Alternatively, if the trend line slopes for the NOM rates are valid then longshore gradients in larger-scale environmental variables at Wanganui would be expected to influence NOM morphodynamics.

Given the possible existence of longshore variation in NOM characteristics, two transects were selected to represent NOM at Wanganui in the global comparison. The chosen representative transects were T1600 and T5000. The NOM parameter values for T1600 and T5000 were derived from the regression models in Figure 5.9. The T1600 and T5000 locations were selected as they maximised the difference in parameter values while avoiding rivermouth proximity. It will be recalled from section 5.1 that data from a rivermouth transect is included in the global analysis. The three Wanganui sites have also been referenced as Wanganui 1 (the rivermouth transect), Wanganui 2 (the 1600 m transect) and Wanganui 3 (the 5000 m transect).

5.5 Global sites

5.5.1 Results

This section will describe the values of NOM parameters for each global site, identify an index parameter to represent the NOM morphological system, and then determine the associations between environmental variables and the index parameter.

NOM parameter values

The average NOM parameter values for the nine different field sites are presented in Figure 5.10. When compared with the Wanganui and Duck sites, The Netherlands sites tend to have NOMs with greater migration widths (305 to 930 m c.f. 195 to 379 m), longer durations (3.7 to 13 yr c.f. 1.2 to 2.4 yr), lower migration rates (34.8 to 85.1 m/yr c.f. 121.9 to 196 m/yr) and longer return periods (3.3 to 14.4 yr c.f. 1.2 to 6.8 yr). Terschelling is notable for its extensive width (930 m). Egmond and Terschelling have particularly long durations (10.6 and 13 yr) and return periods (14.4 and 7.5 yr). Egmond has a very low rate of NOM (34.8 m/yr). The return periods for the Wanganui sites are shorter than at the other sites (1.2 to 1.4 yr c.f. 3.2 to 14.4 yr).

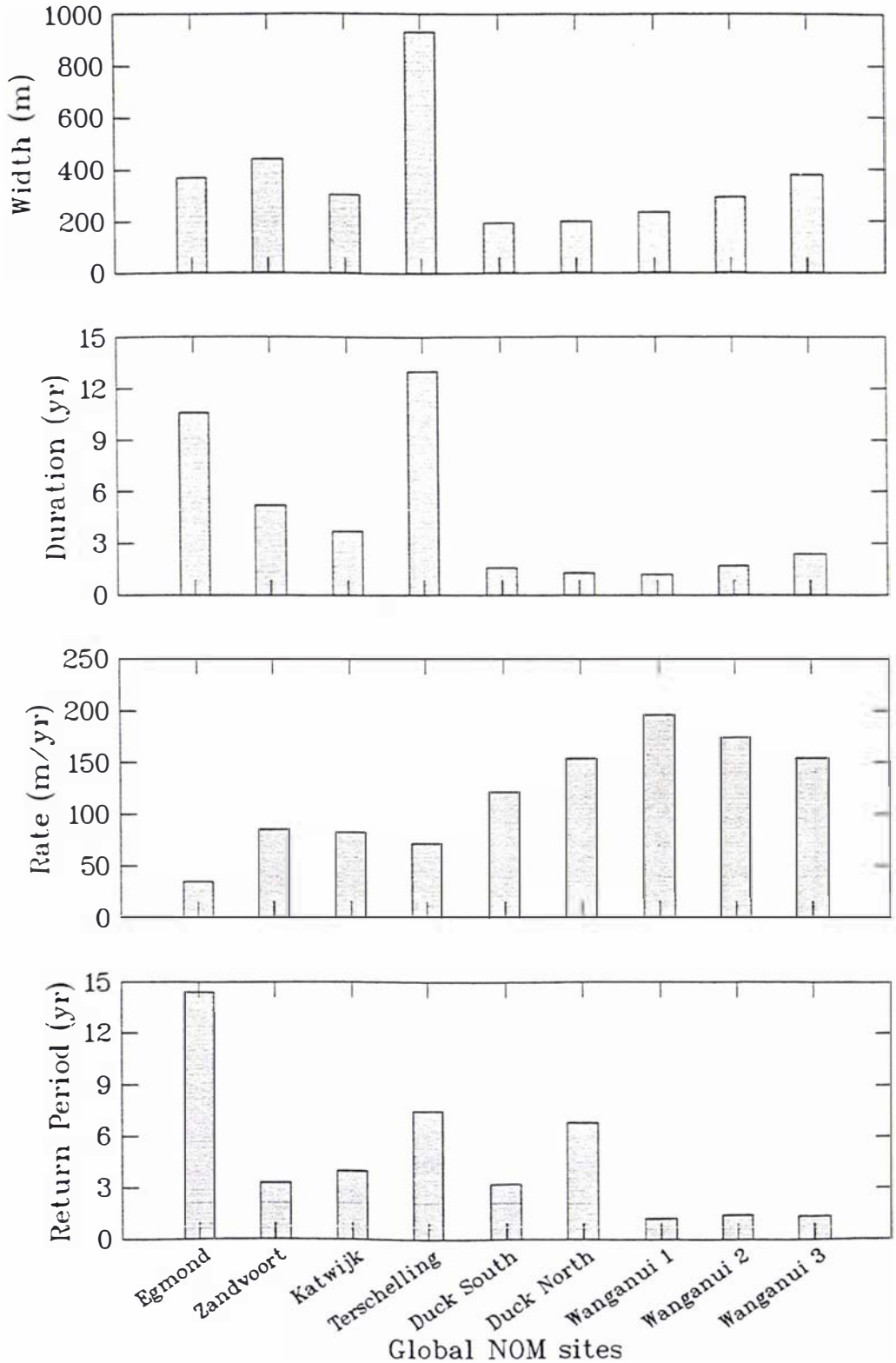

Figure 5.10 Graphs showing average bar migration parameter values for the global NOM sites.

When comparing the NOM parameter values in Figure 5.10 with the values given in Table 1.1 for the earlier NOM studies, it is evident that the durations are lower (1.2 to 13 yr c.f. 2 to 20 yr) and the range of values for rates are less (34.8 to 196 m/yr c.f. 15 to 200 m/yr). This is due to differing time periods over which the data-sets were collected and also because different methods were used to identify the migration end points. In particular, the earlier analysis used an approximation of the initial appearance and final disappearance of each bar, whilst the present study measures bar migration between two cross-shore limits which define the zone of systematic offshore migration.

The results of a linear correlation analysis between the average NOM parameter values are shown in Figure 5.11. These results identify duration as the parameter most strongly associated with the other NOM parameters. Duration was therefore selected as the index parameter to represent NOM behaviour in the subsequent analysis with the environmental parameters.

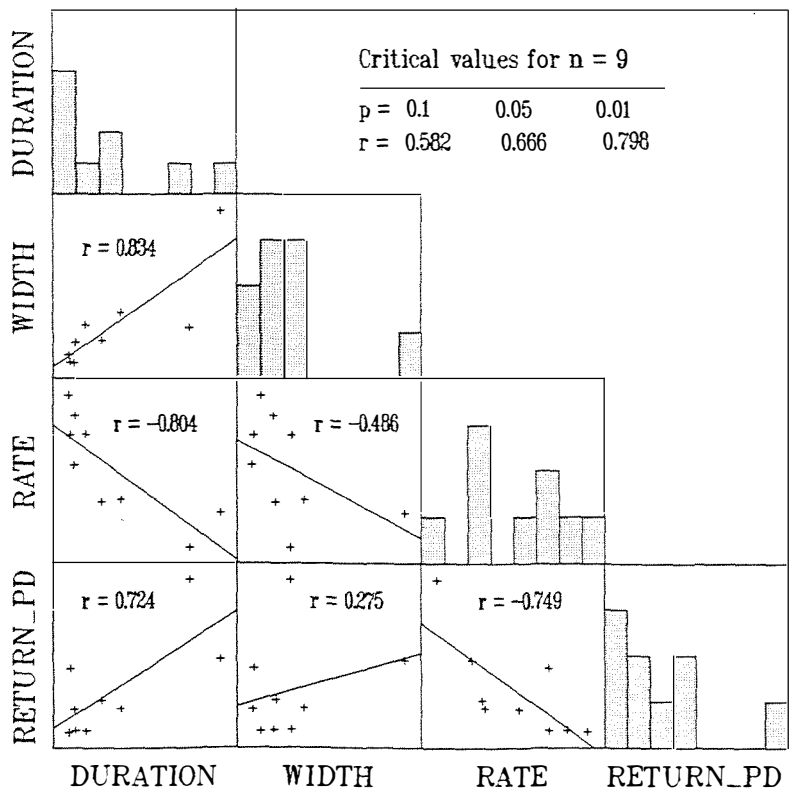

Figure 5.11 Plots of global NOM parameters' values showing fitted linear regression models, Pearson correlation coefficients (r) and critical values for different levels of significance.

Of further note in Figure 5.11 are the positive associations between duration, return period and width, while all three are negatively correlated with the rate parameter. NOM with lower duration values and higher rates will be described as having a 'higher level of NOM activity'.

Environmental conditions and NOM comparison

The result of a linear correlation analysis between NOM duration and the physical boundary variables is given in Table 5.5A. Significant associations at the 10% level of significance, i.e. $p < 0.1$, occurred in all cases except bar number and nearshore sediment size. Curvilinear regression models incorporating power functions appear to better fit the sediment/duration and slope/duration data (see Figure 5.12). Such relationships may be appropriate given the typically non-linear associations that have been found to occur between sediment size and cross-shore slope (see Komar, 1976a; Hardisty, 1990; Stauble, 1992; Hoekstra et al., 1994). Of particular note is the apparent outlier status of Egmond and that the nearshore sediment size only began to show an association with duration, as depicted in Figure 5.12C, when both the Egmond data and the Wanganui Rivermouth (Wanganui 1) data were excluded. Data from the latter site appeared to have been contaminated by finer flood borne river sediment prior to sampling.

The linear correlation coefficients for NOM duration with the process variables are given in Table 5.5B. Mean wave height, extreme wave height and wave period were the only process variables to show significant associations (at $p < 0.1$) with duration. However, the correlation coefficients in Table 5.5B were based on nine independent samples whilst the wave data came from only four recorders as indicated in Table 5.2. To account for this lack of independence in the wave data the NOM durations were averaged to provide only one value per wave height sample and the correlation analysis was then repeated; these results are shown in Table 5.5C. Only extreme wave height now showed a significant association with duration at $p < 0.1$.

The duration/wave height result should be interpreted with caution. Non-equivalency errors in the wave data, short record lengths, and difficulties reconciling various statistics used in the different publications, may have resulted in errors that could significantly affect the correlation, given the similarity in wave height parameter values (Table 5.2).

No linear association is evident between NOM duration and the wind parameters in Table 5.5B; however, Figure 5.13A shows that a strong non-linear relationship appears to exists with wind direction. It will be recalled that the wind direction variable was based on the angle between the shore-line and predominant (storm) wind approach and therefore incorporates

Table 5.5 Pearson correlation matrices for NOM duration with morphological and sediment variables (A), process variables (B) and for independent (see text) wave data (C). The critical correlation values for significant associations are also listed.

A.	Duration	Sediment: foreshore	Sediment: nearshore	Slope: foreshore	Slope: nearshore	Depth: nearshore	Width: nearshore	Bar number
Duration	1.000							
Sediment: foreshore	-0.592	1.000						
Sediment: nearshore	-0.142	0.127	1.000					
Slope: foreshore	-0.653	0.680	0.000	1.000				
Slope: nearshore	-0.739	0.862	0.397	0.620	1.000			
Depth: outer nearshore	0.688	-0.352	0.385	-0.472	-0.322	1.000		
Width: outer nearshore	0.850	-0.728	-0.049	-0.593	-0.823	-0.789	1.000	
Bar number: nearshore	0.297	-0.837	-0.295	-0.541	-0.658	-0.134	0.487	1.000

Number of observations = 9 Critical values (two tailed) p = 0.1 0.05 0.01
r = 0.582 0.666 0.798

B.	Duration	Mean wave height	Extreme wave height	Wave period	Storm wind speed	Wind approach	Spring tide range
Duration	1.000						
Mean wave height	0.740	1.000					
Extreme wave height	0.827	0.960	1.000				
Wave period	-0.582	-0.487	-0.691	1.000			
Storm wind speed	-0.136	0.154	-0.105	0.788	1.000		
Storm wind approach	0.139	0.423	0.395	-0.463	-0.226	1.000	
Spring tide range	0.282	0.424	0.248	0.496	0.860	-0.383	1.000

Number of observations = 9 Critical values (two tailed) p = 0.1 0.05 0.01
r = 0.582 0.666 0.798

C.	Duration	Mean wave height	Extreme wave height	Wave period
Duration	1.000			
Mean wave height	0.830	1.000		
Extreme wave height	0.925	0.963	1.000	
Wave period	-0.623	-0.478	-0.668	1.000

Number of observations = 4,
Critical values (two tailed) p = 0.1 0.05 0.01
r = 0.90 0.95 0.99

A.

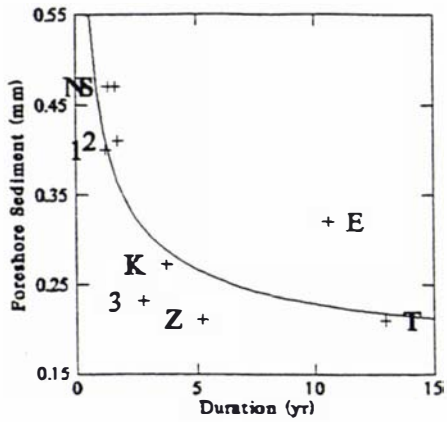

B.

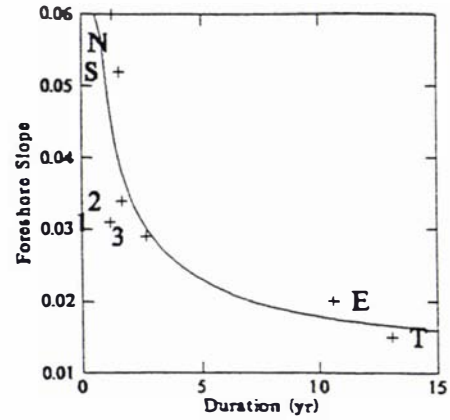

C.

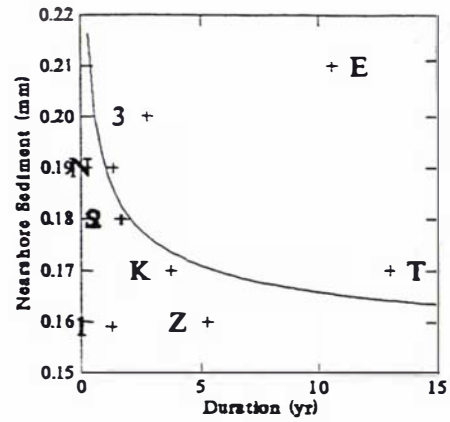

D.

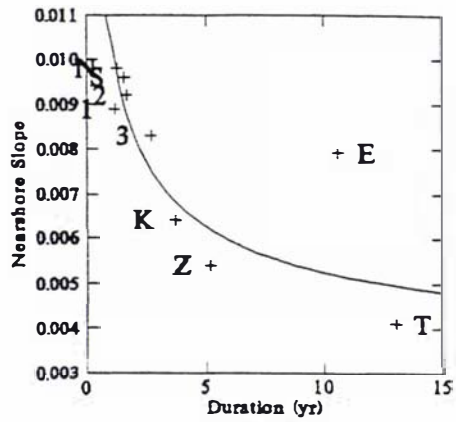

Where:

E = Egmond	T = Terschelling	1 = Wanganui 1
Z = Zandvoort	S = Duck South	2 = Wanganui 2
K = Katwijk	N = Duck North	3 = Wanganui 3

Figure 5.12 Plots of NOM duration with sediment size (Figures A and C) and slope (Figures B and C). Power curves have been fitted to the full data-set in Figures A,B and D but Egmond (E) and the Wanganui Rivermouth (1) have been excluded in Figure C

the boundary condition of coastal orientation. Figure 5.13A shows that duration decreases from a high value at high angle (i.e. predominating wind tending shore-normal) to reach a minimum at approximately 45 degrees. Duration values increase again as the angle decreases toward zero, i.e. predominant wind tending shore-parallel. Repetition of the regression using a quadratic function improved the correlation coefficient from r = 0.133 (Table 5.5B) to r = 0.846. Residuals from the fitted parabolic curve can be observed in Figure 5.13A and these values suggest that the actual relationship is asymmetrical with lower durations being maintained from ~45 degrees toward ~20 degrees before rapidly increasing.

5.5.2 Discussion

5.5.2.1 Underlying drive mechanisms

The environmental parameter values characterising the global sites indicate the type of conditions that are necessary for NOM to occur. Multiple bars, short period waves, and a narrow range of storm strength wind and wave conditions occurred at all sites (Tables 5.1 and 5.2). A drive mechanism for NOM should therefore incorporate these conditions. Spring tide ranges fit within the high micro/low meso categories defined by Davies (1980), and they are consistent with the multiple bar environments identified in Masselink and Short(1993). Storm conditions appear to drive NOM as the relationship between higher energy events and increased seaward bar migration has been well established by laboratory and field results, e.g. Sallenger et al., (1985), Horikawa (1988), Sunamura and Maruyama (1987), Lippmann and Holman (1990), Larsen and Kraus (1992) and Sunamura and Takeda (1993).

The association of NOM with short period waves and storm events is also evident in the following studies from the other NOM sites:

- Analysis of higher resolution data from Duck by Birkemeier (1984) and Lippmann et al. (1993), and from Egmond by Kroon (1994), showed that higher-energy events always accompanied significant offshore migrations.

- Using a theoretical approach to reproduce the bar behaviour at Duck, Plant et al., (1999) showed that in higher wave events seaward bar migration occurred and in lesser events landward bar movement occurred. The net effect was to shift the expected long-term mean sand-bar position offshore. The model explained up to 80% of the

A.

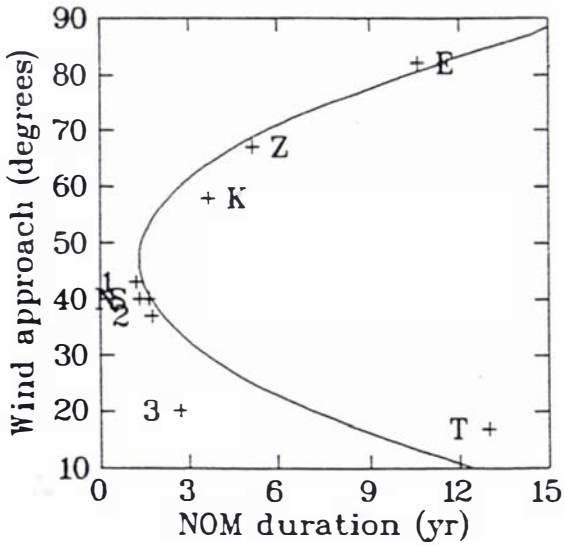

B.

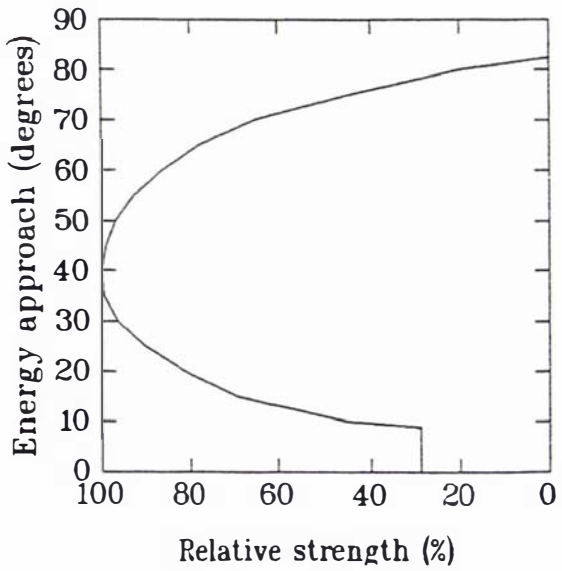

Figure 5.13 Non-linear relationships between the angle of wind approach relative to the shoreline with NOM duration (Figure A), and the angle of wind/wave approach with the relative strength of the longshore energy component (Figure B). Low angle asymmetry in the duration/wind approach data (Figure A) is demonstrated by the deviations from the fitted parabola. The combined influence of both wind and wave energy have been incorporated in Figure B by adapting the method used by Whitford and Thornton (1993) to the average environmental conditions of the NOM sites. The 'relative strength of the longshore energy' in Figure B refers to the ratio of each angle's longshore energy value relative to the maximum possible value.

variance in the observed time-series for bar location. Their modelling was based on assumptions that bars migrated toward a cross-shore equilibrium position that was depth dependent and that the rate of migration was proportional to the wave height.

- Ruessink (1998) analysed sediment transport processes at Terschelling and showed that the greatest annual sediment transport occurred under moderate to high wave conditions. Ruessink subsequently proposed a process-based conceptual model for the NOM cycle in which, at an annual scale, nearshore sediment transport was dominated, during breaking wave conditions, by seaward directed mean flow and this was supplemented by infragravity flow. Further offshore, such seaward transport was balanced by the onshore directed transport induced by incident wave asymmetry.

- Roelvink et al. (1995) developed a process-orientated numerical model to account for the bar behaviour at Terschelling. Their model used the average of the highest waves that occurred 25 times (6.8%) per year as the energy input. While some of the model's components require further field verification, it was able to reproduce the bar morphometry and cyclic NOM behaviour observed in the Terschelling field data.

The occurrence of NOM on storm-dominated coasts, together with the tendency for bars to migrate seaward or landward depending on energy levels, suggests that a general drive mechanism for NOM may involve a long-term imbalance between storm induced seaward bar migrations and the intervening landward migrations associated with lower energy events. This hypothesis is consistent with speculation by Birkemeier (1984, p1511) that the seaward migration trend in bar migration at Duck is "the result of storm erosion/migration sequences at varying time periods of one to two years". The hypothesis is also supported by results from the inter-survey bar migration analysis in chapter 6. For coasts that are characterised by process conditions different to those at the NOM sites, the NOM inducing bar migration would not happen. For example, Ruessink (1998) noted that in a swell-dominated environment the landward sediment flux associated with swell waves would be greater than for sea waves of the same height and at the same depth.

While the NOM sites appear to be located in areas that experience a degree of sediment deficit (section 5.2), Dutch results suggest that this is not a requirement for NOM. Wijnberg (1995) carried out sediment budget calculations on nearshore profiles from the coast of Holland and concluded

that the NOM cycle does not result in a net gain or loss of sediment at any cross-shore location. Wijnberg, and more recently Ruessink (1998) consider the sediment from the degenerating outer bar must be redistributed within the landward bar system. However, data with greater resolution will be required before this sediment redistribution hypothesis can be accepted. Furthermore, the hypothesis requires that bar sediment can move landward independent of the bar. There is some evidence for this such as sequential profile analyses from other field sites which have indicated that landward transport of sediment occurs in the outer nearshore under non-breaking waves (Larsen and Kraus, 1992) and within the surf zone under the action of breaking waves (Carter, 1986). However, other results indicate that sediment cannot be transported landward across troughs in the mid/inner surf zone (Wright et al., 1986; Houwman and Ruessink, 1996). It seems more likely that sediment crosses the mid/inner nearshore troughs by moving landward as part of localised coherent sand bodies and the material is subsequently redistributed longshore. Possible examples of such shoreward return mechanisms include the bar-bifurcation process described by Bailey and Shand (1996), Shand and Bailey (1999), and also in chapter 6 (section 6.1), or the shoaling of horn areas on crescentic bars under fairweather conditions (e.g. Sasaki, 1983; Wright and Short, 1984; Sunamura, 1988; Short and Aagaard, 1993). Further study is required to determine whether NOM is essentially a cross-shore sediment redistribution process, as claimed by Wijnberg (1995), or if net seaward transport occurs and sediment budget deficits play a causal role.

5.5.2.2 Morphodynamic modifications

Energy

Variation in the energy climates at the NOM sites would be expected to cause some difference in the average longer-term NOM characteristics by modifying the magnitude of cross-shore bar migration while preserving the directional imbalance. However, the following evidence indicates that energy climate variation may not be a significant modifying influence:

- The range of climatic variation between the sites is relatively narrow (Table 5.2).
- Variation occurs in average longer-term NOM characteristics at adjacent longshore sites while corresponding gradients in energy parameter values are not evident, e.g. compare the adjacent sites of Egmond and Zandvoort in Figure 5.10.
- An increase in wave height was found to correspond to a decrease in the level of NOM activity (Table 5.5B and C). This result appears to contradict the general drive mechanism for NOM proposed earlier

(section 5.5.2.1) which relies on elevated wave heights. While it is possible that the wave height and NOM activity level relationship may be a result of non-equivalency errors (section 5.5.1), the apparent relationship is consistent with an explanation which involves the influence of larger-scale boundary conditions upon NOM characteristics. This explanation is based on interactions involving incident wave energy and cross-shore slope and will be described below under the heading 'cross-shore slope'.

While variation in the energy climate appears to play a minor or indirect role in the control of average longer-term NOM characteristics, Ruessink (1998) suggested that differences in wave climate may account for fundamental within-cycle variation in NOM behaviour evident between the Dutch and Duck coasts. The nature of such subcyclic aspects of NOM will be considered in chapter 6 (section 6.2.3).

The results in Table 5.1 suggest that differences in average longer-term NOM characteristics are likely to result from variations in physical boundary conditions such as cross-shore slope. This possibility is also supported by the results of the correlation analysis between NOM activity and environmental conditions (Tables 5.5A to C) which shows little association with the process variables but strong association with the physical variables. Possible means by which such large-scale boundary conditions may influence NOM characteristics are discussed in the following sections.

Cross-shore slope

From the results in Table 5.5A and Figure 5.12D, it appears that nearshore slope has a particularly strong positive association with NOM activity, i.e. NOM with high rate and low duration values. The Egmond data point is considered to be an outlier within the global data-set. Wijnberg (1995) noted that Egmond did not demonstrate the typical relationships between cross-shore slope and surf zone width and bar-number that have been observed on other coasts; these relationships are also evident within the correlation matrix of Table 5.5A. The reason why the Egmond value is so different is not clear. However, in a study of large-scale coastal behaviour along the Holland coast, Wijnberg (1995) identified Egmond and Zandvoort/Katwijk belonging to adjacent 'coastal cells', and that the 2.5 km long harbour moles at IJmuiden which separate these two areas (see Figure 5.1B) had enhanced the differences in the associated bar systems.

A possible explanation for the negative nearshore slope/NOM duration association is contained within the following argument which incorporates

both the associations from the correlation matrices in Table 5.5 and also the results from other studies.

- Firstly, cross-shore slope is proportional to cross-shore width. By definition, cross-shore slope equals the depth to width ratio, i.e. $\tan\beta$. The correlation coefficients in Table 5.5A suggest that at the NOM sites the nearshore widths have greater influence over nearshore slope than does the depth at the seaward nearshore boundary. Lower slopes should therefore correspond to wider and somewhat deeper nearshores.

- Secondly, wave height is positively related to near-shore width. This association is indicated by the correlation result between the nearshore width/extreme wave height data from the NOM sites ($r = 0.692$). Furthermore, in a study of multi-barred coasts in the Great Lakes and Gulf of St Lawrence, Davidson-Arnott (1988) found that both cross-shore width and outer bar depth were positively correlated with wave height (using fetch as an analogue). Davidson-Arnott explained this association by the increasing breaking depth achieved by the highest waves. Because of the slope/width association it follows that wave height is negatively associated with cross-shore slope.

- Thirdly, wave height is positively related to bar volume. Davidson-Arnott's (1988) study found that wave height was positively related to bar height, although no causal mechanism was identified. From studies involving the analysis of bar size on multi-bar coasts (see Larsen and Kraus, 1992; and Ruessink and Kroon,1994) it is evident that bar height is proportional to bar volume. It therefore follows that, in general, NOM coasts with lower cross-shore slopes will have larger nearshore bars.

- It is concluded that the negative nearshore slope with NOM duration association (or positive nearshore slope and NOM activity relationship) may occur because bar volume has a positive influence on NOM duration. It is speculated that larger bars take longer than smaller bars to migrate across the surf zone owing to the larger volumes of sediment to be transported.

To test the hypothesis that bar volume is positively related to NOM duration, the sizes of bars at the global study sites were compared with corresponding NOM duration parameter values. Bar volumes were based on the area enclosed by the positive residuals between the bar's profile and the long-term mean profile (per metre alongshore). Where possible, the volumes

were derived for bars just prior to the onset of degeneration. This condition was imposed as bar size appears to increase across the nearshore until degeneration begins (Larsen and Kraus, 1992; Kroon, 1994; Ruessink and Kroon, 1994). However, neither equivalent nor complete bar volume data were able to be acquired for all study sites so the results shown in Table 5.6 are only approximate. Nevertheless, they do support the proposition that the sites with highest NOM durations also have larger bars and those with the lowest durations have the smallest bars.

Nearshore slope may also have some influence on NOM activity by gravitationally induced down-slope sediment transport. However, while such effects have been included as part of the bed-load and suspended load contributions in energetics-based cross-shore sediment transport models (Bowen, 1980; Bailard, 1981), subsequent studies (Stive, 1986; Thornton et al., 1996; and Gallagher et al., 1998) suggest that the gravity driven transport is of relatively minor importance.

Coastal orientation

The influence of coastal orientation on NOM is inferred by the strong non-linear association between wind direction and NOM duration ($r = 0.846$). The wind direction variable was based on the angle between the shore-line and predominant (storm) wind approach and, as noted earlier, therefore incorporates the boundary condition of coastal orientation.

The means by which coastal orientation influences NOM activity may be via longshore currents. Strong local winds with an oblique orientation to the shoreline generate longshore currents via the longshore component of surface wind stress (e.g. Nummedal and Finley, 1978; Hubertz, 1986; Whitford and Thornton, 1993) in combination with changes in the radiation stress from obliquely approaching broken waves (e.g. Longuet-Higgens, 1972; Komar, 1976b; Sherman, 1988). A distinct similarity is evident between the shape of the theoretical curve for longshore current and energy approach angle (see Figure 5.13B), and for the NOM duration and predominant storm wind approach angle relationship identified in this study (Figure 5.13A). Influence of longshore currents on NOM activity may involve a number of mechanisms incorporating edge waves, flow continuity, or morphological configuration and these are briefly described below.

Howd et al. (1991) and Howd et al. (1992) have theoretically shown that progressive edge waves moving in the same direction as a strong longshore current assist seaward bar migration. Progressive edge waves commonly occur in the presence of strong longshore currents and high incident wave energy (Oltman-Shay et al., 1989; Howd et al., 1991; and Howd et al., 1992), both of which characterise the NOM study sites.

Table 5.6 Average NOM durations and bar volumes from global NOM field sites.

Site	NOM duration (years)	Average bar volume (cubic metres)
Duck	1.2 - 1.3	60 - 100
Wanganui	1.7 - 2.4	70 - 120
Zandvoort and Katwijk	3.7 - 5.2	125 - 180
Egmond	10.6	180 - 250
Terschelling	13.0	450 - 700

Sources: Larsen and Kraus (1993), Kroon (1994), Ruessink and Kroon (1994), Wijnberg 1995, Wanganui ground profile data collected during the study period.

Seaward bar migration may result when troughs and topographic constrictions are subjected to increases in longshore flow. Field and modelling evidence from the Terschelling nourishment programme (Hoekstra et al., 1996) gives some support to this mechanism. The study data showed a trough re-establishing across the nourishment zone in association with increased longshore flow. However, additional evidence of greater flow concentration on the seaward side of the trough would be required to account for offshore bar migration. In chapter 6 it will be shown that strong longshore currents in combination with topographic constrictions result in significant morphological configuration changes (bar switching) that are associated with localised seaward bar migration.

Strong persistent longshore currents are associated with shore-parallel topography (Short, 1975; Fox and Davis, 1976) and this type of morphology may promote seaward bar migration for the following reason. Two dimensional (2D) morphological configurations would be expected to increase the longshore uniformity of return flows, while the cellular hydrodynamics associated with 3D morphology (Sonu, 1972; Komar, 1976a) would produce an irregular pattern of seaward flow. Two-dimensional morphology may therefore be capable of forcing more laterally continuous offshore bar migration.

Coastal structures

While the influence of nearshore structures on longer-term NOM characteristics has not been addressed in this chapter, some evidence suggests that such structures may be important. The longshore gradients in NOM characteristics which are apparent along the Wanganui study area (Figure 5.9)

indicate possible influence the river mouth jetties on nearshore morphodynamics. Differing NOM characteristics also occur between the Egmond and Zandvoort/Katwijk sites (Figure 5.1B) which are located on the coast to each side of the IJmuiden jetties.

5.6 Conceptual modelling

Aspects of a conceptual morphodynamic model of NOM that incorporate the above results and discussion, is illustrated in Figure 5.14. The model consists of two parts and these will now be considered.

Figure 5.14A depicts a general drive mechanism for coasts subjected to the NOM energy regime described in Table 5.2. Over time (approximately annual), surf zone bars undergo greater seaward migration under storm conditions than landward migration during intervening periods of lesser energy. This feature of the model is also supported by results from the inter-survey migration frequency analysis detailed in chapter 6. The literature reviewed earlier in this section suggests that net seaward sediment transport during higher energy conditions may result from the dominance of undertow and possibly bound infragravity waves, while net landward transport during the intervening periods may result from the dominance of incident wave asymmetry. However, this sediment transport balance changes when a bar reaches the outer surf zone, i.e. that region where bar degeneration occurs. Outer bar degeneration, and its influence on the behaviour of the landward bars, will be considered further in chapter 6.

Figure 5.14B depicts the morphodynamic interactions which modify the level of NOM activity and produce the range of longer-term NOM characteristics evident in the global data-set (Figure 5.10). The morphodynamic interactions involve incident energy, cross-shore slope and coastal orientation. The cross-shore slope results in differing bar sizes which in turn affect the time taken to transport bar sediment seaward. It will be argued in chapter 6 that bar size may also control characteristics of within-cycle bar migration. The coastal orientation alters the intensity of longshore currents which may affect bar migration in association with edge waves, flow continuity, or morphological configuration. The effect of differences in energy climate parameter values on longer-term NOM characteristics is unclear, although the evidence suggests this to be of less significance than variation in the physical boundary conditions. This situation has been illustrated accordingly in Figure 5.14B.

A. NOM drive mechanism

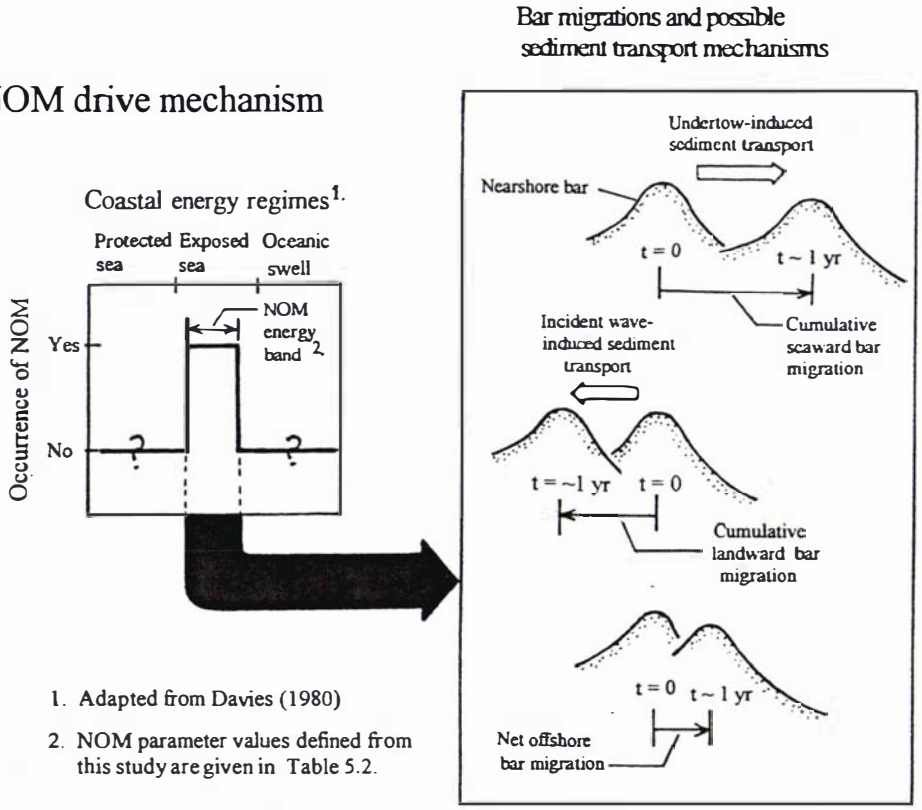

1. Adapted from Davies (1980)
2. NOM parameter values defined from this study are given in Table 5.2.

B. Modifying morphodynamics

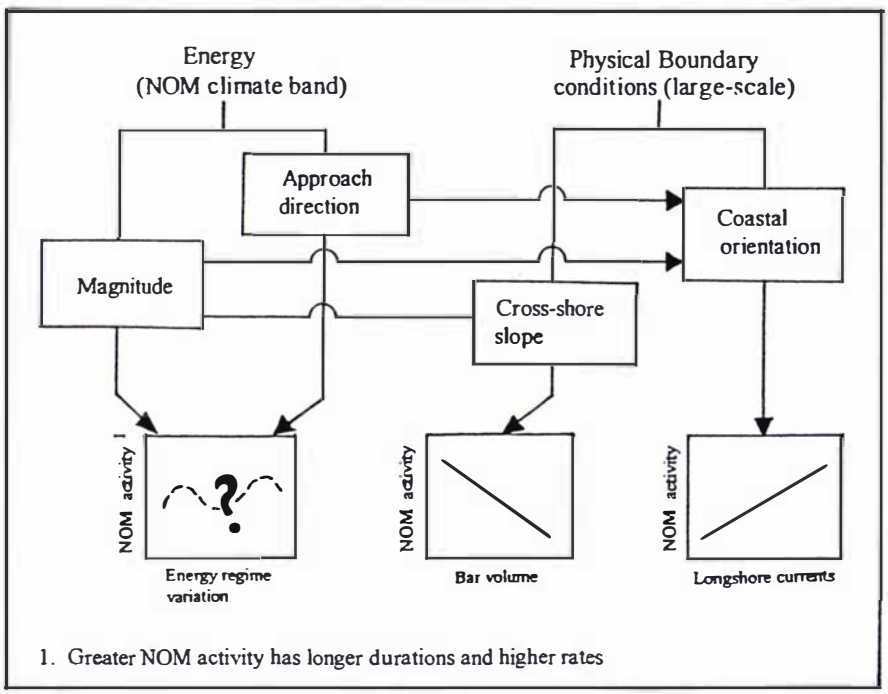

1. Greater NOM activity has longer durations and higher rates

Figure 5.14 Conceptual morphodynamic model for longer-term aspects of NOM. Figure A illustrates the NOM-associated energy regimes identified in this study and the general drive mechanism. Figure B schematically illustrates the morphodynamic interactions responsible for variations in average longer-term NOM characteristics.

5.7 Summary and conclusions

The objectives of this chapter were to identify the longer-term characteristics of NOM, to determine the relationships between these NOM characteristics and environmental conditions, and to conceptually model the associated morphodynamics. To achieve these objectives the bar-crest time-series and environmental conditions for Wanganui and the other locations where NOM has been documented were analysed. A set of parameters were defined to characterise the average NOM behaviour along cross-shore transects, together with a method that located cross-shore boundaries for the zone of systematic offshore migration. The specific research questions addressed in this chapter together with a summary of results and the associated conclusions are given below.

While some data limitations were evident in this chapter, the analysis was able to meet the study objectives. Nonetheless, a longer bar-crest record for Wanganui could confirm the apparent longshore gradients in some NOM characteristics. If such gradients could be substantiated then the calculation of longshore wave height variation would be useful in determining the role of wave energy in modifying longer-term NOM characteristics. The elimination of possible non-equivalency errors in the global process parameter data-set may also help resolve this issue.

What NOM parameter values characterise the Wanganui field site and which values are representative of the Wanganui data?

The NOM parameter values (Figure 5.8) show mean NOM widths vary between 177 m at T200 and 283 m at T5000. Mean durations vary between 1.4 yr at (T200) and 2.4 yr at T5000. Mean rates vary between 130.9 m/yr at T3900 and 169.4 m/yr at T800, and mean return periods vary between 1.3 yr at T1600 and 1.5 yr at T2800. The within-site variability in NOM parameter values (Figure 5.8) for individual cycles suggests that energy inputs influence NOM. However, the inter-site variability in contemporaneous bar behaviour evident in Figure 5.2 indicates that the existing morphology must also have a significant influence on NOM. These two situations are considered further in the following chapter. The longer-term NOM parameter values indicate longshore trends in NOM activity which decrease with increased distance from the river (Figure 5.9). Values for transects located at 1600 m and 5000 m from the rivermouth were selected to represent the Wanganui data in the global data analysis.

What NOM parameter values characterise the global field sites, and which parameter is most representative of the NOM morphological system?

The global average NOM parameter values (Figure 5.10) showed that The Netherlands sites had NOMs with greater migration widths (305 to 930 m c.f. 195 to 379 m), longer durations (3.7 to 13 yr c.f. 1.2 to 2.4 yr), longer return periods (3.3 to 14.4 yr c.f. 1.2 to 6.8 yr), and lower migration rates (34.8 to 85.1 m/yr c.f. 121.9 m to 196.0 m/yr). Duration was selected as the index parameter to represent NOM behaviour on the basis of correlation analysis results (Figure 5.11).

What environmental conditions (physical boundary, process and sediment) occur on the NOM coasts?

The NOM sites are located on multi-bar coasts characterised by relatively short period waves and a narrow range of storm-strength wind and wave conditions (Tables 5.1 and 5.2). These sites also encompass a wide range of geometrical dimensions and a spectrum of higher wind speed approach angles relative to the shoreline.

What associations occur between the NOM characteristics and the corresponding environmental conditions?

Lower cross-shore slope and higher wave energy were statistically associated with longer NOM durations, i.e. decreased NOM activity (Table 5.5). The significant non-linear association between wind direction and NOM duration indicates that coastal orientation also has a strong influence on longer-term NOM characteristics (Figure 5.13A).

How do the longer-term results contribute toward a conceptual morphodynamic model of NOM?

The proposed conceptual modelling incorporates a general drive mechanism (Figure 5.14A) together with modifying morphodynamics to account for regional variation in NOM characteristics (Figure 5.14B). The basic drive mechanism applies to all coasts subjected to the NOM energy regime (Table 5.2). Over time (approximately annual), the surf zone bars undergo greater seaward migration in response to storm induced sediment transport (which is dominated by undertow) than landward migration during intervening periods of lower energy induced transport (which is dominated by incident wave asymmetry). NOM activity is modified as a result of morphodynamic interactions involving incident energy and cross-shore slope (which thereby influences bar size and hence the time required for bar migration), and

coastal orientation (which influence longshore currents and hence bar migration characteristics). Variation of energy parameter values appear to be of lesser significance in controlling average cyclic characteristics of NOM.

Further research is required to determine whether longer-term NOM is a sediment redistribution process within the nearshore, or involves a cross-shore sediment budget imbalance.

Chapter 6 Shorter-term aspects of NOM

It is astonishing and incredible to us, but not to nature;
for she performs with the utmost ease and simplicity
things which are ever infinitely puzzling to our minds.

Galileo

6.1 Introduction

This chapter uses data from the Wanganui field site to investigate cross-shore and plan-view bar-crest behaviour associated with individual cycles of NOM. Such morphological behaviour will be referred to as *within-cycle, subcyclic* or *shorter-term* behaviour. In chapter 5 it was evident that relatively little longshore variation in the longer-term (average cyclic) characteristics of NOM occurred at the local scale, e.g. between sites along the Wanganui coast (Figure 5.8). By contrast, significant variation was evident in the bar migration pattern and NOM characteristics for individual NOM cycles both within and between the sites (Figures 5.2 and 5.8). Such variability supports the observations made in chapter 1 (section 1.2) that longshore synchrony in both bar migration and cycles of NOM did not always occur. Within-cycle variation in bar behaviour which may influence NOM is now investigated by focusing on the following general research objectives from chapter 1 (section 1.4):

- Identification of subcyclic bar behaviours which influence characteristics of the individual NOM cycle, with particular emphasis on longshore non-synchronous situations.
- Identification of the environmental conditions which accompany such within-cycle morphological change.
- Contribution toward conceptual morphodynamic modelling of NOM.

Shorter-term aspects of the NOM phenomenon described in the recent literature are now summarised. Kroon (1994) described regularity in cross-shore bar number and bar spacing. Kroon (1994) also found that the bars at Egmond on the northern coast of Holland tended to reside at certain cross-shore positions and not to remain at other locations; such apparent 'locational preferentiality' formed the basis of the method used earlier in chapter 5 (section 5.3.2) to delineate the zone of systematic offshore migration. Kroon (1994), Ruessink and Kroon (1994), and Wijnberg (1995) described

inter-bar coupling in which seaward bar movement, or a change in the shape of the seaward bar, appeared to coincide with, or to precede, significant offshore migration by the landward bars. This behaviour was earlier observed at Duck by Birkemeier (1984) and Lippmann et al. (1993) and suggests that a causal relationship exists in which the seaward bar morphology controls the migrational behaviour of the landward bars. Other subcyclic morphological behaviour associated with NOM includes episodic seaward 'jumps' in bar location, i.e. rapid and substantial offshore bar movement, and various three-dimensional behaviours. These aspects will now be introduced.

Episodic seaward jumps have been recognised by Birkemeier (1984) and Lippmann et al. (1993) in fortnightly sampled data from Duck, and also by Kroon (1994) who analysed a data-set from Egmond that was sampled at three monthly intervals over an approximately two year period. The early bar-crest data from Wanganui (Figure 1.3) also showed evidence of episodic seaward jumps. Kroon (1994) found that there were differences in timing of the episodic jumps between profiles separated by 500 metres. From the Duck data, Birkemeier (1984) found that bar positions were relatively stable between the episodic jumps, and speculated that the observed offshore migration trend reflected storm erosion/recovery sequences. Both Birkemeier (1984) and Lippmann et al. (1993) found that while high energy events always accompanied offshore episodic movements, at other times such high energy input may have little effect on bar behaviour. The Lippmann et al. (1993) study found that major changes to the morphology at Duck were associated with events during which the significant wave height exceeded three metres for more than six hours. Kroon (1994) found that significant changes in bar-crest location occurred under higher values of a storm parameter based on storm winds (>= 8 Beaufort), storm duration and interval between storms.

Bar bifurcation is a three-dimensional type of bar behaviour that Shand and Bailey (1999) associated with NOM. Bar bifurcation involves a bar splitting longitudinally with the seaward bifurcate migrating further offshore while the inner bifurcate moves into the landward trough. The inner bifurcate subsequently dissipates or migrates shoreward to merge with the adjacent bar or low tide step, causing those features to extend seawards. The term bar bifurcation was first used by Bailey and Shand (1996) to describe this type of nearshore morphological behaviour. Kroon (1990, 1994), and Wijnberg (1995) described the occurrence of 'double bars' on the Holland coast which are probably associated with bar bifurcation. Kroon (1994) suggested that double bar development at Egmond

appeared to be necessary to reinitiate seaward bar migration after a period of inactivity. Other field examples of possible bar bifurcations are shown in Greenwood and Davidson-Arnott (1975), Owens (1977), Holman and Sallenger (1986), Holman and Lippmann (1987), and Bauer and Greenwood (1990). Greenwood and Davidson-Arnott (1975) referred to what appears to be an inner bifurcate as a 'tail', while Holman and Lippmann (1987) used the term 'winged bar' for this feature. In all the documented examples the apparent bifurcations occur where bars broaden, e.g. at the horn area of a crescentic bar. An example of bar bifurcation from the Wanganui coast is shown in Figure 6.1A.

Bar switching is another three-dimensional type of bar behaviour that has been linked with NOM. The term bar switching was first used by Shand and Bailey (1999) and is defined as a type of nearshore morphological behaviour in which longshore bars become discontinuous and the landward bars on one side of the discontinuity realign and join with the seaward bars on the other side. Wijnberg and Wolf (1994), and Wijnberg (1995) first described such bar behaviour along the Holland coast when they observed that NOM cycles could be out-of-phase in the longshore direction. These authors referred to the region separating the different phases of bar behaviour as a transition area. It is therefore within such transition areas, termed *transition zones* in this study, that bar switching occurs. Other published examples of apparent bar switching are shown in Ruessink and Kroon (1994) at Terschelling, Lippmann et al. (1993) at Duck and in Carter (1986) on the Magilligan coast of Northern Ireland. An example of bar switching from the coast of Holland is shown in Figure 6.1B.

Both the Dutch and Duck researchers have speculated that the NOM phenomenon may result from the *longshore translation of obliquely oriented sand-bars* that migrate in the direction of the landward attachment (Kroon, 1990; Lippmann et al., 1993, and Kroon, 1994). Obliquely orientated transverse bars and associated rip channels have been shown to migrate alongshore, e.g. Chappell and Eliot (1979), Hunter et al., (1979), Short (1979). However, as such morphologies are usually transient any longshore translation would result in only a temporary seaward bar-crest migration. Larger-scale oblique bar morphologies within the nearshore have been reported by other researchers e.g. Short(1979), Stewart and Davidson-Arnott (1988), Kroon (1990), Kroon (1994) and Wijnberg (1995). The longshore migration of these substantial features would be associated with more significant cross-shore bar-crest migration which may result in, or influence the characteristics of, a NOM cycle. An example of larger-scale oblique bar translation from the Holland coast is shown in Figure 6.1C.

A.

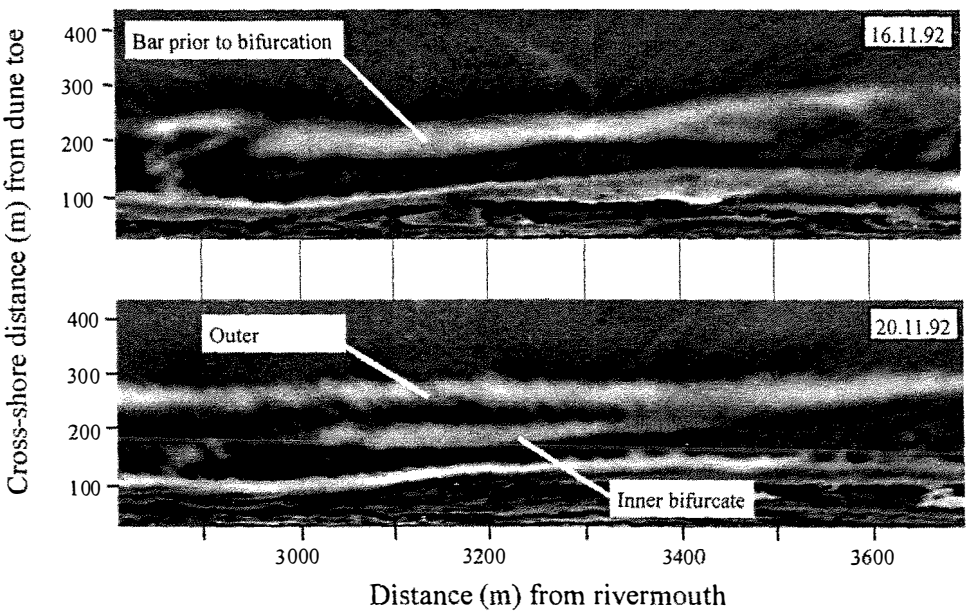

B.

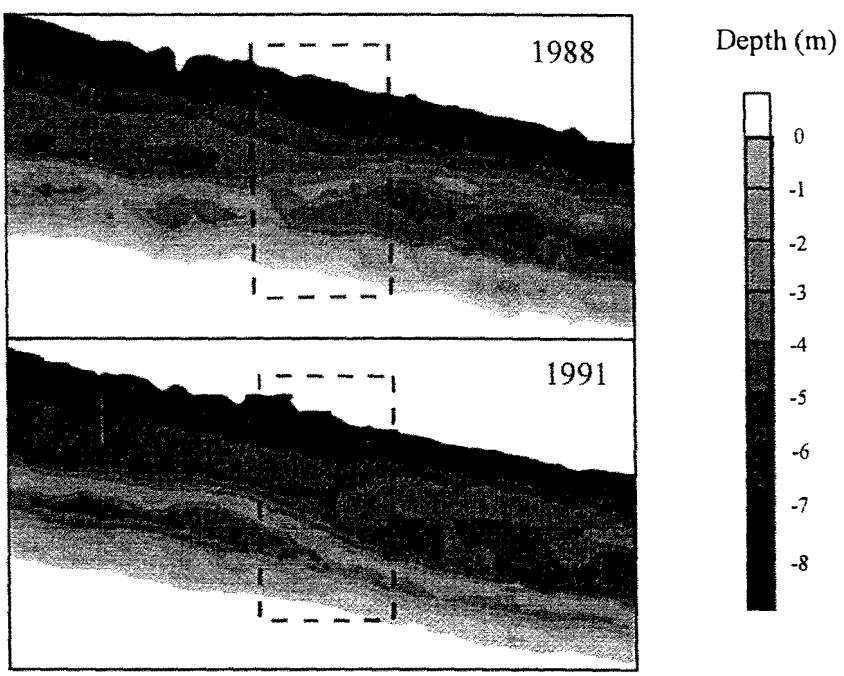

Modified from Wijnberg (1995)

C.

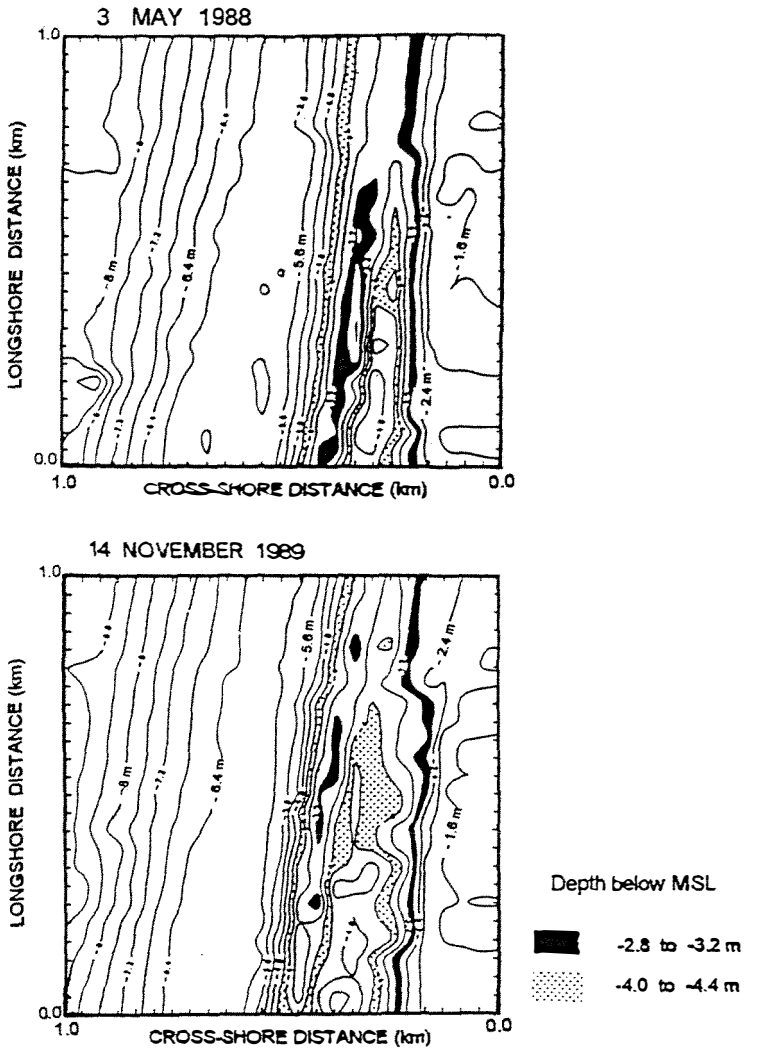

Modified from Kroon (1990)

Figure 6.1 Examples of the three types of bar behaviour previously associated with NOM: bar bifurcation (Figure A), bar switching (Figure B) and oblique bar with longshore translation (Figure C). The example of bar bifurcation (Figure A) is from the Wanganui coast of New Zealand. In the earlier (upper) image the central length of the seaward bar appears relatively broad and has a landward offset. In the subsequent image this 400 m length of bar had split (bifurcated) alongshore with the outer bifurcate having moved seaward and remained longshore-coherent with the original bar to each side. The inner bifurcate had migrated shoreward in the second image and by the 23.1.93 (not shown) had merged with the foreshore. The example of bar switching (Figure B) is from Egmond on the Coast of Holland. The dashed rectangles locate transition zones within which the bar switching occurs. The landward bar on the left of the 1988 image is connected to the outer bar on the right hand side. By 1991 the bar to the left had realigned with, i.e. switched to, the landward bar on the right. The example of oblique bar translation (Figure C) is also from Egmond. The shoreline is located on the right hand side of the figure and the bar-crests are indicated by the black bands. The (longshore) translation (toward the top of the page) of both the seaward bar and the adjacent landward trough are particularly evident as is the consequent seaward bar migration at any given cross-shore transect.

Based on the above considerations the following specific research questions were constructed to investigate shorter-term bar behaviour associated with NOM at Wanganui:

- What are the general cross-shore bar migration characteristics at Wanganui?

- How significant to NOM are episodic seaward jumps and what is the relationship between episodic seaward jumps and longshore non-synchronous bar migration?

- Are episodic seaward jumps preceded by the disappearance or prior seaward movement of the adjacent seaward bar(s)?

- What types of subcyclic (plan-view) morphological behaviour are associated with cross-shore bar migrations capable of influencing the characteristics of individual cycles of NOM?

- Which of these behaviours are associated with contemporaneous longshore variation in cross-shore bar migration, and how does the most frequently occurring behaviour relate to different characteristics of NOM cycles?

- What environmental conditions occur during subcyclic cross-shore and plan-view morphological behaviours.

- How do the shorter-term results from Wanganui contribute towards a conceptual morphodynamic model of NOM?

This chapter proceeds in section 6.2 by considering the general characteristics of cross-shore bar migration at Wanganui. Section 6.3 addresses the characteristics of larger magnitude cross-shore bar migrations, i.e. episodic seaward jumps, and how they may influence NOM activity, and section 6.4 considers the associated (plan-view) bar behaviours. Bar switching was found to be the main type of morphological behaviour associated with longshore non-synchronous cross-shore bar migrations that were capable of influencing NOM; the relationship between bar switching and NOM characteristics is considered in section 6.5. Energy conditions corresponding to inter-survey bar-crest change are considered within sections 6.2 to 6.4. How the results from this chapter contribute to conceptual modelling of NOM is summarised in section 6.6.

6.2 Cross-shore bar migration

This section identifies the general characteristics of inter-survey cross-shore bar migration at Wanganui using data sampled at monthly intervals. All cross-shore bar migrations that occurred along two transects, T1600 and T5000, and within the associated zones of systematic offshore migration, were analysed in a time-independent manner. The significance of migration direction and migration distance to NOM are assessed together with the general energy conditions that occurred during the migrations.

6.2.1 Methods

Bar-crest data from transects located at T1600 and T5000 were chosen for the bar migration analysis in this chapter because of contrast in short-term bar behaviour. This contrast is evident in the range of NOM parameter results in Figure 5.8. In particular, duration values for the individual cycles ranged between 1 and 2.3 years at T1600, while the T5000 values ranged between 1.4 and 4.3 years. It will be recalled that duration was the parameter that best represents the NOM morphological system (chapter 5, section 5.5). The contrast in shorter-term bar behaviour between these two sites is confirmed by variation in the bar-crest migration patterns depicted in Figure 5.2.

Bar-crest locations for T1600 and T5000 were obtained from the time-stack intensity maxima depicted in Figure 5.2 using the image processing algorithm PFIT.VIP described in chapter 3 (section 3.2.6). It will be recalled that these time-stacks were constructed using the monthly data-set which is plotted in Appendix H(i). PFIT.VIP was used with segment widths selected to give a longshore measurement resolution of 200 m (see chapter 4, section 4.3.3.1).

Additional echo-sounded data for T1600 was used to help interpret some of the early aerial-based imagery. For example, the depth of the outer bar during late 1991 prevented a stable intensity signal occurring on the vertical aerial photographs. The echo-sounded data were also used when interpolating between the long sampling intervals which occurred with the aerial photography in early 1992. For example, between 20.2.9 and 17.5.92 only one set of aerial photographs was sampled; this sampling taking place of on the 13.3.92. These supplementary ground contact data are depicted in Appendix J.

The inter-survey bar-crest migration data are influenced by both measurement resolution and irregular sampling intervals; both these error sources will now be described. Bar-crest location measurements have a cross-shore error of ± ~10 m (Figure 4.9). Furthermore, each inter-survey bar migration involves two (independent) bar-crest location measurements. Using equation 4.2, these two errors combine to give a migration error of ± ~14 m. Nevertheless, any relationship identified using the full inter-survey data-set should be indicative of real associations because of the random nature of the errors coupled with the high number of data points (N = 87) used in the analysis. Sample bias may exist if N is small or when individual points are being considered. These situations occur in later sections of this chapter and will be addressed at that time. For statistical purposes, a sample size of 30 is generally used as the division between large and small samples (Shaw and Wheeler, 1985).

Errors also occur because of the variable sampling interval. The monthly data-set used for analysis in this chapter had a a mean sample spacing of 29 days and a standard deviation of 5.8 days (chapter 3, section 3.2.5). Greater migration distances are more likely where inter-sample intervals are longer, and conversely, lower migration lengths are more likely where intervals are shorter. However, as with the migration measurements, this sampling error was random so when the 87 data points are analysed bias should not affect the results. It is also noted that no interpolation was attempted to compensate for sampling variability because ocean waves are a random process (Bendat and Piersol, 1971) and the Wanganui wave height data (Figure 2.21 and Appendix F)) show significant temporal variation at scales of days to months.

The set of bar-crest migrations were compared with the maximum inter-survey wave heights as determined from the daily significant wave height observations (Appendix F). This wave height parameter was used because earlier NOM studies (see section 5.5.2.1) had noted an apparent relationship between significant seaward bar migrations and increased wave height. The global results in chapter 5 (section 5.5.2.2) indicate that longshore currents may also be important in influencing NOM behaviour. However, longshore currents were not incorporated in this general section on inter-survey bar migration because of their strong correlation with wave height (see chapter 2, section 2.5.3). A longshore energy variable was included in later sections (6.3 and 6.4) when analyses of specific bar migrations were carried out.

6.2.2 Results

Inter-survey bar migration distances and the associated descriptive statistics for sites T1600 and T5000 are shown in Figure 6.2 and Table 6.1 respectively. Statistics for positive (seaward directed) migrations, negative (landward directed) migrations and the combined (positive plus negative) migrations were determined. The percentage statistics for positive and negative migrations have also been included because of the differing migration totals at each site (104 at T1600 and 132 at T5000). These differences in total number of bar migrations probably reflect the greater number of nearshore bars existing at any one time at T5000 (see Table 5.1).

The results in Table 6.1 are now described. There was a greater percentage of positive (seaward) migrations compared with negative (landward) migrations; 63.5% at T1600 and 69.7% at T5000. The values in Table 6.1 also show relatively little difference between the statistics for minimum and maximum migrations at the two sites. However, differences become more apparent when considering the means and dispersion. T1600 has positive and negative means of greater magnitude than T5000: 23.5 m c.f. 20.5 m and -13.8 m c.f. -10.9 m respectively. T1600 also has greater standard deviations for both positive and negative migrations than T5000; 20.8 m c.f. 16.5 m and 11.3 m c.f. 10.6 m respectively.

Frequency distributions for the inter-survey migrations are shown in Figure 6.3A for T1600 and in Figure 6.3C for T5000. Both distributions have an asymmetrical shape with a positively directed skew. This asymmetry is more clearly illustrated by the histograms in Figures 6.3B and D. These histograms depict the difference between frequencies of corresponding positive and negative migration classes and these figures will henceforth be referred to as 'difference histograms'. The histograms in Figure 6.3A and C also show evidence of a bimodal migration population with the two groups being separated between positive migrations of 40 to 50 m. The group comprising the higher migration distances for T1600 has 10 samples while T5000 has six. To determine the relative significance of these higher migration distances with respect to NOM, the cumulative distances were analysed. The cumulative seaward migration distance for all migrations at T1600 was 1025 m whereas the cumulative migration distance for the higher group was 641 m, i.e. 62.5% of the total seaward migration distance. By contrast, the cumulative total for all seaward migrations at T5000 was 1450 m and the higher migration group's cumulative total of 395 accounted for 27% of the total.

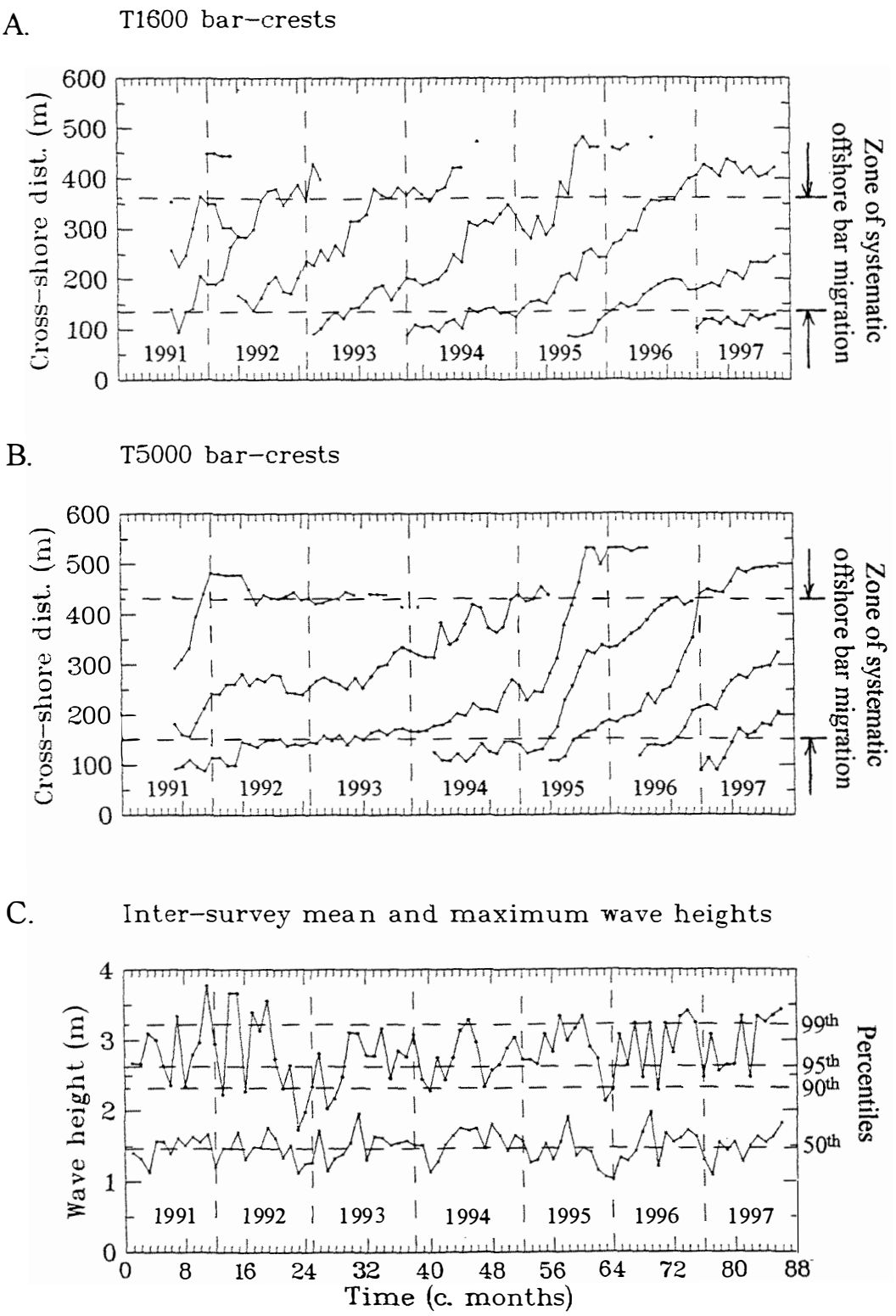

Figure 6.2 Bar-crest time-series for sites T1600 (Figure A) and T5000 (Figure B). Bar-crest locations were obtained from the time-stacks in Figure 5.2; these images had been constructed using the monthly data-set (Appendix H[i]).. The dashed horizontal lines locate the boundaries of the zone of systematic offshore bar migration. Figure C shows the inter-survey mean and maximum wave heights; these values were derived from the daily wave height data depicted in Appendix F and described in chapter 2, section 2.5.1.1. The dashed horizontal lines depict long-term percentile values.

Table 6.1 Descriptive statistics for inter-survey bar-crest migrations at sites T1600 and T5000.

	Positive (seaward) bar migrations (m)		Negative (landward) bar migrations (m)		All migrations (m)	
Site	T1600	T5000	T1600	T5000	T1600	T5000
Number of cases (N)	66	92	38	40	104	132
Percentage of all migrations	63.5	69.7	36.5	30.3	100	100
Minimum	0	0	-46.3	-43.2	-46.3	-43.2
Maximum	85.3	87.7	-0.2	-0.2	85.3	87.7
Range	85.3	87.7	46.1	42.9	131.6	130.9
Mean	23.47	20.53	-13.78	-10.93	9.86	10.99
Standard deviation	20.83	16.49	11.26	10.56	25.38	20.81

Maximum and mean wave parameter values corresponding to each inter-survey bar migration interval are shown in Figure 6.2C. The four horizontal dashed lines locate the long-term mean wave height, the 90th percentile value (i.e. the 10% wave height exceedence value), the 95th percentile value and the 99th percentile value. A comparison of the inter-survey maximum wave height data with the percentile values in Figure 6.2C shows that in 79 of the 86 (92%) cases the values were higher than the 90th percentile with 61 values (71%) exceeding the 95th percentile.

A strong association occurs between the inter-survey maximum wave height values and mean wave height values ($p << 0.01$ for the Pearson correlation coefficient). However, when maximum and mean wave height time-series (Figure 6.2C) are compared there are cases where coupling is not evident. This indicates that some storms are of short duration or occur as isolated events within a period of fairer weather. Storm duration was therefore included as a process parameter when considering NOM-influencing migrations in later sections (6.3 and 6.4).

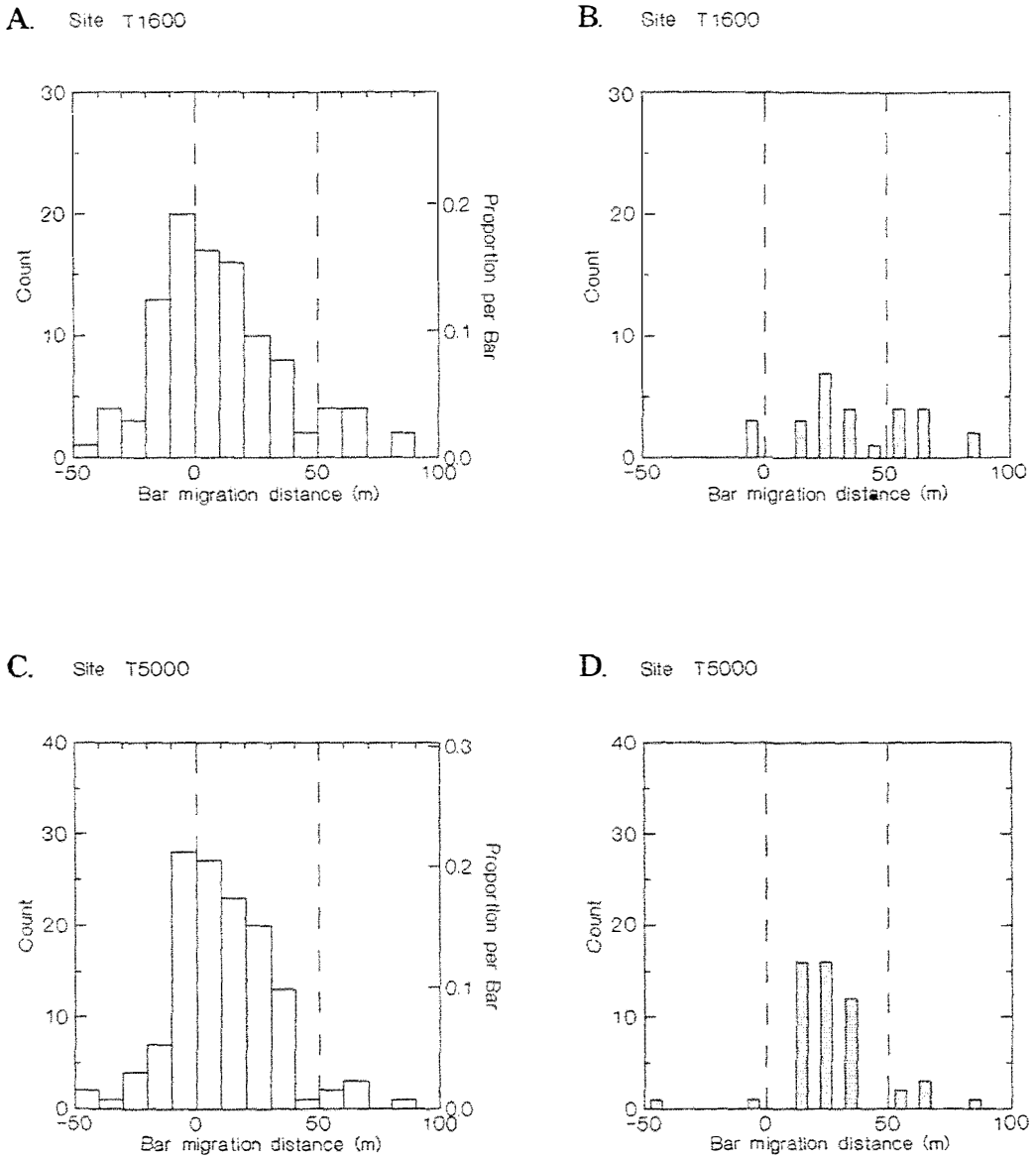

Figure 6.3 Inter-survey bar migration histograms for sites T1600 (Figure A) and T5000 (Figure C). Positive values represent seaward migrations. Figures B and D are frequency 'difference histograms' for T1600 and T5000 respectively; these histograms depict positive migration frequency less negative migration frequency for each class of bar migrations.

Inter-survey wave height maxima and the corresponding migration distances for sites T1600 and T5000 are plotted in Figures 6.4A and 6.4B respectively. Linear correlations differ significantly from zero, i.e. no association, with $p < 0.05$ for the T1600 data and $p < 0.01$ for the T5000 data. Linear regression models fitted to the data have positive slopes and these also differ significantly from zero with F-statistic probabilities of 0.027 for T1600 and 0.001 for T5000.

6.2.3 Discussion

The bimodality evident in the frequency distributions (Figure 6.3) enabled episodic seaward jumps in bar-crest location to be defined. Inter-survey seaward migrations of greater than 50 m will, for the purposes of this study, be referred to as either *episodic seaward jumps* or *episodic offshore migrations*. While the resolution of individual data points may account for some of the extreme bar-crest location values, the number and magnitude of these values indicate that a population of larger migrations does exist. The analysis of such data should therefore provide general results that are indicative of actual relationships.

The results from Figure 6.3 show 62.5% of the cumulative seaward bar migrations at T1600 were due to episodic seaward jumps. Such episodic migrations are therefore likely to have a significant influence on characteristics of NOM cycles at T1600. While only 28% of the cumulative seaward bar migrations at T5000 were from episodic jumps, these migrations also appear to have a significant influence on NOM cycles as all major changes in the bar track pattern (Figure 6.5B) were accompanied by these large seaward migrations. Such subcycle behaviour (episodic jumps) will be the focus of the following sections.

The identification of two positive (seaward) bar migration populations within the difference histograms in Figures 6.3B and D suggests that NOM at Wanganui may result from a combination of two modes of subcyclic cross-shore bar migration. The first mode, referred to as the *episodic mode*, consists of an episodic offshore migration followed by cross-shore directional fluctuations of lesser magnitude such that an overall seaward migration trend occurs. The second mode, referred to as the *regular mode*, consists of bar migrations with more constant directional fluctuations which give a net seaward migration trend. These two migration modes, together with their associated offshore migration trends, are illustrated in Figure 6.6. Both bar migration models can be identified in the Wanganui bar-crest tracks depicted in Figure 6.2. However, the episodic mode appears to predominate at the site closer to the rivermouth, while the regular mode predominates at

A. Site T1600

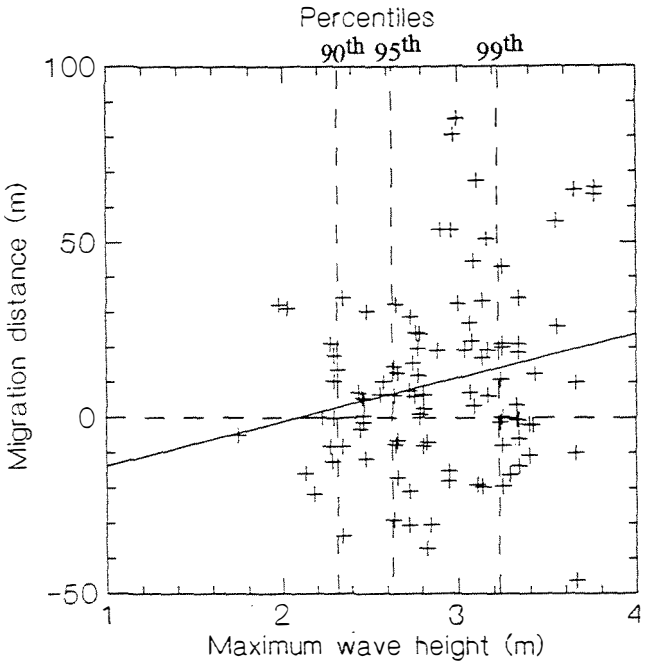

Test statistics and probabilities:

N = 104

r = 0.216
p < 0.05

F = 5.006
p = 0.027

B. Site T5000

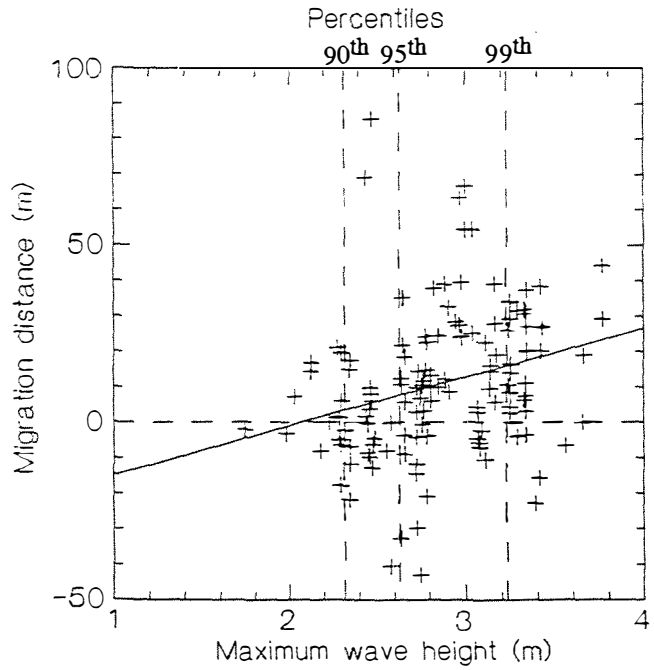

Test statistics and probabilities:

N = 132

r = 0.275
p < 0.01

F = 10.631
p = 0.001

Figure 6.4 Plots of inter-survey bar migration distance versus inter-survey maximum wave height for sites T1600 (Figure A) and T5000 (Figure B). Positive migration distance values indicate seaward directed migrations. The dashed vertical lines denote long-term wave height percentile values. Linear regression models have been fitted to each data-set. Test statistics for correlation (r) and slope (F) are listed, together with the probability (p) of them being equal to zero.

A. T1600 episodic offshore bar migrations

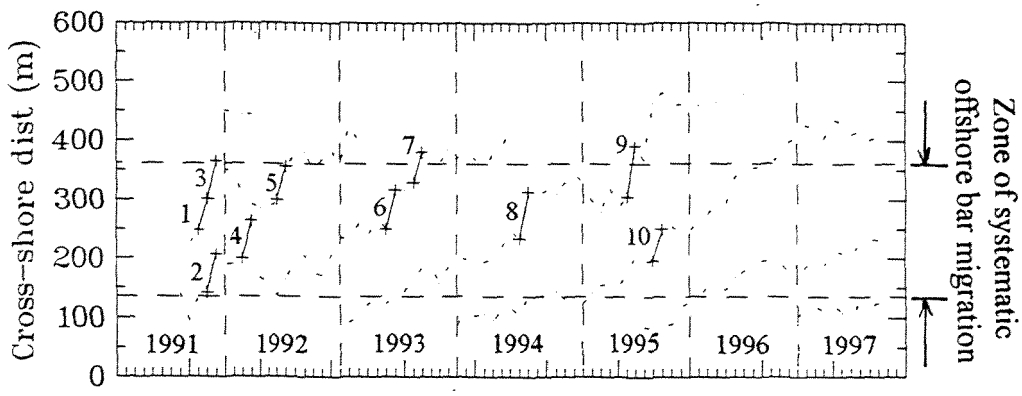

B. T5000 episodic offshore bar migrations

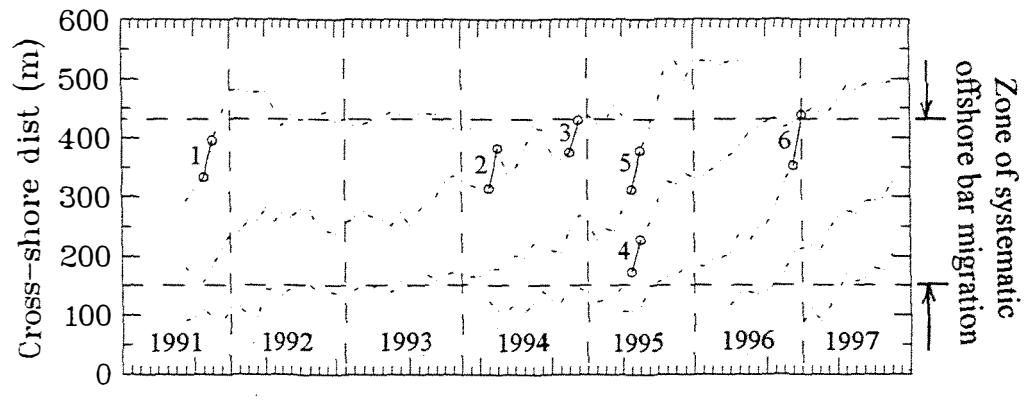

C. Combined (T1600 and T5000) episodic migrations

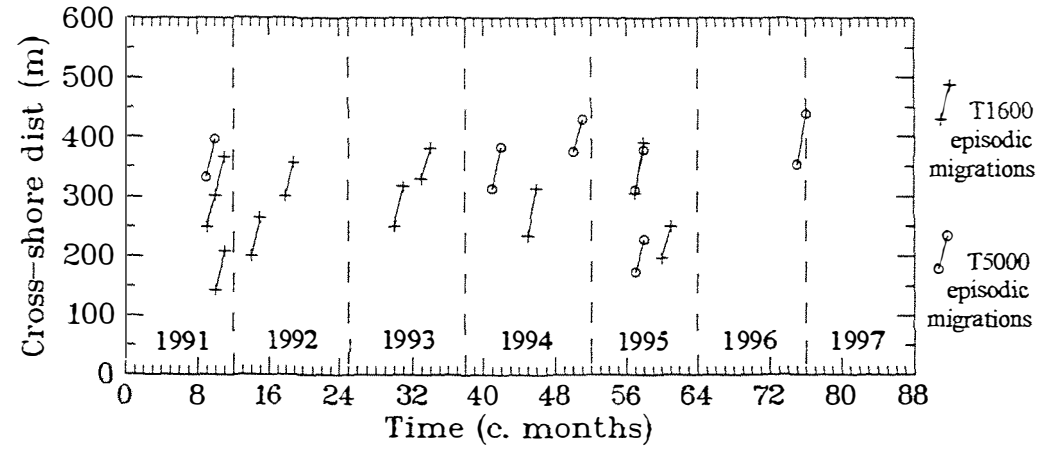

Figure 6.5 Episodic seaward jumps (offshore bar migrations > 50 m) in relation to the bar-crest time-series for sites T1600 (Figure A) and T5000 (Figure B). Each episode has been numbered chronologically. The dashed horizontal lines locate the boundaries of the zone of systematic offshore bar migration. In Figure C the episodic migrations for both sites have been over-lain.

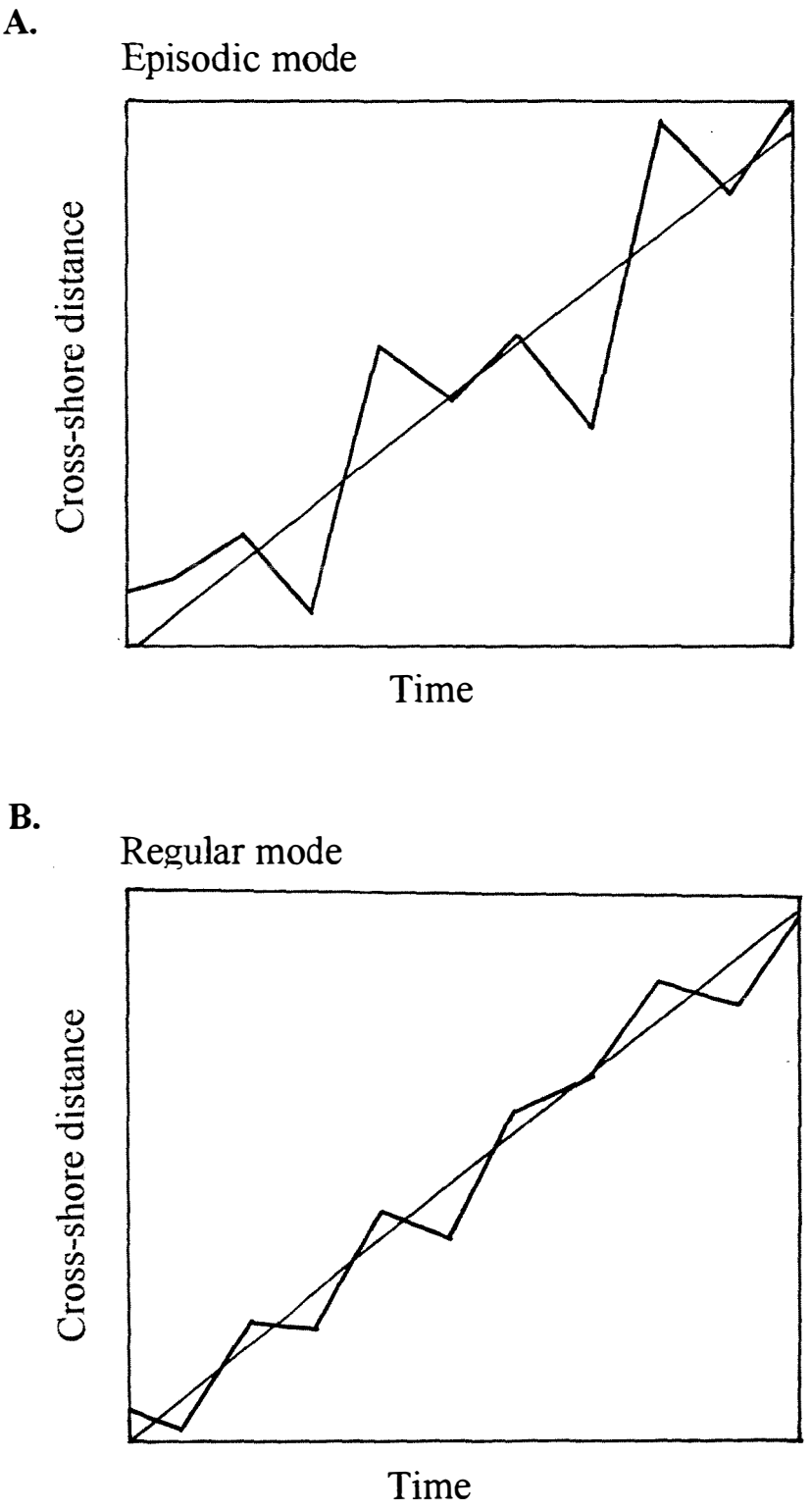

Figure 6.6 Diagrammatic representation of two modes of cross-shore bar migration evident in the Wanganui data that result in the seaward trend depicted by the diagonal lines. Figure A illustrates the episodic bar migration mode and Figure B illustrates the regular bar migration mode as defined in section 6.2.3.

T5000. This observation is supported by the greater number of episodic offshore bar migrations experienced at T1600 (10 compared with 6 at T5000), and also by the greater percentage of the cumulative seaward bar migration distance at T1600 which consisted of episodic jumps (62.5% c.f. 28% at T5000).

Similar modes of NOM behaviour have been recognised at other NOM sites. Ruessink (1998) observed that long-term bar behaviour at Duck appears to have an episodic character, while the Dutch bar cycle has a more regular appearance. Ruessink (1998) speculated that such variation in migrational behaviour at the Duck and Dutch sites may be related to differences in wave climate. Along the Wanganui study area, only a relatively small variation in the incident wave energy climate is expected to occur. However, the longshore gradients which do occur for some larger-scale environmental variables (Table 5.1) may influence subcyclic NOM behaviour and this is explored in the following paragraph.

Steeper slopes and smaller bar sizes at sites with an episodic migration mode may promote the stronger episodic behaviour at T1600 compared with T5000, and also at the Duck sites compared with the Dutch sites. The T1600 site has a steeper nearshore slope than T5000 (Table 5.1), and bar volume data (not shown in Table 5.6)) indicates that the bars at T1600 are approximately 20% smaller than those at T5000. At Duck, the cross-shore slope is steeper (Table 5.1) and the bars are smaller than at the Dutch sites (Table 5.6). It is hypothesised that the size of the outer bar controls the frequency of larger offshore migrations (episodic seaward jumps) by the landward bars. This is based upon the following reasoning:

- In section 6.3.3 it will be demonstrated that an advanced degenerative state of the outer bar promotes the seaward migration of landward bars; this relationship is encompassed within the 'outer bar control concept' (Figure 6.11).
- Given the general similarity in wave conditions at the different Wanganui NOM sites, smaller nearshore bars would, in general, be expected to degenerate more quickly than larger bars. Degeneration mechanisms are discussed in section 6.3.3. Furthermore, results in Table 5.1 and Table 5.6 indicate that smaller bars tend to occur in shallower depths; this should also result in faster degeneration rates for smaller bars.
- The more rapid outer bar degeneration at sites with smaller bars would therefore increase the potential for larger seaward migrations by the landward bars. This should result in more frequent episodic seaward jumps by the landward bars thereby producing an episodic cross-shore migration mode.

The general association between wave energy and the direction and magnitude of bar migration (Figure 6.4) is consistent with the following documentation of such relationships. The direction and rate of cross-shore bar migration has been related to a range of environmental conditions including bar size, cross-shore bar location and profile configuration, migration of 3D morphological configuration, nearshore slope, sediment size and tidal range (see Wolf, 1997 for a review). However, incident waves have been shown in laboratory and field results to be particularly important in determining the direction and rate of bar migration (see Sunamura and Horikawa, 1974; Sallenger and Holman, 1985; Horikawa, 1988; Sunamura and Maruyama, 1987; Lippmann and Holman, 1990; Larsen and Kraus, 1992; and Sunamura and Takeda, 1993). In particular, smaller wave heights, lower event durations and longer wave periods effect landward migrations, while higher waves, longer event durations and shorter periods are associated with increased seaward migration.

The wide spread of wave height and bar migration values in Figure 6.4, however, was not expected. The maximum seaward migrations did not correspond to the largest inter-survey wave heights. Furthermore, in some cases landward migrations of 30 to 50 m were coupled with inter-survey wave energy maxima in excess of the 90th percentile and in one case in excess of the 99th percentile! Landward bar migration under higher incident wave heights have been observed elsewhere (Sallenger and Holman, 1985; Wolf, 1997). In these cases the landward migration was attributed to the longshore migration of rhythmic configurations. Bar switching is another morphological behaviour associated with landward (and seaward) bar migration under high energy conditions and this will be described later in section 6.5.

The inter-survey bar migration results and inter-survey wave data suggest the following drive mechanism for seaward trending subcyclic bar migrations. The frequency distribution for inter-survey bar migration classes (Figure 6.3) showed 63.5% of the monthly migrations at T1600 were directed seaward (Table 6.1) and 69.7% at T5000 were directed seaward. Furthermore, greater seaward bar migration occurred in almost all migration frequency classes at each site. It has already been established that higher wave height events tend to drive bars offshore and regression model results (Figure 6.4) confirmed that this generally occurs at Wanganui. Furthermore, higher energy events happen regularly at Wanganui, e.g. storm wave heights (10 % exceedence) occur at approximately monthly intervals (Figure 6.2C). It therefore appears that at Wanganui, seaward trending

subcyclic sequences of bar migrations result from the frequent occurrence of higher energy events driving bars seaward (via the undertow dominated sediment transport mechanism described in chapter 5, section 5.5.2.1) with migrations during interim lower energy conditions (via the sediment transport mechanism dominated by incident wave asymmetry as described in section 5.5.2.1) accounting for the smaller and less frequent landward movements. This mechanism supports the general drive mechanism proposed in chapter 5 (section 5.6) which states that "over time (approximately annual), surf zone bars undergo greater net seaward migration under storm conditions than landward migration during periods of lesser energy". The frequent occurrence of high energy events and the lack of strong seasonality at Wanganui allow the directional imbalance in bar migrations to be clearly evident over time intervals of much less than (approximately) one year as proposed in the earlier model based on longer-term aspects of NOM.

6.3 Episodic offshore bar migration

This section identifies the characteristics of episodic seaward jumps, i.e. seaward directed bar migration distances greater than 50 m, at Wanganui using the data from transects T1600 and T5000. Two cross-shore bar migration parameters are defined and their values used to identify the characteristics of episodic offshore bar migrations. The longshore synchrony of these episodic migrations is also determined. The relationship between the episodic migrations and behaviour of the most seaward bar is investigated using a classification approach. A range of inter-survey process data are used to identify the general energy conditions that accompanied these larger magnitude seaward bar migrations.

6.3.1 Methods

The episodic offshore bar migrations at sites T1600 and T5000 are described using two parameters: the *cross-shore start location* and the *cross-shore migration distance*. Only those episodic migrations which occurred predominantly within the zone of systematic offshore migration were included in the analysis. Because of the variation in the width of the zone of systematic offshore migration (T1600 = 226 m, T5000 = 280 m) the start distances were normalised with respect to these widths to facilitate inter-site comparison.

A classification procedure is used to determine whether each episodic offshore bar migration at Wanganui is either preceded by, or accompanied by, the disappearance or substantial offshore migration of the adjacent seaward bar. It will be recalled from section 6.1 that such a correlation appears to occur at the other NOM sites. The classification procedure used in the present study is illustrated in Figure 6.7. The seawardmost bar (the classification unit) was first categorised in terms of its existence at the time that the adjacent landward bar underwent episodic seaward migration. If the seaward bar had existed then it was subsequently categorised according to when it had previously undergone a substantial offshore migration (> ~50 m). In those cases where the seaward bar did not exist, the seaward bar was categorised with respect to the length of time since its prior disappearance.

The morphological data used in the episodic seaward bar migration investigation were derived from the same image-based bar-crest data used for the inter-survey bar migration analysis (section 6.2). Additional echo-sounded data for T1600 (Appendix J) were also used to help interpret aerial images in the seaward bar correlation exercise. It is noted that while this supplementary data-set extended the T1600 bar-crest record back to March 1991, episodic seaward jumps within this five month period of pre-image data were not included in the following inter-site comparison exercises; this was to avoid any bias that could result from the unavailability of contemporaneous data for the T5000 site.

The identification of episodic seaward bar migrations are constrained by the same sampling errors which affected the full data-set of inter-survey cross-shore bar migrations used in section 6.2;, i.e. those related to measurement resolution and irregular sampling intervals. While the relatively low number of episodic seaward jumps (N = 16) could result in sampling errors causing analysis bias, the analysis proceeded for the following reasons. Measurement resolution was unlikely to reduce the episodic migration distances enough to transfer them into the lower population, i.e. migration distances less than 40 m which is the lower boundary of the class separating the two migration populations (Figure 6.3). While measurement errors may underestimate migration distance such that some episodic migrations remained undetected, those which were identified should enable the general characteristics to be determined. However, of greater importance to result reliability was the effect of incorrect relative magnitudes and allowance for this is made in the discussion section (6.3.3). Errors associated with irregular sampling intervals were minimised as these migrations were associated with storm events of one to five days duration (see section 6.3.2) and sampling was not carried out during a storm event.

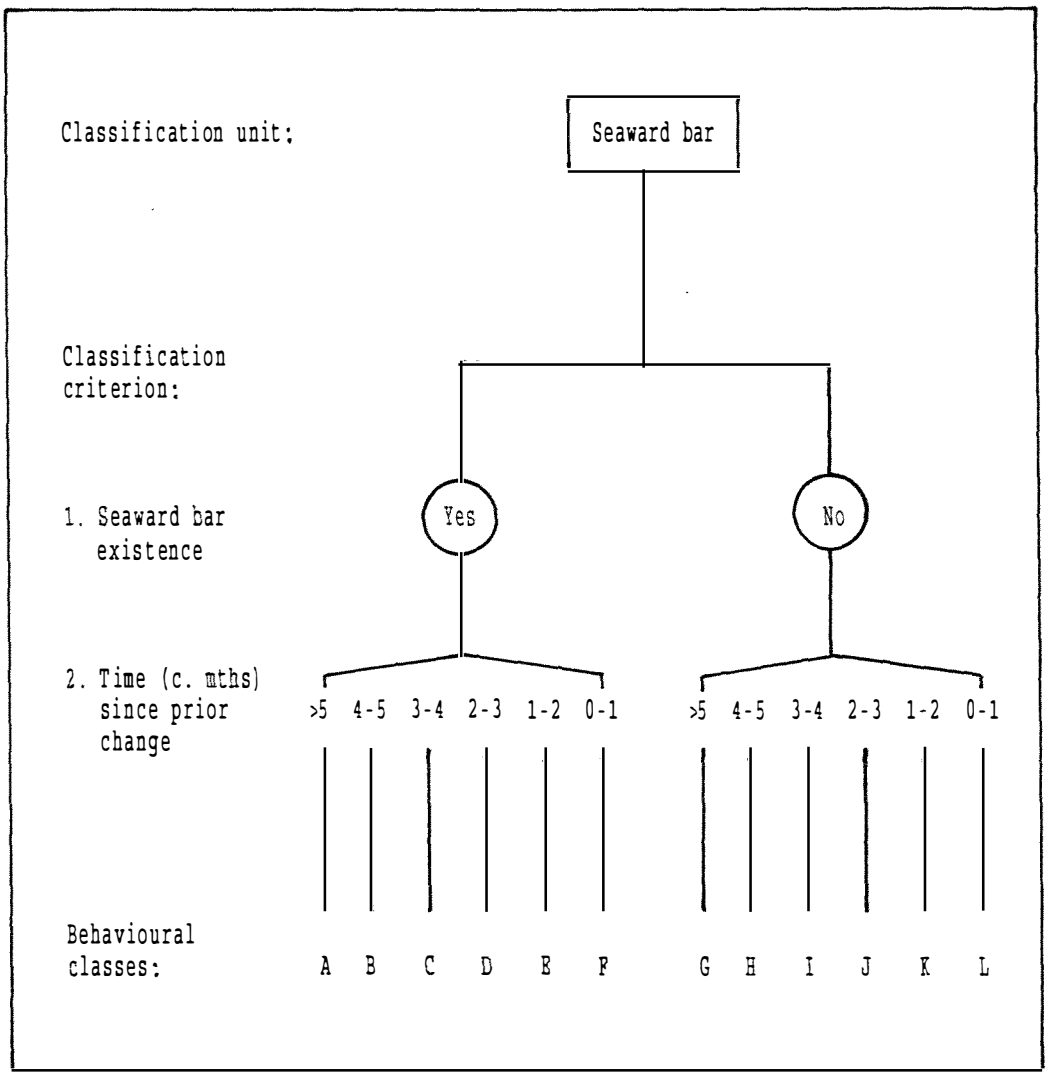

Figure 6.7 Classification scheme for morphological behaviour of the seaward bar relative to episodic offshore bar migrations which occurred further landward. If a seaward bar existed at the time of the episodic migration, then the time period (sampling interval was approximately monthly) since the seaward bar's most recent substantial (> ~50 m) offshore migration was recorded. This classification lead to classes A to F. If no seaward bar existed at the time of the episodic migration then the time of the seaward bar's prior disappearance was recorded. This classification lead to behavioural classes G to L.

Finally, it is noted that statistical inference tests were used to interpret the results as these tests could make some allowance for small sample size (see Siegel, 1956).

The episodic bar migration and process associations were investigated using the inter-survey maximum wave height, storm duration and longshore component of the wind speed (to represent longshore currents). The inter-survey maximum wave height parameter was used rather than the mean wave height as other NOM studies (Birkemeier, 1984; Lippmann et al., 1993; Kroon, 1994) had found that episodic offshore migrations were accompanied by higher wave events. The duration parameter incorporated the number of days for which wave heights exceeded the long-term 90th percentile value (2.32 m). The use of the longshore wind component as an analogue for longshore current was discussed in chapter 2 (section 2.5.3). The longshore current parameter was based on the average nine hours of longshore wind speed corresponding to the sampling time of the inter-survey maximum daily wave height measurement. Nine hours was selected to remove shorter-term fluctuations that often occurred in the wind record. Longshore wind values accompanying the maximum wave heights was used because the effectiveness of longshore currents in sediment transport depends on the corresponding wave height. Empirical and theoretical models for longshore sediment transport (e.g. Bagnold, 1963; Komar and Inman, 1970; CERC, 1984 ; Hardisty, 1990) all incorporate these parameters in the form $h^2 * v$, where h is wave height and v is longshore velocity.

6.3.2 Results

Morphological characteristics

The timing, cross-shore location and migration distance of each episodic offshore bar migration at sites T1600 and T5000 are evident in Figures 6.5A and B respectively, with the episodic bar migrations being superimposed in Figure 6.5C. The 10 episodic seaward jumps at T1600 and the 6 jumps at T5000 have been chronologically numbered in Figure 6.5. Two of the sixteen episodic migrations experienced between-site synchrony; these were episode 1 at T1600 with episode 1 at T5000, and episode 9 at T1600 with episodes 4 and 5 at T5000. There was also one case of within-site synchronous episodic behaviour at each site: episodes 2 and 3 at T1600 and episodes 4 and 5 at T5000.

The cross-shore migration distance and start distance for each episodic migration are depicted in Figure 6.8A and B, while the associated descriptive statistics are given in Tables 6.2A and B. Parameters

A. Migration start location

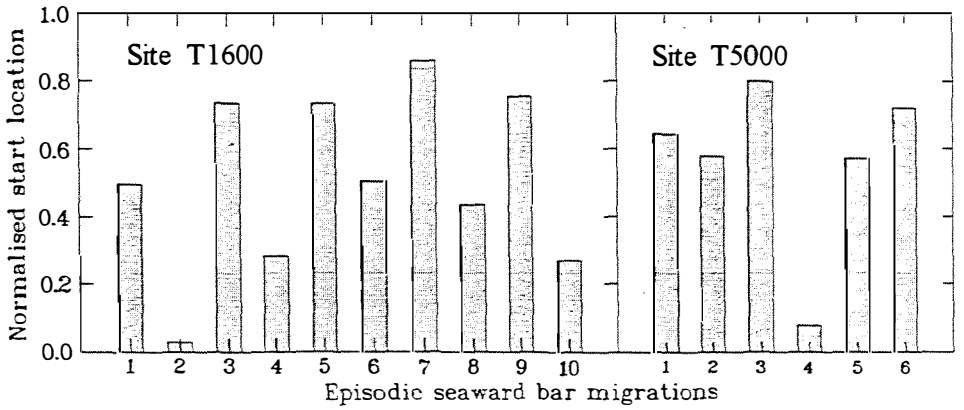

B. Migration distance

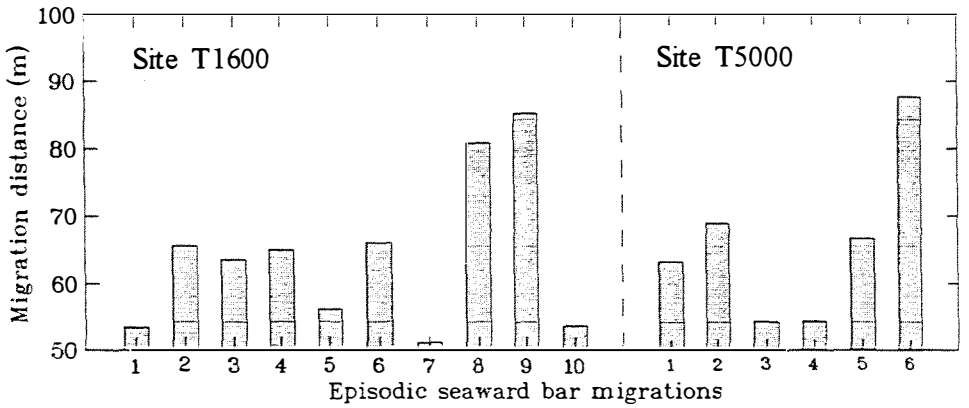

C. Analysis of migration parameters

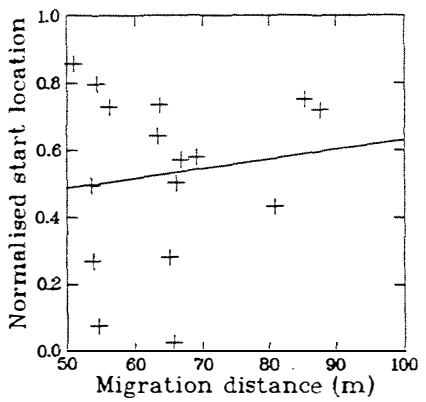

Test statistics and probabilities:

N = 16

r = 0.129 p >> 0.1

F = 0.238 p = 0.633

Figure 6.8 Chronologically numbered episodic seaward bar migrations at sites T1600 and T5000 versus normalised start location (Figure A) and migration distance (Figure B). The cross-shore start locations have been normalised with respect to the width of the zone of systematic offshore migration. Figure C is a plot of migration distance versus normalised start location for the combined data-sets from T1600 and T5000. These data points have been fitted with a linear model and the test statistics are listed.

Table 6.2 Descriptive statistics for episodic seaward bar migration start locations (Table A) and migration distances (Table B) for sites T1600 and T5000. In Table A the start locations (cross-shore distances) have been normalised with respect to width of the zone of systematic offshore migration; the parameter values defining this zone are given in Table C.

A. Migration start location (m)

Site	T1600		T5000	
	RAW	NORMALISED	RAW	NORMALISED
N (sample size)	10	10	6	6
Minimum	142.5	0.029	174.1	0.079
Maximum	330.0	0.858	375.6	0.858
Range	187.5	0.829	201.5	0.829
Mean	251.1	0.509	310.4	0.530
Standard deviation	59.6	0.264	71.0	0.253

B. Migration distance (m)

Site	T1600	T5000
N	10	6
Minimum	51.0	54.3
Maximum	85.3	87.7
Range	34.3	33.4
Mean	64.1	65.9
Standard deviation	11.5	12.3

C. Parameters for the zone of systematic offshore migration. Distances (in metres) are measured relative to dune toe.

Site	T1600	T5000
Landward boundary	136	152
Seaward boundary	362	432
Mid point	249	292
Width	226	280

describing the zone of systematic offshore migration, e.g. cross-shore location of the zone of systematic offshore migration boundaries, are given in Table 2C. As noted earlier, because of the difference in the width of the zone, the start locations were normalised with respect to the zone widths. The results show that at each site episodic migrations began at locations spread across the zone of systematic offshore migration with the average location of onset situated midway across the zone. The plots and descriptive statistics for the migration distances show that values were similarly distributed between 50 and 90 m at each site. No relationship was evident in the plot of start location and migration distance (Figure 6.8C) and this is confirmed by the test statistics ($r = 0.129$, $p >> 0.1$; $F = 0.238$, $p = 0.633$).

Process conditions

The process conditions accompanying the inter-survey interval associated with each episodic seaward bar jump at T1600 and T5000 are shown in Figures 6.9A to C, while the associated descriptive statistics are given in Tables 6.3A to C. The 90^{th} percentile, 95^{th} percentile and 99^{th} percentile values for both the long-term daily significant wave height data, and the long-term nine-hourly longshore wind speed data are denoted by the dashed horizontal lines in Figures 6.9A and 6.9C. The process results in these two figures show that all episodic migrations were associated with wave heights and longshore wind speeds that were greater than the 90^{th} percentile - which was defined as the storm level in chapter 2 (section 2.5.1.1). The results also show that 88% of the episodic migrations had wave height and longshore wind speeds exceeding the 95^{th} percentile value (severe level). Furthermore, 25% percent of episodic migrations occurred with wave heights exceeding the 99^{th} percentile value (extreme level), and 32% of episodic migrations had longshore wind speeds in excess of the 99^{th} percentile value. Storm duration results in Figure 6.9B show that most episodic offshore bar migration (87.5%) occurred during storms that lasted for more than one day, whilst half of the events had storm waves lasting four days.

A lack of statistically significant correlations characterised the associations between the two episodic bar migration parameters and the three energy parameters - see Figure 6.10. Whilst the migration distance and longshore wind data did have a significant correlation at the 10% level, the plot (Figure 6.10E) shows this was caused primarily by 3 of the 16 data points. Should one of these three migration distances be reduced by the measurement resolution error then the correlation coefficient moves above the 10% level of significance, i.e. $p > 0.1$.

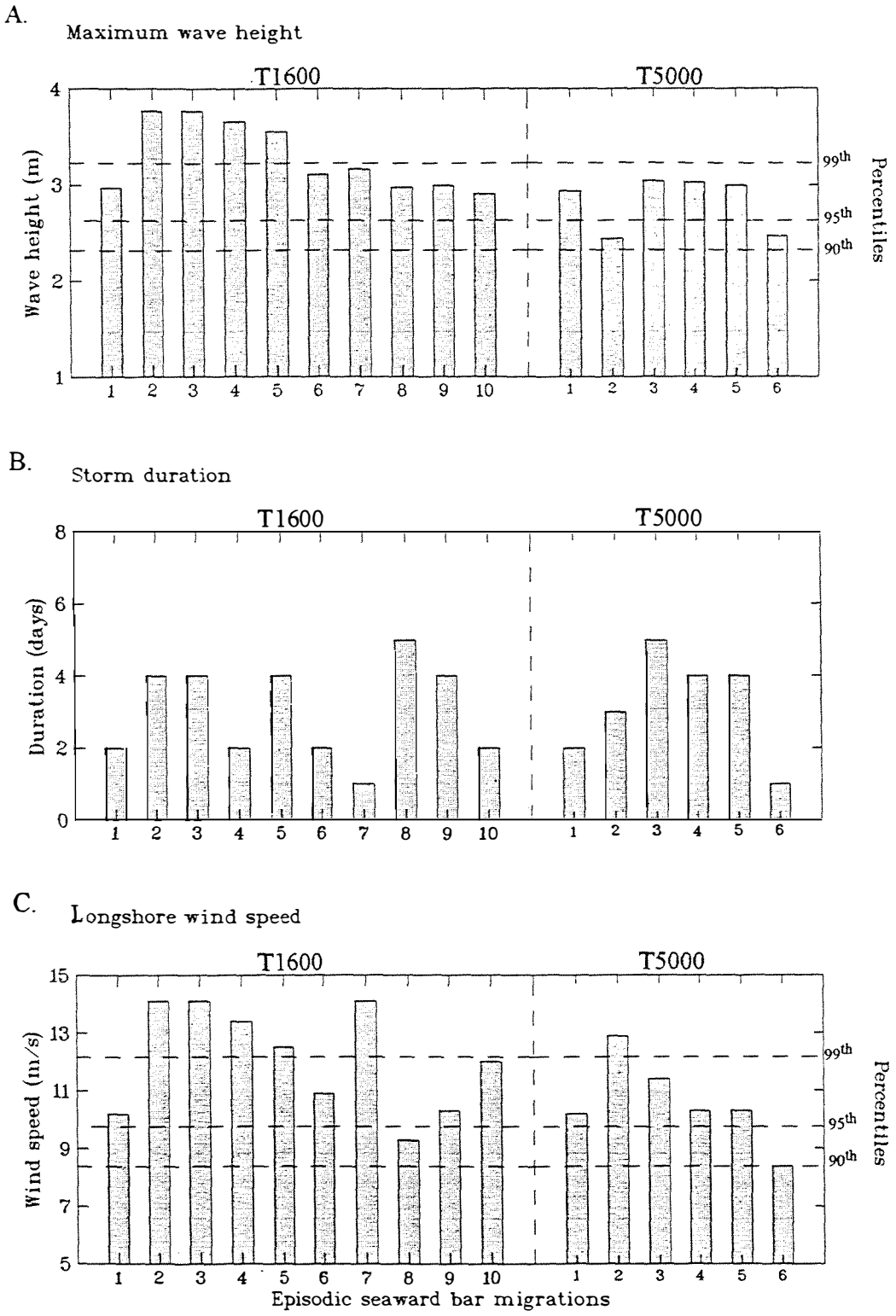

Figure 6.9 Chronologically numbered episodic seaward bar migrations at sites T1600 and T5000 versus corresponding energy parameter values for maximum wave height (Figure A), storm duration (Figure B) and longshore wind speed (Figure C). These parameters are described in section 6.3.1. The horizontal lines in Figures A and C denote long-term percentile values for wave height and longshore wind speed respectively.

Table 6.3 Descriptive statistics for energy parameters accompanying the episodic seaward bar migrations for sites T1600, T5000 and both sites combined. Table A refers to the maximum wave height parameter, Table B to the storm duration and Table C to the longshore wind speed. Parameter definitions are given in the text (section 6.3.1).

A. Maximum wave height (m)

Site	T1600	T5000	Combined
N	10	6	16
Minimum	2.91	2.44	2.44
Maximum	3.77	3.04	3.77
Range	0.86	0.60	1.33
Mean	3.29	2.82	3.11
Standard deviation	0.36	0.28	0.40

B. Storm duration (days)

Site	T1600	T5000	Combined
N	10	6	16
Minimum	1.0	1.0	1.0
Maximum	5.0	5.0	5.0
Range	4.0	4.0	4.0
Mean	3.00	3.17	3.06
Standard deviation	1.33	1.47	1.34

C. Longshore wind speed (m/s)

Site	T1600	T5000	Combined
N	10	6	16
Minimum	9.3	8.4	8.4
Maximum	14.1	12.9	14.1
Range	4.8	4.5	5.7
Mean	12.09	10.68	11.53
Standard Dev	1.83	1.49	1.82

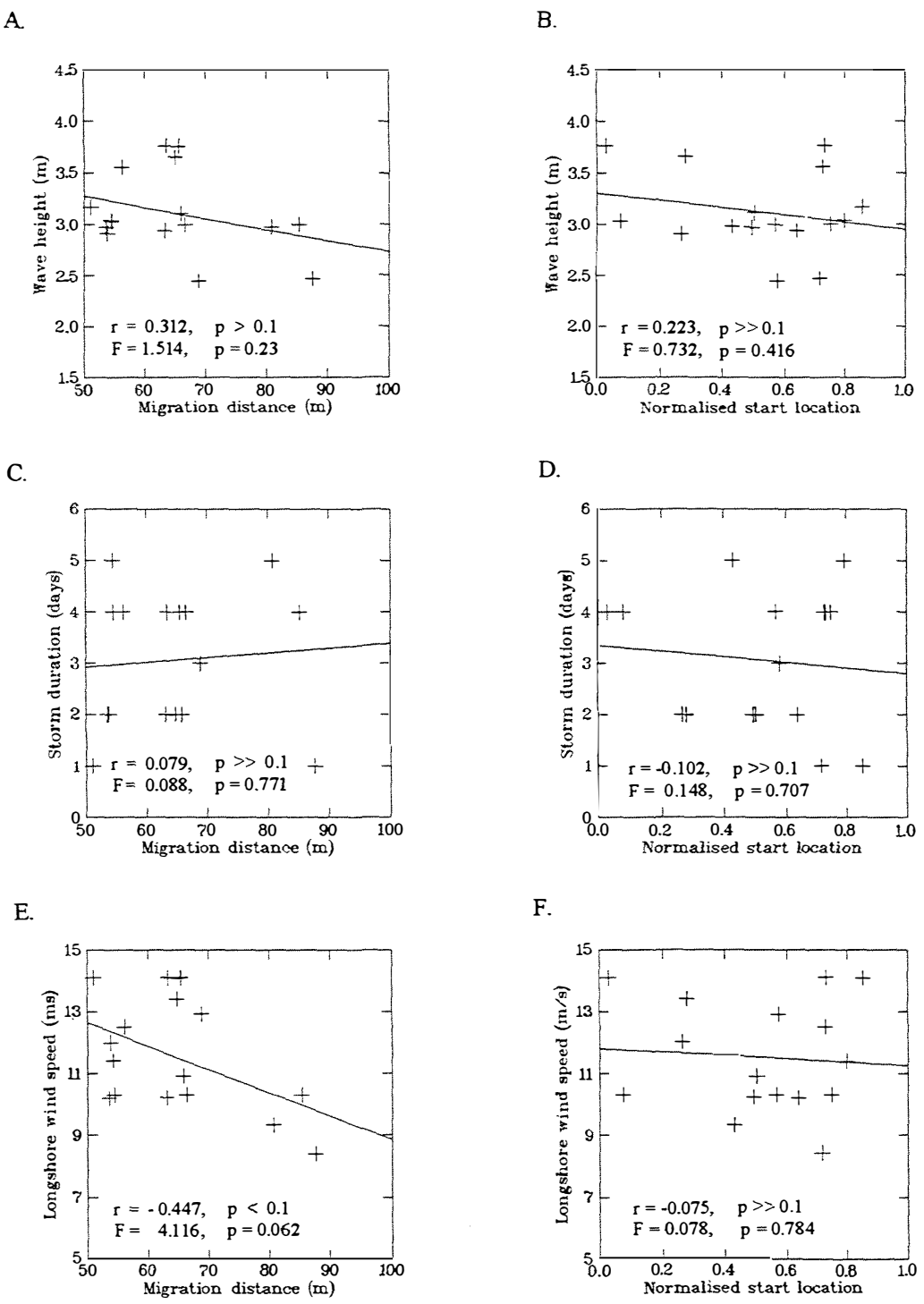

Figure 6.10 Plots of migration distance and normalised start location of episodic seaward bar migrations versus energy parameter values for maximum wave height (Figures A and B), storm duration (Figures C and D) and maximum longshore wind speed (Figures E and F). These parameters are described in section 6.3.1. Migration data for sites T1600 and T5000 have been combined. Linear models have been fitted to each set of data points and the test statistics for N = 16 are listed within each plot.

Seaward bar associations

The seaward bar classification results are shown in Table 6.4. Fifteen of the sixteen episodes that occurred at the two study sites could be fitted into one the 12 behavioural classes. The only case not included in this classification was the first episode for T5000 which could not be processed owing to a lack of ground profile data prior to the onset of imaging on 11.8.91. The classification results are now described.

In 5 of the 15 episodic offshore bar migrations a seaward bar was present at the time of episodic event. The times when each of these five seaward bars had undergone a substantial offshore migration are shown in Table 6.4A. In four of the five cases (for episodes 1, 2, 3 and 10 at T1600) the seaward bar underwent a substantial offshore migration at least one month before the episodic event. In the remaining case (number 4 at T5000), the seaward bar experienced a substantial migration during the same inter-survey period as the episodic migration event.

Ten of the 15 episodes did not have a seaward bar at the time of the episodic offshore bar migration. The times when these ten seaward bars had previously disappeared from the rectified images are shown in Table 6.4B. In 6 of the 10 cases (numbers 6, 7 and 9 at T1600, and 2, 3 and 5 at T5000) the seaward bar had disappeared at least one month before the episodic event. In the remaining four cases (episodes 4, 5 and 8 at T1600, and 6 at T5000) the seaward intensity signal had disappeared during the same month in which the episodic jump had occurred.

6.3.3 Discussion

Most episodic seaward bar migrations (80%) are longshore non-synchronous (Figure 6.5C). As significant longshore variations in incident energy are unlikely to occur between the two sites, the lack of longshore coupling between episodic seaward bar migrations probably results from the influence of differing antecedent morphology on incoming energy.

A notable lack of relationship occurred between the two episodic migration parameters (start location and migration distance, see Figure 6.8C), and also between these episodic seaward bar migration parameters and the three process parameters (maximum wave height, storm duration and longshore wind speed, see Figure 6.10). While this lack of association may indicate the importance of antecedent morphology to the system morpho-dynamics, it may also reflect the sampling errors described earlier.

Table 6.4 Classification results for seaward bar behaviour associated with episodic offshore bar migrations. The classes are those depicted in Figure 6.7. Table A relates to seaward bars which did exist at the time of the episodic offshore bar migration and the data in this table denote the times (inter-survey periods which are at approximately monthly intervals) when those seaward bars had previously undergone a substantial (> 50 m) seaward migration. Table B relates to situations when a seaward bar did not exist at the time of the episodic migrations and the data in this table summarise the times when seaward bars had previously disappeared from the intensity record.

A. Seaward bar did exist

Class	A	B	C	D	E	F
Time (c. months)	>5	4-5	3-4	2-3	1-2	0-1
T1600 episode number		3	1		2,10	
T5000 episode number						4
Number of cases	0	1	1	0	2	1

B. Seaward bar did not exist

Class	G	H	I	J	K	L
Time (c. months)	>5	4-5	3-4	2-3	1-2	0-1
T1600 episode number	7,9		6			4,5,8
T5000 episode number	3			2	5	6
Number of cases	3	0	1	1	1	4

The occurrence of very high wave height values during all episodic seaward bar migrations at Wanganui is consistent with earlier results from Duck (Birkemeier, 1984; Lippmann et al., 1993) and Egmond (Kroon, 1994). However, results from the present study (Figure 6.9), suggest that various combinations of wave height, storm duration and longshore currents may achieve the necessary threshold level to trigger an episodic migration. While a positive correlation occurs between wave height and longshore wind speed (chapter 2, section 2.5.3), relatively low waves sometimes coincided with relatively high longshore wind speeds e.g. episode 2 at T5000 (Figure 6.9). Furthermore, in some situations the duration parameter values combined with the other parameter values to give a higher overall energy input, e.g. episode 6 at T1600. However, in one case the energy parameter combination resulted in a particularly low energy input, e.g. episode 6 at T5000. This particular migration distance (87.7 m) appears to be real as even if it was reduced by the maximum resolution error the result is still well above the episodic migration threshold of 50 m. This result is a further indication that antecedent morphology has a significant influence on the morphodynamics of episodic seaward bar migration.

The associations between episodic seaward jumps and prior disappearance or substantial offshore migration of the seaward bar (Table 6.4), are consistent with the earlier results from the other NOM sites (section 6.1). In 10 of the 15 cases of episodic bar migration at Wanganui the seaward bar change clearly preceded the episodic event. In the remaining five cases the seaward bar change was evident during the same month in which the episodic jump occurred. Temporal sampling resolution prevented a more accurate determination of event relativity. It is therefore possible that the seaward bar change in these five cases did precede episodic offshore migration of the landward bar as occurred in the other 10 cases.

The Wanganui data is considered to be indicative of a causal relationship between seaward bar change and episodic offshore bar migration of the landward bars. This causal relationship appears to be based on the degenerative state of the outer bar for the following reasons. When 10 of the 15 episodic seaward migrations occurred the seaward bar either had been in an advanced state of degeneration or had disappeared completely. In the remaining five cases the seaward bar had previously undergone substantial seaward migration which placed it in the outer surf zone; it was therefore probably undergoing degeneration. It is therefore concluded that the degenerative state of the outer bar appears to control the seaward migration potential of the landward bar(s). This concept will henceforth be referred to as the *outer bar control concept* and is diagrammatically illustrated in Figure 6.11.

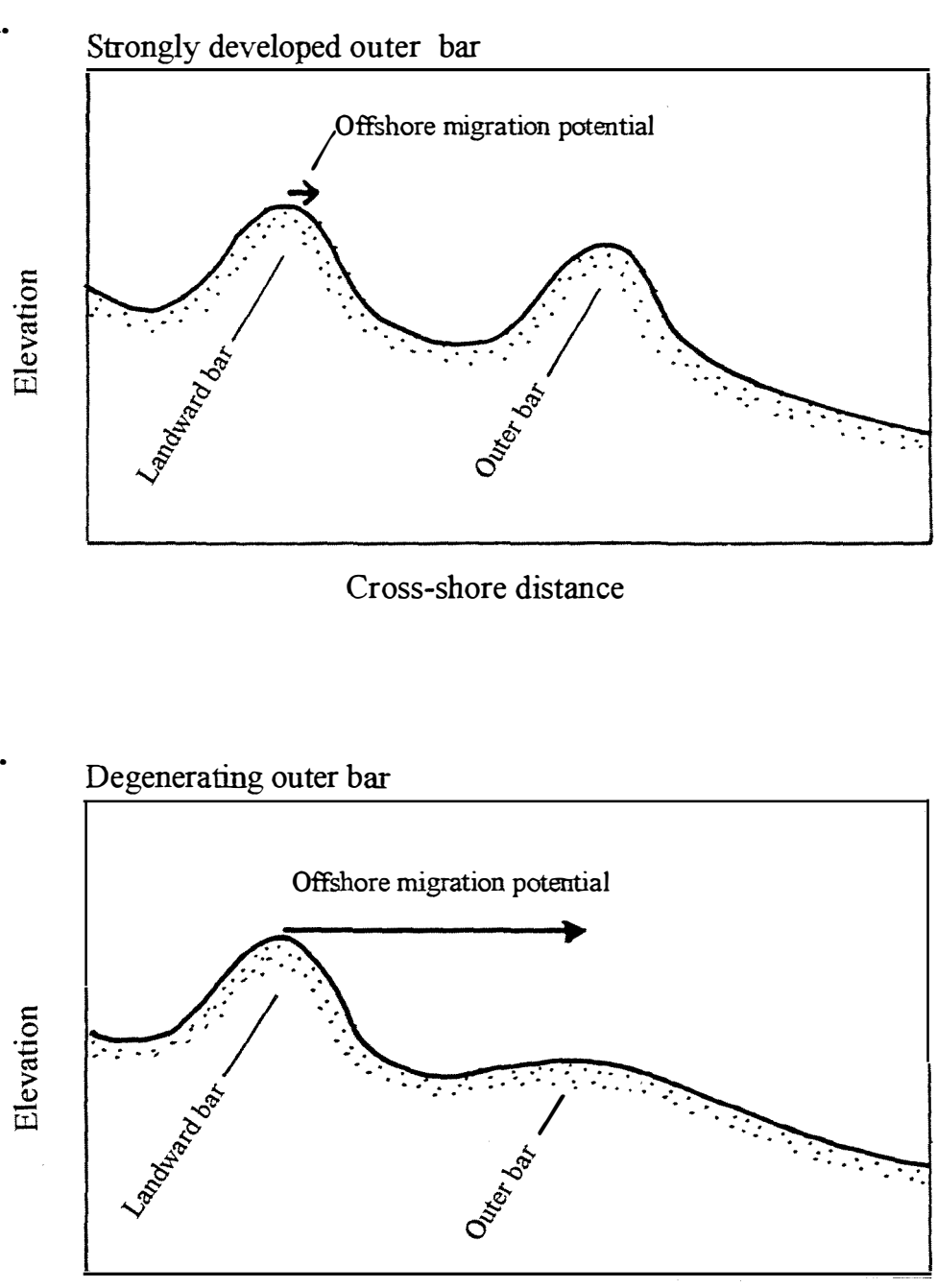

Figure 6.11 Diagrammatic illustration of the outer bar control concept in which the landward bar's offshore migration potential (depicted by horizontal arrows) is determined by the degenerative state of the seaward bar.

The outer bar control concept for episodic seaward bar migration is intuitively attractive because the outer bar exerts a control on the wave field before it reaches the landward bar system, especially during high wave conditions (Davidson-Arnott, 1988; Carter, 1988). Possible mechanisms by which an outer bar's behaviour may control (constrain or facilitate) the seaward migration of the landward bar have been proposed by Kroon (1994) and Kroon and Ruessink (1994). These researchers speculate that the seaward bar could control both the cross-shore wave height distribution and the cross-shore structure of standing infragravity waves. They then argue that whether landward bars are 'fixed' or 'free' to move offshore is governed by break-point and/or standing wave-based sediment transport mechanisms. These mechanisms are described in, for example, Kirby et al. (1981) and Thornton and Guza (1983).

The following bar degeneration mechanism has recently been hypothesised by Wijnberg (1995, 1996). Bar degeneration in the outer nearshore occurs under highly asymmetrical waves while bar maintenance occurs under conditions of intense wave breaking. As the depth of the outer bar increases the frequency of occurrence of bar-diminishing conditions increase while the frequency of occurrence of bar-maintaining conditions decrease. Positive feedback therefore ensures that bar degeneration continues and significant bar regeneration cannot occur. Ruessink (1998) modified the hypothesis by proposing that morphological inactivity (bar maintenance) under intense wave breaking was due to the hourly balance between onshore and offshore sediment transports associated with wave asymmetry and undertow. Both researchers used applied/theoretical analysis of Dutch data to support these hypotheses.

The temporal variation in cross-shore response to hydrodynamic forcing suggests that during a cycle of NOM the system alternates between self-organised and nonself-organised morphological behaviour. These concepts and their application to coastal geomorphology are described in Carter et al. (1993), Phillips (1992, 1995) and Southgate and Beltran (1995). The self-organised response in the NOM system occurs when the outer bar is well formed. Incident wave energy is absorbed by the outer bar as waves frequently break on this bar. However, relative stability can exist at this time within the landward morphology which is able to self-organise and increase its level of morphological pattern, i.e. three-dimensionality. It therefore exists in a state 'far from equilibrium' with the incident energy and the bar is unable to migrate very far in a seaward direction. In contrast, a nonself-organised response occurs when outer bar degeneration proceeds beyond a threshold level. Energy fluctuations pass into the mid/inner bar zone with less modification. Instability occurs within the

landward system which is unable to develop morphological pattern and has a nonself-organised character. The landward bar morphology responds 'toward equilibrium' with the incident energy and the bar is forced to migrate offshore.

6.4 Morphological behaviour

This section determines the type of morphological (plan-view) behaviour associated with episodic seaward jumps. In section 6.2.3 it was found that such episodic migrations appear to have a significant influence on cycles of NOM at Wanganui. Once the different types of morphological behaviour have been determined they will be compared with the corresponding inter-survey process data. Those behaviours associated with longshore non-synchronous cross-shore bar migration are identified.

6.4.1 Methods

The morphologies which temporally bracketed each episodic bar migration for sites T1600 and T5000 were identified on rectified and straightened images from the monthly data-set (Appendix H[i]). The morphological changes encompassed within the bracketing images were then determined using the sequencing algorithm SEQVIEW.VIP (chapter 3, section 3.2.6) and categorised into four classes. Three of these classes were based on the NOM-associated behaviours described earlier in section 6.1: bifurcating bars, switching bars and the longshore translation of obliquely orientated bars. The fourth class included all samples which did not fit into the other three; this class was therefore referred to simply as *'other'*.

The relationships between morphological behaviour and energy conditions were investigated by comparing each behaviour with inter-survey wave height, storm duration and longshore wind speed, i.e. the parameters described earlier in section 6.3.1.

6.4.2 Results

The results of the morphological behaviour analysis are shown in Table 6.5. Nine of the 16 episodic offshore migrations fitted the 'other' class of behaviours. Five of the episodic migrations were associated with bar switching and the remaining two episodic migrations were associated with bar bifurcation. In all 'other' cases, the initial configuration consisted

Table 6.5 Episodic seaward bar migrations at sites T1600 and T5000 associated with the four categories of (plan-view) morphological behaviours described in the text (section 6.4). The numbers in the table refer to the chronology of episodic bar migrations as depicted in Figure 6.5.

Site	Type of morphological behaviour			
	Oblique	Switching	Bifurcation	Other
T1600		4 5	8 10	1 2 3 6 7 9
T5000		2 3 6		1 4 5

of bar-crests and troughs with essentially linear (longshore) form. The post-migration configurations also tended to be linear, with the bar migrating seaward in an approximately uniform manner at longshore locations to either side of the transect where the episodic migration occurred. Examples of bracketing morphologies for the three behavioural classes present, i.e. bar bifurcation, bar switching and linear bars with uniform migration, are provided in Figure 6.12. While no cases of oblique bar with longshore translation were observed, in some instances a linear bar had a slightly oblique alignment (e.g. see Figure 6.12C); this orientation may have facilitated longshore translation of the bar, thereby contributing to the observed episodic offshore bar migration.

The process conditions that occurred during each morphological behaviour are shown in Figures 6.13A to C. The parameter values for bar switching had greater ranges than for the other types of behavioour. The average wave height and longshore wind speed for bifurcating bars appear to be somewhat lower and the storm duration longer, than for the switching and linear bars with uniform migration. However, grouped t-tests showed there to be no significant difference.

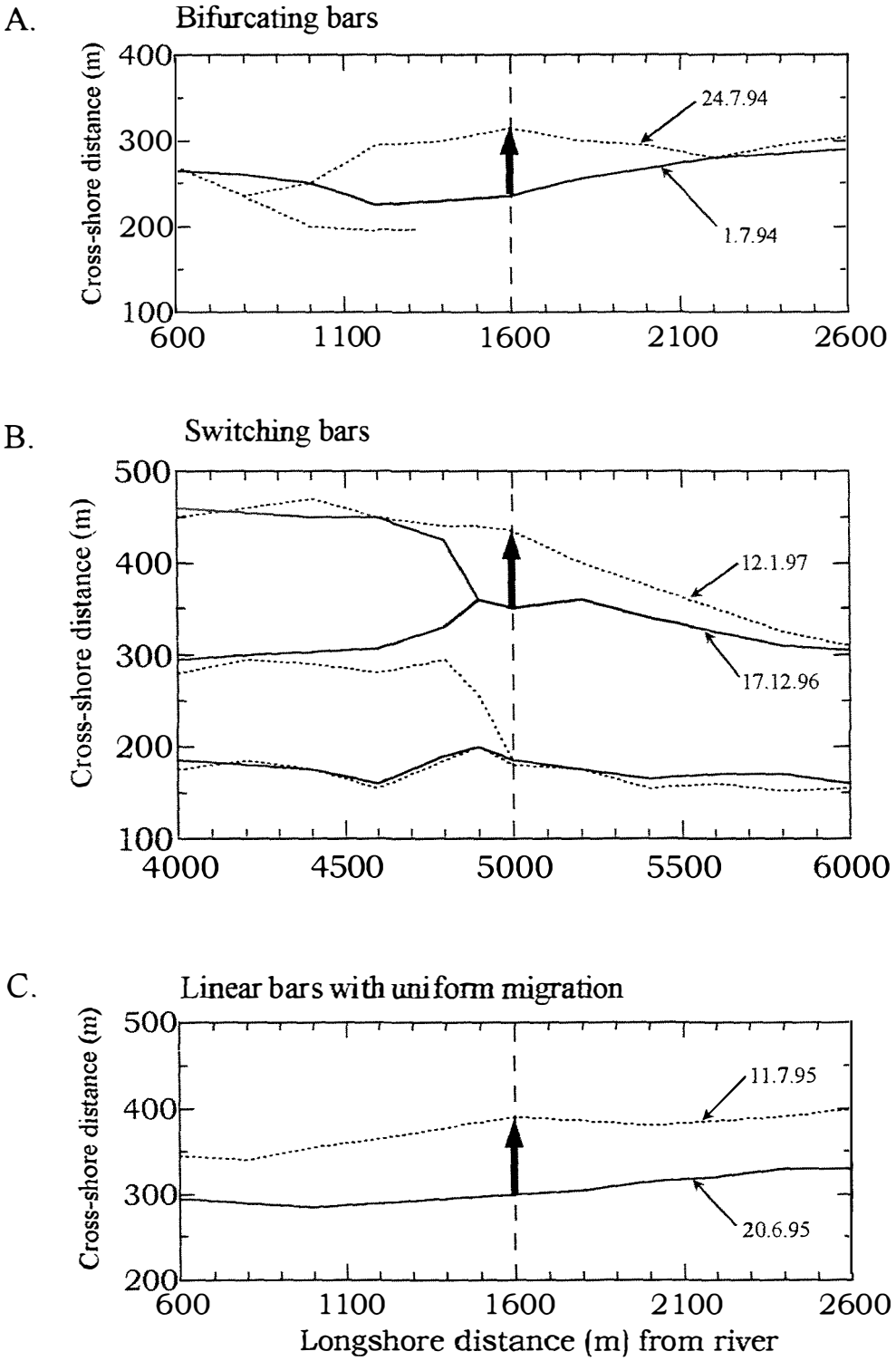

Figure 6.12 Examples of the morphological behaviour associated with the 16 episodic offshore bar migrations at T1600 and T5000 (see Figure 6.5). Figure A illustrates bar bifurcation, Figure B illustrates bar switching and Figure C shows a linear bar undergoing uniform cross-shore migration. These bar-crest data were obtained from the rectified images which bracket the episodic migrations. The solid line represents pre-episodic migration bar-crest data and the dashed line represents post-episodic migration bar-crest data. The dashed vertical line in each figure locates the transect where bar migrations were identified and the arrows denote the episodic migrations (> 50 m).

A. Maximum wave height

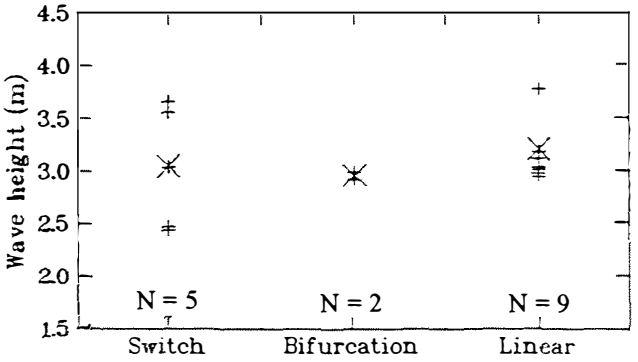

B. Storm duration

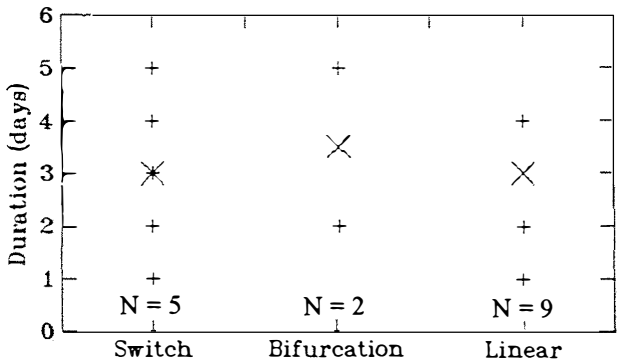

C. Maximum longshore wind speed

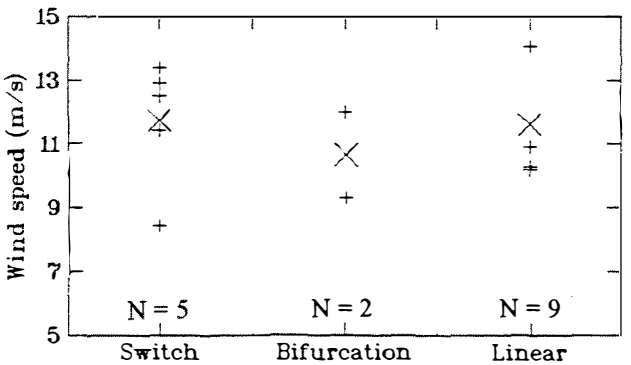

Figure 6.13 Plots of morphological behaviour versus energy parameters values for maximum wave height (Figure A), storm duration (Figure B) and longshore wind speed (Figure C). The three types of morphological behaviour are described in sections 6.1 and 6.4, and the episodic offshore bar migrations that correspond to each type are shown in Table 6.5. The number of samples (N) in each behavioural class are marked. The energy parameters are described in section 6.3.1. The X symbol locates the mean energy parameter value for each type of morphological behaviour.

6.4.3 Discussion

Comparison of the morphological behaviour results in Table 6.5 with the episodic seaward migrations in Figure 6.5 shows that longshore non-synchronous episodic bar migrations were associated with each of the five cases of bar switching, with both cases of bar bifurcation, and in two of the nine cases of linear bars with uniform migration. Bar switching was therefore the most frequently occurring behaviour associated with contemporaneous longshore variation in cross-shore bar migrations that were capable of influencing NOM. How this type of morphological behaviour relates to different characteristics of NOM cycles will be investigated in the subsequent section (6.5).

Comparison of the results in Table 6.5 and Figure 6.5 also show that all cases of longshore synchronous episodic migrations and all cases of cross-shore synchronous episodic migrations, were associated with longshore bars with uniform migration.

The most reliable morphological behaviour and process variable results in Figure 6.13 were for linear bar with uniform migration and for bar switching which had nine and five samples respectively (Table 6.5). The similarity in the mean values of all energy parameters for both these types of behaviour suggests that morphological configuration has a strong influence on the system morphodynamics. However, such topographic influence may be somewhat stronger with bar switching as the dispersion of parameter values were greater for this type of behaviour.

6.5 Bar switching

This section investigates the relationship between bar switching and the characteristics of NOM cycles. In the previous section it was determined that bar switching was the type of morphological behaviour most frequently associated with longshore non-synchronous cross-shore bar migrations that were capable of influencing NOM. It will be recalled from chapter 1 (section 1.2) that the study of morphological non-synchronous behaviours was hoped to provide an additional means of achieving the thesis aim, i.e. to elaborate on the behaviour and causal processes of net offshore bar migration. The relationship between bar switching and characteristics of NOM cycles will be identified by analysing cross-shore bar migrations from examples of bar switching observed at Wanganui during the study period.

6.5.1 Methods

Separate periods of bar switching during the study period were identified from the monthly image data-set (Appendix H[i]). In some cases additional images were used to provide increased temporal detail; these images have been reproduced in Appendix H(ii). A period of bar switching consisted of a set of individual interrelated bar realignments, i.e. bar switches, which occurred in the same area. Such a set of switches will also be referred to as an *episode of bar switching*. Each individual realignment was defined by a *transition zone* as described in section 6.1. The time-space distribution for the nine episodes of bar switching that were identified during the study period are depicted in Figure 6.14. The location of each episode relates to the average longshore distance of the set of transition zones used to define the episode of switching. The data in Figure 6.14 shows that periods of bar switching occurred throughout the study period, with the mean interval between episodes being 22.3 weeks (range 0 to 64.3 weeks). The mean duration of the switch episodes (data not shown) was 13 weeks with values ranging between 7.6 and 26.7 weeks. All episodes were located between approximately T1500 and T5000.

The following episodes of bar switching were selected for analysis. Bar-crest data from episode 7 were used to identify the association between bar switching and cross-shore bar migration, and also to identify the relationship between bar switching and the characteristics of NOM cycles. Episode 7 was selected because the associated set of images clearly depict bar switching and this episode comprised a typical sequence of realignments (see paragraph 1, section 6.5.2). Bar-crest data from switch episodes 5 and 9 were used to determine how cross-shore bar migration on each side of a transition zone could change with increasing longshore distance from the zone. These two periods of switching were selected for analysis firstly because they depict positive and negative switching (see subsection 'cross-shore bar migration' in section 6.5.2)), and secondly because they occurred toward the northwestern end of the study area (see Figure 6.14), thereby providing the greatest possible distance overwhich to observe the occurrence of cross-shore bar migration between the transition zone and rivermouth.

Cross-shore bar migration data used in this section were obtained by applying the time-stack algorithm MORPHSTK.VIP (chapter 3, section 3.2.6) to the image sequence which depicted the episode of bar switching under consideration. The sequencing algorithm SEQVIEW.VIP (chapter 3, section 3.2.6) was used extensively to help identify the episodes of switching and determine associated plan-view morphological behaviour.

6.5.2 Results

As switch episode 7 provides most of the data used in the following analysis of bar switching, it will first be described in relation to the set of morphological configurations displayed in Figure 6.15A to E. Each image depicts a nearshore area that is 2800 m long by 500 m across. Two images (A and B) represent pre-switch morphological behaviour. It is evident that bar configurations in the lead up to switching were shore-parallel. The weaker or patchy seaward intensity signal on the right side of these images is indicative of outer bar degeneration (chapter 3, section 3.2.7). Bar switching is occurring within the transition zones marked on images C and D. The landward shift in transition zone location between these two images indicates bar realignment began with the bars in the outer surf zone and then progressed landward. This same pattern was evident in the other episodes of bar switching with the exception of the fourth and sixth episodes; in these cases the realignments occurred more centrally within the zone of systematic offshore migration. A new bar formed on the lower foreshore to the right side of the transition zone in Figure D.

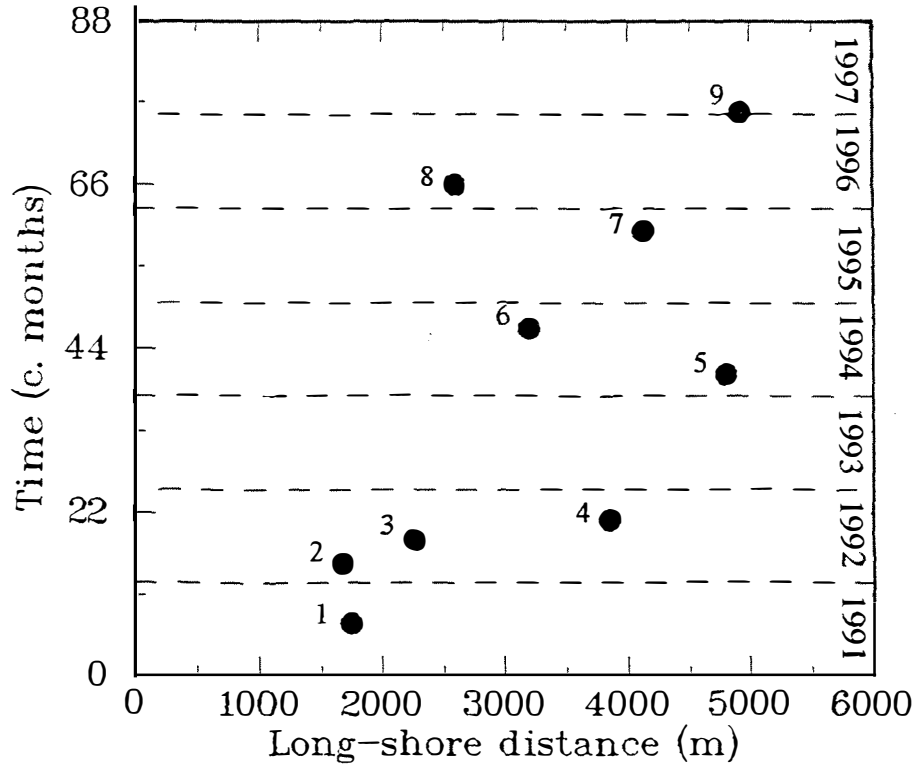

Figure 6.14 Plot of longshore location for each period (episode) of bar switching versus time during the study period. Each episode of switching is numbered chronologically.

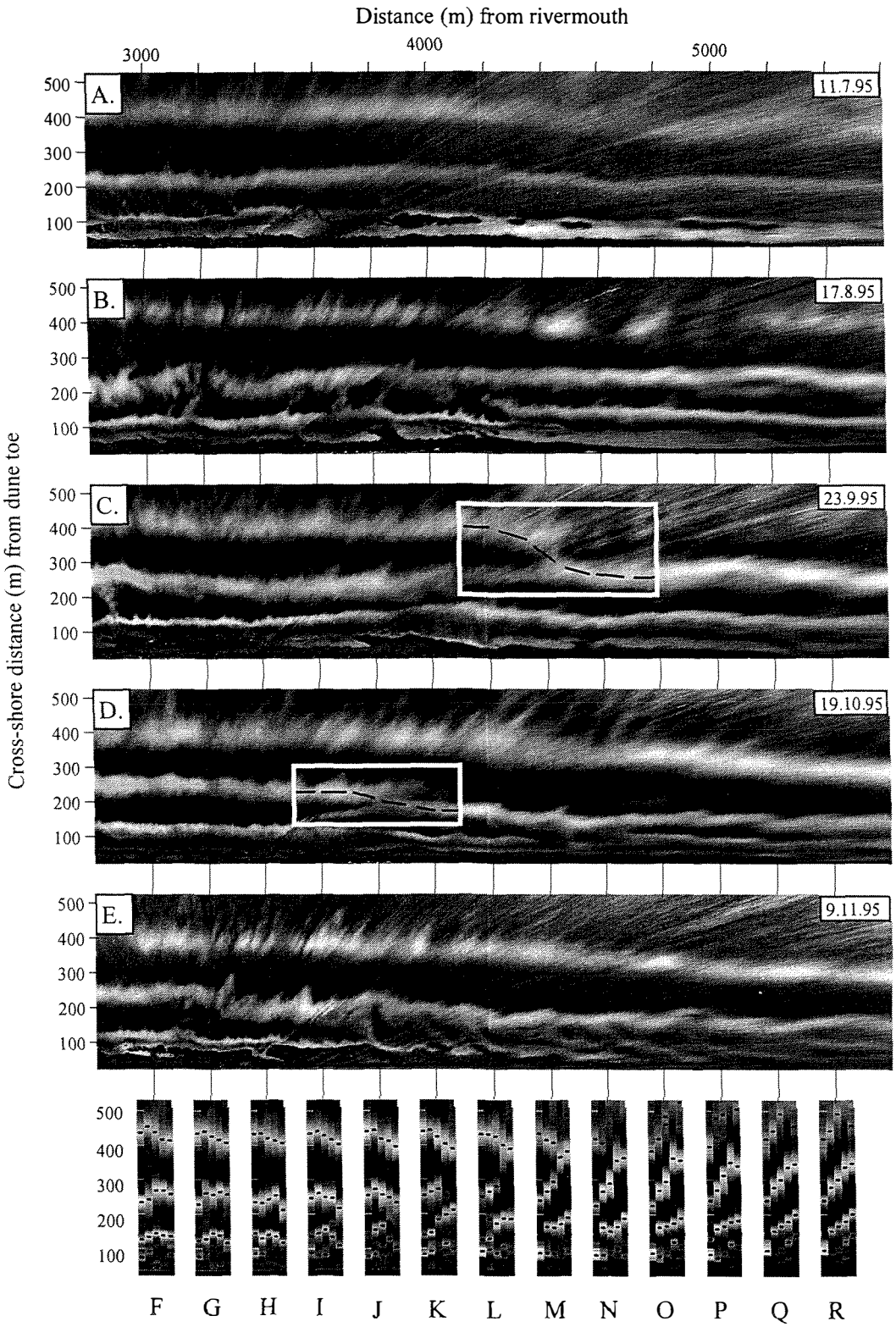

Figure 6.15

Sequence of images (A to E) depicting morphological configurations associated with switch episode 7 (see Figure 6.14), together with time-stacks (F to R) showing the associated cross-shore bar migrations at 200 m intervals alongshore. The two white rectangles define transition zones within which the bar realignments (switching) occur. The dashed black lines within each transition zone show bar-crest alignments that the switching is about to achieve.

Bar switching is complete in Figure E with the bars having essentially regained a shore-parallel configuration. However, a close inspection of Figure E shows that beach-states for the foreshore and inner bar on each side of the transition zone where switching had last occurred, are different. The beach-state of 'longshore bar and trough' (Appendix A[i]) characterises the morphology on the left while 'transverse bar and rip' or 'rhythmic bar and beach' states occur on the right. Subsequent images (see Appendix H[i]) show the beach-state ('longshore bar and trough') developed along the entire 2800 m of coast over the following three months.

Cross-shore bar migration

Cross-shore bar migration during switch episode 7 is depicted by the series of time-stacks arranged along the base of Figure 6.15 and labelled F to R. These time-stacks illustrate cross-shore bar migration at 200 m intervals. The bar tracks show that cross-shore migration differed markedly to each side of the transition zone. While bars on the left of the transition zone (Figures F to H) remained approximately stationary, bars on the right (Figures N to R) moved rapidly seaward. These two situations will be referred to as *negative* and *positive switching* respectively. Time-stacks within the transition zone itself show variable and complex cross-shore bar behaviour; this included discontinuous migration tracks (Figure K) and merging migration tracks (Figure M). A migration track within the transition zone may also split; however, this situation did not occur during switch episode 7.

Longshore variation

To determine how cross-shore bar migration on each side of a transition zone can change with increasing longshore distance, the rates of cross-shore bar migration were analysed. Average migration rates at 200 m intervals (in the longshore direction) for switch episodes 5 and 9 are depicted in Figure 6.16A and B respectively. Each longshore data point (rate) in Figure 6.16 was determined from the slope of the linear regression model fitted to the bar migration time-series, i.e. the relevant series of black rectangles on time-stacks similar to those appearing along the base of Figure 6.15 (which were for switch episode 7). The data for switch episode 5 represents positive switching, while the data for switch episode 9 represents negative switching. It is noteworthy that switch episodes 5 and 9, as depicted in Figure 6.16, demonstrate how the location of positive (or negative) switching may occur either on the left hand side, i.e. the river side, of the transition zone or on the right hand side.

A. Episode 5: positive switching

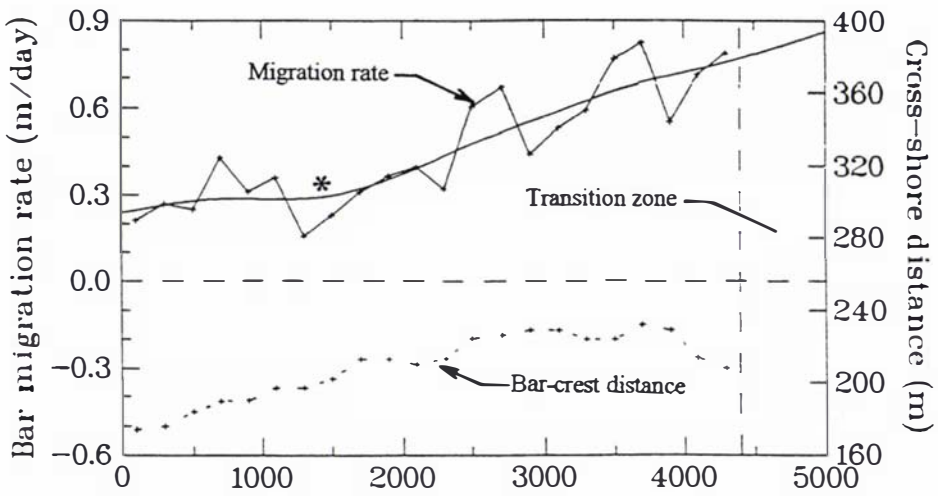

B. Episode 9: negative switching

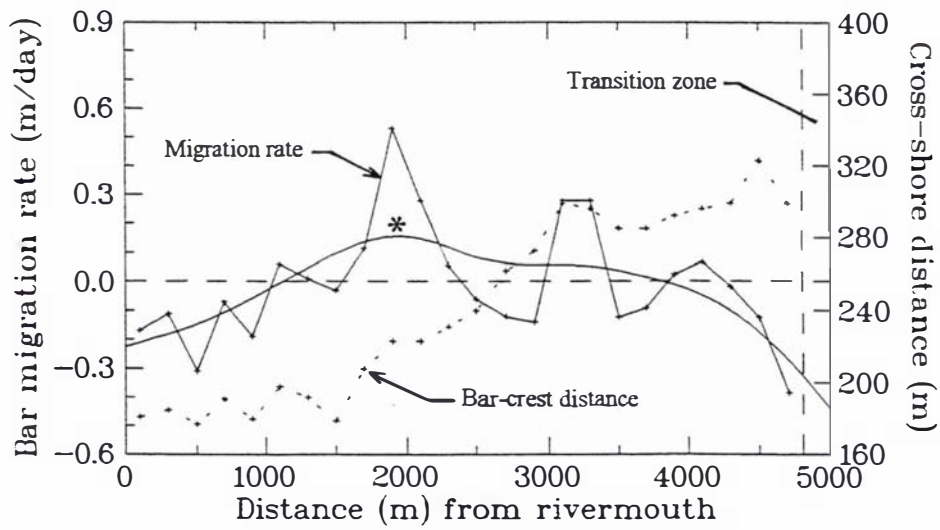

Figure 6.16 Cross-shore bar migration rate (bold line segments) between the rivermouth and the boundary of the transition zone (dashed vertical line) for positive switching (Figure A) and negative switching (Figure B). The positive switching is associated with episode 5, while the negative switching is from episode 9; terms are defined in section 6.5.1. Data points for bar migration rate were determined from the slope of linear regression models. These models were fitted to time-stacks constructed from the image sequence depicting the switching episode. The continuous curves were obtained by filtering the migration rate data using a distance weighted least squares routine. The dashed curve denotes the average cross-shore distance to the bar-crest under consideration at each longshore location. The asterisk marks the longshore limit of cross-shore bar migration associated with the episode of bar switching as proposed in section 6.5.2.

Despite considerable noise, the graphs in Figure 6.16 are indicative of how cross-shore bar migration changes with increasing longshore distance from the transition zone. These two bar-crest time-series display longshore fluctuations in their cross-shore migration rate. Furthermore, the wavelength of these fluctuations decreases closer to the rivermouth. Longshore fluctuations of similar wavelength and phase are also evident in the cross-shore bar-crest location data (dashed line). To identify any migration rate signal within the migration rate fluctuations, a distance weighted least squares filter was applied to the data points. The resulting curves overlay the raw data in Figures 6.16A and B. These curves show significant gradient changes at approximately T1500 for episode 5 and at approximately T2000 for episode 9. These locations, marked by asterisks on Figure 6.16, are interpreted as the longshore limit of the association between switching and cross-shore bar migration for these two episodes of bar switching. From the transition zone boundary to the asterisks, the migration rate can be seen to decrease for positive switching and increase for negative switching; in each case this occurred for a distance of ~3000 m.

NOM characteristics

To identify the relationship between bar switching and NOM characteristics, the time-series for individual bar-crests on each side of the transition zone for switch episode 7 were compared with the corresponding NOM characteristics for those bars. These data were obtained from the time-stacks for sites T2800 and T5000 (Figure 5.2). These sites are approximately equidistant from the average transition zone location for switch episode 7 which was centred approximately 4000 m from the rivermouth. The data for the two bar-crests are depicted in Figure 6.17. These bars were selected because they were both at a similar stage in their NOM life-cycle, in that prior to the onset of switching they had both entered the zone of systematic offshore migration at about the same time. At T5000, the seaward movement of the bar during episode 7 shows that positive switching occurred on this side of the transition zone, while at T2800, the minimal net bar migration indicates negative switching occurred in this area.

The NOM parameter values for these two offshore bar migrations are given in Table 6.6. The bar at T5000 has a substantially faster average rate of seaward migration (177 m/yr) than the bar at T2800 (>= 87 m/yr). The durations also show a marked variation, with the T5000 net offshore bar migration being shorter (1.6 yr) than that of the T2800 bar (>= 3 yr). These results indicate that areas which have undergone positive switching will be

A. Site T2800: negative switching

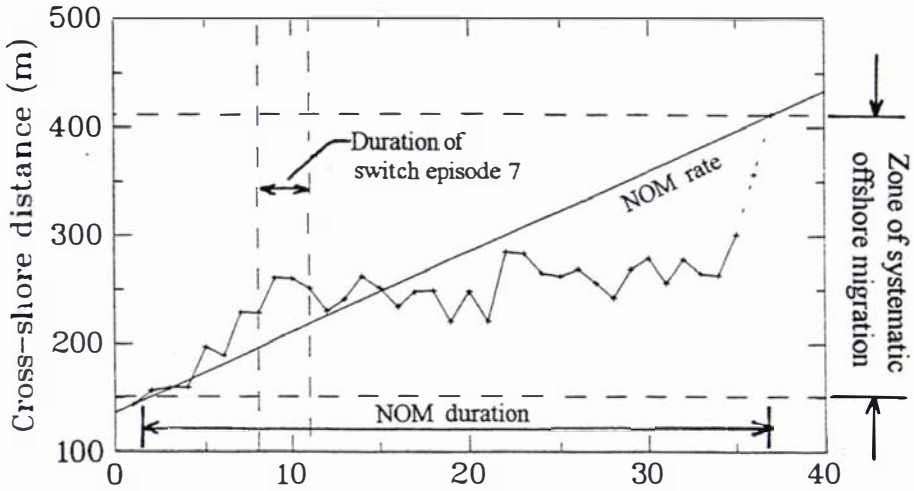

B. Site T5000: postive switching

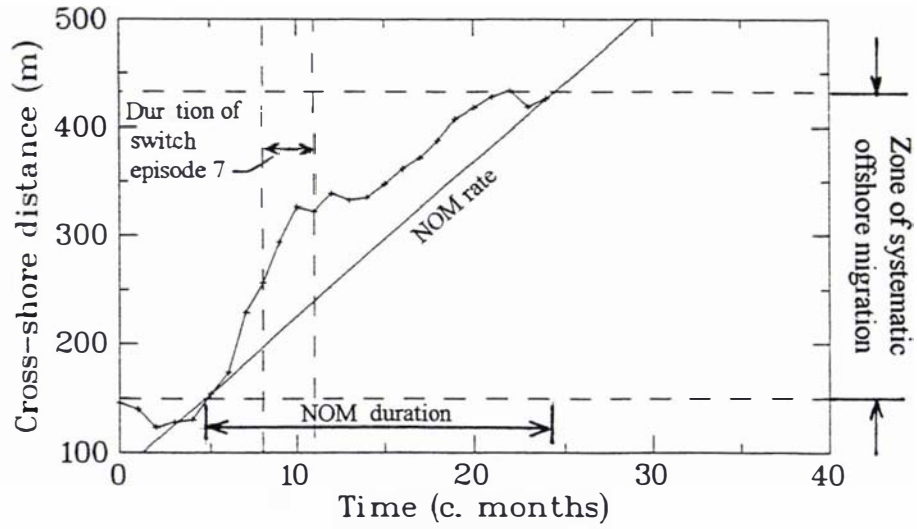

Figure 6.17 Time-series depicting the cross-shore location of selected bars at sites T2800 (Figure A) and T5000 (Figure B) between 8.12.94 (Time = 0) and the end of the study period on 22.11.97 (Time = 35). Sampling intervals were approximately one month apart (Appendix H[i]). The dashed vertical lines mark the time interval in which switch episode 7 occurred. The dashed horizontal lines locate the boundaries of the zone of systematic offshore bar migration. The straight diagonal lines define the average offshore migration rate of each NOM cycle. The NOM durations are also depicted. The method used to extrapolate between the final bar-crest location and the seaward boundary of the zone of systematic offshore migration is described in chapter 5, section 5.3.2. Resulting parameter values for the two NOM cycles are given in Table 6.6.

Table 6.6 NOM parameter values for bars located at sites T2800 and T5000. The bar-crest time-series are depicted in Figure 6.17. The T2800 bar was affected by negative switching associated with switch episode 7 (Figure 6.14) and the T5000 bar was affected by positive switching associated with switch episode 7.

Transect locations	NOM rate (m/yr)	NOM duration (years)
T2800	<=87	>=3
T5000	177	1.6

associated with NOM cycles characterised by higher levels of NOM activity (faster rates and shorter durations), while areas that undergo negative switching will be associated with cycles characterised by lower levels of NOM activity.

6.5.3 Discussion

The above results support the conclusion in section 6.2.3 that episodic offshore jumps have a significant influence on the characteristics of NOM cycles, for the following reasons. Positive switching is associated with large seaward bar migrations (see Figure 6.12B and Figure 6.17B). As positive switching has been shown to increase the level of NOM activity (previous subsection), episodic seaward jumps can also have this effect.

Morphological change evident in the bar switching example (Figure 6.15) strongly supports the outer bar control concept (section 6.3.3) for the following reasons. The seaward bar degeneration on the right side of Figure 6.15A to E preceded any large offshore bar migrations. Degeneration of the outer bar therefore appears to facilitate the offshore migration of the landward bar(s) for subsequent offshore migration in response to higher energy conditions. By contrast, the seaward bar to the left of the transition zone did not undergo degeneration and this appears to have constrained the landward bar(s) from undergoing substantial offshore migration.

Bar switching at Wanganui appears to be a consequence of longshore contrast in the degeneration status of the seaward bar. If bars along one section of coast are able to undergo substantial seaward migration while bars along an adjacent section of coast are constrained, then bar-crests have to undergo realignment in the longshore direction, i.e. bar switching must occur. A similar explanation may apply to bar switching on other coasts as Wijnberg (1995, p140) observed that on the Coast of Holland "small longshore differences in position and depth of the outer bar exist prior to the bar system getting out of phase".

The question to now be addressed is why does outer bar degeneration vary, at times, in the longshore direction? An empirical approach to answering this question would require high resolution elevation data (e.g. ± 0.1 m) covering a substantial area (e.g. 5 km^2) and sampled at intervals of about two weeks. To the authors knowledge, such a data-set is presently unavailable for any location; indeed it is unlikely that the technology exists to acquire such data. Nonetheless, it is possible to provide speculative answers on the basis of both theory and field results; two such possibilities are outlined below.

Changes in nearshore and/or shoreface sediment supply may result in longshore variation in the degeneration of the outer bar. Field evidence of such a relationship is suggested in data from a nourishment project at Terschelling (Hoekstra et al., 1996) where seaward bar degeneration slowed down following sediment deposition in the vicinity of the outer bar. Natural longshore variation in sediment supply, in terms of the occurrence of migrating low amplitude sand-waves or blankets, have been documented on a variety of coasts, e.g. along the Nile delta (Inman et al., 1992), along the eastern USA seaboard (Trowbridge, 1995), along the Danish coast (Brunn, 1955) and along the German coast (Antia 1996). Such features have been observed on the shoreface at Wanganui using side-scan sonar (Wallen, pers. comm.)[1]. The mechanism by which encroachment of such sedimentary features into the outer nearshore may locally affect seaward bar degeneration is a matter of conjecture. One possible explanation is that localised increase in sediment availability may increase the volume of bars, which then take longer to dissipate.

Standing edge waves may be capable of initiating longshore variations in seaward bar degeneration for the following reasons. Standing edge waves alter nearshore hydrodynamics by causing longshore variation in breaker height (Bowen and Inman, 1969) and by imposing a drift velocity

---

1. Lieutenant Commander overseeing the 1993 survey of bathymetric chart 4612 by the Hydrographic Office of the Royal New Zealand Navy.

pattern on the bottom boundary layer (Carter et al., 1973). These effects may cause local variations in degeneration morphodynamics. For example, outer bar size/shape changes may occur at edge wave nodes or antinodes. Infragravity and seiche waves that may be associated with standing edge waves at a range of periods (and wavelengths) have been observed to occur at Wanganui (chapter 2, section 2.5.1).

6.6 Conceptual modelling

Shorter-term bar behaviour considered in this chapter contributes to a conceptual morphodynamic model of NOM in three areas: the drive mechanism; modes of seaward bar migration; and the characteristics of NOM cycles. These three aspects are now summarised.

The positive skew evident in the frequency distribution for bar migration classes (Figure 6.3, Table 6.1) indicates that NOM is driven by morphodynamics associated with frequently occurring storm events. In particular, the seaward bar migrations associated with higher energy driven undertow are greater than the landward migrations associated with incident wave asymmetry experienced during intervening periods. Such morphodynamics are consistent with the general NOM drive mechanism proposed earlier in chapter 5 (sections 5.5.2.1 and 5.6).

NOM at Wanganui appears to result from the combination of two modes of subcyclic cross-shore bar migration: an episodic offshore jump followed by smaller cross-shore fluctuations; or more regular fluctuations that have a net seaward trend. These two modes are schematically illustrated in Figure 6.6. Offshore bar migration at other global sites also appears to fit these two behavioural modes. A proposed explanation for modal preference at particular sites is given within the following paragraph which deals with the role of outer bar degeneration in subcyclic bar behaviour.

The Wanganui results for inter-survey cross-shore bar migration (Table 6.4), together with the cross-shore migration analysis for bar switching (Figure 6.15), clearly demonstrate a causal relationship whereby the degeneration status of the outer bar appears to control the offshore migration potential of the landward bar(s). In particular, a degenerated outer bar enables the landward bar to undergo substantial seaward migration, while a well developed outer bar constrains significant offshore migration by the landward bar. This *outer bar control concept* is illustrated in Figure 6.11. The degenerative state of the outer bar appears to control the magnitude of cross-shore bar migration and

characteristics of individual NOM cycles, by determining when the landward bars are exposed to intense seaward directed sediment transport. Where a longshore contrast exists in the degenerative state of the outer bar, a marked longshore difference can occur in cross-shore bar migration. This causes bar switching and results in bars on each side of the transition zone having different NOM characteristics. Such longshore variation in outer bar degeneration may be a consequence of longshore differences in the size of the most seaward bar because a smaller bar could dissipate more rapidly than a larger bar. Contrasting size of the outer bar may also result in the two modes of bar migration described in the preceding paragraph. Where outer bars have relatively smaller volumes, the degeneration will occur more rapidly and lead to large migrations by landward bars. Under such circumstances an episodic mode of cross-shore bar migration would occur in contrast to a regular mode occurring where bars have a greater volume.

In terms of systems theory, a cycle of NOM involves two temporally alternating subsystems: one characterised by self-organisation and the other by nonself-organisation. A well developed seaward bar dissipates incident wave energy. The landward bars can then become organised into distinct three-dimensional patterns, but they are unable to migrate very far seaward. However, when outer bar degeneration proceeds past a depth and/or shape threshold then a nonself-organised subsystem is triggered. Landward bars are forced to migrate seaward to attain equilibrium with the incident energy. Antecedent morphology and positive form-process feedback are therefore particularly important controls in these subsystems. In the case of bar switching, the two subsystems occur contemporaneously and are located next to each other in the longshore direction.

6.7 Summary and conclusions

The objectives of this chapter were firstly to identify shorter-term bar behaviour that may influence the individual NOM cycle, with particular emphasis on longshore non-synchronous behaviour; secondly to identify the process associations that occur with these types of subcyclic behaviour, and thirdly to use these results to further the development of a conceptual model for NOM. These objectives were achieved by analysing Wanganui data with respect to bar migration along two cross-shore transects, and change within selected (plan-view) morphological sequences. The specific research questions used to address these objectives, together with a summary of results and the associated conclusions, are given below.

While sampling errors associated with measurement resolution and irregular sampling intervals influenced bar migration data, bias was minimised by either analysing large samples or by allowing for errors when interpreting the results. More detailed future studies into NOM, however, would benefit from a reduction in sampling errors.

What are the general cross-shore bar migration characteristics from the Wanganui data?

Directional asymmetry characterised the frequency distributions of the cross-shore bar migration data (Figure 6.3). Net seaward migration occurred for most migration distance classes. Approximately 64% percent of all bar migrations at T1600 and ~70% at T5000 were in a seaward direction.

Two populations of cross-shore migrations were evident in the data from each sites (Figure 6.3). The populations separate at migration distances of 40 to 50 m in the seaward direction. All migrations in excess of 50 m were defined as episodic seaward jumps or episodic offshore bar migrations. Ten such events occurred at site T1600 and six at T5000.

How significant to NOM are episodic seaward jumps?

Episodic jumps are a particularly important subcyclic influence on NOM for the following reasons. Such migrations could account for a high proportion of the total seaward migration distance, e.g. 62.5% at T1600. Episodic seaward jumps were often associated with significant changes in cross-shore bar migration patterns (see Figure 6.5B). Episodic seaward jumps appear to increase the level of NOM activity for individual cycles (section 6.5.3).

Are episodic seaward jumps non-synchronous in the longshore direction?

Episodic seaward bar migrations at Wanganui are predominantly (80%) non-synchronous in the longshore direction (Figure 6.5C). This is likely to result in longshore variation in the characteristics of contemporaneous NOM cycles.

Are episodic seaward jumps preceded by the disappearance or prior seaward movement of the adjacent seaward bar(s)?

Episodic seaward bar migrations at Wanganui were usually (10 of 15 cases) preceded by either the disappearance of the adjacent seaward bar or by a substantial offshore migration of the adjacent seaward bar (Table 6.4). In the remaining five cases, change in the seaward bar appeared to coincide with the episodic migration. More precise event relativity could not be established because of the monthly sampling interval. It is therefore

possible that in all 15 cases the seaward bar change preceded the episodic seaward migration. The Wanganui results are consistent with observations made at other NOM sites. The bar switching analysis (Figure 6.15) provided additional evidence that a seaward bar change preceded substantial offshore migration of the landward bars. The bar migration results (section 6.3) together with the bar switching results (section 6.5) provide strong evidence that a causal relationship exists at Wanganui in which the outer bar behaviour controls the potential for offshore migration of the landward bar; this is referred to as the *outer bar control concept* and is diagrammatically illustrated in Figure 6.11. General mechanisms have been proposed to explain the degeneration of the seaward bar (Wijnberg, 1995; Ruessink, 1998), and also how a degenerated bar could control cross-shore migration of landward bars (Kroon, 1994; Ruessink and Kroon, 1994).

What types of subcyclic (plan-view) morphological behaviour are associated with cross-shore bar migration which may be capable of influencing the characteristics of individual cycles of NOM?

Three different types of plan-view morphological behaviours occurred during episodic offshore bar migrations at Wanganui. These types of behaviour (Figure 6.12) were bar switching (N=5), bar bifurcation (N=2), and linear bar with uniform cross-shore migration (N=9).

Which of these behaviours are associated with contemporaneous longshore variation in cross-shore bar migration, and how does the most frequently occurring behaviour relate to different characteristics of NOM cycles?

Bar switching was the predominant morphological behaviour associated with contemporaneous longshore variation in NOM characteristics. Bar switching was investigated further by analysing cross-shore bar migration associated with three of the nine episodes of bar switching that occurred at Wanganui during the study period. Cross-shore bar migration was found to differ markedly on each side of the transition zone with bars on one side moving rapidly offshore whilst bars on the other side underwent minor net cross-shore migration (Figure 6.15). These two situations are referred to as positive and negative switching respectively. Increased levels of NOM activity were shown to accompany positive switching, while decreased levels accompanied negative switching (Figure 6.17) and this appeared to be responsible for marked contrasts in characteristics of individual cycles of NOM at Wanganui. Bar switching appears to result from longshore variation in the level of degeneration of the outer bar. Positive switching occurs where the outer bar degeneration is in an advanced state; this is in accord with the outer bar control concept. It therefore appears that both bar switching and NOM characteristics are interrelated because both are

strongly dependent upon outer bar degeneration, rather than than one influencing, or being a consequence of, the other. Finally, the association between cross-shore bar migration and switching was shown to extend ~3000 m from the transition zone (Figure 6.16). However, the strength of the association tends to decrease with increased distance from the transition zone so the effect on NOM characteristics should also lessen.

What environmental conditions occur during subcyclic cross-shore and plan-view morphological behaviours?

At Wanganui, episodic seaward bar migrations and the associated morphological plan behaviours usually occur under very high levels (>95th percentile value) of wave height and longshore wind speed (Figure 6.9A and C). In most cases (77%) these events lasted from two to four days.

While episodic seaward bar migrations occur under higher energy levels, the following evidence suggests that antecedent morphology has a significant influence on subcycle morphodynamics:

- Most (80%) episodic offshore bar bar migrations were longshore non-synchronous (Figure 6.5).
- There were no strong associations between episodic bar migration and the three process parameters (Figure 6.9).
- Negative (landward) migrations of up to 50 m occurred under higher energy levels (Figure 6.4).
- The process parameters for the predominant types of morphological (plan) behaviours (Figure 6.13) have similar values.

How do the shorter-term results from Wanganui contribute towards a conceptual morphodynamic model of NOM.

Contribution to conceptual modelling includes a NOM drive mechanism based on morphodynamics associated with frequently occurring storm-recovery sequences. In particular, the seaward (undertow driven) bar migrations associated with higher energy levels are greater than the landward (incident wave asymmetry driven) migration experienced during intervening periods. Such a mechanism is consistent with the general NOM drive mechanism proposed in chapter 5 (section 5.5.2.1 and 5.6).

A further modelling contribution concerned control by the outer bar over cross-shore migration of the landward bar(s), i.e. the outer bar control

concept. In particular, higher levels of degeneration facilitate substantial offshore bar migration (Figure 6.11). Such substantial bar migration was shown to increase the level of NOM activity (Figure 6.17 and Table 6.6). Lower levels of degeneration have the opposite effect.

Contrasting cross-shore bar migrations occur where the level of outer bar degeneration varies in the longshore direction. This can result in bar switching and longshore variation in the characteristics of NOM cycles.

The modelling contribution also includes the identification two modes of seaward bar migration. These modes, referred to as episodic and regular, are diagrammatically illustrated in Figure 6.6.

A cycle of NOM can be explained with respect to systems theory. Briefly, two temporally alternating subsystems develop in response to the changing degeneration state of the outer bar (section 6.3.3). In the case of bar switching, the two subsystems occur contemporaneously and are adjacent in the longshore direction.

Chapter 7 CONCLUSIONS

So Man, who here seems principal alone,
Perhaps acts second to some sphere unknown,
Touches some wheel, or verges to some goal;
T'is but a part we see, and not a whole.

Pope: An Essay on Man, Epistle 1.

In this chapter the conclusions pertaining to the thesis aim are summarised (section 7.1) and directions for further research are discussed (section 7.2).

7.1 NOM objectives

The aim of this thesis was to **elaborate on the behaviour and causal processes of net offshore bar migration** (chapter 1, section 1.1). This was to be achieved by addressing the general research objectives listed in chapter 1 (section 1.4) and the associated specific objectives and questions formulated in subsequent chapters. The general objectives consisted of:

- The development of photogrammetric methods of data acquisition and analysis;
- Determination of longer-term (average cyclic) characteristics of NOM behaviour based on the analysis of multiple cycles;
- Determination of shorter-term (within-cycle or subcycle) characteristics of NOM behaviour, with emphasis on longshore non-synchronous variation;
- Comparison of the Wanganui results with those from other NOM sites;
- Identification of the environmental conditions which accompany the NOM-associated morphological behaviour;
- Development of a conceptual model to explain the observed NOM behaviour.

Conclusions are now presented under the following general headings: image-based data acquisition; longer-term NOM characteristics; shorter-term NOM characteristics; and conceptual modelling of NOM.

7.1.1 Image-based data acquisition

Photogrammetric techniques of data acquisition were developed that produced bar-crest data for the study area with a cross-shore resolution of ~20 m and a longshore resolution of ~200 m. By comparison, the data requirements outlined in chapter 1 (section 1.3.2) had stipulated resolutions of ~10 m and ~100 m respectively. While the 20 X 200 m resolution combination imposed a limitation on the detection of bar migration, these data were still able to identify morphological change at a level of detail which satisfactorily met the NOM study objectives.

Intensity maxima defining surf zone bars became less well defined at both the seaward and landward extremes of the zone. At the seaward limit the signal became less intense and patchy, which indicated that bar degeneration was occurring. Intensity maxima located on the foreshore could relate to features other than bar-crests because most of this area was exposed during photographic sampling. While these limitations often prevented accurate identification of bar generation and the location of bars during degeneration, suitable ground survey data were available for these purposes. However, within the zone of systematic offshore bar migration where NOM analysis was carried out, the image-based data were able to meet the study objectives. This was because the method used to define this zone enabled the problem areas to be excluded.

Differences were found to occur between bar-crest location data obtained by aerial and terrestrial photogrammetry and also between data obtained from image and ground profiles. Corrections for these systematic errors were determined - thereby enabling data fusion to occur and hence the subsequent analysis of otherwise incompatible data.

While greater accuracy in determining some of the errors was desirable, the use of either 95% confidence intervals or a 'worst case' approach, resulted in an overestimation of many errors and hence conservative (higher) estimates for combined errors. Reliable bar-crest data should therefore have been acquired for the NOM analysis.

Photogrammetric sampling occurred over a 6.3 year period. While weekly, fortnightly and monthly data-sets were obtained, the monthly data was usually found to define NOM adequately for the purposes of this study. In situations where the definition was not clear, supplementary data were incorporated into the analysis.

A range of image processing algorithms was written which enabled the extensive set of field samples (1894 photographs) to be processed and analysed.

7.1.2 Longer-term NOM characteristics

The longer-term or average cyclic NOM characteristics at Wanganui and the other global NOM sites were determined using a set of parameters that were applied to a pre-determined zone of systematic offshore bar migration. These parameters consisted of the cross-shore width of the zone, the NOM duration, the NOM return period and the NOM rate. NOM duration was the parameter used to represent the NOM morphological system; this parameter was positively associated with width and return period and negatively associated with rate. Analysis of time-series data from longshore sites at Wanganui showed relatively small variation in average duration (1.4 to 2.4 years). While values increased further from the rivermouth, the existence of a longshore trend was not conclusive. By comparison, average duration showed much greater variation for the global sites with values ranging from 1.2 to 13.0 years. Furthermore, a distinction was evident between the Wanganui/Duck sites and the Dutch sites with the former tending to have NOMs with shorter average durations (1.2 to 2.4 yr c.f. 3.7 to 13 yr), smaller migration widths (195 to 379 m c.f. 305 to 930 m), shorter average return periods (1.2 to 6.8 yr c.f. 3.3 to 14.4 yr) and faster average migration rates (121.9 to 196 m/yr c.f. 34.8 to 85.1 m/yr).

The global NOM sites are located on coasts characterised by multiple sand-bars. Nearshore widths varied between 313 m (Duck) and 1250 m (Terschelling), and nearshore slopes varied between 0.0098 (Duck) and 0.0041 (Terschelling). Process conditions were charactrised by a narrow range of storm strength wind and wave conditions, the predominance of sea waves, and low to moderate tide ranges. In particular, extreme wave height (1% exceedence) parameter values varied between 3.05 m at Duck and 4.3 m at Terschelling, wind speed (10% exceedence) parameter values ranged between 12.3 m/s at Duck and 14.8 m/s at Wanganui, wave period parameter values ranged from 6 seconds for the Dutch sites to 7.8 seconds at Wanganui, and spring tide ranges varied between 1.2 (Duck) and 2.5 m (Terschellilng). In contrast to the similarity of these energy parameter values, storm wind directions were highly variable and ranged between 17 degrees (to the coastline) at Terschelling and 82 degrees at Egmond.

NOM characteristics were associated with the following environmental variables. Gentler cross-shore slopes and higher wave energy were positively related to NOM duration. A strong non-linear association occurred between wind direction relative to the coastline and NOM duration. This indicates that coastal orientation is related to longer-term NOM characteristics. However, the role of the sediment budget or coastal structures in either initiating or influencing longer-term NOM remains unclear.

While the data used in this study enabled the objectives for longer-term NOM to be generally met, the following limitations were encountered. The apparent longshore gradients in some NOM characteristics at Wanganui could not be confirmed because of insufficient length of the data. Furthermore, the role of wave climate variation in modifying longer-term characteristics of NOM could not be resolved because of possible non-equivalency errors in process parameter values for the global sites.

7.1.3 Shorter-term NOM characteristics

The shorter-term (subcyclic or within-cycle) bar behaviours which may influence the characteristics of individual cycles of NOM at Wanganui were investigated by analysing both cross-shore bar migration data (at sites T1600 and T5000), and selected morphological configuration sequences. Frequency distributions of inter-survey bar migration distance showed most bar migrations (63.5 to 69.7%) were directed seaward and net seaward bar movement occurred in most of the migration classes. Furthermore, the migration population appeared to be bimodal. The group of migrations with inter-survey distances greater than 50 m were referred to as episodic seaward jumps or episodic offshore bar migrations. At site T1600, 10 such migrations occurred, while six occurred at T5000. Episodic seaward jumps were a significant influence on NOM and were observed to increase the level of NOM activity, i.e. cause shorter NOM duration and faster NOM rate. Eighty percent of these larger seaward migrations were non-synchronous in the longshore direction.

Most episodic jumps were preceded by the seaward bar either moving significantly further offshore or undergoing substantial degeneration. This relationship had previously been suggested by other researchers (see section 6.1). Further analysis showed that in all the Wanganui cases the offshore migration potential of a landward bar depended on the outer bar being in an advanced state of degeneration.

Three different types of morphological (plan) behaviour occurred at Wanganui during episodic seaward jumps: linear bars with uniform offshore migration; bar switching; and bar bifurcation. Bar switching was the behaviour most often associated with contemporaneous longshore variation in episodic offshore bar migration and was therefore studied in greater detail.

Bar switching involves the realignment of nearshore bars such that the bars become discontinuous in the longshore direction with landward bars on one side of the discontinuity joining with seaward bars on the other side.

This type of morphological behaviour appears to be a result of a longshore contrast in the degeneration state of the outer bar on each side of the transition zone, i.e. that area within which bar switching takes place. In most episodes of bar switching at Wanganui (78%), the bars underwent rapid seaward migration (positive switching) on one side of the transition zone, but remained relatively stationary (negative switching) on the other side. The outer bar was in a degenerated state when positive switching occurred and in a well developed state when negative switching occurred. The NOM cycles on each side of a transition zone had markedly contrasting characteristics with higher rates and shorter duration occurring for bars that underwent positive switching.

Episodic seaward bar migrations were usually associated with severe wave energy and longshore winds (> 95th percentile value) which lasted from two to four days. While such high energy events drive these bar migrations, morphological control is also important to the system morphodynamics. Antecedent morphology appears to be particularly significant when bar migrations were associated with bar switching.

The determination of short-term bar behaviour at Wanganui was subject to a variety of sampling errors. However, analysis bias was minimised either by using a large number of samples or by accounting for the errors when interpreting results.

7.1.4 A conceptual model for NOM

This section combines the various aspects of conceptual modelling in chapters 5 (section 5.6) and 6 (section 6.6) into a general conceptual morphodynamic model for NOM. The proposed model applies to coasts subject to the environmental conditions detailed in Tables 5.1 and 5.2. The focus of the model is on bar migration across the zone of systematic offshore migration, i.e. the second stage of the three stages which define the NOM 'life-cycle' (sections 1.1 and 5.1). While the model is therefore not concerned with a morphodynamic-based explanation of bar generation or degeneration, the latter process affects the morphodynamics of bars within the zone of systematic offshore migration so this aspect has been incorporated into the modelling. The model consists of a basic drive mechanism, a morphodynamic modification mechanism and a timing mechanism. These components account for the average cyclic NOM characteristic observed in the longer-term bar-crest time-series, and also for the variation observed within individual cycles of NOM at Wanganui.

NOM is driven by greater seaward directed forces (undertow) which predominate under storm conditions, compared with landward directed forces (incident wave asymmetry) which predominate under lower energy conditions. The drive mechanism concept is illustrated in Figure 5.14A and Figure 6.6. The storm characteristics of a site influence the length of time required for net offshore bar migration to become evident. For example, at Wanganui, frequent storm events tend to result in the net seaward bar migration signal being evident within a relatively short time period (c. 0.25 to 0.5 yr), while at Duck less frequent storm events result in a longer time span (c. 0.5 to 2 yr) being necessary to detect the signal. NOM morphodynamic modifiers such as bar size, also influence signal detection time.

Longer-term NOM characteristics are modified as a result of morphodynamic interactions involving incoming energy and physical boundary conditions (Figure 5.14B). Cross-shore slope appears to influence the bar size and hence the time required for bars to migrate across the zone of systematic offshore migration, with smaller bars resulting in higher levels of NOM activity (shorter NOM duration and faster NOM rate). Coastal orientation appears to influence longshore currents, with stronger currents associated with an oblique wind and wave approach resulting in a higher level of NOM activity.

The characteristics of individual NOM cycles are controlled by the timing of large offshore bar migrations. The potential of a nearshore bar to undergo substantial offshore migration in response to elevated incident energy levels is explained by the *outer bar control concept.* This concept incorporates the results of both bar migration analysis and bar switching analysis. It states that landward bars are only able to undertake substantial offshore migration if the outer bar is in an advanced state of degeneration (Figure 6.11). Conversely, if the outer bar is well developed then the landward bars are relatively fixed in cross-shore location. Bar degeneration may vary both temporally and spatially so successive NOM cycles at the same site, or contemporaneous NOM cycles at different longshore sites, may have contrasting NOM characteristics. For example, if a longshore contrast develops in the degenerative state of the outer bar then bar switching may occur and characteristics of adjacent longshore NOM cycles can vary dramatically (e.g. Figure 6.17, Table 6.6). The two modes of cross-shore bar migration (Figure 6.6) appear to result from differing rates of outer bar degeneration, with more rapid degeneration producing more frequent larger offshore bar migrations and hence an episodic mode of behaviour. It is hypothesised that outer bar degeneration is influenced by bar size, such that larger bars take longer to degenerate. Bar switching would therefore be a product of longshore variation in bar size, and differing bar migration

modes would occur at sites with contrasting bar size. This latter result is consistent with the varying levels of longer-term NOM activity associated with differing bar size noted above, in that smaller bars facilitate larger offshore migrations which in turn should result in shorter NOM durations and faster NOM rates.

Possible mechanisms by which the behaviour of an outer bar may control the seaward migration (potential) of the landward bar have been proposed by Kroon (1994) and Kroon and Ruessink (1994). These researchers speculate that the seaward bar controls both the cross-shore wave height distribution and the cross-shore structure of standing infragravity waves; so whether landward bars are able to undergo (substantial) offshore migration is governed by break-point and/or standing wave-based sediment transport mechanisms. Mechanisms have also recently been hypothesised by Wijnberg (1995 and 1996) and Ruessink (1998) to account for the degeneration of the outer bar.

A cycle of NOM can be viewed in terms of systems theory with two temporally alternating subsystems developing in response to the changing degenerative state of the seaward bar (see section 6.3.3). In the case of bar switching, the two subsystems occur contemporaneously and are located next to each other in the longshore direction.

Finally, NOM can be viewed as a complex system operating at a range of time scales. At a shorter time scale, a seaward bar migration trend is the product of successive bar migrations. At a short to medium time scale, the characteristics of individual NOM cycles are controlled by the antecedent morphology (of the outer bar in particular) which influences the incident energy's potential to effect off-shore bar migration. Longer-term (average cyclic) NOM characteristics reflect the relationships between the climatic energy regime and the physical boundary conditions.

7.2 Further research

The recognition of additional coasts that experience NOM will lead to the identification of stronger environmental associations and more detailed conceptual models. However, an important consideration is the minimum length of bar-crest time-series necessary to accurately determine the NOM characteristics of a site. While parameter values at Wanganui appeared to be stabilising after 6.3 years, small changes would probably have occurred if the bar-crest record had been extended. An ongoing monitoring programme which updates the NOM parameter values until no further (statistically significant) change is evident would be a preferred approach to

future longer-term NOM investigations. Present developments in automated video monitoring systems, e.g. http://www.minvenw.nl/projects/netcoast/argus/argus.htm for international sites or http://www.niwa.cri.nz/cam-era/ for New Zealand sites, coupled with image processing algorithms similar to those used in this project, will provide cost effective methods of obtaining these data.

The analysis of video images can also provide a comprehensive range of process data which can be utilised when developing more detailed morphodynamic models for NOM. Recent developments include the measurement of wave speed by Lippmann (1992), automated swash-front tracking by Bailey and Shand (1994), the measurement of wave period at different nearshore locations by Redondo et al. (1994), and the measurement of longshore current by Leon and Holman (1994) and Osborne et al. (1999). Intensity patterns on time-stack images constructed from video frames, such as in Figure 3.12A, could provide a means of obtaining breaking wave height at different locations within the surf zone.

This study has confirmed that outer bar degeneration plays a key role in controlling the characteristics of NOM cycles. Further investigation is required into the nature of outer bar degeneration and how this affects the migration potential of the landward bars. A spatially and temporally extensive data-set of high resolution three-dimensional measurements will be required for this analysis.

The possibility that longer-term NOM involves a sediment redistribution process within the nearshore, or a cross-shore sediment budget imbalance, requires further research.

NOM-associated bar generation and shoreline stability could also be investigated. Bar generation during the NOM cycle occurs on the lower foreshore (Shand and Bailey, 1999). The study of such repetitive, and hence somewhat predictable, bar formation provides an opportunity to further investigate bar generation and field test existing models; see Holman and Sallenger (1993) for a review. In addition, bar-crest data presented in the Wanganui time-stack images (Figure 5.2) suggest that the foreshore widens until the time of bar formation and then narrows. This appears to be consistent with a correlation between cross-shore excursion of the dune toe and the NOM cycle that was recently identified in data from the Holland coast by Stive et al. (1996). This process may have relevance for shoreline modelling and hence warrants further investigation.

Future study into NOM may be facilitated by carrying out investigations in an area where bar switching is occurring. This is because the three NOM stages of bar generation near the shoreline, systematic offshore migration across the surf zone and bar degeneration in the outer surf zone, all occur during an episode of positive bar switching. These stages are all completed within shorter time-spans, and within more localised areas, than for nonswitch-associated NOM.

The relationship between NOM and beach-state models should be investigated. It will be recalled from chapter 1 (section 1.1) that a major implication of NOM for coastal geomorphology was how this phenomenon could be integrated with existing conceptual surf zone models, i.e. the beach-state models summarised in Appendix A. While such a task was beyond the scope of the present study, the thesis has provided necessary background understanding of NOM thereby making such an investigation more feasible. In addition, image-based methods of data acquisition, such as those developed for, or described in, the present study, can provide the necessary data for this next step in the advancement of beach and nearshore modelling.

References

Aagaard, T., 1990. Infragravity waves and nearshore bars in protected, storm-dominated coastal environments. *Marine Geology*, 94, 181-203.

Aagaard, T., and Holm, J., 1989. Digitisation of wave run-up using video records. *Journal of Coastal Research*, 5(3), 547-551.

Abbott, S.T. and Carter, R.M., 1991. The sequence architecture of Mid-Pleistocene (c.1.1-0.4 Ma) cyclotherms from New Zealand: facies development during a period of orbital control on sea-level cyclicity. In De Boer, P.I., and Smith, D.G. (eds.), *Orbital Forcing and Cyclic Sequences*, ISA Special Publication 1.

Anders, F.J., and Byrnes, M.R., 1991. Accuracy of shoreline change rates as determined from maps and aerial photographs. *Shore and Beach*, 59(1), 17-26.

Antia, E.E., 1996. Shoreface-connected ridges in German and U.S. Mid-Atlantic Bights: similarities and contrasts. *Journal of Coastal Research*, 12(1), 141-146.

Bagnold, R.A., 1963. Beach and nearshore processes. Part 1, mechanics of marine sedimentation. In: Hill, M.N., (ed.), *The Sea: Volume. 3.* Wiley-Interscience, New York, pp. 507-528.

Bailard, J.A., 1981. An energetics total load sediment transport model for a plane sloping beach. *Journal of Geophysical Research* 86, 10938-10954.

Bailey, D.G., 1985. *Hardware and software developments for applied digital image processing.* PhD thesis, University of Canterbury, New Zealand.

Bailey, D.G., and Hodgson, R.M., 1988. VIPS - a digital image processing algorithm development environment. *Image and Vision Computing*, 6, 176-184.

Bailey, D.G., and Shand, R.D., 1993. Determining large-scale sand-bar evolution. *Proceedings of the 1st New Zealand Conference on Image and Vision Computing*, pp. 109-116.

Bailey, D.G., and Shand, R.D., 1994. Determining wave run-up using automated video analysis. *Proceedings of the 2nd New Zealand Conference on Image and Vision Computing*, pp. 2.11.1 - 2.11.8.

Bailey, D.G., and Shand, R.D., 1996. Determining large-scale sand-bar behaviour. *Proceedings of the IEEE International Conference on Image Processing*, Lausanne, Switzerland, (2), 637-640.

Bailey, D.G., and Shand, R.D., 1997. Data fusion issues in analysing coastal morphodynamic systems. *Proceedings of the 1st joint Australian and New Zealand conference on Digital Image and Vision Computing: Techniques and Applications*, New Zealand, pp. 107-112.

Balsillie, J.H., and Carter, R.W.G., 1984. The visual estimation of shore-breaking wave heights. *Coastal Engineering*, 8, 367-385.

Barford, N.C., 1985. *Experimental measurements: Precision, Error and Truth*. John Wiley and Sons, New York, 157p.

Bauer, B.O., and Greenwood, B., 1990. Modification of a linear bar-trough system by a standing edge wave. *Marine Geology*, 92, 177-204.

Bell, R., 1990. Oceanography of Wanganui Coastal Waters. *Final Report of the Wanganui District Council on the Recommended Scheme for Wastewater treatment and Disposal for the City of Wanganui*. Water Quality Centre, Department of Scientific and Industrial Research, New Zealand, 33p.

Bell, R., 1991. Oceanography of Wanganui Coastal Waters. *Environmental Impact Assessment Report for the Wanganui Wastewater Working Party*. Water Quality Centre, Department of Scientific and Industrial Research, New Zealand, 24p.

Bendat, J.S. and Piersol, A.G., 1971. *Random Data: Analysis and Measurement Procedures*. John Wiley and Sons, Inc., New York, 407p.

Birkemeier, W.A., 1984. Time scales of nearshore profile change. *Proceedings of the 19th International Conference on Coastal Engineering*, ASCE, pp. 1507-1521.

Birkemeier, W.A., 1985. Field data on the seaward limit of profile change. *Journal of Waterway, Port, and Coastal Engineering*, 111(3), 598-602.

Blauberg, I.V.; Sadovsky, V.N., and Yudin, E.G, 1980. The systsemic approach: prerequisites, problems, and difficulties. *General Systems*, XXV, 1-31.

Bowen, A.J., 1980. Simple models of nearshore sedimentation; beach profiles and longshore bars. In: McCann, S.B (ed.), *The Coastline of Canada, Geological Survey Canada*, Paper 80-10, pp. 1-11.

Bowen, A.J., and Inman, D.L., 1971. Edge waves and crescentic bars. *Journal of Geophysical Reset*, 76, 8662-8671.

Bowman, M.J.; Jones, D.A., and Kibblewhite, A.C., 1982. Tidal studies. In: Kibblewhite, A.C., (ed.), *Maui Development Environmental Study: report on phase two, 1977-81*, University of Auckland, pp. 49-59.

Brodie, J.W., 1960. Coastal surface currents around New Zealand. *New Zealand Journal of Geology and Geophysics*, 3(2), 235-252.

Bruun, P. 1955. Migrating sand waves or sand humps, with special reference to investigations carried out on the Danish North Sea coast. *Proceedings of the 5th Conference on Coastal Engineering*, pp. 269-295.

Bruun, P., 1978. *Stability of Tidal Inlets - Theory and Engineering*. Developments in Geotechnical Engineering 23. Elsevier Scientific Publishing Company, Amsterdam, 506p.

Bruun, P., and Gerritson, F., 1960. *Stability of Coastal Inlets*. North-Holland Publishing Company, Amsterdam, 123p.

Bryant, E., 1983. Coastal erosion and accretion , Stonewall Park Beach, N.S.W., 1890-1980. *Australian Geographer*, 15, 382-390.

Bunge, M., 1977. General systems and holism. *General Systems*, XXII, 87-90.

Burgess, J.S., 1971. *Coastline change at Wanganui, New Zealand.* Unpublished PhD thesis, University of Canterbury, New Zealand, 99p.

Capra, F., 1995. A systems view of the world. *Resurgence*, 151, 34-37.

Carter, R.W.G., 1986. The morphodynamics of beach-ridge formation: Magilligan, Northern Island. *Marine Geology*, 73(2), 191-214.

Carter, R.W.C., 1988. *Coastal Environments: An Introduction to the Physical, Ecological and Cultural Systems of Coastlines.* Academic Press, London, 611p.

Carter, R.W.C.; Forbes, D.L.; Orford,J.D.; Jennings, S.C.; Shaw, J., and Taylor, R.B., 1993. Long-term morphodynamic evolution of beaches and barriers: examples from paraglacial coasts. In: List, J.H., (ed.), *Large-Scale Coastal Behaviour '93.* U.S. Geological Survey, Open-File Report 93-381: 25-28.

Castleman, K.R., 1979. *Digital Image Processing.* Prentice-Hall, Englewood Cliffs, New Jersey, USA.

CERC, 1984. *Shore Protection Manual, Vol. 1.* US Coastal Engineering Research Centre.

Chandler, J.H.; Cooper, M.A.R., and Robson, S., 1989. Analytical aspects of small format surveys using oblique aerial photographs, *Journal of Photographic Science*, 37, 235-240.

Chandler, J.H, and Moore, R., 1989. Analytical photogrammetry: a method for monitoring slope instability. *Quarterly Journal of Engineering Geology*, 22, 97-110.

Chappell, J., and Eliot, I.G., 1979. Surf-beach dynamics in time and space - an Australian case study, and elements of a predictive model. *Marine Geology*, 32, 231-250.

Chapple, L.J.B., and Veitch, H.C., 1939. *Wanganui.* Hawera Star Publishing Company, New Zealand, 312p.

Chorley, R.J., and Kennedy, B.A., 1971. *Physical Geography: A Systems Approach.* Prentice-Hall International Inc., London, 360p.

Chorley, R.J., Schumm, S.A., and Sugden, D.E., 1984. *Geomorphology.* Methuen, London, 607p.

Crowell, M.; Leatherman, S.P., and Buckley, M.K., 1991. Historical shoreline change: error analysis and mapping accuracy. *Journal of Coastal Research*, 7(3), 839-852.

Dahm, J., 1988. Wanganui Estuary and Bar. *Evidence of the Department of Conservation, presented to the Central Districts Catchment Board in the matter of the Wanganui River Minimum Flow Review,* Department of Conservation, New Zealand, 23p.

Dally, W.R., 1990. Random breaking waves: a closed-form solution for planar beaches. *Coastal Engineering*, 14, 223- 263.

Davidson-Arnott, R.G.D., 1988. Controls on bar formation and forms of barred nearshore profiles. *The Geographical Review*, 78, 185-193.

Davies, J.L., 1980. Geographical variation in coastal development. In: Clayton, K.M., (ed)., *Geomorphology Texts 4*. Longman, London, 212p.

Davis, R.A., and Fox, W.T., 1972. Coastal processes and nearshore sand bars. *Journal of Sedimentary Petrology*, 42(2), 401-412.

Davis, R.A., and Fox, W.T., 1975. Process-response patterns in beach and nearshore sedimentation: 1. Mustang Island, Texas. *Journal of Sedimentary Petrology*, 45(4), 852-865.

Davis, R.A., and Hayes, M.O., 1984. What is a wave-dominated coast? *Marine Geology*, 60, 313-329.

DCE, 1980. *Coastal Management in Western Australia.* Department of Conservation and Environment, Australia, Bulletin 49.

De Boer, D.H., 1992. Hierarchies and spatial scale in process geomorphology: a review. *Geomorphology* 4, 303-318.

De Vriend, H.J., 1991. Mathematical modelling and large-scale coastal behaviour, Part 1: Physical Processes, *Journal of Hydraulic Research*, 29(6) 727-740.

De Vroeg, J.H.; Smith, E.S.P., and Bakker,W.T., 1988. Coastal genesis. *Proceedings of the 21st International Conference on Coastal Engineering*, ASCE, pp. 2825-2839.

Dean, R.G., 1977. *Equilibrium Beach Profiles: U.S. Atlantic and Gulf coasts.* University of Delaware, Department of Civil Engineering, Ocean Engineering Technical Report 12, 45p.

Dolan, R., and Haden, B., 1983. Patterns and prediction of shoreline change. In: Komar, P., (ed.), *Handbook of Coastal Processes and Erosion.* CRC Press, pp. 123-149.

Douglas, S.C., and Weggel, J.R., 1988. Laboratory experiments of the influence of wind on nearshore wave breaking. *Proceedings of the 21st International Conference on Coastal Engineering*, ASCE, 632-643.

Everitt, I.H.; Escobar, D.E., and Villarreal, R., 1988. Evaluation of single-band-video and video-band-based indices for grassland phytomass assessment. *Photogrammetric Engineering and Remote Sensing*, 54, 1177-1180.

Fenster, M., and Dolan, R., 1994. Large-scale reversals in shoreline trends along the U.S mid-Atlantic coast. *Geology*, 22, 543-546.

Fleming, C.A., 1953. *Geology of the Wanganui Subdivision*. Geological Survey Bulletin n.s. 52, Department of Scientific and Industrial Research, New Zealand, 362p.

Fox, W.T., 1985. Modelling coastal environments. In Davis, R.A., (ed), *Coastal Sedimentary Environments*, pp. 665-705.

Fox, W.T., and Davis, R.A., 1976. Weather patterns and coastal processes. In: Davis, R.A., and Ethington, R.C., (eds.), *Society of Economic Palaeontologists and Mineralogists, Special Publication*, 24, 1- 23.

Frisby, R.B., and Goldberg, E., 1981. Storm wave run-up levels at Onepoto Bay, East Coast, North Island, New Zealand. *Water and Soil,* Technical Publication, 21: 59-63.

Gable, C.G., and Wanetick, J.R., 1984. Survey techniques used to measure nearshore profiles. *Proceedings of the 19th International Conference on Coastal Engineering*, ASCE, pp. 1879-1895.

Gallagher, E.L., Elgar, S., and Guza, R.T., 1998. Observations of sand-bar evolution on a natural beach. *Journal of Geophysical Research*, 103, 3203-3215.

Gibb, et. al., 1962. *Tongariro River Power Development, Wanganui Harbour. Report to the New Zealand Ministry of Works by Sir Alexander Gibb and Partners,* London, 39p.

Gibb, J.G., 1979. *Late Quaternary Shoreline Movements in New Zealand.* Unpublished PhD thesis, Victoria University of Wellington, New Zealand.

Gilbeaut, J.G., and Davis, R.A., 1991. Computer simulation modelling of ebb-tidal deltas. *Proceedings of Coastal Sediments'91*, ASCE, pp. 1389-1403.

Goda, Y., 1983. Wave measurements and utilisation of wave data. *Proceedings of the 6th Australian Conference on Coastal and Ocean Engineering*, Gold Coast, Australia, pp. 1-9.

Goldsmith, V.; Bowman, D., and Kiley, K., 1982. Sequential stage development of crescentic bars: Hahoterim Beach, southeastern Mediterranean. *Journal of Sedimentary Petrology*, 52, 233-249.

Gonzalez, R.C., and Wintz, P., 1987. *Digital Image Processing.* Addison-Wesley, Sydney.

Greenwood, B., and Davidson-Arnott, G.D., 1975. Marine bars and nearshore sedimentary processes, Kouchibouguac Bay, New Brunswick. In: Hails, J., and Carr, A., (eds.), *Nearshore Sediment Dynamics and Sedimentation.* John Wiley and Sons, New York, pp. 123-150.

Guza, R.T. and Thornton, E.B., 1982, Swash oscillations on a natural beach. *Journal of Geophysical Research*, 87(C1), 483-491.

Hallermeier, R.J., 1978. Uses for a calculated limit depth to beach erosion. *Proceedings of the 16th Conference on Coastal Engineering*, ASCE. pp. 1493-1512.

Hayes, M.O., 1991. Geomorphology and sedimentation patterns of tidal inlets: a review. *Proceedings of Coastal Sediments'91,* ASCE, pp. 1343-1355.

Hardisty, J., 1990. *Beaches: Form and Process.* Unwin Hyman, London, 319p.

Hardisty, J., 1993. Time series analysis using spectral techniques: oscillatory currents. *Earth Surface Process and Landforms,* 18, 855-862.

Hesp, P., and Hilton, M.J., 1996. Nearshore-surf zone system limits and the impacts of sand extraction. *Journal of Coastal Research,* 12(3), 726-747.

Hoekstra, P.; Houwman, K.T.; Kroon, A.; Van Vessem, P., and Ruessink, B.G., 1994. The NOURTEC experiment of Terschelling: Process-orientated monitoring of a shoreface nourishment (1993-1996). *Proceedings of Coastal Dynamics '94,* ASCE pp. 402-416.

Hoekstra, P.; Houwman, K.T.; Kroon, A.; Ruessink, B.G.; Roelvink, J.A., and Spanhoff, R., 1996. Morphological development of the Terschelling shoreface nourishment in response to hydrodynamic and sediment transport processes. *Proceedings of the 25th International Conference on Coastal Engineering,* ASCE pp. 2897-2910.

Holland, K.T., and Holman, R.A., 1993. The statistical distribution of swash maxima on natural beaches. *Journal of Geophysical Research,* 98(C6), 10,271-10,278.

Holman, R.A., 1981. Infragravity energy in the surf zone. *Journal of Geophysical Research,* 86, 6442-6450.

Holman, R.A., 1983. Edge waves and the configuration of the shore-line. In: Komar, P., (ed.), *Handbook of Coastal Processes and Erosion.* CRC Press, pp. 21-33.

Holman, R.A., and Bowen, A.J., 1982. Bars, bumps, and holes: models for the generation of complex beach topography. *Journal of Geophysical Research,* 84, 457-468.

Holman, R.A., and Lippmann, T.C., 1987. Remote sensing of nearshore bar systems - making morphology visible. *Proceeding of Coastal Sediments'87,* ASCE, pp. 927-944.

Holman, R.A., and Sallenger, A.H., 1986. High energy nearshore processes. *EoS Trans.* AGU 67, 1369-1371.

Holman, R.A., and Sallenger, A.H., 1993. Sand-bar generation: a discussion of the Duck Experiment Series. *Journal of Coastal Research, Special Issue,* 15, 75-92.

Hom-ma, M., and Sonu, C., 1962. Rhythmic patterns of longshore bars related to sediment characteristics. *Proceedings of the 8th International Conference on Coastal Engineering,* ASCE, pp. 248-278.

Horikawa, K., 1988. *Nearshore Dynamics and Coastal Processes.* University of Tokyo Press, 522p.

Houwman, K.T and Ruessink, B.G., 1996. Cross-shore sediment transport mechanisms in the surf zone on a time scale of months to years. *Proceedings of the 25th International Conference on Coastal Engineering*, ASCE, pp. 4793-4806.

Howd, P.A; Bowen, A.J.; Holman, R.A., and Oltman-Shay, J., 1991. Infragravity waves, longshore currents and linear sand-bar formation. *Proceedings of Coastal Sediments'91*, ASCE, 72-84.

Howd, P.A; Bowen, A.J., and Holman, R.A., 1992. Edge waves in the presence of strong longshore currents. *Journal of Geophysical Research*, 97-C7, 11357-11371.

Hubertz, J.M., 1986. Observations of local wind effects on longshore currents. *Coastal Engineering*, 10, 275-288.

Huggett, R.J., 1985. *Earth Surface Systems*. Springer-Verlag, New York, 263p.

Hunter, R.E.; Clifton, H.E., and Phillips, R.L., 1979. Depositional processes, sedimentary structures, and predicted vertical sequences in barred nearshore systems, Southern Oregon coast. *Journal of Sedimentary Petrology*, 49(3), 711- 726.

Ingham, A.E., 1975. *Sea Surveying*. John Wiley and Sons, London, 235p.

Inman, D.L.; Hany, M; Elwany, S; Khafagy, A.A., and Abraham, G., 1992. Nile delta profiles and migrating sand blankets. *Proceding of the 23rd International Conference on Coastal Engineering*, pp. 3273-3284.

Jamshidi, M., 1983. *Large-scale systems.* Elsevier Science Publishing Co., New York.

Jaques, W.F., 1981. *Chart N.Z.46: Wellington to Patea including Cook Strait, scale 1:200,000*. Hydrographic Office of the Royal New Zealand Navy.

Johnston, R.M.S., 1985a. Coastal change and hazard delineation on the Rangitikei-Wanganui coast. *Proceedings of the 8th Australasian Conference on Coastal and Ocean Engineering*, pp. 411-420.

Johnston, R.M.S., 1985b. *Coastal Resource Survey - Progress Report 2*. Rangitikei-Wanganui Catchment Board and Regional Water Board, New Zealand, 52p.

Kaufman, A.E., 1994. Visualisation. *Computer*, 27(7), 18-19.

King, C.H.M., 1972. *Beaches and Coasts*. Butler & Tanner Ltd., 570p.

King, S.M, 1964. *History of the Port of Wanganui and its influence on the City of Wanganui.* Unpublished MA thesis, Victoria University, New Zealand.

Kinsman, B., 1965. *Wind waves.* Englewood Cliffs, New Jersey: Prentice-Hall, 676p.

Kirby, J.T.; Dalrymple, R.A., and Liu, P.L.F., 1981. Modification of edge waves by barred-beach topography. *Coastal Engineering*, 5, 35-49.

Kolbl, O.R., 1976. Metric and non-metric cameras. *Photogrammetric Engineering and Remote Sensing*, 42(1), 103-113.

Komar, P. D., 1976a. *Beach Processes and Sedimentation*. Prentice-Hall, Englewood Cliffs, New Jersey, 429p.

Komar, P.D., 1976b. Evaluation of wave-generated longshore current velocities and sand transport rates on beaches. In Davis, R.A., and Ethington, R.C. (eds.), *Beach and Nearshore Sedimentation*. Society of Economic Palaeontologists and Mineralogists, Special Publication 24, pp. 48-53.

Komar, P.D., 1983a. Beach Processes and Erosion. In Komar, P.D., (ed.), *Handbook of Coastal Processes and Erosion*. CRC Press, pp. 1-20.

Komar, P.D., 1983b. Coastal erosion in response to the construction of jetties and breakwaters. In Komar, P.D., (ed.), *Handbook of Coastal Processes and Erosion*, CRC Press, pp. 191-204.

Komar, P.D., and Inman, D.L., 1970. Longshore transport on beaches. *Journal of Geophysical Research*, 76, 713-721.

Kroon, A., 1990. Three-dimensional morphological changes of a nearshore bar system along the Dutch coast near Egmond aan Zee. *Journal of Coastal Research, Special Issue*, 9, 430-451.

Kroon, A., 1994. *Sediment transport and morphodynamics of the beach and nearshore zone near Egmond, The Netherlands*. PhD thesis, Utrecht University, The Netherlands, 275p.

Kroon, A., and Hoeskstra, P., 1993. Nearshore bars and large-scale coastal behaviour. In: List, J.H., (ed.), *Large-Scale Coastal Behaviour '93*. U.S. Geological Survey, Open-File Report 93-381, pp. 92-95.

Lakhan, V.C., and Trenhaile, A.S., 1989. Models and Coastal Systems. In Trenhaile, A. S., (ed.), *Applications in Coastal Modelling*, Elsevier Oceanographic Series 49, pp. 1-10.

Lane, S.N.; Richards, K.S., and Chandler, J.H., 1993. Developments in photogrammetry; the geomorphological potential. *Progress in Physical Geography*, 17(3), 306-328.

Larsen, M., and Kraus, N.C., 1989. *SBEACH: Numerical model for simulating storm-induced beach change. Report 1. Empirical foundation and model development*. Technical Report CERC-89-9, 267p.

Larsen, M., and Kraus, N.C., 1992. *Analysis of cross-shore movement of natural longshore bars and material placed to create longshore bars*. Technical Report CERC DRP-29-5, 115p.

Larson, R.J., and Marx, M.L., 1986. *An Introduction to Mathematical Statistics and its Applications*. Prentice-Hall International Inc., London, 625p.

Lee, G., and Birkemeier, W.A., 1993. *Beach and Nearshore Data: 1985-1991 CERC Field Research Facility*. Technical Report CERC-93-3, 13p.

Leon, P.F., and Holman, R.A., 1994. *The estimation of longshore currents from video imagery.* Abstract 012F-9, Transactions of the American Geophysical Union, EOS, 75(44), 322.

Lewis, K.B., 1979. A storm-dominated inner shelf, Western Cook Strait, New Zealand. *Marine Geology,* 31, 31-43.

Lilienfeld, R., 1978. *The rise of systems theory: an ideological analysis.* John Wiley and Sons, New York, 249p.

Lillisand, T.M., and Kiefer, R.W., 1987. *Remote Sensing and Image Interpretation.* John Wiley and Sons.

Lippmann, T.C., and Holmam, R.A., 1989. Quantification of sand-bar morphology: a video technique based on wave dissipation. *Journal of Geophysical Research,* 94, 995-1011.

Lippmann, T.C., and Holmam, R.A., 1990. The spatial and temporal variability of sand-bar morphology. *Journal of Geophysical Research,* 95, 11,575-11,590.

Lippmann, T.C.; Holmam, R.A., and Hathaway, K.K., 1993. Episodic, non-stationary behaviour of a double bar system at Duck, North Carolina, U.S.A., 1986-1991. *Journal of Coastal Research, Special Issue,* 15, pp. 49-75.

Lithgow, N.A., 1986. *A textural and mineralogical study of the beach sands along the southwest coast of the North Island.* Unpublished MSc thesis, Massey University, New Zealand.

Longuet-Higgins, M.S., 1972. Recent progress in the study of long-shore currents. In Meyer, R.E. (ed.), *Waves on Beaches and resulting sediment transport.* Academic Press, New York. pp. 203-248.

McLean, R.F., and Burgess, J.S., 1969. *Investigations of the entrance to Wanganui Harbour. Collected Interim Reports to the Engineer Wanganui Harbour Board.* University of Canterbury, Geography Department, 105p.

McLean, R. F., and Burgess, J. S., 1974. Bar depth and beach changes around a New Zealand rivermouth port: Wanganui 1850-1970. *Proceedings of the 2nd Australian Conference on Coastal and Oceanographic Engineering,* pp. 69-74.

Macky, G.H., 1991. Correlation between wind, waves and river bar changes at Wanganui. *Proceedings of the 10th Australasian Conference on Coastal and Ocean Engineering,* pp. 283-288.

Macky, G.H.; Cumming. R, J., and Valentine, E. M., 1988. *Measurements of ocean wave climate at Wanganui and Himitangi Beach.* Hydrology Centre, Department of Scientific and Industrial Research, Christchurch, New Zealand.

Marion, A., 1991. *An Introduction to Image Processing.* Chapman and Hall.

Marra, J. J., 1992. *Swash zone dynamics in a rhythmic black sand beach system.* Unpublished PhD thesis, University of Canterbury, 235p.

Masselink, G., 1993. Simulating the effects of tides on beach morphodynamics. *Journal of Coastal Research, Special Issue*, 15, 180-197.

Masselink, G., and Short, A.D., 1993. The effect of tide range on beach morphodynamics and morphology: a conceptual beach model. *Journal of Coastal Research*, 9(3), 785-800.

Meisner, E.M., and Lindstrom, O.M., 1985. Design and operation of a colour infrared aerial video system. *Photogrammetric Engineering and Remote Sensing*, 51(5), 555-560.

Miller, H.C.; Birkemeier, W.A., and DeWall,A.E., 1983. Effects of CERC research pier on nearshore processes. *Proceedings of the International Conference on Coastal Structures '83*, New York, pp. 765-782.

Ministry of Transport, 1982. *The climatology of Wanganui Airport. New Zealand Meteorological Service*, Miscellaneous publication 171 (25) , Ministry of Transport, New Zealand.

Ministry of Transport, 1989. *New Zealand Nautical Almanac 1989-90.* Marine Transport Division, Ministry of Transport, New Zealand, 176p.

Morang, A.; Larson, R., and Gorman, L., 1997. Monitoring the coastal environment; part 111: geophysical and research methods. *Journal of Coastal Research*, 13(4), 1064-1085.

Naish, T., and Kamp, P.J.J., 1995. Pliocene-Pleistocene marine cyclotherms, Wanganui Basin, New Zealand: a lithostratigraphic framework. *The New Zealand Journal of Geology and Geophysics*, 38, 223-243.

Nummedal, D., and Finley, R.., 1978. Wind-generated longshore currents. *Proceedings of the 16th Conference of Coastal Engineering*, pp. 1428-1438.

Nummedal, D.; Sonnenfeld, D.L., and Taylor, K., 1984. Sediment transport and morphology at the surf zone of Presque Isle, Lake Erie, Pennsylvania. *Marine Geology*, 60, 99-122.

Oltman-Shay, J.; Howd, P.A., and Birkemeier, W.A., 1989. Shear instabilities of the mean longshore current; 2 field observations. *Journal of Geophysical Research*, 94, 18031- 18042.

Osborne, P.D.; Mavoa, F.D., and Holman, R.A., 1999. Video remote sensing of longshore currents in a high-energy surf zone. *Proceedings of the Canadian Coastal Conference '99*, CCSEA.

Owens, E.H., 1977. Temporal variations in beach and nearshore dynamics. *Journal of Sedimentary Petrology*, 47(1), 168-190.

Patterson, D.C., 1985. *Low cost visual determination of surf zone parameters.* Unpublished MSc thesis, University of Queensland, Australia, 143p.

Patterson, D.C., 1991. *Wanganui Port Development: Coastal Engineering Considerations. A report for Ocean Terminals and the Wanganui District Council, New Zealand*, 48p.

Patterson, D.C., 1992. *Wanganui Port development feasibility studies: coastal engineering aspects. A report for Ocean Terminals and the Wanganui District Council, New Zealand*, 51p.

Patterson, D.C., and Blair, R.J., 1983. Visually determined wave parameters. *Proceedings of the 6th Australian Conference on Coastal and Ocean Engineering*, Australia, pp. 151-155.

Peltier, W.R., 1987. Mechanisms of relative sea-level change and the geophysical responses to ice-water loading. In: Devoy, R.J.N., (ed.), *Sea Surface Studies*. London, Croom and Helm, pp. 57-91.

Phillips, J.D., 1992. The end of equilibrium? *Geomorphology*, 5, 349-361.

Phillips, J.D., 1995. Self-organisation and landscape evolution. *Progress in Physical Geography*, 19(3), 305-321.

Pillans, B.J., 1983. Late Quaternary marine terrace chronology and deformation, South Taranaki, New Zealand. *Geology*, 11, 292-297.

Pillans, B.J., 1990. *Late Quaternary marine terraces South Taranaki - Wanganui. New Zealand Geological Survey Miscellaneous Series Map 18.* Department of Scientific and Industrial Research, New Zealand, 46p.

Plant, N.G., and Holman, R.A., 1999. Extracting morphologic information from field data. *Proceedings of the 26th International Conference on Coastal Engineering*, ASCE, pp. 2773-2784.

Plant, N.G.; Holman, R.A.; Freilich, M.H., and Birkemeier, W.A., 1999. A simple model for interannual sand bar behaviour. *Journal of Geophysical Research*, 104(C7), 15755-15776.

Rangitikei-Wanganui Catchment Board, 1988. *Review of the Minimum Flow Set for the Wanganui River. Technical Report for the Wanganui River Minimum Flows Hearing*, New Zealand 55p.

Redondo, J.M.; Rodrigues, A.; Bahia, E.; Falques, A.; Gracia, V.; Sanchez-Arcilla, A, and Stive, M.J.F., 1994. Image analysis of surf zone hydrodynamics. *Proceedings of Coastal Dynamics'94*, pp. 350-365.

Roelvink, J.A.; Meijer, J.G.P.; Houwman, K.; Bakker, R., and Spanhoff, R., 1995. Field validation and application of a coastal profile model. *Proceedings of Coastal Dynamics'95*, ASCE,pp. 818-828.

Ruessink, B.G., 1992. *The nearshore morphology of Terschelling (1965-1991).* Institute for Marine an Atmospheric Research Utrecht, IMAU report R92-11, 30p, (cited in Ruessink and Kroon, 1994).

Ruessink, B.G., 1998. *Infragravity waves in a dissipative multiple bar system.* PhD thesis, Utrecht University, The Netherlands, 245p.

Ruessink, B.G., and Kroon, A., 1994. The behaviour of a multiple bar system in the nearshore zone of Terschelling, the Netherlands: 1965-1993. *Marine Geology*, 121, 187-197.

Sallenger, A.H, and Holman, R.A, 1985. Wave energy saturation on a natural beach of variable slope. *Journal of Geophysical Research*, 90: 11939-11944.

Sallenger, A.H; Holman, R.A, and Birkemeier, W.A., 1985. Storm-induced response of a nearshore-bar system. *Marine Geology, 64,* 237-257.

Sallenger, A.H, and Holman, R.A, 1987, Infragravity waves over a natural barred profile. *Journal of Geophysical Research*, 92(C9), 9531-9540.

Samtaney, R.; Silver, D.; Zabusky, N., and Cao, J., 1994. Visualising features and tracking their evolution. *Computer*, 27(7), 20-27.

Sasaki, T., 1983. *Three-dimensional topographic changes on the foreshore zone of sandy beaches.* University of Tsukuba: Institute of Geoscience, Science Report A-4, pp. 69-95.

Saville, T., and Caldwell, J.M., 1953. *Accuracy of hydrographic surveying in and near the surf zone.* Technical Memorandum Number 32, Beach Erosion Board Corps of Engineers, 28p.

Shand, R.D., 1990. *The subaqueous morphology at the entrance to a jetty controlled river mouth on a moderate to high energy littoral drift dominated coast: Wanganui, New Zealand 1981-1987.* Research project: Post-graduate Diploma in Science, Massey University, New Zealand, 102p.

Shand, R.D., and Bailey, D.G., 1999. A review of net offshore bar migration with photographic illustrations from Wanganui, New Zealand, *Journal of Coastal Research*, 15(2), 365-378.

Shand, R.D.; Bailey, D.G., and Shepherd, M.J., 1999. An inter-site comparison of net offshore bar migration characteristics and environmental conditions. *Journal of Coastal Research*, 15(3), 750-765.

Shaw, J., 1985. Beach Morphodynamics of an Atlantic Coast Embayment: Runkerry Strand, County Antrim. *Irish Geography*, 18, 51-58.

Shaw, G., and Wheeler, D., 1985. *Statistical Techniques in Geographical Analysis.* John Wiley and Sons, New York, 361p.

Sherman, D.J., 1988. Empirical evaluation of longshore-current models. *Geographical Review*, 78, 158-168.

Short, A.D., 1975. Offshore bars along the Alaskan Arctic coast. *Journal of Geology*, 83, 209-221.

Short, A.D., 1979. Three-dimensional beach-stage model. *Journal of Geology*, 87, 553-571.

Short, A.D., 1991. Macro-meso tidal beach morphodynamics - an overview. *Journal of Coastal Research*, 7(2), 417-436.

Short, A.D., 1992. Beach systems of the central Netherlands coast: processes, morphology, and structural impacts in a storm driven multi-bar system. *Marine Geology*, 107, 103-127.

Short, A.D., and Aagaard,T., 1993. Single and multi-bar beach change models. *Journal of Coastal Research, Special Issue*, 15, 141-157.

Siegel, S. 1956. *Non-parametric Statistics for the Behavioural Sciences.* McGraw-Hill Kogakusha, Ltd., Tokyo, 303p.

Slama, C.C., 1980. *The Manual of Photogrammetry.* American Society of Photogrammetry, 1049p.

Smith, R.K. and Ovenden, R., 1998. *Wanganui District Council Coastline Stability Investigation Between Kai Iwi and Harakeke. Report: WNG80202. National Institute of Water and Atmospheric Research Ltd, New Zealand*, 32p.

Smith, E.J., and Wagner, E., 1991. Littoral environment observation programme. *Journal of Coastal Research*, 7, 595-605.

Stive, M.J.F., 1986. A model for cross-shore sediment transport. *Proceedings of the 20th International Conference on Coastal Engineering,* ASCE, pp. 1550-1564.

Sonnenfeld, D.L., and Nummedal, D., 1987. Morphodynamics and sediment dispersal of a tideless surf zone. *Proceedings of Coastal Sediments'87*, ASCE, pp. 1938-1949.

Sonu, C.J., 1972. Field observation of nearshore circulation and meandering currents. *Journal of Geophysical Research*, 77(18), 3232-3247.

Sonu, C. J., 1973. Three-dimensional beach changes. *Journal of Geology,* 81, 42-64.

Southgate, H.N., and Beltran, L.M., 1995. Time series analysis of long-term beach level data from Lincolnshire, UK. *Proceedings of Coastal Dynamics'95,* pp. 1006-1017.

Stauble, D.K., 1992. *Long-term profile and sediment morphodynamics: Field Research Facility case history.* Technical Report CERC-92-7,pp 69.

Stern, T.A. and Davey, F.J., 1989. Crustal structure and origin of basins formed behind the Hikurangi subduction zone, New Zealand. In Price, A.P., (ed.), *Origin and Evolution of Sedimentary Basins and Their Energy and Mineral Resources.* International Union of Geodesy and Geophysics, and American Geophysical Union, Geophysical Monograph 48, IUGG 3, pp. 73-85.

Stewart, C.J., and Davidson-Arnott, R.G.D., 1988. Morphology, formation and migration of longshore sandwaves; Long Point, Lake Erie, Canada. *Marine Geology*, 81, 63-71.

Stive, M.J.F.; Guillen, J., and Capobianco, M., 1996. Bar migration and duneface oscillation on decadal scales. *Proceedings of the 25th International Conference on Coastal Engineering*, ASCE, pp. 2884-2896.

Sunmaura, T., 1988. Beach morphologies and their change. In Horikawa, K., (ed.), *Nearshore Dynamics and Coastal Processes.* University of Tokyo Press, pp. 133-166.

Sunamura, T., and Horikawa, K., 1974. Two-dimensional beach transformation due to waves. *Proceedings of the 14th International Conference on Coastal Engineering*, pp. 920-938.

Sunamura, T., and Takeda, I., 1984. Landward migration of inner bars. *Marine Geology*, 60, 63-78.

Sunamura, T., and Maruyama, K., 1987. Wave induced geomorphic response of eroding beaches - with special reference to seaward migrating bars. *Proceedings of Coastal Sediments'87*, ASCE, 788-801.

Sunamura, T., and Takeda, I., 1993. Bar movement and shoreline change: predictive relations. *Journal of Coastal Research, Special Issue*, 15, 125-140.

Sutherland, A.J., Lumsden, J.L. and Sewell, D.W., 1990. *Wanganui Harbour development prefeasibility study. A report prepared for Ocean* Terminals Ltd., Wanganui, Canterprise, University of Canterbury, 39p.

Thompson, S.M., 1988. *Evidence of the Electricity Corporation of NZ Ltd., presented before the Central Districts Catchment Board in the matter of the Wanganui River Minimum Flow Review, Electricity Corporation of NZ Ltd., New Zealand* 23p.

Terwindt, J.H.J., and Kroon, A., 1993. Theoretical concepts of parameterization of coastal behaviour. In: List, J.H., (ed.), *Large-Scale Coastal Behaviour '93*. U.S. Geological Survey, Open-File Report 93-381, pp. 193-196.

Terwindt, J.H.J., and Wijnberg, K.M., 1991. Thoughts on large scale coastal behaviour. *Proceedings of Coastal Sediments'91*, ASCE, pp. 1476-1487.

Thornton, E.B., and Guza, R.T., 1983. Transformation of wave height distribution. *Journal of Geophysical Research*, 88, 5925-5938.

Thornton, E.B.; Humiston, R.T., and Birkemeier, W., 1996. Bar/trough generation on a natural beach. *Journal of Geophysical Research*, 101, pp. 12097-12110.

Tomlinson, A.I., 1976. Climate. In Woods, I., (ed.), *New Zealand Atlas,* Government Printer, New Zealand, pp. 82-89

Tonkin and Taylor, 1978. *Water Resources of the Wanganui River. A report prepared by Tonkin and Taylor, Consulting Engineers, for the Rangitikei-Wanganui Catchment Board, New Zealand, 167p.*

Torlegard, A.K.I., 1976. State-of-the-art of close range photogrammetry. *Photogrammetric Engineering and Remote Sensing,* 42(1), 71-79.

Trowbridge, J.H., 1995. A mechanism for the formation and maintenance of shore-oblique sand ridges on storm-dominated shelves. *Journal of Geophysical Research*, 100-C8, 16071-16086.

Van Alphen, J.S.L.J., and Damoiseaux, M.A., 1987. *A morphological map of the Dutch shoreface and adjacent part of the continental shelf (1:250,000).* Rijkswaterstaat. Nota NZ-N-87.21/ MDLK-R-87.18, 20p. (cited in Ruessink, 1998).

Van Wijk, M.C., and Ziemann, H., 1976. The use of non-metric cameras in monitoring high speed processes. *Photogrammetric Engineering and Remote Sensing,* 42(1), 91-102.

Veitch, J., 1995. A model of innovation. In Riley, B., (ed.), *Kiwi Ingenuity: A Book of New Zealand Ideas and Inventions,* AIT Press, New Zealand, pp. 151-158.

Wallingford Hydraulic Research Station, 1967. *Wanganui Harbour. A report prepared for the Wanganui Harbour Board. New Zealand,* 14p.

Westlake, S.J. 1995. *Behaviour of a shoreface nourishment, Terschelling, The Netherlands.* MSc thesis, International Institute for Infrastructural, Hydraulic and Environmental Engineering, Delft, The Netherlands, report HH249, 95p.

Whitford, D.J., and Thornton, E.B., 1993. Comparison of wind and wave forcing of longshore currents. *Continental Shelf Research,* 13(11), 1205-1218.

Wijnberg, K.M., 1995. *Morphologic behaviour of a barred coast over a period of decades*. PhD thesis, Utrecht University, The Netherlands, 245p.

Wijnberg, K.M., and Wolf, F.C.J., 1994. Three-dimensional behaviour of a multiple bar system. *Proceedings of Coastal Dynamics '94,* ASCE, pp. 59-73.

Williams, B.L., 1985. More on coastal currents. In: Williams, B.L., (ed.), *Ocean Outfall Handbook.* Water and Soil Miscellaneous Publication Number 76, Ministry of Works and Development, New Zealand, pp. 152-165.

Willett, R.W., 1959. Tongariro river power development: effect of diversions on Wanganui Harbour. In Gibb, et. al., *Tongariro River Power Development, Wanganui Harbour. Report to the New Zealand Ministry of Works, New Zealand,* 39p.

Wolf, F.C.J., 1997. *Hydrodynamics, sediment transport and daily morphological development of a bar-beach system.* PhD thesis, Utrecht University, The Netherlands, 267p.

Wolf, P.R., 1974. *Elements of Photogrammetry.* McGraw-Hill, New York.

Worley, Downey, Muir and Associates, 1970. *Report on Sewerage Investigations and a Comprehensive Scheme for Collection and Disposal of Wastes. A report prepared for the Wanganui City Council,* New Zealand, 69p.

Wright, L.D.; Nielsen, P,; Shi, N.C., and List, J.H., 1986. Morphodynamics of a bar-trough surf zone. *Marine Geology,* 70, 251-285.

Wright, L.D., 1977. Sediment transport and deposition at river mouths: a synthesis. *Geographical Society of America Bulletin,* 88, 857-868.

Wright, L.D., 1993. Micromorphodynamics of the inner continental shelf: a middle Atlantic Bight case study. *Journal of Coastal Research, Special Issue*, 15, 93-124.

Wright, L.D.; Chappell, J.; Thom, G.B,; Bradshaw, M.P., and Cowell,P., 1979. Morphodynamics of reflective and dissipative beaches and inshore systems: Southeastern Australia. *Marine Geology*, 32, 105-140.

Wright, L.D., and Coleman, J.M., 1973. Variations in morphology of major river deltas as functions of ocean wave and river discharge regimes. *American Association of Petroleum Geologists Bulletin*, 57 (2), 370-398.

Wright, L.D., and Short, A.D., 1984. Morphodynamic variability of surf zones and beaches: a synthesis. *Marine Geology*, 56, 93-118.

Wright, L.D., and Thom, B.G., 1977. Coastal depositional landforms: a morphodynamic approach. *Progress in Physical Geography*, 1(3), 412-459.

Wright, L.D., Thom, B.G., and Higgens, R.J., 1980. Wave influence on river-mouth depositional process: examples from Australia and Papua New Guinea. *Estuarine and Coastal Marine Science*, 11, 263-277.

Appendix A Conceptual surf zone models

Distinguishing features of the six beach-states (i) and the configuration sequences for one, two and three bars (ii) as proposed by Wright and Short (1984) and Short and Aagaard (1993) respectively. In Appendix A(ii), Ω refers to the dimensionless fall velocity parameter where Hb = breaker height, w_s = sediment fall velocity and T = wave period. B* refers to the bar number parameter where Xs = cross-shore distance to the point of zero slope (i.e. tanβ = 0), g = gravitational acceleration and Ti = infragravity period.

i. Beach-states

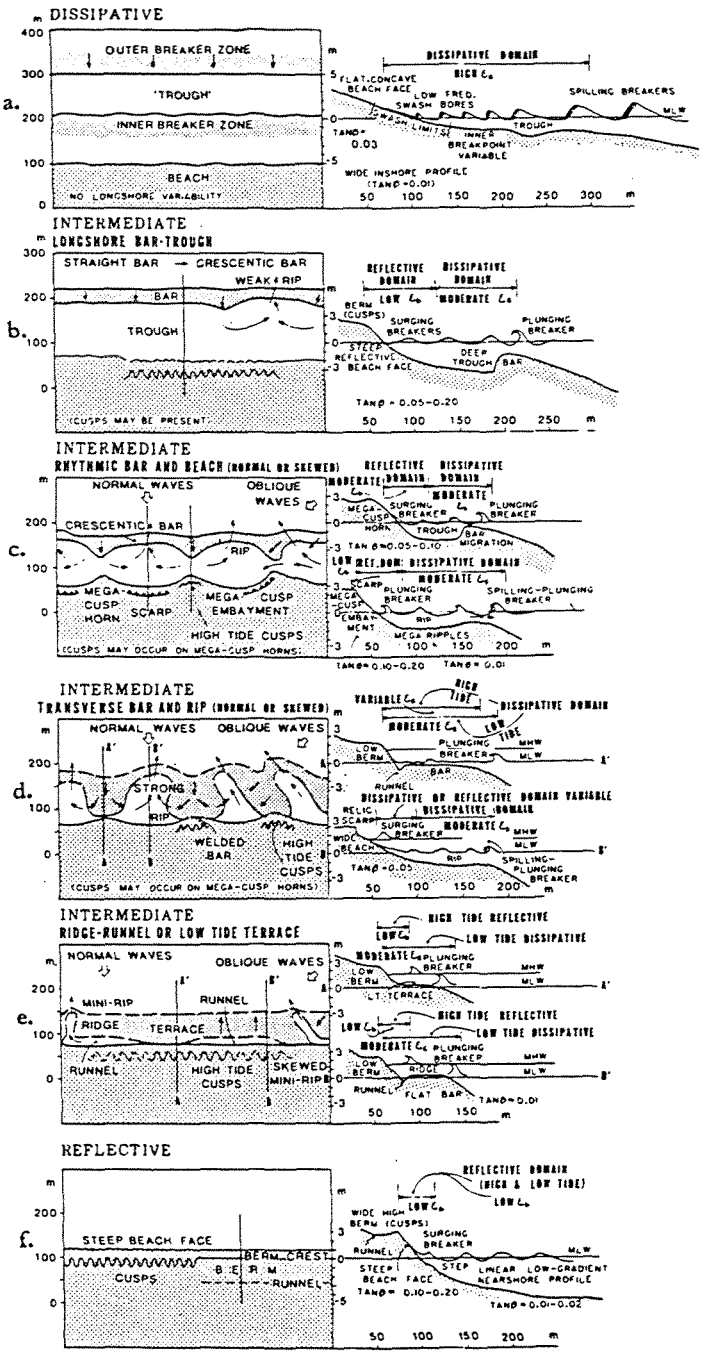

ii. Multiple bar sequences

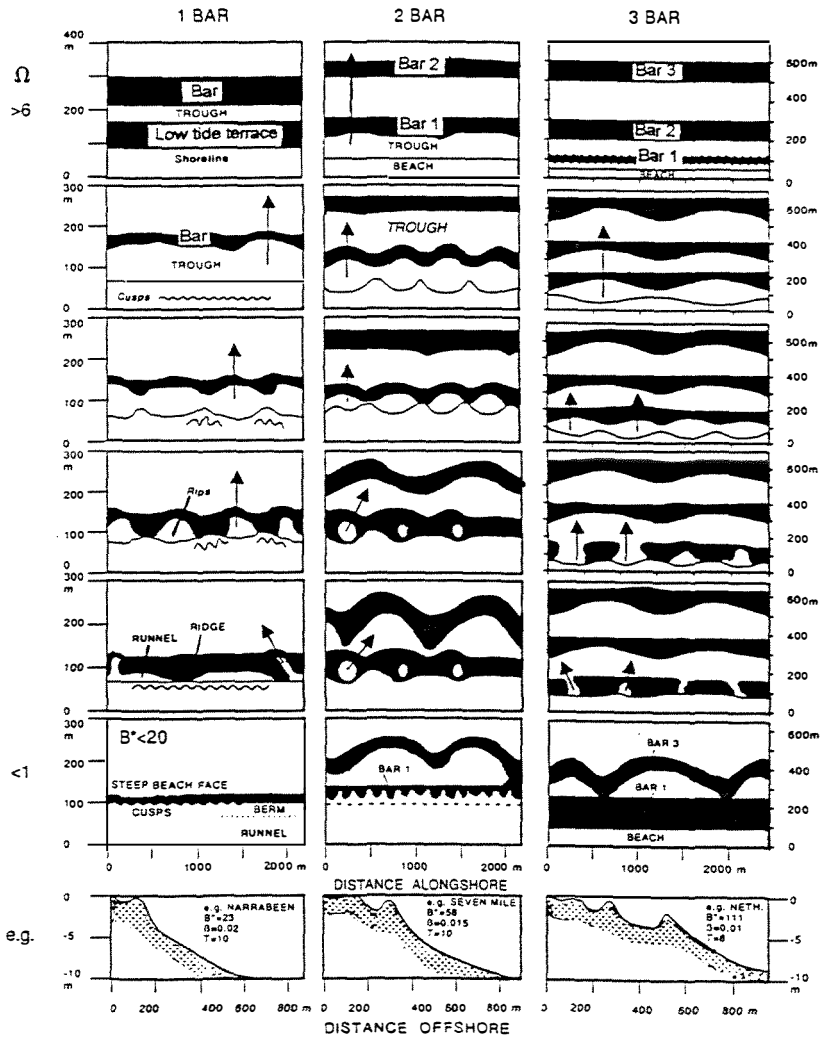

$\Omega = Hb/Tw_s$, $B^* = Xs/g \tan\beta Ti^2$

Appendix B Littoral drift estimates for the Wanganui coast.

Method of estimation	Sampling interval	NW → SE (m^3)	SE → NW (m^3)	Gross (m^3)	Net (NW → SE) (m^3)
Sediment accumulation *	1885-95	275 000			
Sediment accumulation *	1921-29	142 000			
Calculation: wave energy #	1968/9	306 000	122 000	428 000	184 000
Calculation: wind & wave @	1968/9	355 000	60 000	415 000	295 000
Calculation: wind & wave @	1986/7	597 000	277 000	874 000	320 000

Where NW → SE indicates sediment transport directed from northwest to southeast.
Information sources given below and further details are provided in text.

Sources: * Reported in Wallingford Research Station (1967),
Burgess (1971),
@ Patterson (1992).

Appendix C Shoreline change background information

Reference code *	Survey year	Data source	Shoreline indicator #	Reference @
A	1876	cadastral map	HWM	DOLSI
B	1879	bathymetric profiles	HWST	Gibb et al. (1962)
C	1885	bathymentric chart	HWST	Gibb et al. (1962)
D	1894	bathymentric chart	HWST	WHB archive
E	1912	general plan	HWM	WHB archive
F	1921	bathymentric chart	HWST	WHB archive
G	1927	bathymentric chart	HWST	Burgess (1971)
H	1942	aerial photo (SN90148)	dune-toe	DOLSI
I	1949	aerial photo (SN59242)	dune-toe	DOLSI/NZAM
J	1956	bathymentric chart (4612)	HWST	HBND
K	1960	aerial photo (SN243406)	dune-toe	DOSLI/NZAM
L	1962	aerial photo (SN3402/3)	dune-toe	DOSLI/NZAM
M	1965	aerial photo (1791 C/3,4)	dune-toe	DOSLI/NZAM
N	1968	aerial photo (1791 c/4)	dune-toe	DOSLI/NZAM
O	1974	aerial photo (SN3761)	dune-toe	DOSLI/NZAM
P	1976	aerial photo	dune-toe	DOSLI/NZAM
Q	1983	aerial photo	dune-toe	DOSLI/NZAM
R	1988	ground survey	debris line	author
S	1992	ground survey	debris line	author
T	1994	ground survey	debris line	author

Notes: * Codes as used in Figure 2.6

\# HWM = high water mark, HWST = high water (mean) spring tide, dune toe identified by seaward vegetation limit, debris line = seaward extent of back-shore drift wood etc.

@ DOSLI = Department of Land and Survey Information.
WHB = Wanganui Harbour Board. The Board was terminated in 1990 and the port operation taken over by a port company (Ocean Terminals Ltd.), with the Wanganui District Council taking over ownership of the assets.
HBND = Hydrographic Branch Navy Department.
NZAM = New Zealand Aerial Mapping, Hastings, New Zealand.

Compatibility and accuracy of shoreline indicators

When interpreting shoreline-change based on these data, the following limitations should be considered. Uncertainty exists as to the location of HWM for the cadastral survey (1876) as this mark is a function of the spring tide - neap tide cycle, of wind and wave conditions prior to survey, and of beach morphology at the survey time. It is also uncertain whether HWST was based on elevation or approximated; in the latter situation environmental conditions would also be relevant. Based on observations at the field site,

these uncertainties may result in location errors of ± 5 m for individual measurements. The vertical aerial photo data is more accurate with the dune toe location error estimated at ± 2.5 m (Johnston, 1985a). The debris line measurements are estimated to be within two metres of the actual location. Furthermore, the four shoreline indicators are not compatible. The dune toe is usually landward of the debris line, the debris line is landward of the HWST line, and the HWST line is landward of the HWM. The difference between the dune toe and HWM is estimated to range between 5 and 20 m at this field site. In spite of the data incompatibility and measurement errors outlined above, the magnitude of shoreline change during the study period ensures that the results depicted in Figure 2.6 and 2.7 are qualitatively valid and quantitatively indicative of the actual changes.

For a thorough discussion regarding compatability and accuracy of data for use in shoreline change analysis the reader is referred to Anders and Byrnes (1991), and Crowell et al. (1991).

Appendix D Ground profile data-sets

All data have been reduced to MSL elevation datum and cross-shore distances are measured relative to benchmarks located at the dune toe (see chapter 3 for details).

i. One-monthly data-set

Date	Foreshore transects			Date	Nearshore transects		
	T200	T1500	T5000		T200	T1500	T5000
Monthly foreshore surveys were carried out on 53 occations. These surveys have not been included in this table, however, as they were not utilised in the present study.				16.2.91	no	yes	no
				14.3.91	no	yes	no
				16.4.91	no	yes	no
				27.5.91	no	yes	no
				14.6.91	no	yes	no
				11.7.91	yes	yes	yes
				27.8.91	no	yes	no
				9.9.91	no	yes	no
				21.10.91	yes	yes	no
				6.11.91	no	yes	no
				6.12.91	no	yes	no
				23.1.92	no	yes	no
				7.2.92	yes	yes	yes
				4.3.92	yes	yes	no
				7.4.92	yes	yes	no
				4.5.92	yes	yes	yes
				3.6.92	yes	yes	no
				1.7.92	yes	yes	no
				19.8.92	yes	yes	yes

ii. Three-monthly data-set

Date	Foreshore transects			Date	Nearshore transects		
	T200	T1500	T5000		T200	T1500	T5000
31.12.89	yes	yes	no	14.3.91	no	yes	no
27.2.90	yes	yes	no	27.5.91	no	yes	no
25.5.90	yes	yes	no	11.7.91	yes	yes	yes
21.8.90	yes	yes	no	22.10.91	yes	yes	no
18.11.90	yes	yes	no	7.2.92	yes	yes	yes
17.2.91	yes	yes	no	4.5.92	yes	yes	yes
20 5 91	yes	yes	yes	19.8.92	yes	yes	yes
16.7.91	yes	yes	yes	29.10.92	yes	yes	yes
24.10.91	yes	yes	yes	10.2.93	yes	yes	yes
7.2.92	yes	yes	yes	11.5.93	yes	yes	yes
4.5.92	yes	yes	yes	12.8.93	yes	yes	yes
28.8.92	yes	yes	yes	27.10.93	yes	yes	yes
28.10.92	yes	yes	yes	28.1.94	yes	yes	yes
8.2.93	yes	yes	yes	9.5.94	yes	yes	yes
11.5.93	yes	yes	no				
4.8.93	yes	yes	yes				
27.10.93	yes	yes	yes				
29.1.94	yes	yes	yes				
14.5.94	no	yes	yes				

Appendix E Mineralogy of beach sediment

Longshore dispersal pattern of minerals in beach sand along the northern flank of the Cook Strait western embayment. Composite grains are sedimentary and volcanic fragments. 'Magnetic' feldspar is andesine and labradorite with magnetite inclusions. Miscellaneous minerals include garnet, zircon, micas and olivine.

Source: Gibb (1979)

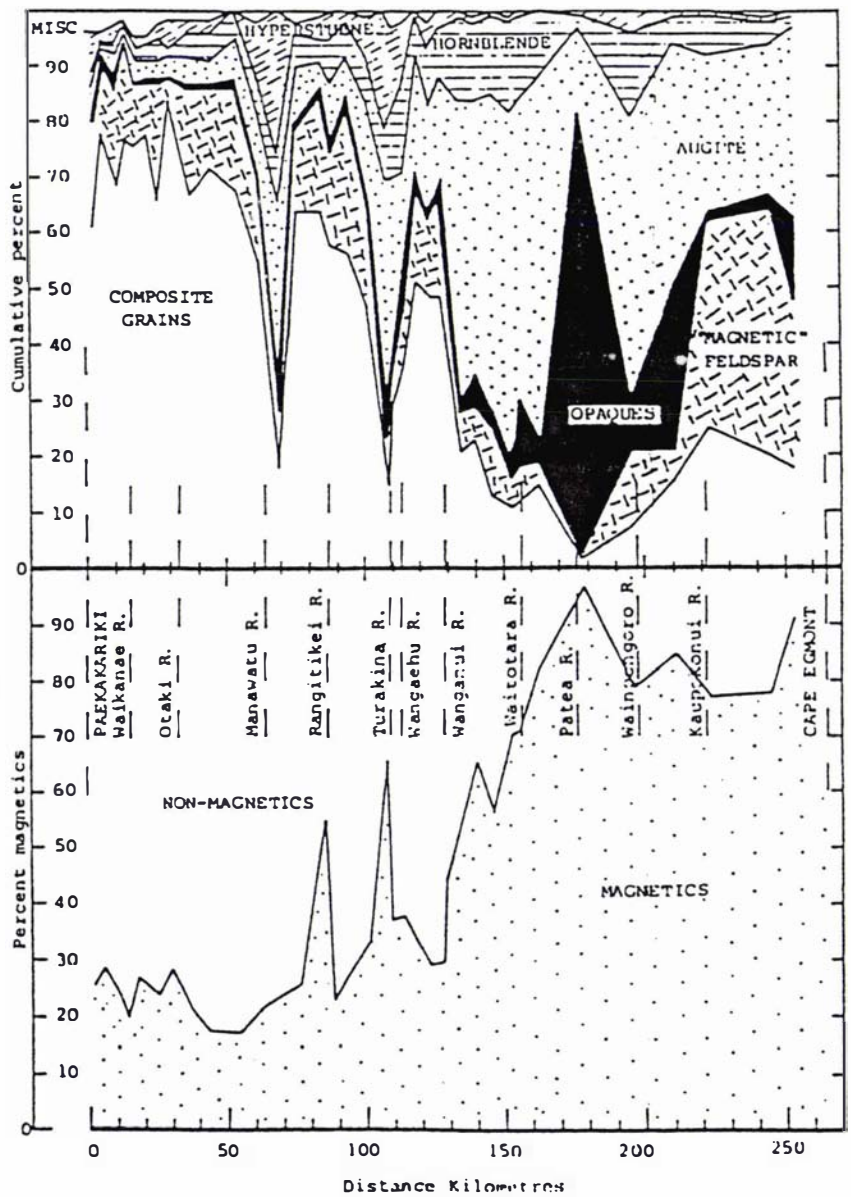

Appendix F Line-of-sight wave height data

Daily wave heights for the period 1.1.90 to 1.1.98. Measurements were made using the line-of-sight method described in the text (see section 2.5.1).

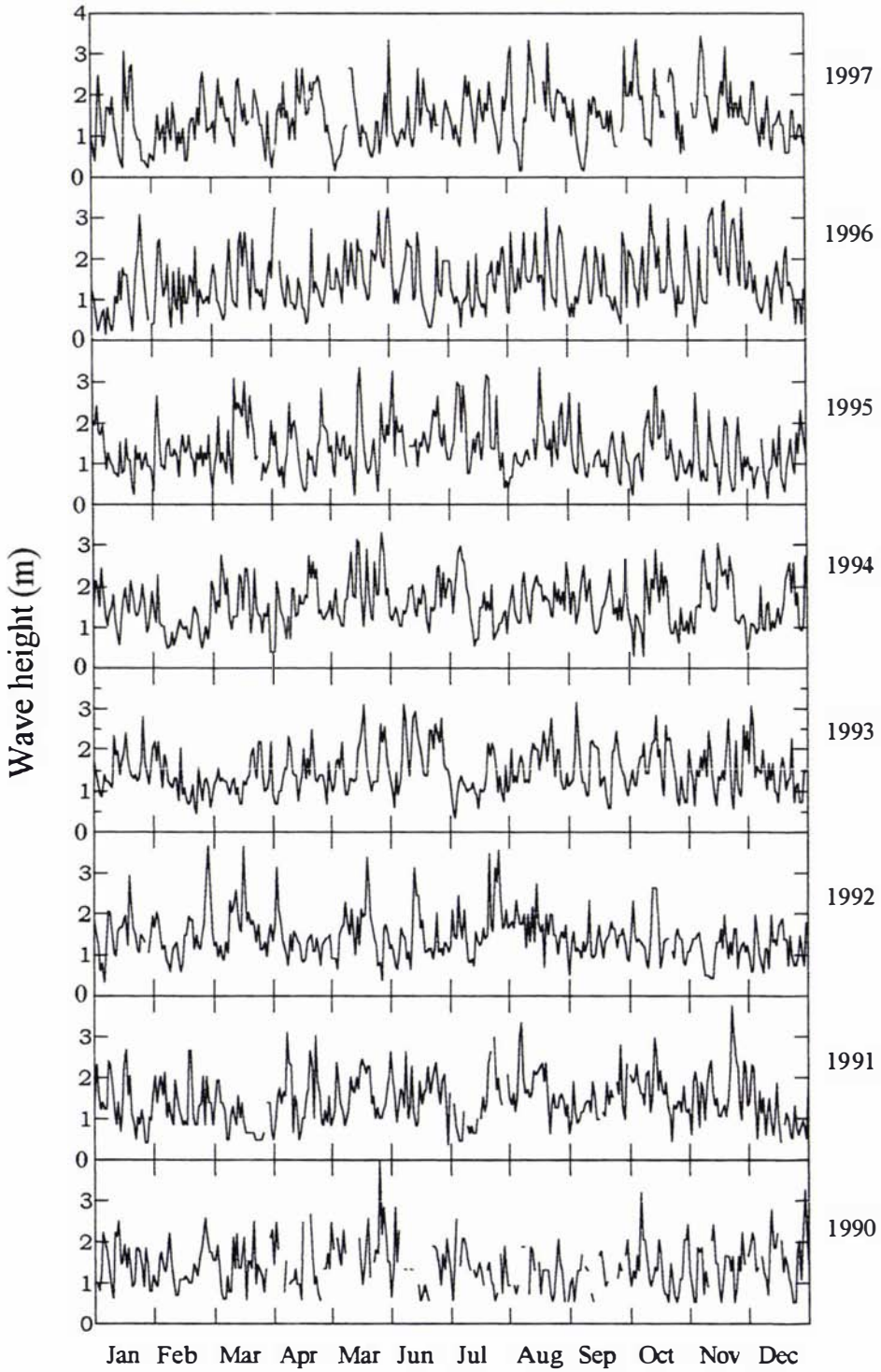

Appendix G Details of the oblique terrestrial rectification algorithm ETM_MAIN.VIP

The following material is adapted from Bailey and Shand (1993) and (1996).

Image preprocessing

A 512 x 512 image is captured of each photograph, with a 2:3 aspect ratio. While capturing the photographs, it is ensured that the top and bottom edges are visible in the image since these are required for determining the camera tilt. It is also ensured that the left and right edges of the photographs are out of the field of view, otherwise artefacts may be introduced when mosaicing the photographs.

Since the panorama spans about 160° there is a considerable variation in lighting from one photograph to another because of differing sun angles. In addition to this, there may be sun glare from the sea or clouds and vignetting caused by the lens and neutral density filters. These effects are all exacerbated by reciprocity failure caused by the long exposures required. The first step is to normalise the contrast range of each image as much as possible. This contrast normalisation is performed using the following steps:

1. The image is filtered by selecting the minimum pixel value within a 21 x 21 pixel box. This effectively shrinks the lighter regions of the bars preventing them from being removed by the process. At this stage we are interested in finding the background level.
2. This image is then filtered using the average pixel value within a 55 x 55 pixel box to obtain an estimate of the local average density. Variations in this image correspond to density variations in the original image.
3. The average is subtracted from the original image to remove the density variations. An offset of 128 is added to allow negative differences to be represented conveniently.
4. Finally, the contrast of the image is enhanced using a linear stretch to expand the range of pixel values from 116 to 208 to fill the available range (0 to 255).

The resulting contrast normalised image is shown in figure 1.

Figure 1: A typical image after normalising variations in lighting and enhancing the contrast.

Correction of perspective distortion

The first step in this process is to correct for the perspective distortion present in each of the images. At this stage, a convenient coordinate system is based on map co-ordinates. We have actually used rotated map co-ordinates since the stretch of coast under study runs SE to NW, resulting in unnecessarily large images to contain the detail of interest.

If we assume that the earth is flat (a reasonable assumption since the ranges of interest are within 3.5 km from the camera location) the perspective correction equation may be represented by

$$X = \frac{a_0 x + a_1 y + a_2}{a_6 x + a_7 y + a_8}, \quad Y = \frac{a_3 x + a_4 y + a_5}{a_6 x + a_7 y + a_8} \tag{1}$$

where (x,y) are the pixel coordinates in the image before rectification, and (X,Y) are the corresponding rectified coordinates. Note that this equation will only correctly transform one 2-D plane to a second 2-D plane. The input plane is the film plane of the camera, and the output plane corresponds to sea-level. The 9 unknowns in equation (1) are solved by knowing the camera position, the positions of two surveyed ground control points (GCPs) within each image, the sea-level, and the horizon. The common denominator of the perspective transformation represents the perspective vanishing line in the photographs.

$$a_6 x + a_7 y + a_8 = 0 \tag{2}$$

If the earth were truly flat, this line would correspond to the horizon. However, because of the curvature of the earth, the apparent horizon will be below the true "flat earth" horizon (figure 2). It can be shown that the angle between the true and apparent horizon is

$$\theta \approx \sqrt{\frac{2h}{R}} \tag{3}$$

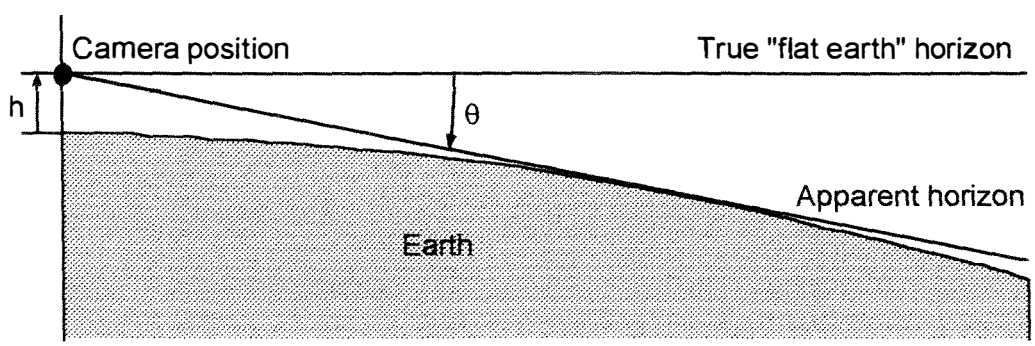

Figure 2: Error between true horizon and apparent horizon.

where h is the height of the camera above sea-level, and R is the radius of the earth. Although this angle is small (θ =0.21 for h =43 m), the error is significant, giving a 4 pixel shift in the horizon for photographs taken using a 55 mm lens and a 9.5 pixel shift with a 135 mm lens.

From the positions of the ground control points in the image, the position of the apparent horizon is estimated. A linear edge detection operation is applied within that region to detect the maximum intensity gradient (corresponding to the horizon). A least squares fit is applied to the detected points to give the line of the horizon. This is then corrected for θ to give a_6, a_7 and a_8. Note that equation (2) is normalised so that

$$a_6^2 + a_7^2 = 1 \tag{4}$$

The program draws the detected horizon on the input image and asks the user if it has been detected correctly. If not, the user defines the correct horizon by entering two points. This step is necessary because the position of the horizon may not be detected accurately if the weather is hazy or if the sea has rough and calm patches on it.

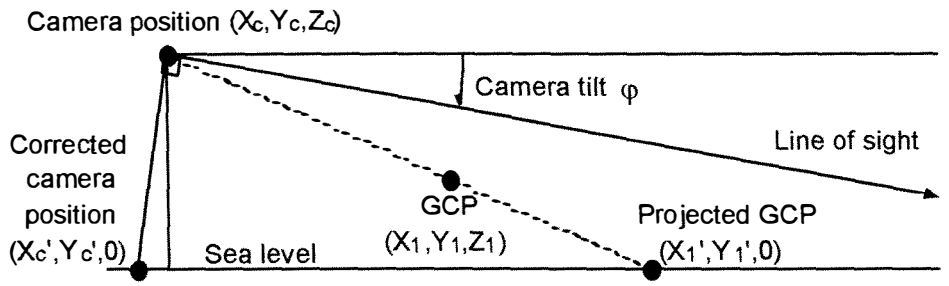

Figure 3: Correcting for camera tilt and projecting ground control points to sea-level.

The next step is to reference the camera and ground control points to sea-level (the reference plane for our perspective corrected image). The GCPs are projected to sea-level as shown in figure 3. This projection may be represented as in equation (5).

$$X_1' = \frac{Z_1 X_c - Z_c X_1}{Z_1 - Z_c}, \quad Y_1' = \frac{Z_1 Y_c - Z_c Y_1}{Z_1 - Z_c} \tag{5}$$

Lines perpendicular to the horizon on the input image all fall on planes which pass through the camera. Therefore these lines all converge at the camera point in the rectified image. If the camera is tilted below the true horizon, the point of intersection of the horizon perpendiculars will move behind the camera as shown in figure 3. It is assumed that the pixel midway between the top and bottom edge of the photograph is along the line of sight of the camera (that is normal to the film plane). The tilt is calculated knowing the angle of the line of sight below the true horizon. The camera position may be referenced to sea-level as

$$X_c' = X_c - Z_c \tan\varphi \sin\gamma, \quad Y_c' = Y_c - Z_c \tan\varphi \cos\gamma \tag{6}$$

where γ is the direction of the line of sight. In practise, the direction of the line of sight is calculated by solving equation (1) assuming no tilt (using (X_c, Y_c)). The centre pixel of the image (256,256) is then transformed to give the direction of the line of sight. This is used to correct the camera position for tilt and equation (1) is solved again. Figure 4 shows the input image with the key features labelled.

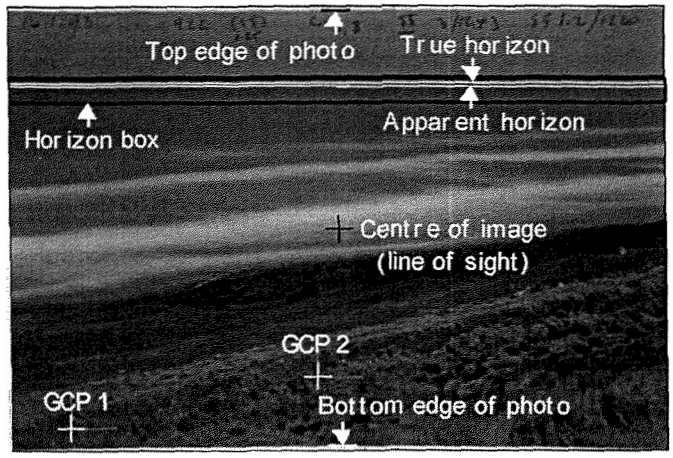

Figure 4: The input image with key features labelled.

Lines perpendicular to the horizon intersect at the corrected camera position after transformation. These lines may be parameterised by

$$x = a_6 t + b_0, \quad y = a_7 t + b_1 \tag{7}$$

where b_0 and b_1 are arbitrary constants. Substituting these into equation (1) gives

$$X_c' = \underset{t\to\infty}{Limit} \frac{a_0(a_6 t + b_0) + a_1(a_7 t + b_1) + a_2}{a_6(a_6 t + b_0) + a_7(a_7 t + b_1) + a_8} \tag{8}$$
$$= \frac{a_0 a_6 + a_1 a_7}{a_6^2 + a_7^2} \quad = a_0 a_6 + a_1 a_7$$

Each GCP gives a further independent equation in a_0, a_1 and a_2, as in equation (9).

$$X_1' = \frac{a_0 x_1 + a_1 y_1 + a_2}{a_6 x_1 + a_7 y_1 + a_8} \tag{9}$$
$$= \frac{a_0 x_1 + a_1 y_1 + a_2}{H_1}$$

where H_1 is a constant (all its terms are known). Equation (8) and equation (9) for each GCP give three simultaneous equations that are solved to give

$$a_0 = \frac{X_c'(y_1 - y_2) - a_7(H_1 X_1' - H_2 X_2')}{a_6(y_1 - y_2) - a_7(x_1 - x_2)}$$
$$a_1 = \frac{a_6(H_1 X_1' - H_2 X_2') - X_c'(x_1 - x_2)}{a_6\ y_1 - y_2) - a_7(x_1 - x_2)} \tag{10}$$
$$a_2 = X_1' H_1 - a_0 x_1 - a_1 y_1$$

Similar equations may be obtained for a_3, a_4 and a_5. Equation (1) is then used to transform each pixel in the input image, giving figure 5. The transformed image is sampled with 2 m resolution.

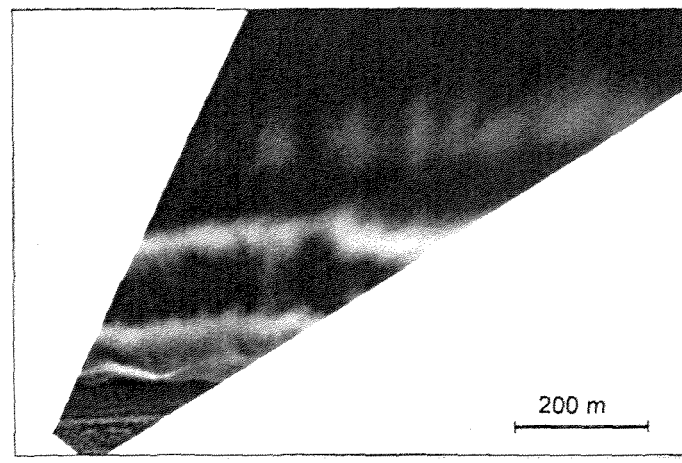

Figure 5: The perspective corrected image

Mosaicing

After correcting for perspective distortions in each of the eight input photographs, the images are combined into a single view of the coast. The views provided by the individual photographs overlap slightly. To reduce the possibility of artefacts from the joins, in the region of overlap between adjacent views, the images are merged using a linear spline as shown in figure 6. The resulting mosaic is shown in figure 7.

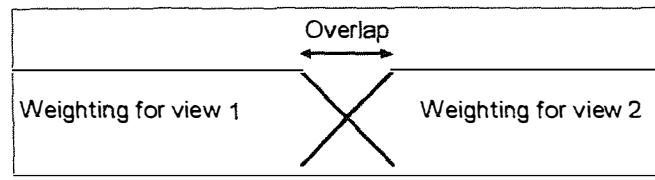

Figure 6: Linear spline applied to the overlap between images.

Figure 7: Mosaic of eight perspective corrected images.

Appendix H Rectified images of the study area

The following rectified images have been utilised in the present study of NOM. All images have been rectified to geodetic co-ordinates. Appendix H(i) contains the images from the monthly data-set. Appendix H(ii) contain supplementary images used in other parts of the study, with the relevant section(s) being noted on each image. In addition, each image has been identified by its file name which is printed in the upper left corner. The file notation identifies the sampling method, the survey date and the spatial coverage in the following manner:

[method of field sampling][date of survey].[spatial coverage]

The following codes have been used within the file name:

Field methods:
AV = vertical aerial photography.
AO = oblique aerial photography.
LE = oblique terrestrial photography.

Date:
YYMMDD, where Y = year, M = month, D = day.

Spatial coverage:
FUL = the entire study area.
CEN = central portion of study area, as photographed with 55 mm lens.
PRT = some other partial coverage of the study area.

For example, the image LE920707.FUL was sampled using oblique terrestrial photography on the 7th of July 1992 and covers the entire study area.

Appendix H(i) page 1 of 8

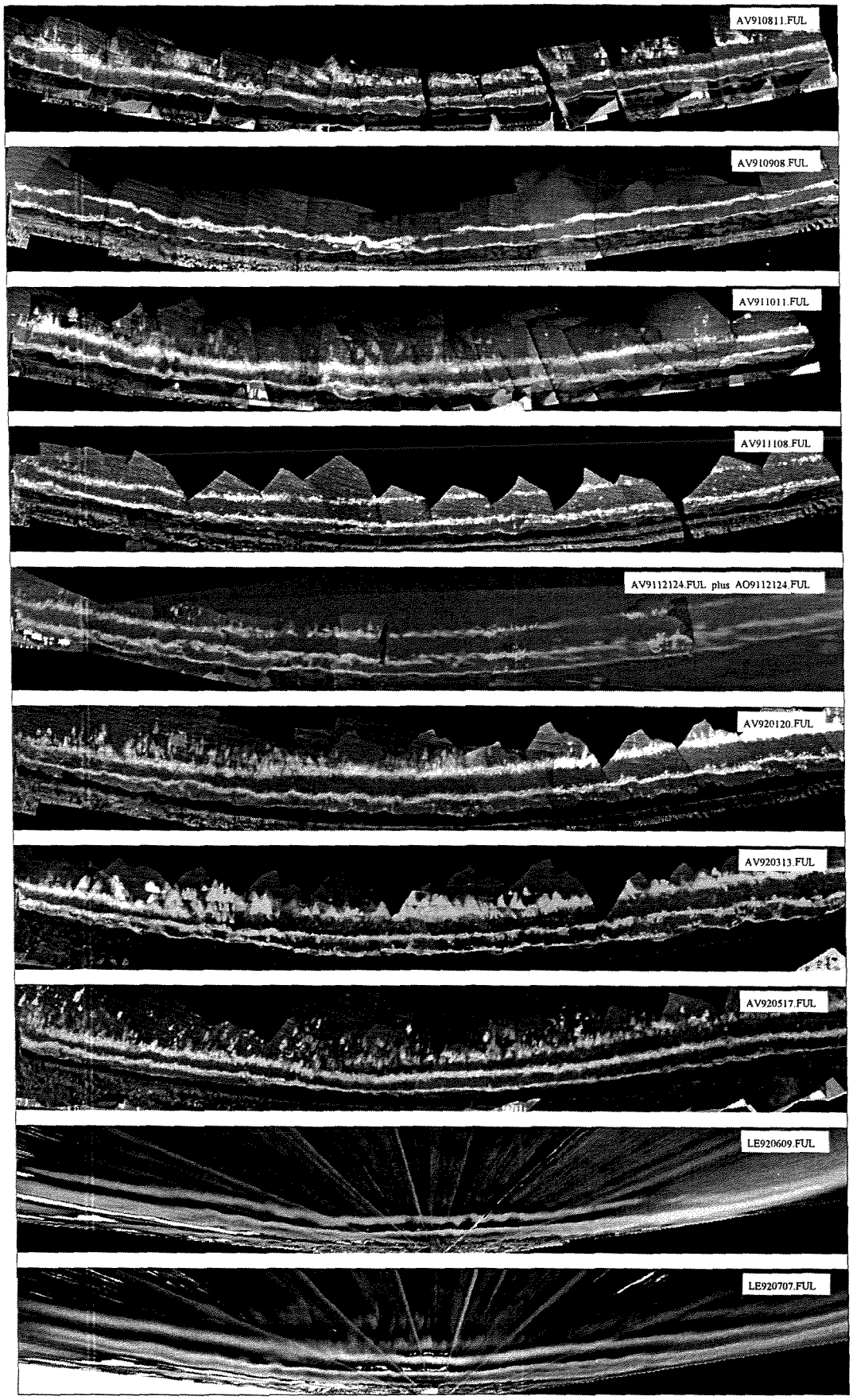

Appendix H(i) page 2 of 8

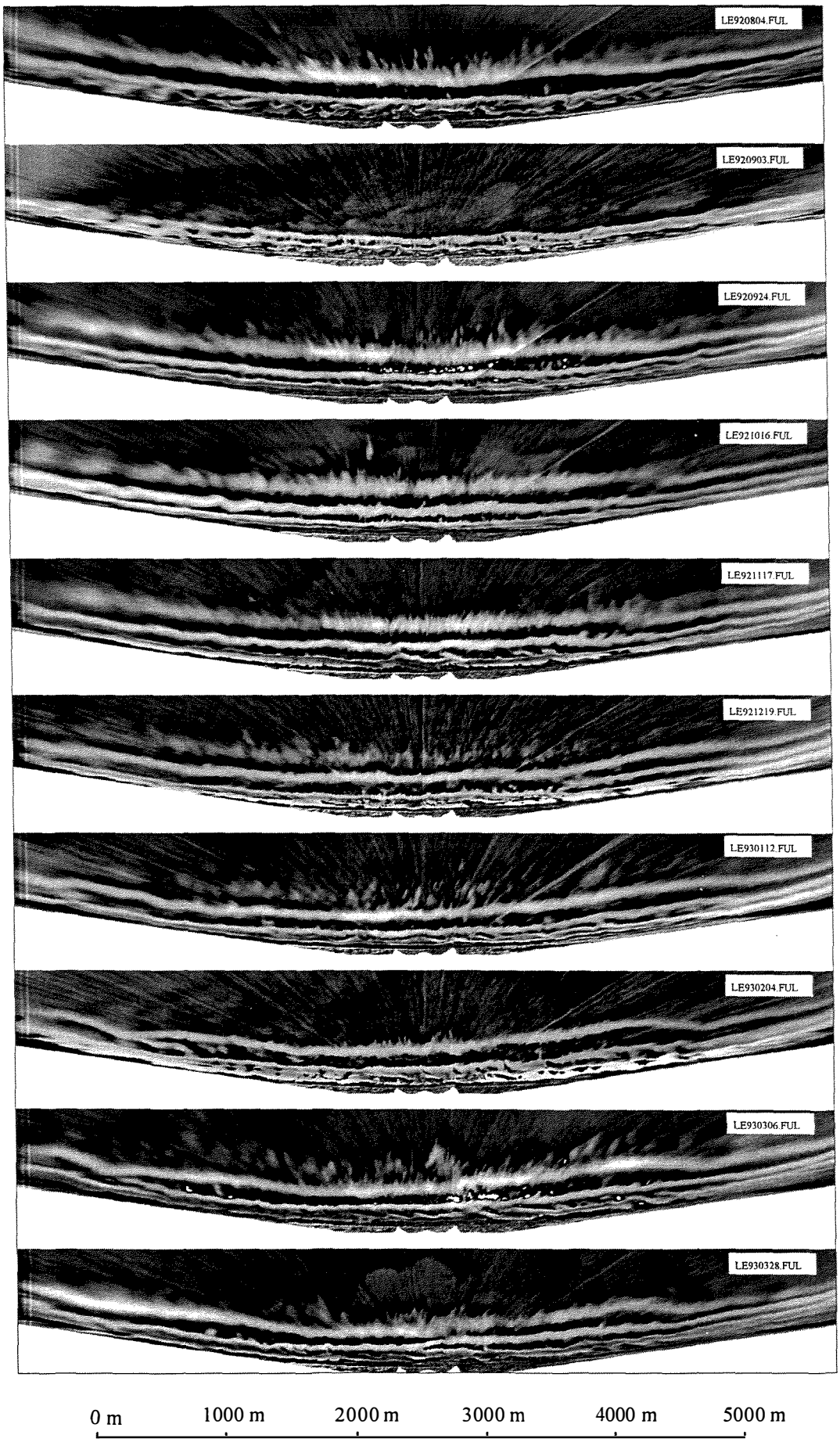

Appendix H(i) page 3 of 8

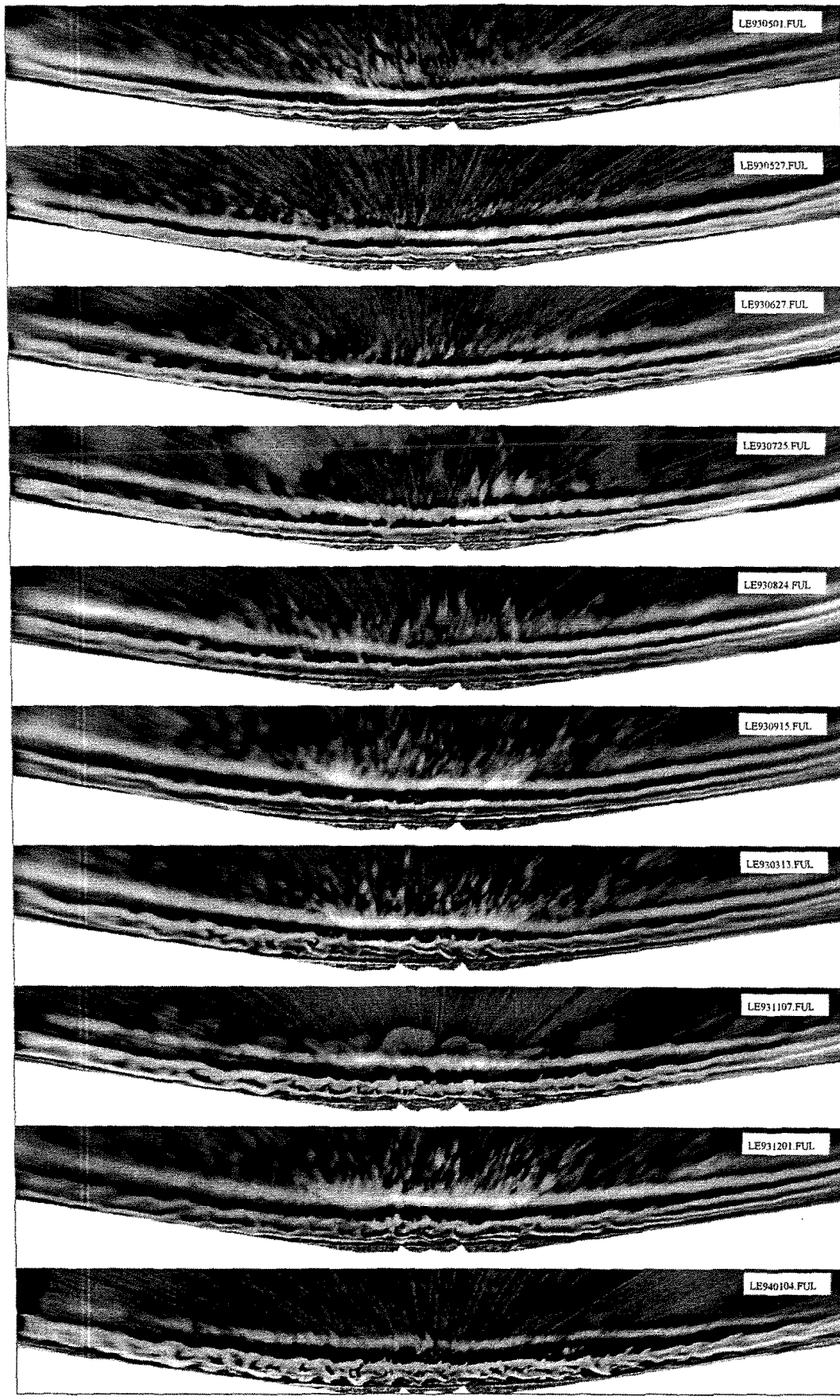

Appendix H(i) page 4 of 8

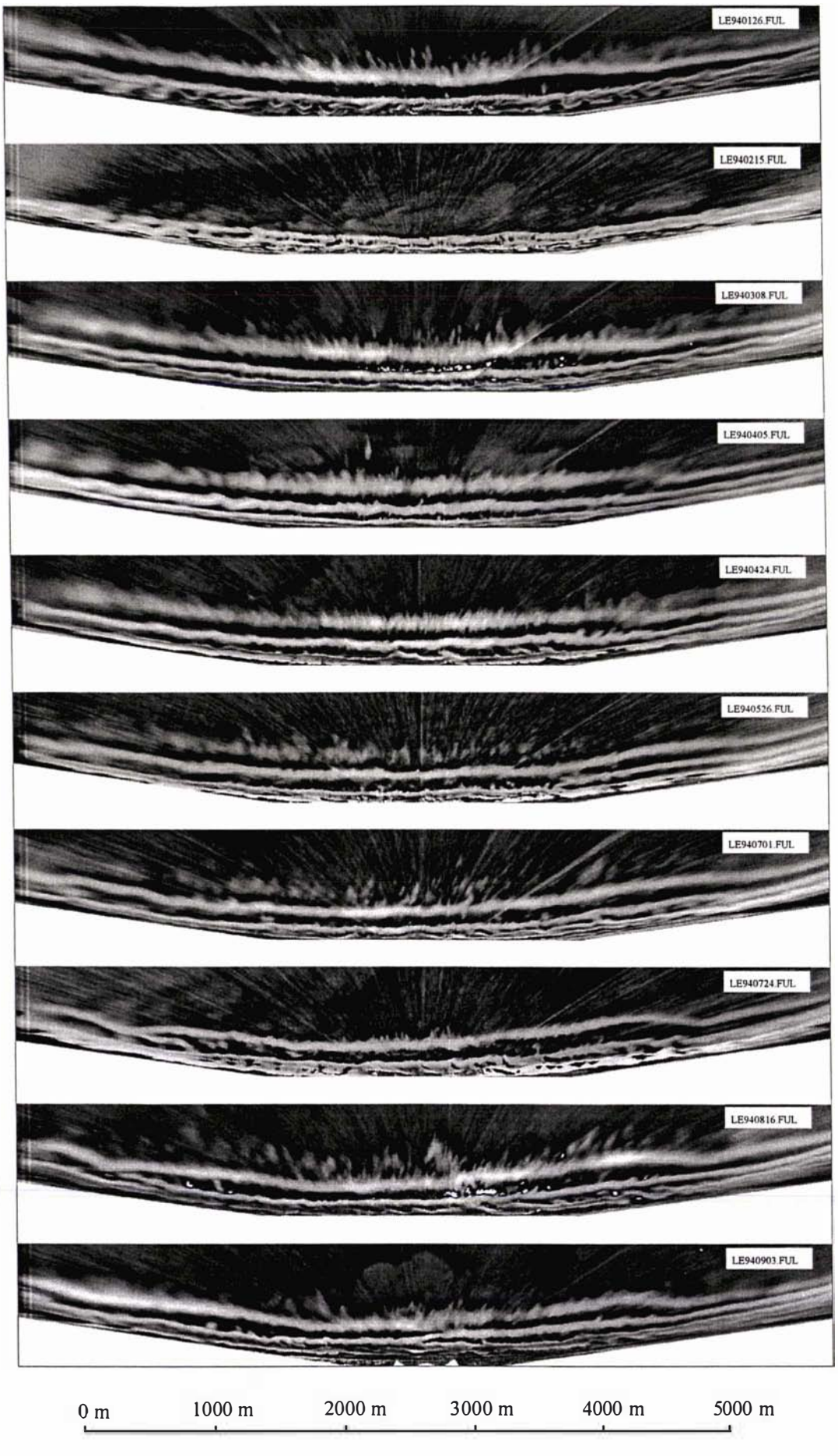

Appendix H(i) page 5 of 8

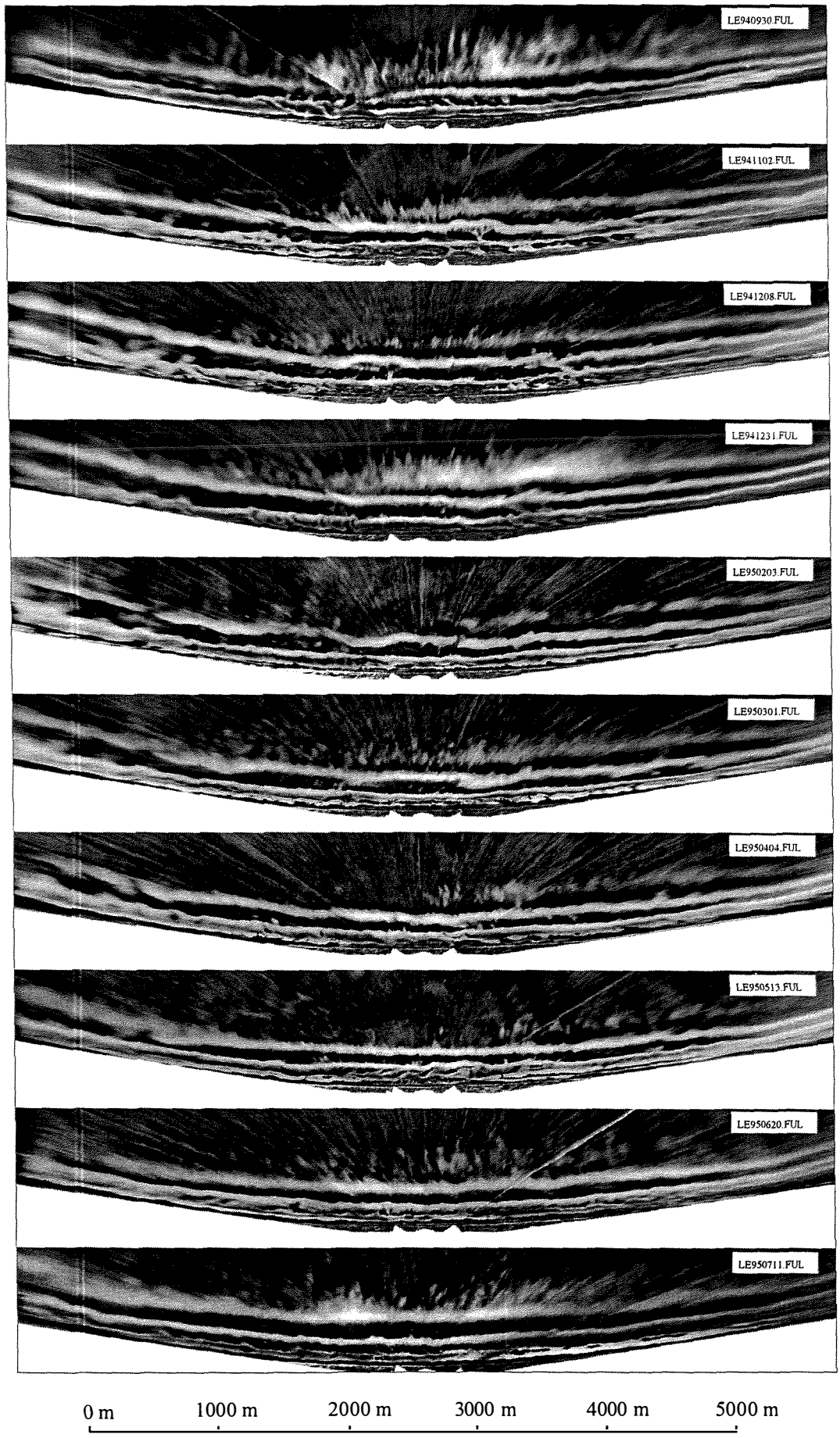

Appendix H(i) page 6 of 8

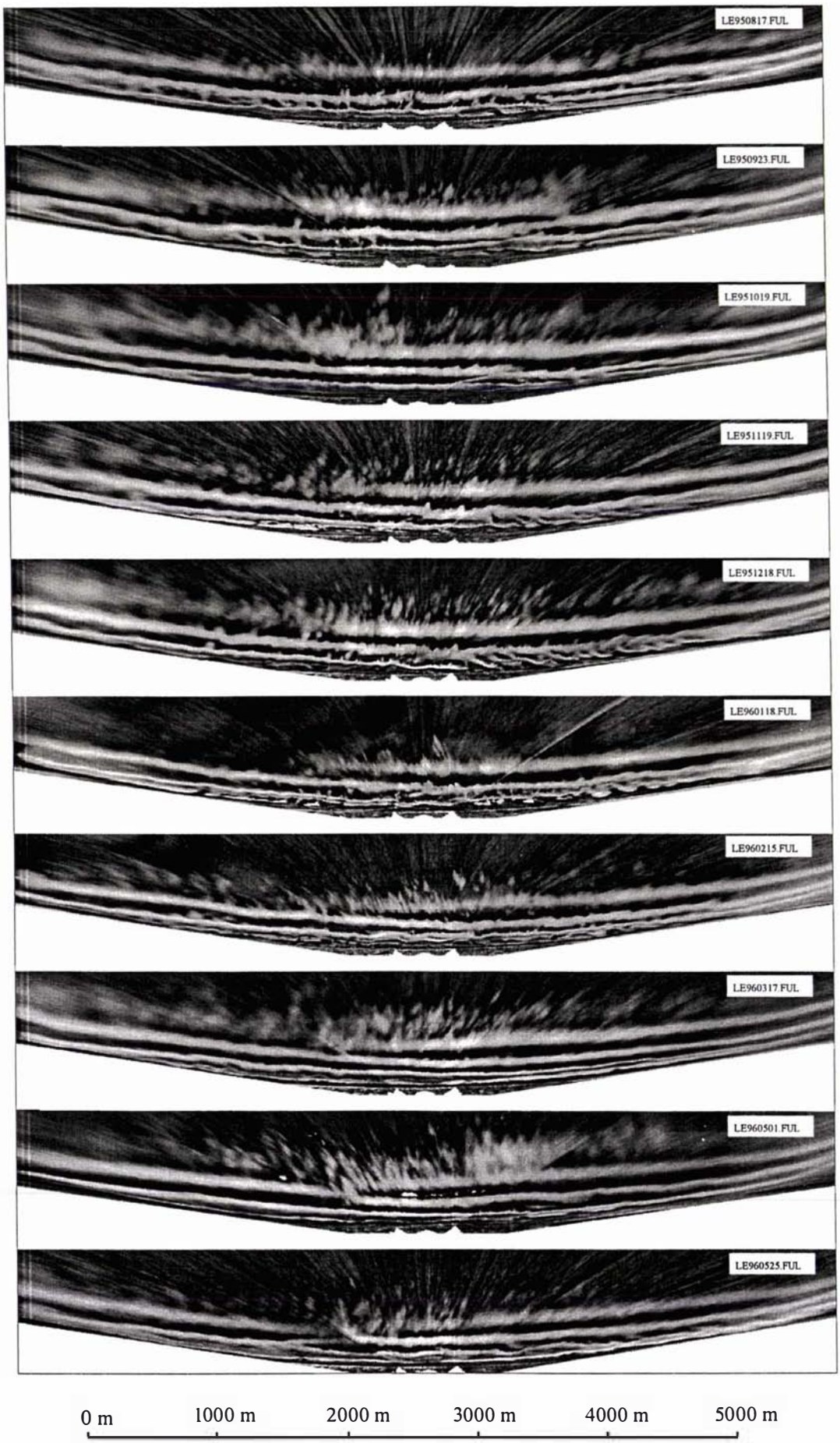

Appendix H(i) page 7 of 8

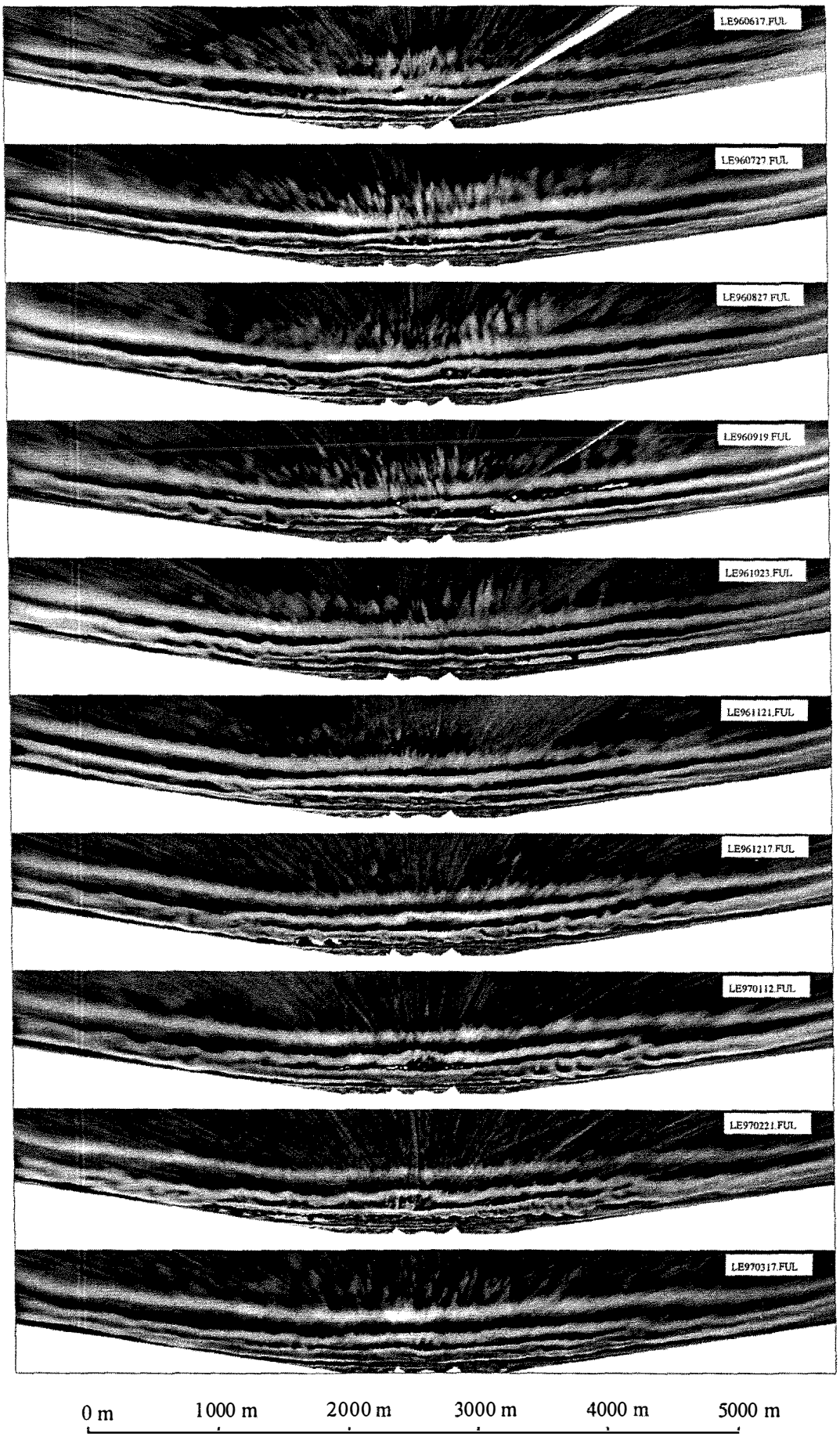

Appendix H(i) page 8 of 8

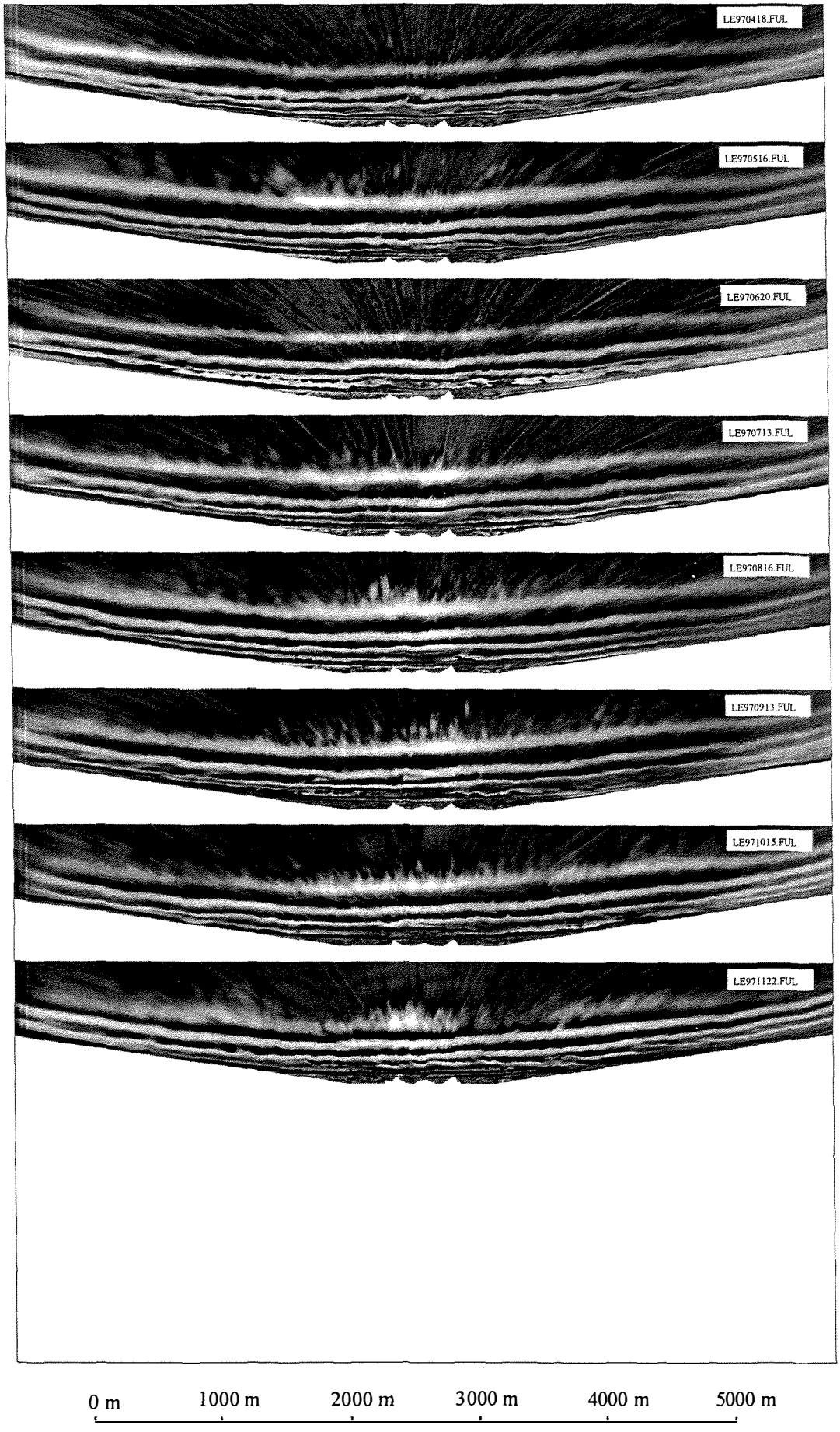

Appendix H(ii) page 1 of 2

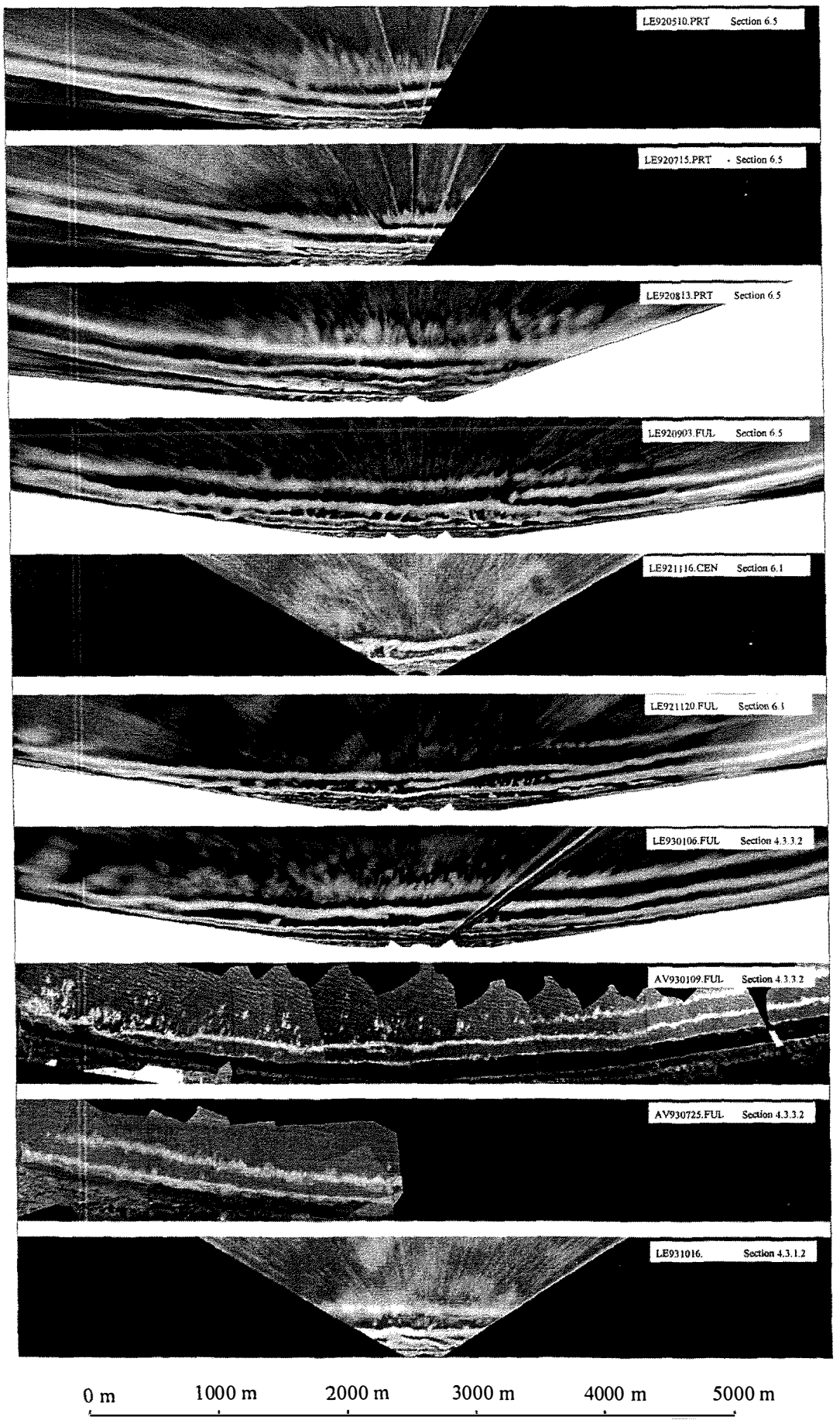

Appendix H(ii) page 2 of 2

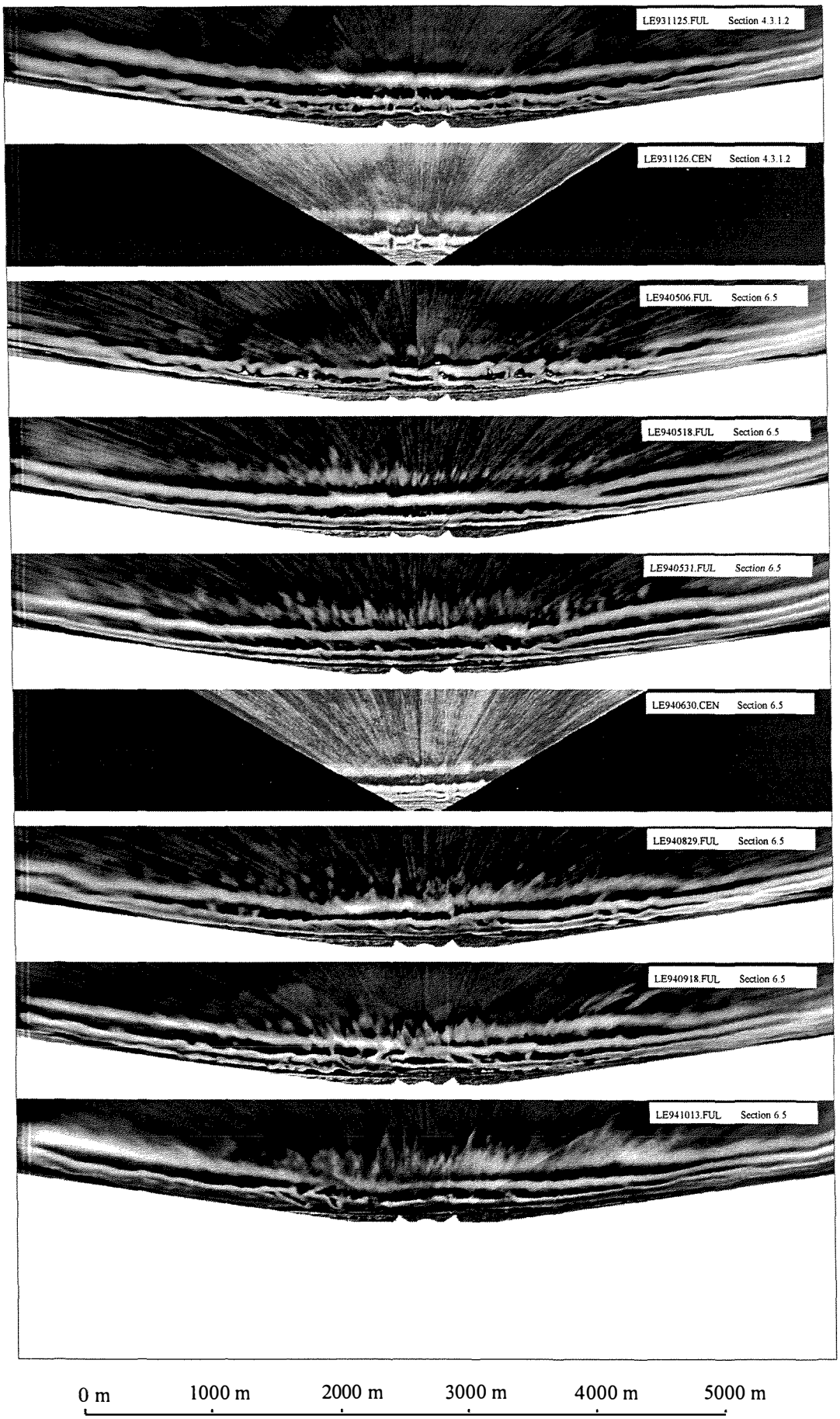

Appendix I Environmental conditions during error assessment sampling

Parameter values defining the environmental conditions which occurred during the field sampling for data used in the morphological error analysis (chapter 4). The particular use that the data from each sampling was put to is given in parenthesis on the following line.

Date of sampling	Time of sampling (hours)	Sampling method*	Incident wave height (m)	Wave Period (seconds)	Tide (MSL) (m)	Wind direction (degrees)	Wind speed (m/s)	Barometric pressure (hPa)	Seiche wave height (m)
910131	1420 to 1550	PS	1.44	6.9	0.4 to -0.45	285	15.0	1004.5	0.71
(Seiche modelling, equation 4.4)									
910201	1505 to 1635	PS	1.89	9.2	0.3 to -0.5	280	12.0	1004.6	0.69
(Seiche modelling, equation 4.4)									
910202	1545 to 1715	PS	1.26	9.2	0.35 to -0.45	290	13.0	1002.9	0.93
(Seiche modelling, equation 4.4)									
910204	1650 to 1820)	PS	1.89	6.9	0.25 to -0.3	300	11.8	1011.9	1.00
(Seiche modelling, equation 4.4)									
910210	1025 to 1155	PS	0.72	14.0	0.1 to -0.15	040	1.5	1017.8	0.41
(Seiche modelling, equation 4.4)									
910212	1215 to 1345	PS	1.44	15.7	0.2.to -0.3	275	7.5	1012.5	0.44
(Seiche modelling, equation 4.4)									
910217	0850 to 1020	PS	0.72	8.5	-0.55 to 0.4	070	2.0	1011.6	0.18
(Seiche modelling, equation 4.4)									
910218	1550 to 1720	PS	2.52	8.5	0.4 to -0.45	295	6.0	999.2	1.18
(Seiche modelling, equation 4.4)									
910219	1635 to 1805	PS	2.52	9.2	0.3 to -0.55	170	14.0	1005.4	1.12
(Seiche modelling, equation 4.4)									
910222	1245 to 1415	PS	0.72	8.5	-0.3 to 0.2	210	3.5	1018.7	0.31
(Seiche modelling, equation 4.4)									
910223	0615 to 0745	PS	1.17	8.5	0.35 to -0.1	010	1.0	1017.6	0.26
(Seiche modelling, equation 4.4)									
910224	1535 to 1705	PS	1.26	7.9	-0.3 to 0.2	280	7.5	1017.0	0.25
(Seiche modelling, equation 4.4)									
910225	1650 to 1820	PS	1.89	5.5	-0.35 to 0.2	190	5.7	1020.4	0.54
(Seiche modelling, equation 4.4)									
910227	1225 to 1405	PS	1.89	6.5	0.45 to -0.4	290	12.0	1008.0	1.24
(Seiche modelling, equation 4.4)									
910301	1350 to 1520	PS	1.26	9.2	0.35 to -0.4	190	6.5	1010.0	0.99
(Seiche modelling, equation 4.4)									
910302	0820 to 0950	PS	0.72	14.0	-0.55 to 0.45	020	1.0	1011.2	0.22
(Seiche modelling, equation 4.4)									

continued

Date of sampling	Time of sampling (hours)	Sampling method	Incident wave height (m)	Wave Period (seconds)	Tide (MSL) (m)	Wind direction (degrees)	Wind speed (m/s)	Barometric pressure (hPa)	Seiche wave height (m)
910303 (Seiche modelling, equation 4.4)	0850 to 1020	PS	1.17	12.2	-0.3 to 0.4	320	3.5	1006.3	0.22
910304e (Seiche modelling, equation 4.4)	1530 to 1700	PS	1.80	11.0	0.4 to -0.4	260	7.0	1014.7	0.68
910305 (Seiche modelling, equation 4.4)	1605 to 1735	PS	1.84	6.9	0.2 to -0.3	290	12.8	1013.7	1.26
910307 (Seiche modelling, equation 4.4)	1705 to 1835	PS	1.26	7.0	0.2 to -0.3	160	7.7	1027.0	0.48
930106 (Aerial/terrestrial data comparison, Figure 4.10)	1400 to 1500	TOP	1.41	8.1	-1.0 to -0.7	290	14.9	1005.2	ND
930109 (Aerial/terrestrial data comparison, Figure 4.10)	1745 to 1800	AV	1.18	10.0	-1.35 to -1.15	290	11.3	1016.1	ND
930112 (Aerial/terrestrial data comparison, Figure 4.10)	0840 to 0940	TOP	1.88	8.3	-1.4 to -1.0	300	7.0	1018.9	ND
930725 (Aerial/terrestrial data comparison, Figure 4.10)	0915 to 0945	AV	2.03	16.8	-1.0 to -0.9	360	2.0	1028.6	ND
930725 (Aerial/terrestrial data comparison, Figure 4.10)	1030 to 1130	TOP	2.03	16.8	-0.65 to -0.15	060	2.6	1028.2	ND
931016 (Tide change effect on intensity maximum location, Table 4.4 and Figure 4.3)	0745 to 0800	TOP	1.88	9.3	-1.53	280	3.6	1018.4	ND
931016 (Tide change effect on intensity maximum location, Table 4.4 and Figure 4.3)	1640 to 1650	TOP	1.88	9.3	-0.51	350	4.6	1020.4	ND
931125 (Wave height change effect on intensity maximum location, Table 4.5 and Figure 4.4) continued	1340 to 1350	TOP	2.27	12.8	-0.75	210	4.6	1010.5	ND
931126 (Wave height change effect on intensity maximum location, Table 4.5 and Figure 4.4)	1400 to 1415	TOP	1.25	10.0	-0.8	210	5.7	1014.5	ND
940131 (Detection of infragravity wave motion, Figure 2.23)	0930 to 1230	TOV	1.72	9.5	1.1 to 2.7	320	4.3	1015.5	ND
940131 (Seiche influence on cross-shore variation in intensity maximum location, Figure 4.2)	1710 to 1810	TOV	1.72	9.5	-0.2 to -0.7	230	6.7	1015.7	ND
940201 (Identification of seiche period from 180 minute video-based runup record Figure 2.24D)	1300 to 1600	TOV	1.41	12.0	1.0 to 0.8	180	10.5	1020.1	ND
940316 (Seiche height; predicted and observed values in Table 4.2)	1030 to 1130	SES	2.04	10.0	-0.2 to 0.35	030	2.8	1009.5	0.34
940502 (Seiche height; predicted and observed values in Table 4.2)	1200 to 1300	SES	1.72	9.7	-0.3 to -0.1	340	7.0	1026.0	0.21+

Where: PS = pressure sensor, SES = stationary echo-sounding, AV = vertical aerial photography, TOP = oblique terrestrial photography, TOV = oblique terrestrial video, ND = no data.

Appendix J Ground profile bar-crest data for T1500

Echo-sounded bar-crest location data for site T1500, i.e. 1500 m northwest of the Wanganui Rivermouth. These data were used when investigating shorter term morphological behaviour associated with cycles of NOM (chapter 6). Surveys were carried out at approximately monthly intervals between 14.3.91 and 3.6.92; the dates are listed in Appendix D[i]. Bar-crests were detected using the 'maximum residual method' described in chapter 3, section 3.3.4.